

Spring 2017

Numerical and experimental studies on coastal marsh erosion under hurricane induced wave and current

Minhaz M. Shahriar
Louisiana Tech University

Follow this and additional works at: <https://digitalcommons.latech.edu/dissertations>

 Part of the [Civil Engineering Commons](#), and the [Geotechnical Engineering Commons](#)

Recommended Citation

Shahriar, Minhaz M., "" (2017). *Dissertation*. 59.
<https://digitalcommons.latech.edu/dissertations/59>

This Dissertation is brought to you for free and open access by the Graduate School at Louisiana Tech Digital Commons. It has been accepted for inclusion in Doctoral Dissertations by an authorized administrator of Louisiana Tech Digital Commons. For more information, please contact digitalcommons@latech.edu.

**NUMERICAL AND EXPERIMENTAL STUDIES ON
COASTAL MARSH EROSION UNDER
HURRICANE INDUCED WAVE
AND CURRENT**

by

Minhaz M. Shahriar, B.Sc., M.Sc.

A Dissertation Presented in Partial Fulfillment
of the Requirements of the Degree
Doctor of Philosophy

COLLEGE OF ENGINEERING AND SCIENCE
LOUISIANA TECH UNIVERSITY

May 2017

ProQuest Number: 10644143

All rights reserved

INFORMATION TO ALL USERS

The quality of this reproduction is dependent upon the quality of the copy submitted.

In the unlikely event that the author did not send a complete manuscript and there are missing pages, these will be noted. Also, if material had to be removed, a note will indicate the deletion.



ProQuest 10644143

Published by ProQuest LLC(2017). Copyright of the Dissertation is held by the Author.

All rights reserved.

This work is protected against unauthorized copying under Title 17, United States Code.
Microform Edition © ProQuest LLC.

ProQuest LLC
789 East Eisenhower Parkway
P.O. Box 1346
Ann Arbor, MI 48106-1346

LOUISIANA TECH UNIVERSITY

THE GRADUATE SCHOOL

April 07, 2017

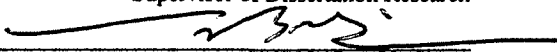
Date

We hereby recommend that the dissertation prepared under our supervision
by Minhaz Mohammad Shahriar, M.Sc.

entitled "NUMERICAL AND EXPERIMENTAL STUDIES ON COASTAL MARSH
EROSION UNDER HURRICANE INDUCED WAVE & CURRENT"

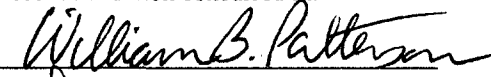
be accepted in partial fulfillment of the requirements for the Degree of
Ph.D. in Engineering (Civil Engineering)

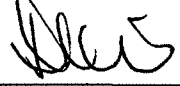


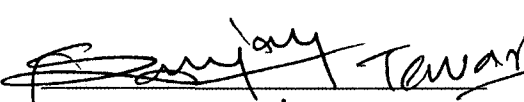
Supervisor of Dissertation Research


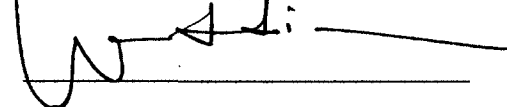
Head of Department
Civil Engineering
Department

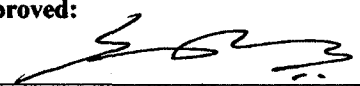
Recommendation concurred in:







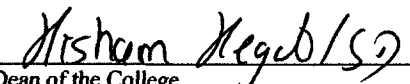
Advisory Committee


Approved: 

Director of Graduate Studies

Approved: 

Dean of the Graduate School



Dean of the College

ABSTRACT

Considering the past history and future risks of hurricanes in the USA, well understood storm protection plans are needed to shelter the important areas of the population and economy, especially within southeastern Louisiana. It is extensively assumed that marshes offer protection from hurricane though the degree of this protection is not well measured or understood due to the complex physics involved in this overall system. Moreover, marshes experience significant erosion while serving as a barrier for important areas. Consequently, a particular method to quantify the effects on marshes during a coastal hurricane period is necessary to mitigate major marsh loss.

A study comprised of experimental work and numerical simulation was undertaken to evaluate the effect of marsh vegetation on resisting hurricane induced erosion and erosion of the marsh itself. Local vegetation *Spartina alterniflora* was selected as principal marsh vegetation for this study. Contribution from *Spartina alterniflora* had been analyzed from two different directions such as contribution of roots and contribution of shoots.

The overall research was divided into three different phases. The first phase was the laboratory experiments of collected soil samples with and without roots of *Spartina* from the study area (Cycle-1 of CS-28 project). Direct shear tests were performed on the samples to study the effect of roots on soil shear strength. Tensile strength of the roots was also studied. In the second phase, Delft3D wave flow coupled model was applied on the

Louisiana coastal marsh near Calcasieu Lake to assess the contribution of marsh vegetation in reducing hurricane induced wave and current actions. The objective of this phase was to develop an integrated wind, current, wave modeling system for the Louisiana coast under hurricane conditions. Hurricane Ike in 2008 was chosen as an example to study the marsh's contribution during hurricane. The wave flow coupled model was generated covering a significant part of Calcasieu Lake, surrounding marshes and a part of the Gulf of Mexico. The coupled model was calibrated and validated against observed data gathered from NOAA and CPRA observation stations. Later after validation, Hurricane Ike forcing condition was introduced to the wave flow coupled model. Moreover, to originate the extreme scenario, the hurricane was introduced by excluding the precipitation and flooding effect of a previous hurricane named Gustav that made landfall 13 days prior to Hurricane Ike. Delft3D vegetation model was also analyzed to investigate the effect of a hurricane on vegetated mud bed. In the third phase, based on the experimental results from the tensile and direct shear tests and hurricane stress results from Delft3D analysis, slope stability analyses were performed for 16 different scenarios by utilizing Slope/W to predict erosion of vegetated and non-vegetated mud surface during different phases of a hurricane.

Experimental results suggested that the marshes do have the potential to enhance soil shear strength. Results suggested that the additional cohesion developed from plant roots played a vital role in enhancing shear strength of marsh soil, especially near the surface. A correlation between *Spartina alterniflora* root tensile strength and root cohesion was proposed for dredged soil. The validation of the coupled wave flow model showed that the water level computed by Delft3D agrees fairly well with the measured data. Results from Delft3D vegetation model study indicated a major reduction in the current velocity in

presence of the *Spartina alterniflora* shoot system. Results from the hurricane induced wave flow model showed that the wave induced bed shear stress up to 90 Pa can be the result while hurricane reached its peak time.

It was found that the edge and flat soil mass of the marsh reacted differently under hurricane induced wave and current action especially when time dependent analysis is considered. It was also observed that the presence of a shoot system around the weak spot reduces bed shear stress significantly, especially while the marsh bed is submerged or under a low wave energy field. Yet, completely exposed vegetation during the peak of a hurricanes was found to be most vulnerable and supposed to experience severe mass erosion/marsh shears.

It was also noticed from the erosion prediction analysis that the hurricane damage could have been severe if there was no prior hurricane before Hurricane Ike. From the summary of erosion prediction analysis output, it was observed that the uprooting or mass erosion only occurred during two scenarios among sixteen scenarios. Near the marsh edge, mass erosion occurred during the hurricane landfall with the condition that the marsh edge was above water prior to hurricane impact. On marsh flat, mass erosion occurred during the peak of the hurricane when analyzed with drought condition prior to the hurricane.

The combined experimental and numerical analysis of Louisiana coastal marsh under hurricane-induced waves and currents provided useful insights of actual scenarios and probable cases. The findings could be used effectively in the design and construction of future marsh creation projects in Louisiana.

APPROVAL FOR SCHOLARLY DISSEMINATION

The author grants to the Prescott Memorial Library of Louisiana Tech University the right to reproduce, by appropriate methods, upon request, any or all portions of this Dissertation. It is understood that "proper request" consists of the agreement, on the part of the requesting party, that said reproduction is for his personal use and that subsequent reproduction will not occur without written approval of the author of this Dissertation. Further, any portions of the Dissertation used in books, papers, and other works must be appropriately referenced to this Dissertation.

Finally, the author of this Dissertation reserves the right to publish freely, in the literature, at any time, any or all portions of this Dissertation.

Author 

Date 07/28/2017

DEDICATION

Dedicated to my father, Mohammed Abdus Sabur and my mother, Afroza Akhter.

TABLE OF CONTENTS

ABSTRACT.....	iii
DEDICATION.....	vii
LIST OF TABLES.....	xiv
LIST OF FIGURES.....	xvi
ACKNOWLEDGMENTS.....	xiii
CHAPTER 1 INTRODUCTION.....	1
1.1 Background.....	1
1.2 Objective.....	7
1.3 Site Description.....	8
1.3.1 Cameron Parish.....	8
1.3.2 Calcasieu-0Sabine Basin.....	9
1.4 Research Tasks.....	9
1.5 Layout of the Thesis.....	10
CHAPTER 2 LITERATURE REVIEW.....	12
2.1 Hydrology of the Study Area.....	12
2.2 Reference Project: The Sabine Refuge Marsh Creation (CS-28).....	14
2.2.1 Cycle-1 of CS-28 Project.....	16

2.3	Coastal Marsh.....	17
2.3.1	Smooth Cordgrass.....	20
2.4	Delft3D Modeling	22
2.4.1	Delft3D FLOW Module.....	23
2.4.2	The Delft3D-WAVE Module	26
2.4.3	Vegetation Model.....	27
2.4.4	Bed Shear Stress	28
2.5	Wave Induced Normal Stress.....	29
2.6	Composite Shear Strength of Rooted Soil.....	31
2.7	Stability Analysis to Predict Erosion	33
2.7.1	Analysis of the Roots-Reinforced Slope.....	33
2.7.2	Slope/W and Root Reinforcement Analysis	34
CHAPTER 3 FIELD AND LABORATORY ANALYSIS OF		
MARSH VEGETATED SOIL.....		36
3.1	Introduction	36
3.2	Field Study	37
3.3	Laboratory Study.....	38
3.3.1	Direct Shear Test.....	39
3.3.2	Root Distribution Analysis	40
3.3.3	Tensile Strength Test on Roots	42
3.3.4	Root Area Ratio Calculations	43

3.4	Results	44
3.4.1	Tensile Strength of Roots.....	44
3.4.2	Shear Strength of Plain and Rooted Soil.....	45
3.4.3	Root-Induced Cohesion in Soils	48
CHAPTER 4 DELFT3D HYDRODYNAMIC MODEL		
CALIBRATION AND VALIDATION.....		
50		
4.1	Introduction	50
4.2	Chapter Structure.....	52
4.3	Gathered Data.....	52
4.3.1	Bathymetry.....	52
4.3.2	Reference Level	53
4.3.3	Water Level Data	53
4.3.4	Wind and Precipitation Data.....	56
4.4	Model Setup	57
4.4.1	Model Grid.....	57
4.4.2	Model Bathymetry	61
4.4.3	Model Initial Condition.....	63
4.4.4	Flow Model Forcing Conditions.....	64
4.4.5	Additional Parameters for Flow Model	68
4.4.6	Wave Model.....	69
4.4.7	Model Calibration.....	70

4.4.8	Model Validation	74
4.4.9	Model Circulation Characteristics	76
CHAPTER 5 STUDY ON THE IMPACT OF HURRICANE IKE		
OVER <i>SPARTINA ALTERNIFLORA</i> MARSH SYSTEM		
82		
5.1	Introduction	82
5.2	Chapter Structure.....	83
5.3	Hurricane Ike.....	83
5.4	Model Setup	86
5.4.1	Model Grid and Bathymetry	86
5.4.2	Initial Condition	89
5.4.3	Boundary Condition.....	91
5.4.4	Model Coupling	94
5.4.5	Model Validation	95
5.4.6	Vegetation Model.....	96
5.5	Model Scenarios.....	97
5.6	Results	98
5.6.1	Result Analysis for Mudflat (Without Vegetation)	99
5.6.2	Result Analysis for Marsh Mudflat (With Vegetation)	117
5.6.3	Result Comparison for Vegetated and Non-Vegetated Mudflat.....	120
5.6.4	Summary	127

CHAPTER 6 EROSION PREDICTION STUDY OF *SPARTINA*

<i>ALTERNIFLORA</i> MARSH SYSTEM UNDER HURRICANE IKE.....	128
6.1 Introduction	128
6.2 Erosion Prediction Model.....	129
6.2.1 Model Setup.....	129
6.2.2 Material Properties.....	131
6.2.3 Model Scenarios.....	132
6.2.4 Model Loading Condition.....	133
6.2.5 Results.....	134
6.2.6 Summary.....	140

CHAPTER 7 SUMMARY, CONCLUSIONS AND

RECOMMENDATIONS.....	142
7.1 Summary	142
7.2 Conclusions.....	143
7.3 Recommendations.....	145
APPENDIX A DELFT3D MODEL INPUTS.....	147
APPENDIX B DELFT3D VEGETATION INPUT FILES.....	154
B.1 Delft3D Vegetation Map File for <i>Spartina alterniflora</i>	156
APPENDIX C DELFT3D MODEL FILES.....	159
C.1 Delft3D Wave Boundary File	160
C.2 Wave Flow Coupled Run Script.....	161

C.3 Wave Run Script	162
REFERENCES	163

LIST OF TABLES

Table 1-1: Wetland loss estimates (km ²) following hurricanes Katrina and Rita (2005) and Gustav and Ike (2008) by geographic province (Barras et al. 2009).....	4
Table 2-1: Sabine refuge marsh creation project (CS-28) summary (obtained from CWPPRA project fact sheets).....	16
Table 2-2: Dominant height of <i>Spartina alterniflora</i> Loisel (shoot system) at different vegetation stations in the project area (CS-28 - Cycle-1).	21
Table 3-1: Root Physical Properties.	42
Table 3-2: Physical properties of roots and resulted strength for each root.	45
Table 3-3: Soil strength parameter comparison.	48
Table 3-4: Root cohesion for both models.....	49
Table 4-1: Summary of boundary and observation stations.	55
Table 4-2: Grid characteristics.....	59
Table 4-3: Parameters used in Flow model.....	69
Table 4-4: Wave parameters used for boundary conditions.	69
Table 4-5: Comparison of RMAE and skill for calibration study.....	73
Table 4-6: RSME and Skill comparisons for observation points.....	76
Table 5-1: Summary of Significant Times and Characteristics of Hurricane Ike.....	84
Table 5-2: Location of observation station.	95
Table 5-3: Vegetation input parameters.....	97
Table 5-4: Result observation condition.	98
Table 5-5: Description of result extraction section.....	104

Table 5-6: Extraction point location.	117
Table 6-1: Material properties used in erosion model.	132
Table 6-2: Model scenarios for erosion analysis.	133
Table 6-3: Model input conditions.	134
Table 6-4: Erosion prediction model results	135
Table 6-5: Model results.	141

LIST OF FIGURES

Figure 1-1: The basin boundaries defined by CWPPRA Task Force and wetland loss rate (Barras, 1994).....	1
Figure 1-2: Marsh vegetation loss under wave and current action.	3
Figure 1-3: Tracks of Hurricanes in Coastal Louisiana (Source: NOAA Coastal Services Center).....	5
Figure 1-4: Map depicting the area selected for study in Calcasieu-Sabine basin.	8
Figure 2-1: Reference project location (left) and the boundary of the reference project (right).	15
Figure 2-2: Vegetation types in the study area (extracted from Sasser (2014)).	18
Figure 2-3: Location of vegetation station.....	18
Figure 2-4: (a) Marsh classification. (b) Marsh vegetation data.....	19
Figure 2-5: Plant morphology of smooth cordgrass.	20
Figure 2-6: Location of observation stations.	21
Figure 2-7: Sigma model example (Deltares 2011).....	24
Figure 2-8: Rotational sliding proposed by Hankel (1970).	30
Figure 2-9: Root reinforcement model scheme.	32
Figure 2-10: Stress and strength illustration along with a potential slip surface: Shear strength along the slip surface in the presence and absence of root reinforcement (Left) and Typical slice and bottom forces for the method of the slice (Right).	34
Figure 3-1: Vegetated Marsh (left) Penetration test (right).	37
Figure 3-2: Cone penetration resistance distribution with depth in the area of Cycle-1.....	38

Figure 3-3: Collected marsh soil with vegetation from Cycle-1.	38
Figure 3-4: Sample preparation for the direct shear test.....	40
Figure 3-5: (a) Roots during the washing stage (b) Roots distribution of two plants (c) Root distribution of one single plant (d) Near surface root distribution.....	41
Figure 3-6: Root distribution of <i>Spartina alterniflora</i>	42
Figure 3-7: (a) Types of Roots. (b) Tensile Test on Root.	43
Figure 3-8: Sample for RAR calculation.	44
Figure 3-9: Tensile stress vs. root diameter comparison.	44
Figure 3-10: Stress-strain curve for plain and rooted soil for normal stress of 0.7 kPa.	46
Figure 3-11: Stress-strain curve for plain and rooted soil for normal stress of 2.3 kPa.	46
Figure 3-12: Stress-strain curve for plain and rooted soil for normal stress of 3.2 kPa.	47
Figure 3-13: Stress-strain curve for plain and rooted soil for normal stress of 5.47 kPa.	47
Figure 3-14: Stress-strain curve for plain and rooted soil.	48
Figure 4-1: Sample data for floodplain (left) and overall model domain(right) bathymetry.	52
Figure 4-2: Photographs of Station 8768094 Calcasieu Pass, LA.	54
Figure 4-3: Tidal datum explanation for Calcasieu Pass station.....	54
Figure 4-4: Boundary and observation stations.	56
Figure 4-5: Delft3D FLOW grid.....	57
Figure 4-6: Layer distribution for Flow grid.....	58
Figure 4-7: Delft3D WAVE grid.	59
Figure 4-8: Delft 3D model grid.	61

Figure 4-9: Flow model bathymetry.	62
Figure 4-10: Wave model bathymetry.	62
Figure 4-11: Initial condition of the Hydrodynamic model (water level).....	64
Figure 4-12: Model bathymetry and station locations.	65
Figure 4-13: West boundary condition of the model.	65
Figure 4-14: East boundary condition of the model.	66
Figure 4-15: South boundary condition of the model.	66
Figure 4-16: Wind rose (speed and direction) at Calcasieu Pass for the period of 15 August, 2008 to 15 September, 2008 used in Hydrodynamics model.	67
Figure 4-17: Location of precipitation data collection stations.	68
Figure 4-18: Extreme precipitation data used in Hydrodynamics model.	68
Figure 4-19: Regular/normal wave height data near study area.	70
Figure 4-20: Model calibration for OS1.	71
Figure 4-21: Model calibration for OS2.	71
Figure 4-22: Model calibration for OS3.	72
Figure 4-23: Model calibration for OS4.	72
Figure 4-24: Model calibration for OS5.	73
Figure 4-25: Model validation for OS1.....	74
Figure 4-26: Model validation for OS2.....	75
Figure 4-27: Model validation for OS3.....	75
Figure 4-28: Model validation for OS4.....	75
Figure 4-29: Model validation for OS5.....	76
Figure 4-30: Sections of the model area to extract flow velocity results.	77
Figure 4-31: Flow velocity at the inlet section where maximum ebb velocities occur.....	78

Figure 4-32: Flow velocity at the inlet section where maximum flood velocities occur.....	79
Figure 4-33: Flow velocity at the middle section where maximum flood velocities occur.....	80
Figure 4-34: Flow velocity at the middle section where maximum flood velocities occur.....	80
Figure 4-35: Flow velocity at the study section where maximum ebb velocities occur.....	81
Figure 4-36: Flow velocity at the study section where maximum flood velocities occur.....	81
Figure 5-1: Hurricane Ike tracking with corresponding wind speed data.....	85
Figure 5-2: Model flow grid.....	86
Figure 5-3: Model wave grid.....	87
Figure 5-4: Flow bathymetry	88
Figure 5-5: Wave bathymetry	88
Figure 5-6: Submerged initial condition.....	89
Figure 5-7: Dry initial condition.....	90
Figure 5-8: West boundary condition of the model.....	91
Figure 5-9: East boundary condition of the model.....	92
Figure 5-10: South boundary condition of the model.....	92
Figure 5-11: Wind rose (speed and direction) at Calcasieu Pass for the period of 12 September, 2008 to 15 September, 2008 used in the Hydrodynamics model.....	93
Figure 5-12: Significant wave height boundary data for the simulation period.....	94
Figure 5-13: Significant wave height boundary data for the simulation period.....	94
Figure 5-14: Validation time-series plot for Calcasieu Pass station.....	96
Figure 5-15: Validation time-series plot for USGS LA-CAM-003.....	96

Figure 5-16: Polygon for Cycle-1 vegetation map input in the model.	97
Figure 5-17: Modeling scenarios for Delft3D wave flow coupling with Hurricane Ike forcing.	98
Figure 5-18: Segment of the overall domain to extract results for Cycle-1 mudflat.	99
Figure 5-19: Wave and current induced bed shear stress on mudflat for submerged (top) and dry (right) initial condition during hurricane landfall.	100
Figure 5-20: Wave and current induced bed shear stress on mudflat for submerged (top) and dry (right) initial condition during hurricane peak.	101
Figure 5-21: Water depth on mudflat for submerged (top) and dry (right) initial condition during hurricane landfall.	102
Figure 5-22: Water depth on mudflat for submerged (top) and dry (right) initial condition during hurricane peak.	103
Figure 5-23: Sections for result extraction.	104
Figure 5-24: Wave current shear stress on LS1.	105
Figure 5-25: Water depth on LS1.	106
Figure 5-26: Wave current shear stress on LS2.	107
Figure 5-27: Water depth on LS2.	108
Figure 5-28: Wave current shear stress on LS3.	109
Figure 5-29: Water depth on LS3.	110
Figure 5-30: Wave current shear stress on CS1.	111
Figure 5-31: Water depth on CS1.	112
Figure 5-32: Wave current shear stress on CS2.	113
Figure 5-33: Water depth on CS2.	114
Figure 5-34: Wave current shear stress on CS3.	115
Figure 5-35: Water depth on CS3.	116
Figure 5-36: Sections for result extraction.	117

Figure 5-37: Wave and current induced bed shear stress on vegetated mudflat for submerged (top) and dry (right) initial condition during hurricane landfall,	118
Figure 5-38: Wave and current induced bed shear stress on vegetated mudflat for submerged (top) and dry (right) initial condition during hurricane peak.....	119
Figure 5-39: Wave and current induced bed shear stress with time at location “A” from submerged (top) and dry (bottom) condition analysis for vegetated and non-vegetated mudflat.	121
Figure 5-40: Water depth with time at location “A” from submerged (top) and dry (bottom) condition analysis for vegetated and non-vegetated mudflat.....	122
Figure 5-41: Wave and current induced bed shear stress with time at location “A” from submerged (top) and dry (bottom) condition analysis for vegetated and non-vegetated mudflat.....	123
Figure 5-42: Water depth with time at location “A” from submerged (top) and dry (bottom) condition analysis for vegetated and non-vegetated mudflat.....	124
Figure 5-43: Velocity profile at location A during peak (submerged condition).	125
Figure 5-44: Velocity profile at location A during peak (dry condition).	125
Figure 5-45: Velocity profile at location B during peak (submerged condition).	126
Figure 5-46: Velocity profile at location B during peak (dry condition).....	126
Figure 6-1: Mudflat section for plain soil (top) and rooted soil (bottom).....	130
Figure 6-2: Marsh edge section for plain soil (top) and rooted soil (bottom).....	131
Figure 6-3: Layer distribution of marsh soil.	132
Figure 6-4: Factors of safety for scenario 1.	135
Figure 6-5: Factors of safety for scenario 2.	136
Figure 6-6: Factors of safety for scenario 3.	136
Figure 6-7: Factors of safety for scenario 4.	136
Figure 6-8: Factors of safety for scenario 5.	137
Figure 6-9: Factors of safety for scenario 6.	137

Figure 6-10: Factors of safety for scenario 9.	137
Figure 6-11: Factors of safety for scenario 10.	138
Figure 6-12: Factors of safety for scenario 11.	138
Figure 6-13: Factors of safety for scenario 12.	138
Figure 6-14: Factors of safety for scenario 13.	139
Figure 6-15: Factors of safety for scenario 14.	139
Figure 6-16: Factors of safety for scenario 15.	139
Figure 6-17: Factors of safety for scenario 16.	140
Figure A-1: Delft3D Flow grid input though GUI.	148
Figure A-2: Delft3D Flow depth input though GUI.	148
Figure A-3: Delft3D Flow roughness input though GUI.	149
Figure A-4: Delft3D Flow process input though GUI.	149
Figure A-5: Delft3D Flow constant input though GUI.	150
Figure A-6: Delft3D Flow numerical parameters input though GUI.	150
Figure A-7: Delft3D Flow observation points input though GUI.	151
Figure A-8: Delft3D Wave grid input though GUI.	151
Figure A-9: Delft3D Wave physical parameters input though GUI.	152
Figure A-10: Delft3D Wave physical parameters input though GUI.	152
Figure A-11: Delft3D Wave numerical parameters input though GUI.	153

ACKNOWLEDGMENTS

I would like to express the deepest appreciation to my committee chair, advisor and mentor Dr. Xingran Wang, who has the attitude and the substance of a genius: he continually and convincingly conveyed a spirit of adventure in regard to research and scholarship, and an excitement in regard to teaching. Without his guidance and persistent help this dissertation would not have been possible. I would also like to thank my committee members, Dr. William B. Patterson, Dr. Don Liu, Dr. Sanjay Tewary and Dr. Nazimuddin M. Wasiuddin.

I am also grateful to Louisiana Tech University for providing me the wonderful opportunity to study here and for all the essential support and services it has provided.

Apart from the efforts of myself, the success of any project depends largely on the encouragement and guidelines of many others. I take this opportunity to express my gratitude to the people who have been instrumental in the successful completion of this project. I must acknowledge the support and encouragement from CPRA (Coastal Protection and Restoration Authority) officials. I am grateful for their constant support and help.

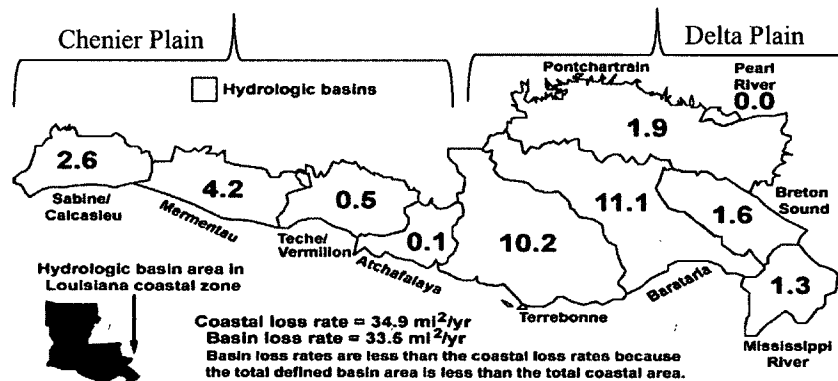
Lastly, I would like to thank my family members, father, Mr. Mohammad Abdus Sabur, mother, Mrs. Afroza Akhter, siblings, Sabrina, Muntasir and Nila and my wife Ikra for their love and affection and endless support throughout my life.

CHAPTER 1

INTRODUCTION

1.1 Background

Coastal Louisiana suffers a high rate of erosion from storm surge flooding generated by hurricanes. The proximity to the Gulf of Mexico and lower elevation of the area made it vulnerable to the coastal process. In the USA, Louisiana alone has 70% of the total wetlands which are equivalent to an area of 3 million acres (Gosseline *et al.* 1998). This zone of interest in Louisiana can be divided into two distinct regions based on the formation and coastal process. One region is named as the Chenier Plain which extends into Texas from Vermilion Bay, Louisiana. The other region is Deltaic Plain, which is located between east of Vermilion Bay to the Pearl River Basin on the Mississippi state line. The Coastal plain region and associated historical loss are shown in **Figure 1-1**.



Figure+ 1-1: The basin boundaries defined by CWPPRA Task Force and wetland loss rate (Barras, 1994).

Formations of both areas are mainly controlled by erosion and sedimentation process from Mississippi River over a long period of time. Influence from the Gulf of Mexico also played a vital role in the formation of Chenier Plain. These coastal processes eventually formed more than four million acres of wetland leading to one of the most dynamic ecosystems on earth. On the contrary, Louisiana also suffers from the highest land loss rate in the USA. Over the last 30 years, Louisiana lost 35-40 sq miles per year and the amount of loss is 90% of coastal marsh loss in the United States (USACE 2004). During the late 1980's, U.S. Army Corps of Engineers (COE) estimated the annual loss to be 40-50 sq miles (Benoit 1997; Johnston *et al.* 1995). Since the 1930s, coastal Louisiana has lost over 1.2 million acres of land. It was estimated in 2000 that coastal Louisiana would experience an additional loss of 431,000 acres by 2050 (USACE 2004). The projected loss over the next 50 years, with current restoration efforts considered, is estimated to be approximately 320,000 acres (Barras *et al.* 2003).

The process for wetland loss can start with the result of the gradual decline of marsh vegetation due to inundation and saltwater intrusion eventually leading to complete loss of marsh vegetation or the result of storm surge events. The most damaging coastal storms are either extratropical cyclones (winter storms) or tropical cyclones (hurricanes) that form around centers of low barometric pressure (Morton, 1988). In the Gulf of Mexico, a major hurricane causes dramatic land losses and substantial property damage (Fig. 4b) about every 10 years (Hayes, 1967; Nummedal *et al.* 1980; Morton *et al.* 1985).

As marsh vegetation is lost, underlying soils are more susceptible to erosion and are typically lost as well, leading to deeper water and precluding marsh regeneration as shown in **Figure 1-2**. Unfortunately, the benefit of vegetation in erosion control is not well

understood and is not as well appreciated within the engineering community. As Gray *et al.* (1982) remarked, the oversight on the importance of vegetation in reinforcing soil is surprising, whereas Gray *et al.* (1996) stated that the loss of vegetation on a slope may lead to a higher rate of erosion or greater rates of slope failure. Significant accretion of sediments is then required for marsh habitat to reestablish. Perhaps the most serious and complex problem in the concerned area lies in the failure of this soil vegetation root combination, which leads to the overall coastal loss.

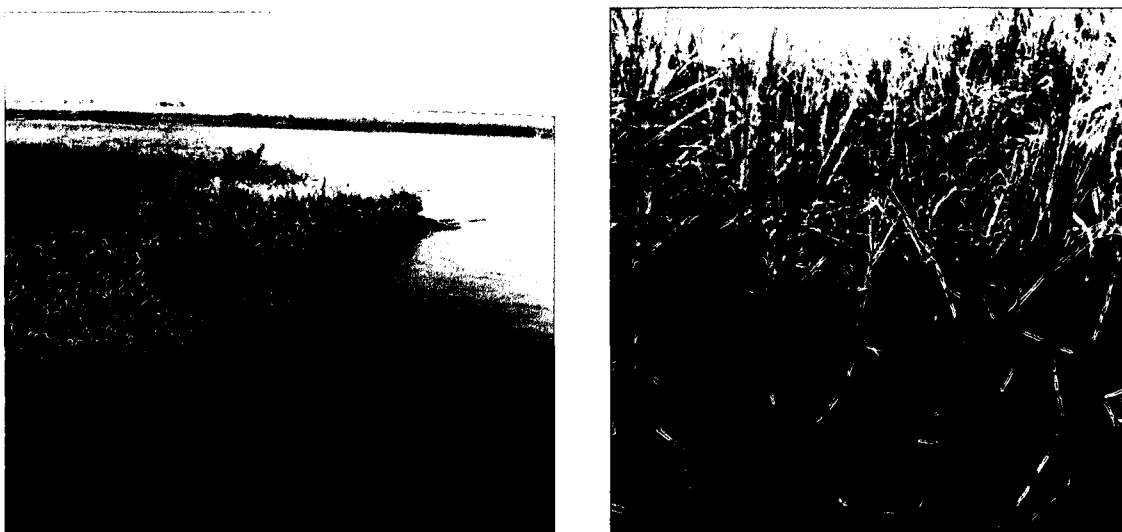


Figure 1-2: Marsh vegetation loss under wave and current action.

Greenway (1987) indicated that roots reinforce the soil by increasing soil shear strength, roots bind soil particles at the ground surface by reducing their susceptibility to erosion, and roots extract moisture from the soil, leading to lower pore-water pressures (Menashe, 2001). Zeimer *et al.* (1977) found that the roots improve soil strength by vertical anchoring along the soil mass to failures in the bedrock and by laterally tying the weak zones of a slope. Gray *et al.* (1982) summarized the mechanical influence of vegetation in terms of root reinforcement, soil moisture modification, buttressing and arching, and surcharge. In certain cases, the weight of vegetation improves the stability by increasing

the confining stress. Plants not only support the soil slope mechanically but also support the surrounding ecology. Native plants enhance wildlife habitat by providing nesting and hiding cover, food, and safe travel corridor. Soil scouring aversion and slope stabilization in some areas in the US have benefited from the felicitous utilization of riparian vegetation. Locally available marshes flourishing on the Louisiana coastline play a very important role in shoreline protection and tidal marsh restoration because of its aggressive spreading habit and tolerance to salinity (Walkup *et al.* 1991).

The effects of recent hurricanes have accelerated marsh loss. **Table 1-1** includes estimates of wetland loss attributed to the major hurricanes of 2004 to 2008 in the Chenier Plain and throughout coastal Louisiana.

Table 1-1: Wetland loss estimates (km²) following hurricanes Katrina and Rita (2005) and Gustav and Ike (2008) by geographic province (Barras *et al.* 2009).

Period	Storms	Chenier Plain	Marginal Delta Plain	Delta Plain	Coastal Louisiana
2004-2006	Katrina+Rita	-292	-2.6	-230	-525
2006-2008	Gustav+Ike	-139	-59	-124	-323
2004-2008	All storm	-432	-62	-354	-848

Among the hurricanes, Katrina was a category-5 storm with winds up to 175 miles an hour but weakened to a Category 3 before making landfall below New Orleans in Plaquemines and Saint Bernard Parishes. Rita came ashore as a Category 3 between Sabine Pass, Texas and Johnson Bayou, Louisiana. Hurricane Gustav made landfall near Cocodrie along the Louisiana coast and Hurricane Ike made US landfall at Galveston, Texas both as category 2. It should be noted that the Rita and Ike made US landfall near Chenier Plain where Katrina and Gustav made landfall near Delta Plain. Moreover, Katrina and Rita attacked Louisiana shores in 2005 August-September at two furthest points where Gustav

and Ike made land fall at a very close distance as shown in **Figure 1-3** in August-September of 2008.

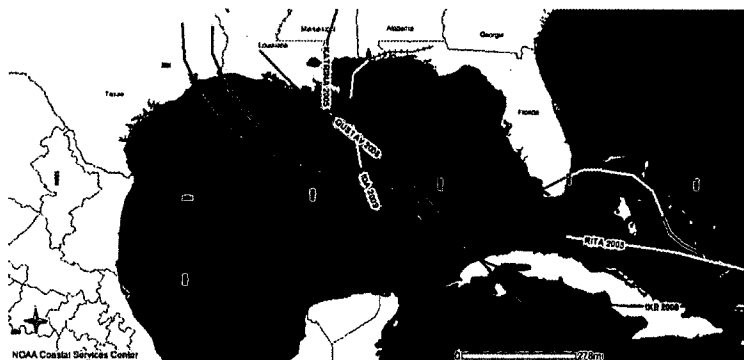


Figure 1-3: Tracks of Hurricanes in Coastal Louisiana (Source: NOAA Coastal Services Center).

The distribution of new water areas after Hurricanes Gustav and Ike shared similar morphologies but varied in magnitude and distribution. Surge impacts of Hurricane Gustav in the Deltaic Plain are smaller in scale and magnitude than surge impacts of Hurricane Ike in the Chenier Plain.

Surge impacts of Hurricane Ike in 2008 were very similar to those of Hurricane Rita in 2005. The 2008 water levels were visibly higher, causing the scours to appear as ponds. In some instances, Hurricane Ike's surge formed significant new ponds and expanded existing ponds formed by Hurricane Rita in almost identical locations within intermediate marshes. After Hurricane Ike, some of these surge-formed features where the marsh was completely removed exceeded 405 ha in size. Furthermore, during Ike's landfall, north to south anastomosing channels were cut through the intermediate marsh located 11.5 km north-northwest of Johnsons Bayou. The 2008 storms impacted a coastal landscape that was still incorporating the impacts from two significant category 3 storms in 2005 (Barras, 2006; Barras, 2007a, b). Normal seasonal variations with short-term fluctuations in water levels affect the interpretation of land area based on satellite imagery

and can cause area changes of 5 percent (Morton, 2005; Bernier, 2007). Combining these normal, short-term land area variations with the effects of multiple episodic impacts over a short 3-year period will cause even greater variations in the classification of land-water configurations (Barras, 2008). Although the net reduction in land from 2004 to 2008 (849.5 km²) exceeds that from 1978 to 2004 (743.3 km²) (Barras, 2008), it is likely that the 2004–08 estimate will decrease, given time for the coast to recover from those hurricane seasons. Nevertheless, it is likely that the cumulative loss from these hurricane seasons will remain significant.

Much of the research relating to wetland loss reflects the threat of submergence due to a failure to keep pace with sea level. However, in their role as a coastal buffer, marshes may experience a range of damage including vegetation death because of wrack deposition during high waters, salt intrusion into freshwater wetlands, enhanced wave erosion at the marsh edge, or the bulk removal of the vegetation mat. The extent of this damage will affect recovery time and the health of the post-storm marsh and its effectiveness as a buffer, and it may lead to permanent wetland loss. Arguably, cannibalization of sediment from one region of the marsh may provide the input necessary to bolster neighboring zones, but the result is still one of net loss.

Within our study site, near Browns Lake, most of the marshes are medium to high saline marshes that can survive during salt water intrusion. Still, major hurricanes always cause significant damage to the marshes in terms of wave and current induced stresses. It is important to quantify the stresses over vegetated marshes and non-vegetated flatland/mud during Hurricane to extensively study the erosion failure of this marsh wetland during a Hurricane.

Where most researches of marsh loss were conducted through satellite image analysis, little attentions were given to combined analysis of flood and erosion resistance ability of coastal marshes. The goal of this thesis is to predict and quantify the contribution of Louisiana coastal marshes in resisting hurricane-induced wave, currents and associated erosion in the coastal area of Louisiana and to understand the marsh erosion under different extreme scenarios.

1.2 Objective

The key objective of this research is to develop a simple and efficient method to study the marsh contribution in resisting erosion as well as investigate marsh erosion under high wave and tide action. The research program focus is directed towards i) Conducting laboratory experiments to measure the physical and strength properties of marsh soil and vegetation roots. Key lab tests involve direct shear test and tensile strength test. Direct shear test on rooted and non-rooted soil samples will measure vegetation root contribution in shear strength enhancement. Tensile strength test on the individual root will provide information on root capacity in resisting tension which is the principle failure mood when soil experience shear. ii) Modeling the hydrodynamics and waves in Louisiana coastal marshes by wave flow coupling to create different extreme hurricane scenarios and study the generated stresses on marsh vegetated and non-vegetated bed. The well-known tool Delft3D will be used during the hydromorphodynamic modeling. iii) Developing a new method to predict the coastal marsh erosion and significance of marsh vegetation in resisting erosion or erosion type and depth in case of failure. A slope stability analysis software Slope/w will be used for this study. Failure of marsh edge and flat/ mild slope

under hurricane-induced wave and current action will provide useful information on erosion failure.

1.3 Site Description

A part of the Calcasieu-Sabine Basin, Louisiana was taken as the area of investigation in order to navigate the role of marshes that protects Louisiana coastal wetland. The Gulf of Mexico is at the south boundary of the site, and at the north boundary, there is Starks North Canal. The site incorporates the majority of the Calcasieu Lake. Cameron Parish is adjacent to the study area as displayed in **Figure 1-4**.

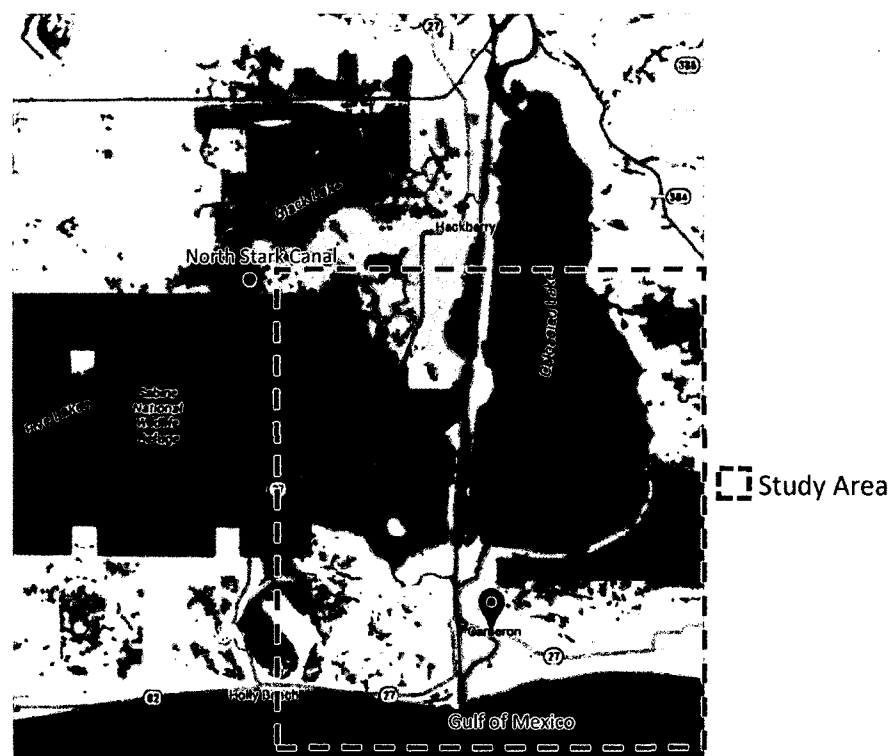


Figure 1- 4: Map depicting the area selected for study in Calcasieu-Sabine basin.

1.3.1 Cameron Parish

Cameron Parish is situated in the southwest corner of Louisiana and is adjacent to the southern boundary of the parish which stretches alongside the Gulf of Mexico. Eighty-

two percent of Cameron Parish is comprised of coastal marshes. Geographically, very few parishes in Louisiana are as large as this one. The parish mostly is pastoral and the principal communities of the vicinity are Cameron and Hackberry. Location of both Cameron and Hackberry are positioned along LA-82 and LA-27, respectively. Creole, Johnsons Bayou, and Holly Beach are other mentionable smaller communities.

1.3.2 Calcasieu-Sabine Basin

Two semi-distinct hydrologic units, the Calcasieu River Basin and the Sabine River Basin, which is unremitting between Louisiana and Texas, holistically form the Calcasieu-Sabine Basin. This particular study comprises only the analysis of the Louisiana region, specifically east of the Calcasieu River to Louisiana Highway 27. This delta is dictated by fresh, intermediary and briny marshes.

1.4 Research Tasks

The research tasks can be summarized by the following:

1. Perform lab tests on collected soil and marsh vegetation sample to find soil and vegetation root's physical and strength parameters.
2. Develop coastal hydrodynamic model capable of representing the dominant processes in a fully three-dimensional manner with well described initial and boundary forcing condition.
3. Validate the wave flow coupling model against available theories and field data.
4. Apply online wave coupling to the total hydrodynamic model in a complex coastal environment with a well-known hurricane (Hurricane Ike 2008) forcing conditions.
5. Quantify the wave and current induced stress developed on marsh flat for different hurricane conditions.

6. Include marsh vegetation in the coupled model to study the effect of vegetation cover on hurricane wave and current generated stress.
7. Finally, conduct detailed numerical studies to predict the erosion of vegetated and non-vegetated marsh flat by using the lab results and wave-current coupled results as input and taking erosion as slope instability issue. The studies will provide insight to quantify erosion of coastal marshes under extreme hurricane conditions.

1.5 Layout of the Thesis

The thesis is organized into seven chapters. This chapter presents the background, objective, site description, methodology, and the layout of the thesis.

Chapter Two provides a literature review that includes theoretical background on the processes and methods that are necessary for explaining the research studies presented in this thesis. First, an explanation will be given on the historical hydrologic modification and important hydrologic units in the study area. Later, a description of coastal marshes in the study area will be provided. After that, the reference project used in this study will be discussed in detail. Lastly, the theory and process involved in the study will be explained.

Chapter Three discusses the laboratory analysis of soil and root samples collected from the reference project area.

Chapter Four provides a description of the Delft3D hydrodynamic model that is used in this thesis. The focus of the chapter has been directed to the calibration and validation of the wave flow coupling model.

Chapter Five presents different extreme condition hurricane wave forcing to calibrate wave flow coupling model. A study involving vegetation is also discussed in this chapter.

Chapter Six proposes an alternative model for predicting erosion of marsh soil under extreme hurricane wave and current condition. Erosion prediction model study was conducted based on the laboratory analysis and coupled flow wave model results. The model takes into account the wave generated stresses on marsh surface during different hurricane periods. In addition, the model also quantifies the significance of full-scale vegetation structure (both root and shoots) in a highly erosive environment.

Finally, conclusions and recommendations and suggestions for future research studies are presented in Chapter Seven.

CHAPTER 2

LITERATURE REVIEW

2.1 Hydrology of the Study Area

Calcasieu/Sabine Basin marshes began to form around 3,500 years ago. Each time the Mississippi River established a westerly course, it allowed a large amount of sediment deposition along the gulf shore, resulting in southerly growth of the shoreline. Again, whenever the course of the Mississippi River shifted to east, the sediment supply decreased. As a result, the shoreline converted to a more typical beach-like nature and gradually retreated. The repetitive occurrence of these pulses of sediment due to change in the Mississippi River's course helped to build the systems of cheniers (oak ridges) in the basin.

The pro-gradation process helped to create an undulating land form along the Gulf Coast. The areas between the cheniers were collecting points for water and, over time, built up by decomposition and regeneration of plant materials to form low-salinity marshes. These interior marsh areas would occasionally receive pulses of mineral sediment input due to storm tides.

The main source of fresh water flowing into this region is the Calcasieu River. It follows the north-south gradient. The hydrology of the region is influenced by the complex occurrences of riverine freshwater inflow including precipitation, Gulf of Mexico tides and wind effects on the level and direction of the water flow. The U.S Fish and Wildlife Service personnel observed that strong persistent south and southeast winds influence the pushing

of large volumes of water from the Gulf of Mexico into Calcasieu Lake causing a rise in water level in the marshes (Paille, 1996).

There has been the maintenance of the lower Calcasieu River and the Calcasieu Ship Channel (CSC) for navigation since 1874. This is when a 5-ft-deep x 80-ft-wide x 7,500-ft-long navigation channel was constructed by the U.S. Army Corps of Engineers (USACE) through the outer bar of Calcasieu between the Gulf of Mexico and the Calcasieu Lake. The CSC depth was increased to 13ft in 1903. The channel was then enlarged between 1937 and 1940 to 250 ft. wide and 30 ft. deep. The final enlargement of the ship channel was in 1968 where it was increased to 400 ft. wide and 40 ft. deep (Waldon, 1996). Before the CSC began being dredged, the mouth of the Calcasieu River had a 3.5 ft. deep shoal (War Department 1897).

The hydrology of the marshes between Sabine and Calcasieu Lakes has also been altered by numerous relatively small access canals. The GIWW and this web of canals have generated a hydrologic connection between the Calcasieu and Sabine Estuaries. Furthermore, a number of bayous which once drained adjacent marshes into either of the estuaries have been connected to one another. Consequently, marshes among Sabine and Calcasieu Lakes have become a large interlinked system with water draining and circulating to the northern, eastern, and western portions of the basin.

The water circulation patterns allow for higher salinity water to enter the interior marshes (saltwater intrusion). The basin soils, which are 87 percent organic and support lower salinity marsh vegetation, are infiltrated by the more saline waters. This leads to increased stress and loss of the plant communities, and eventually erosion and sediment transport out of the inner marsh areas. The changes made are removal of the channel mouth

and subsequent deepening and widening of the CSC enabled the intrusion of more saltwater and tidal into the estuary. This led to the drastic marsh loss, large volumes of organic marsh substrate being exported by the tide and an overall change in the region to a more saline habitat (USDA). The CSC also allows the upriver flow of denser and saltier water as a saltwater wedge. The CSC introduces saltwater to floodplain marshes through the West Cove Canal and Back Ridge Canal (Miller, 1997).

2.2 Reference Project: The Sabine Refuge Marsh Creation (CS-28)

There are coastal restoration and protection projects underway in the study area. The issue being solved dictates the techniques to be used in the projects and other factors specific to the site such as landscape of the project area, habitat type, wave climate, substrate and proximity to freshwater and sediment resources, open water and major waterways. To study the contribution of marsh vegetation in resisting erosion and the restoration project of creating marsh were most relevant to this study.

Dredged material is used for the restoration or nourishment of existing marsh. A deteriorated wetland is then covered with the dredged material at specific elevations which influences the desired marsh plants to grow and form new marsh. Booster pumps are utilized by the dredging technique by projects further from the sources of sediment for the transportation at greater distances.

The Sabine Refuge Marsh Creation (CS-28) is the principal restoration project in the selected study area. Canals built and hurricanes from the 1950s and 1970s led to an extensive land loss in the study area by saltwater intrusion through the Gulf Intracoastal Waterway and the Calcasieu Ship Channel. The project involved the design of five cycles for the creation of marsh, prevention of saltwater intrusion, reduction of wave energy and

nourishment of the existing marsh in the project region. The reference project of this study is the first cycle (Cycle-1) of CS-28 project. **Figure 2-1** shows the project location and boundary.

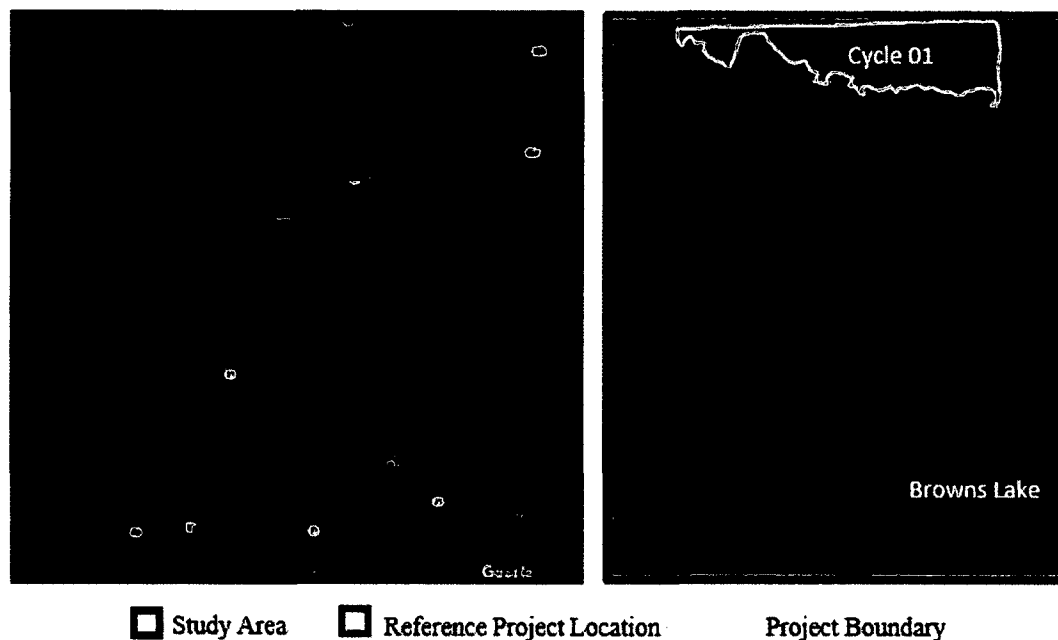


Figure 2- 1: Reference project location (left) and the boundary of the reference project (right).

The Sabine National Wildlife Refuge, west of Los Angeles Highway 27, hosted the Sabine Refuge Marsh Creation Project in the vast, open water regions north of Browns Lake in Cameron Parish, Louisiana. There is the placement of dredged substance from the Calcasieu Ship Channel into 3 of 5 cycles of planned marsh creation in the Brown Lake area in the northeast corner of Sabine National Wildlife Refuge. A brief summary of the CS-28 project is presented in **Table 2-1**.

Table 2-1: Sabine refuge marsh creation project (CS-28) summary (obtained from CWPPRA project fact sheets).

Location	In Cameron Parish in southwest Louisiana lies the Sabine National Wildlife Refuge composed of 3,300 acres. The project area is just west of LA Hwy. 27.	
Cost	Cycle-1	\$3.4 million.
	Cycle-2	\$14.3 million.
	Cycle-3	\$4.77 million.
	Cycle-4 & Cycle-5	\$10.7 million.
Date	Start: August 2001	
Type	Marsh Creation Project	
Sponsors	Federal	U.S. Fish and Wildlife Service, and U.S. Army Corps of Engineers
	Local	Coastal Protection & Restoration Authority (CPRA)
Summary	The project will create marsh in large, exposed water areas of the Sabine National Wildlife Refuge. The completed project will also deliver benefits to minimize wind-induced erosive conditions and saltwater introduction and freshwater loss. Increase nourishment in nearby marshes will reduce exposed fetch length and erosion of marsh.	

2.2.1 Cycle-1 of CS-28 Project

The maintenance of dredging the Calcasieu River was done in January 2001 by the Operations Division of the US Army Corps of Engineers – New Orleans District and an estimated 1,000,000 cubic yards of sediment dredged from the Calcasieu Ship Channel between 8.3 to 10.4 miles in Cycle-1. Dredged sediment was then placed in a confined area within the Sabine National Wildlife Refuge. An estimated 200 acres of the vegetated marsh was created during the first cycle. Pumping of the sediments was up to 4.0 to 4.4 ft. MLG.

Spartina alterniflora was the principle vegetation utilized in the Cycle-1. A total of 36,000 plants were planted along the constructed canals in the Cycle-1 dredge placement region and along the edges of the perimeter. However, when this was accomplished, there was a quick re-vegetation of the interior of the new marsh by itself. Cycle-1 did not use

plantings since it seemed to have vegetated from windborne seed sources and soil seed bank. By February 26, 2002, the construction of the Cycle-1 was complete.

2.3 Coastal Marsh

A marsh is a wetland prevalent of herbaceous plant species other than the woody. The coastal marshes can be classified into two groups which are the high salinity marsh and low salinity marsh. The vegetation mapping depends on the character of salinity regimes: grouping of freshwaters is described by 'low salinity' in addition to the intermediate marsh in relation to oligohaline and limnetic conditions. Saline and brackish marsh are included in 'high salinity' which is equal to meso and polyhaline conditions. An aerial survey was jointly completed in 2013 by the Louisiana Department of Wildlife and Fisheries Coastal, the University of Louisiana at Lafayette and Nongame Resources Division on the types of vegetation in Louisiana coast. There was a listing of the plant species and classification of their abundance. With respect to the abundance and composition, the sampling marsh stations were marked with a marsh type: Saline, brackish, intermediate, or fresh marsh. The study area was noted to have a high presence of salinity marshes in addition to some low salinity marsh as shown in **Figure 2-2**.

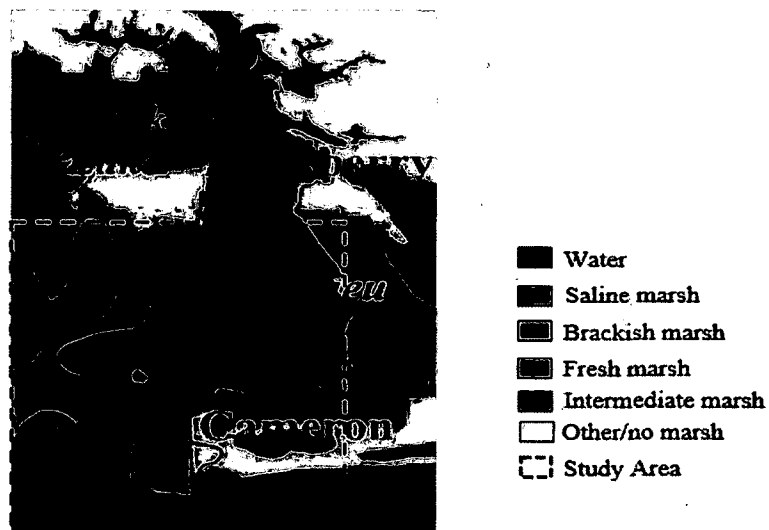


Figure 2- 2: Vegetation types in the study area (extracted from Sasser (2014)).

In the research presented in this dissertation, marsh vegetation has been extensively studied on the basis of field and laboratory study. Selection of marsh vegetation has been made by analyzing field data collected from a vegetation station located in Cycle-1 of the CS-28 project. The station CRMS-6301 as shown in **Figure 2-3** has been used to collect the vegetation information.

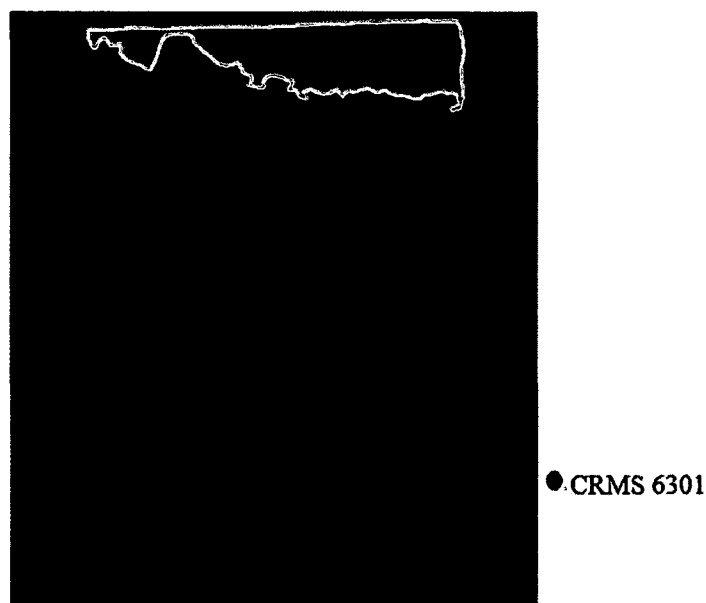
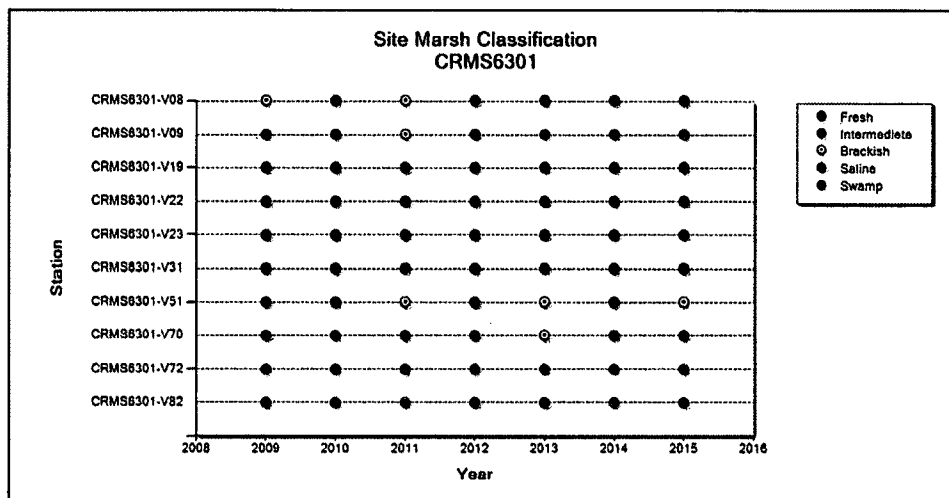
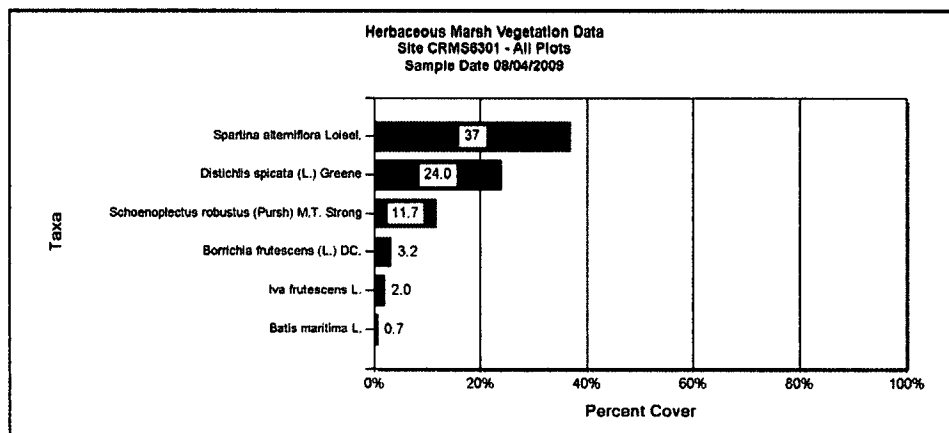


Figure 2- 3: Location of vegetation station.

After analyzing the collected field data, it has been found that the saline marsh is the most common marsh type in Cycle-1 as shown in **Figure 2-4(a)**. It has also been found that one type of salt marsh commonly referred to as smoothed cordgrass (*Spartina alterniflora* Loisel) dominating the study area as in **Figure 2-4(b)** and were selected for the study.



(a)



(b)

Figure 2- 4: (a) Marsh classification. (b) Marsh vegetation data.

2.3.1 Smooth Cordgrass

These are true marsh communities consisting of surface water most times. The smooth cordgrass in Louisiana occurs with salt grass (*Distichlis Spicata*) or pure stands and black rush (*Juncus Roemerianus*) as less prevalent associates.

The smooth cordgrass is large, coarse grass growing in the warm season and physiologically inhabits the salt marsh habitat. Morphology of the *Spartina alterniflora Loisel* can be generally described as two systems namely root system and shoot system as shown in **Figure 2-5**. The shoots can reach up to 2.5 m tall under good conditions while those that grow in high salt marshes, especially at salt pans only grow to 40 cm tall together with inflorescence.

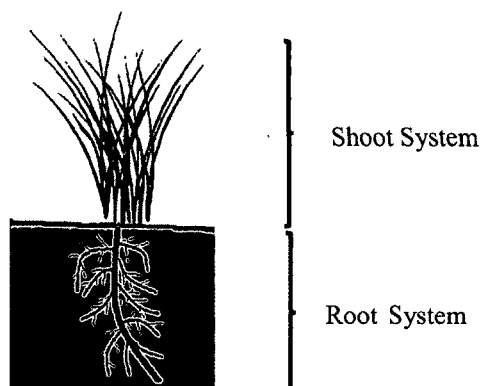


Figure 2- 5: Plant morphology of smooth cordgrass.

A thick stand of this tall grass resembles a tiny forest of dark green plants that do not allow light to reach the mud beneath the plants. The tidal currents are strong in the areas that favor growth while washing away the dead leaves which leave the stand free of debris and clean almost throughout the year. The root system of *Spartina alterniflora Loisel* have been analyzed in the laboratory during this study and the shoot system analysis has been conducted by evaluating data obtained from the available station. Two stations have

been selected for this study and they are CRMS-6301 and CS28-101A as shown in **Figure 2-6**.

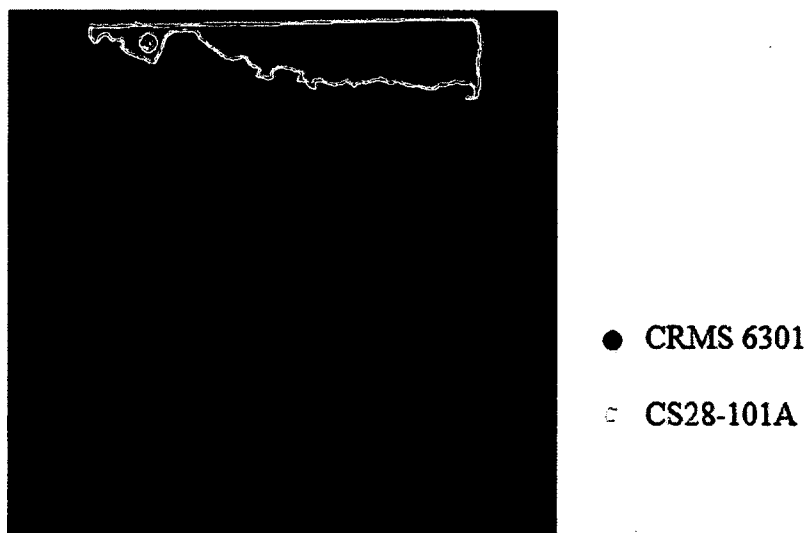


Figure 2-6: Location of observation stations.

Based on the available data, it has been found that the maximum dominant height of *Spartina alterniflora Loisel* shoots is 177 cm and the minimum height is 67 cm in the project location as shown in **Table 2-2**.

Table 2-2: Dominant height of *Spartina alterniflora Loisel* (shoot system) at different vegetation stations in the project area (CS-28 - Cycle-1).

Station ID	Average Height Dominant (cm)
CRMS6301-V08	123.13
CRMS6301-V19	113.99
CRMS6301-V22	79.85
CRMS6301-V23	72.54
CRMS6301-V31	140.20
CRMS6301-V51	67.66
CS28-100A	143.00
CS28-101A	177.00

2.4 Delft3D Modeling

Delft3D is a computer software developed for a multi-disciplinary approach to morphodynamic and nearshore modeling. Hence, it consists of several modules which enable the user to perform simulations of flow (Delft3D-FLOW), ecology (Delft3D-ECO), water quality (Delft3D-WAQ and Delft3D-PART), waves (Delft3D-WAVE) and sediment transport (Delft3D-SED) (Deltares, 2011a). Since the study concentrates on the wave and hydrodynamic model, this section also discusses the literature based on the two processes.

The wave and hydrodynamic modules (Delft3D-WAVE and Delft3D-FLOW) are capable of performing coupled simulations (online interactions) and uncoupled simulations (offline). Online interactions can be viewed as a two-way exchange of data. In this case, the hydrodynamic data from the Delft3DFLOW is used by the Delft3DWAVE module to recalculate the wave conditions. The new wave field is hence a Delft3DFLOW module input (Treffers, 2009). The study will hence concentrate on the interaction between the wave and hydrodynamic modules which are used to estimate wave set-up and compute wave driven long shore currents.

Other than the six modules, there are other programs included in Delft3D that enable the handling of raw data, such as Delft3D-RFGRID, Delft3D-QUICKIN and Delft3D-RGFGRID. They assist in the modification and generation of curvilinear or orthogonal grids. This program hence functions based on a process of grid generation that satisfies the requirements of Delft3D-WAVE and Delft3D-FLOW regarding orthogonality and smoothness (Deltares, 2011d). The main role of Delft3D-QUICKIN is the creation, editing, and visualization of the bathymetric data which represents an input for the Delft3D-WAVE and Delft3D-FLOW modules. For instance, if there is the addition of

bathymetric samples (raw data) to Delft3D-QUICKIN, interpolation tools can be used to generate a Digital Model of 5 of the Terrain inside a grid domain. There is also the capacity to smoothen rapidly varying bathymetry with the help of a depth smoothing option (Deltares, 2011b).

Finally, numerical results can be visualized and animated with the help of Delft3D-QUICKPLOT. A seamless integration with the MATLAB environment is also enabled by this program (Deltares, 2011c)

2.4.1 Delft3D FLOW Module

The Navier-Stokes equations for incompressible flow are solved by the Delft3DFLOW. The continuity equation is used to compute vertical velocities in 3D models. A structured grid is used to solve a set of initial and boundary conditions together with a set of partial differential equations (Deltares, 2011).

With regards to the horizontal directions, an orthogonal curvilinear coordinate system is supported by Delft3D. There are two options available: Spherical coordinates (λ, ϕ) and Cartesian coordinates (ξ, η) . The top lid of the domain is viewed as flat in Cartesian coordinates. Here, Φ is the latitude and λ is the longitude in spherical coordinates. This coordinate involves the top of the lid adopting the Earth's curvature. Spherical coordinates are significant with regards to the orthogonal curvilinear grid.

Where

$$\xi = \lambda; \eta = \phi$$

$$\sqrt{G_{\xi\xi}} = R \cos\phi; \sqrt{G_{\eta\eta}} = R$$

$R = 6378.137$ km radius of the Earth, $\sqrt{G_{\eta\eta}}$ and $\sqrt{G_{\xi\xi}}$ are coefficients utilized in the transformation of curvilinear coordinates into a rectangular grid.

The vertical direction involves definition of the system with regards to the boundary fitting coordinate referred to as the sigma (σ) coordinate system represented by the equation:

$$\sigma = \frac{z - \zeta}{d + \zeta} = \frac{z - \zeta}{H}. \quad \text{Equation (2-1)}$$

where z represents the vertical coordinate in physical space; ζ represents the free surface elevation above the plane of reference (at $z = 0$); the depth below the reference plane is d , while the total depth of the water is H represented as $H = d + \zeta$ (Deltares, 2011).

Layers bound by the two sigma planes are presented by the vertical σ system and which follow the free surface and bottom topography. The vertical coordinate is scaled by a sigma coordinate system in relation to the local water column depth which results in a constant number of layers over the whole model domain (Robson, 1999; Van Ballegooyen *et al.* 2001). There is the capacity to distribute the relative layer thickness non-uniformly so that vertical resolution may increase in the region of interest. This system consists of free surface at $\sigma = 0$ and bottom corresponds $\sigma = -1$ as seen in **Figure 2-7** (Deltares, 2011).

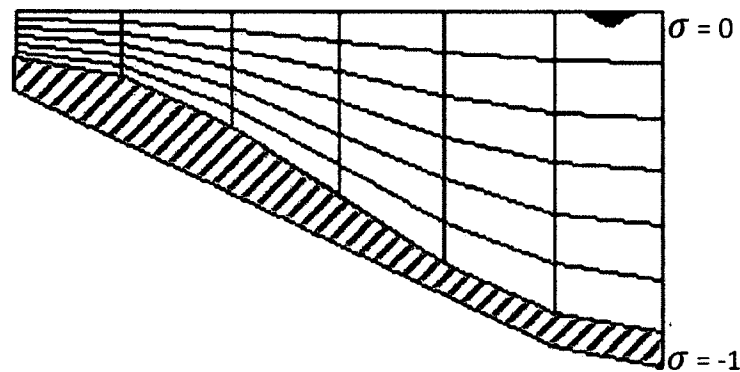


Figure 2- 7: Sigma model example (Deltares 2011).

The continuity equation is given by:

$$\begin{aligned} \frac{\partial \zeta}{\partial t} + \frac{1}{\sqrt{G_{\xi\xi}}\sqrt{G_{\eta\eta}}} \frac{\partial [(d + \zeta)U\sqrt{G_{\eta\eta}}]}{\partial \xi} \\ + \frac{1}{\sqrt{G_{\xi\xi}}\sqrt{G_{\eta\eta}}} \frac{\partial [(d + \zeta)V\sqrt{G_{\eta\eta}}]}{\partial \eta} = Q. \end{aligned} \quad \text{Equation (2-2)}$$

where U represents the depth-averaged velocity in ξ -direction, the depth velocity in η -direction is V and the coefficients used for the transformation of curvilinear to rectangular coordinates are $\sqrt{G_{\xi\xi}}\sqrt{G_{\eta\eta}}$. Q represents the contribution per unit area with regards to the withdrawal or discharge of water, evaporation and precipitation:

$$Q = H \int_{-1}^0 (q_{in} - q_{out}) d\sigma + P - E. \quad \text{Equation (2-3)}$$

Conservation of momentum in x-direction:

$$\begin{aligned} \frac{\partial u}{\partial t} + \frac{u}{\sqrt{G_{\xi\xi}}} \frac{\partial u}{\partial \xi} + \frac{v}{\sqrt{G_{\eta\eta}}} \frac{\partial u}{\partial \eta} + \frac{w}{d + \zeta} \frac{\partial u}{\partial \sigma} - \frac{v^2}{\sqrt{G_{\xi\xi}}\sqrt{G_{\eta\eta}}} \frac{\partial \sqrt{G_{\eta\eta}}}{\partial \xi} \\ + \frac{uv}{\sqrt{G_{\xi\xi}}\sqrt{G_{\eta\eta}}} \frac{\partial \sqrt{G_{\xi\xi}}}{\partial \eta} - f_v \\ = -\frac{1}{\rho\sigma\sqrt{G_{\xi\xi}}} P_\xi + F_\xi + \frac{1}{(d + \zeta)^2} \frac{\partial}{\partial \sigma} \left(v_v \frac{\partial u}{\partial \sigma} \right) \\ + M_\xi. \end{aligned} \quad \text{Equation (2-4)}$$

Conservation of momentum in y-direction:

$$\begin{aligned} \frac{\partial v}{\partial t} + \frac{u}{\sqrt{G_{\xi\xi}}} \frac{\partial v}{\partial \xi} + \frac{v}{\sqrt{G_{\eta\eta}}} \frac{\partial v}{\partial \eta} + \frac{w}{d + \zeta} \frac{\partial v}{\partial \sigma} - \frac{u^2}{\sqrt{G_{\xi\xi}}\sqrt{G_{\eta\eta}}} \frac{\partial \sqrt{G_{\eta\eta}}}{\partial \eta} \\ + \frac{uv}{\sqrt{G_{\xi\xi}}\sqrt{G_{\eta\eta}}} \frac{\partial \sqrt{G_{\xi\xi}}}{\partial \xi} + f_u \\ = -\frac{1}{\rho\sigma\sqrt{G_{\eta\eta}}} P_\eta + F_\eta + \frac{1}{(d + \zeta)^2} \frac{\partial}{\partial \sigma} \left(v_v \frac{\partial v}{\partial \sigma} \right) + M_\eta. \end{aligned} \quad \text{Equation (2-5)}$$

where w , v and u are the flow velocities in σ –direction, η - direction and ξ -direction respectively. Here, v_V represents the three-dimensional turbulence that is the vertical eddy viscosity as:

$$v_V = v_{mol} + \max(v_{3D}, v_V^{back}). \quad \text{Equation (2-6)}$$

v_V^{back} is the background vertical mixing coefficient; v_{mol} is the kinematic viscosity of water, and v_{3D} is computed by a 3D turbulent closure model.

Density variations are neglected, except for the pressure gradients, and P_ξ and P_η and the horizontal Reynold's stresses are represented by the forces F_ξ and F_η .

2.4.2 The Delft3D-WAVE Module

This module focuses on the third-generation wave model SWAN (Simulating Waves Nearshore) developed by Delft University of Technology. The wave action balance equation represents the model's prognostic equation (Booij *et al.* 1999; Holthuijsen 2007). The action density spectrum N is the most considered spectrum in SWAN (σ, θ) instead of the energy density spectrum $E(\sigma, \theta)$ since action density is conserved in the presence of currents while energy density is not (Whitham, 1974).

The relative frequency σ represents the independent variables (as seen in a frame reference moving along with the current velocity) and the direction of wave θ (the usual direction to the wave crest of each spectral component).

When the energy density is divided by the relative frequency, it gives the action density: $N(\sigma, \theta = \frac{E(\sigma, \theta)}{\sigma}$ the spectrum has the capacity to vary in space and time in SWAN).

The wave spectrum evolution in SWAN is defined by the equation of spectral action balance (Hasselmann *et al.* 1973):

$$\frac{\partial}{\partial t} N + \frac{\partial}{\partial x} c_x N + \frac{\partial}{\partial y} c_y N + \frac{\partial}{\partial \sigma} c_\sigma N + \frac{\partial}{\partial \theta} c_\theta N = \frac{S}{\sigma} \quad \text{Equation (2-7)}$$

The local rate of action density shift in time is the initial term on the left-hand side of the equation. The propagation of action in geographical space is represented by the second and third terms (with propagation velocities c_y and c_x in y - and x -space, respectively). The change of relative frequency due to variations in currents and depth is represented by the fourth term (the propagation velocity is c_σ in σ space). The depth and current induced refraction are represented by the fifth term (The propagation velocity is c_θ in σ space). The linear wave theory is where the expressions for these propagation speeds are derived (Whitham, 1974; Mei, 1983; Dingemans, 1997). The term S ($S(\sigma, \theta)$) at the right-hand side of the action balance equation represents the source term with regards to energy density based on the effects of the non-linear wave, dissipation and generation wave interactions.

2.4.3 Vegetation Model

Shear stresses are exerted by the vegetation on the passing flow. Rough coefficient of type Ch'zy characterizes the magnitude of the bed's shear stresses. The local conditions of the alluvial bed (bed form characteristics and bed composition) usually determine the shear stresses within the main stream flow. In the intertidal regions of estuaries and the floodplains of rivers, a combination of alluvial bed forms or non-alluvial bed and vegetation determines the flow resistance. A couple of features have been added to Delft3D-FLOW for an accurate representation of certain conditions in the numerical models. These features include vegetation models and bed form roughness predictors. A

2D numerical model can be utilized in resolving these forms of flow resistance with the help of trachytopo approach. In the 3D model, it will use a comprehensive representation of vegetation over the depth of water and a combination of bed resistance formulations.

2.4.3.1 Directional Point Model (DPM) for vegetation

The vertical variations in characteristics of vegetation can be represented in a detailed numerical model to assist in the study of the impact of vegetation on turbulence and 3D flow.

The theory of integrating the impacts of vegetation upon turbulence and momentum equations was implemented by Uittenbogaard (2000) on the 'directional point model' (Wintewerp *et al.* 1997) that has been widely tested and related to experiment (HKV).

The number of stems per unit area based on height $n(z)$ represents the basic input parameters together with the stem width based on the height $\phi(z)$. The effect of vegetation on the momentum equation is represented by the vertical distribution of the friction as influenced by the cylindrical elements in oblique flow:

$$F(z) = \frac{1}{2} \rho_0 C_D \phi(z) n(z) |u(z)| u(z). \quad \text{Equation (2-8)}$$

with $u(z)$ the horizontal flow velocity profile and C_D the cylindrical resistance coefficient (default value 1.0).

The horizontal cross-sectional plant area is given by:

$$A_p(z) = \frac{\pi}{4} \phi^2(z) n(z). \quad \text{Equation (2-9)}$$

2.4.4 Bed Shear Stress

Currents and Waves are two substantial hydrodynamic factors which prevail in the coastal region. The model concentrates on the current generation by waves such as

longshore currents and undertow. Shear instabilities related to mean sheared currents develop with the use of depth-averaged shallow water equations that are time dependent.

The waves in the model promote the current's bed shear stress. The interaction of a non-linear wave current within the bottom boundary layer describes bed shear where turbulent shear stress is proportional to a square of the velocity $\tau \propto u^2$ (Soulsby *et al.* 1993). The bed shear stresses of the waves and currents are calculated separately and then combined. In 3D approach bed shear stress is related to the current just above the bed. The formulation of current shear stress is:

$$\tau_{b_{3D}} = \frac{g\rho_0 u_b |u_b|}{C_{3D}^2} \quad \text{Equation (2-10)}$$

where $|u_b|$ is the magnitude of the horizontal velocity in the first layer just above the bed.

The formulation for bed stress magnitude with regards to the wave is:

$$\tau_w = \frac{1}{2} \rho f_w U_{orb}^2 \quad \text{Equation (2-11)}$$

where U_{orb}^2 represents the amplitude of the near bottom wave orbital velocity and the wave friction factor is f_w .

2.5 Wave Induced Normal Stress

There can be cyclic variations of pressure on the seafloor due to storm generated surface waves. Henkel presented an early publication that showed the importance of storm-induced bottom pressures on the slope stability of submarine with the use of an equilibrium approach which assumes a circular failure surface (Henkel 1970). In this case, movements could be highly influenced by the bottom pressure pulses caused by ocean waves. Ocean waves have the capacity to generate pressure changes within the water below the surface and on the sediment's surface. Pressure increases with the passing of a wave above the mean hydrostatic bottom pressure usually present below the crest, while pressure decreases

beneath the trough. The depth of water d , the wave height H , the wave period T and the wave length L , determine the magnitude of the excess pressure which is in line with the wave (Wiegel, 1964) and represented as:

$$\delta p = \frac{H \cosh k(z + d)}{Z \cosh kd} \cos(kx - \sigma t). \quad \text{Equation (2-12)}$$

where

$$k = \frac{2\pi}{L}$$

and

$$\sigma = \frac{2\pi}{T}$$

There is distribution of excess pressure at the mud line ($Z = -d$) as indicated in **Figure 2-8** and computed as:

$$\delta p = K_p \eta. \quad \text{Equation (2-13)}$$

where $K_p = \frac{1}{\cosh kd}$ is the pressure response factor on the top of the sediment, and

$\eta = \frac{H}{2} \cos(kx - \sigma t)$ is the fluctuation of the water level due to the wave.

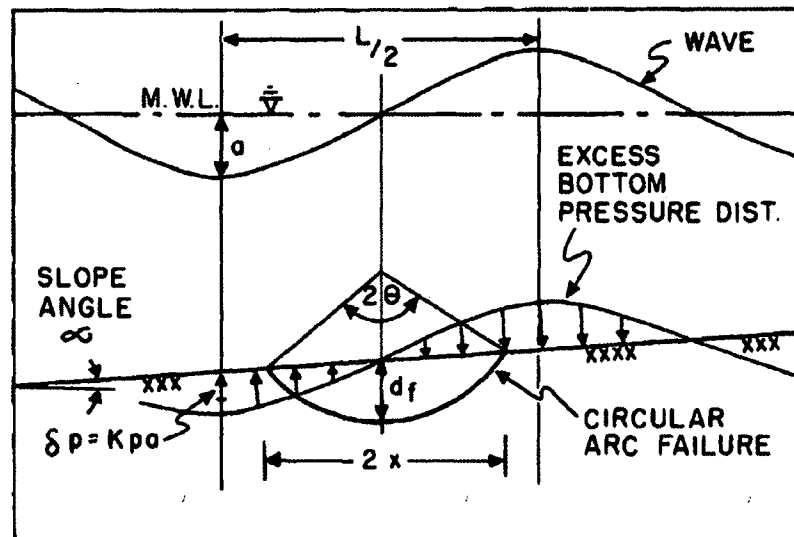


Figure 2- 8: Rotational sliding proposed by Hankel (1970).

It may be noted that if the depth of water is more than half of the wavelength L the excess pressure is negligible.

2.6 Composite Shear Strength of Rooted Soil

Plant roots tend to bind the soil together in a monolithic mass and contribute to the strength by providing an apparent additional cohesion (Abernethy *et al.* 2001). If the soil is rooted, the increased soil shear strength can be expressed as an additional cohesion:

$$S_r = s + C_r. \quad \text{Equation (2-14)}$$

where s is soil shear strength (kPa), s_r (kPa) is the shear strength of the soil reinforced by the roots and C_r (kPa) is the increase in shear strength due to the presence of the roots.

A modified shear strength equation for rooted soils has been developed by K.M. Schmidt *et al.* (2001) following the work done by Endo *et al.* (1969); O'Loughlin (1974); Waldron (1977):

$$S_r = C_s' + C_r + (\sigma - u)\tan\phi'. \quad \text{Equation (2-15)}$$

where C_s' is the effective cohesion of soil without roots, C_r is the cohesion of root-induced soil, σ is the normal stress induced by the weight of the moist sliding mass, u is the soil pore-water pressure, and ϕ' is the effective internal friction angle of the soil which is unaltered by the presence of roots.

Wu (1977) and Wu *et al.* (1979) pioneered a model that was applied in numerous studies for the assessment of how roots contribute to soil shear reinforcement. The model, based on the force equilibrium principle, has been applied to both vertical roots and inclined roots as shown in **Figure 2-9** and allows evaluating the shear strength increment that can be provided by the roots. The deformation of the soil and the associated stresses and forces were described by Wu *et al.* (1979).

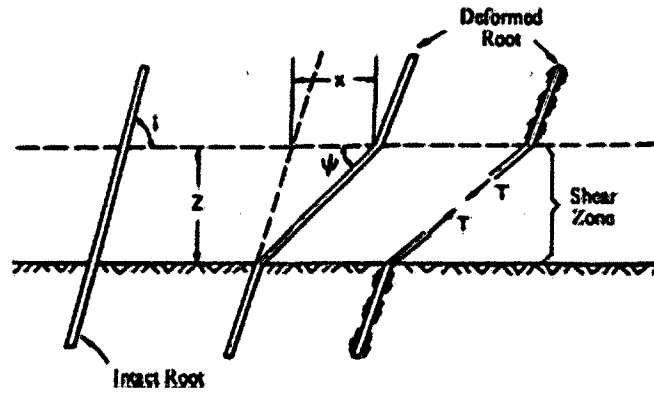


Figure 2- 9: Root reinforcement model scheme.

Using the scheme in **Figure 2-9**, the force equilibrium models developed by Waldron (1982) and Wu *et al.* (1979) allow computing the additional shear strength, Δc , for vertical roots with the following equation:

$$\Delta c = t_R(\sin\theta + \cos\theta \tan\phi). \quad \text{Equation (2-16)}$$

where t_R is the mobilized tensile force in roots per unit area of soil, $\theta (= \tan^{-1} x/z)$ is the angle of the root relative to vertical after shear distortion, z is the thickness of the shear zone and x is the shear displacement. The mobilized force in roots is dependent on elongation and fixity of roots in soils. The mobilized tensile force in roots per unit area of soil, t_R , can be computed by the following equation:

$$t_R = T_r \frac{A_R}{A}. \quad \text{Equation (2-17)}$$

where T_r is the tensile stress developed in roots, A is the area of the soil shear surface, A_R is the total cross-sectional area of all roots crossing the shear surface, and A_R/A is defined as the RAR. Based on experimental results, Wu *et al.* (1979) observed that the value of the term $(\sin\theta + \cos\theta \tan\phi)$ in **Equation (2-16)** is relatively insensitive to the normal variations relatively insensitive to the normal variations and proposed an

average value of 1.2 for this term, avoiding to assess the value of the angle θ by following equation:

$$\Delta c \cong 1.2t_R. \quad \text{Equation (2-18)}$$

Gray *et al.* (1982) analyzed the additional shear strength provided by root reinforcement for a root inclined from the vertical. In this case, the additional shear strength provided by roots can be estimated by the following equation:

$$\Delta c = t_R[\sin(90 - \psi) + \cos(90 - \psi) \tan \phi]. \quad \text{Equation (2-19)}$$

where ψ is the angle of shear distortion and is expressed as $\tan^{-1} [1/(m+(\tan i) - 1)]$, i is the initial angle of inclination with respect to the shear surface, and m is the shear distortion ratio ($m=x/z$).

2.7 Stability Analysis to Predict Erosion

2.7.1 Analysis of the Roots-Reinforced Slope

The analyses of conventional slope stability involve bounding the equilibrium of a soil mass using an assumed potential slope surface below and the slope surface above. Moments and forces that influence instability of the masses are related to the ones that resist instability. There is the adoption of a 2D cross-section under the plane strain condition in most cases for analysis. Strength and stress conditions are briefly depicted in **Figure 2-10** for a potential slip surface where **Figure 2-10** (left) indicates a potential slide mass described using a candidate slip surface. **Figure 2-10** (right) shows a comprehensive strength-stress condition in a rooted soil slice that was utilized in the Ordinary Method of Slices.

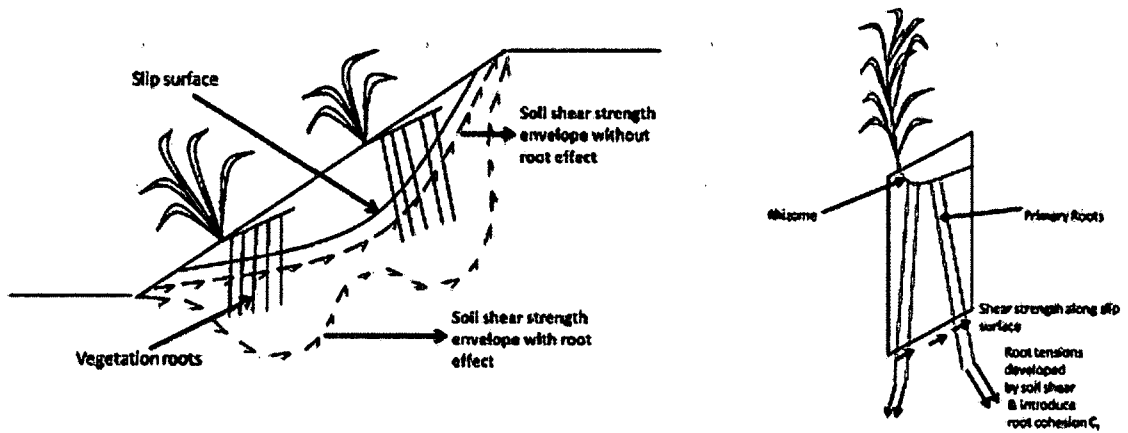


Figure 2- 10: Stress and strength illustration along with a potential slip surface: Shear strength along the slip surface in the presence and absence of root reinforcement (Left) and Typical slice and bottom forces for the method of the slice (Right).

The stability of a slope is characterized by conventional analysis with calculation of a safety factor. Definition of a factor of safety (F.S.) is based on the soil's shear strength as the ratio of the present shear strength to guaranteed shear stress for equilibrium; therefore:

$$F.S. = \frac{\text{Available shear strength}}{\text{Equilibrium shear stress}} = \frac{s}{\tau} \quad \text{Equation (2-20)}$$

When shear strength is defined based on the effective stress, the factor of safety is then expressed as:

$$F.S. = \frac{c' + (\sigma - u) \tan \phi'}{\tau} \quad \text{Equation (2-21)}$$

where c' and ϕ' are the effective stress-based cohesion and friction angle, respectively.

2.7.2 Slope/W and Root Reinforcement Analysis

The commercially available software displays root as an independent model during the analysis of soil slope reinforcement. That the soil block is divided into a certain number of slices is conjectured by the software. The base of each slice has reached the shear strength through the critical equilibrium condition. The contribution of the tensile strength

component (if any) and the summation of the shear strength of the soil collectively forms this shear strength from the roots as displayed in Equation (2-16), where S_m depicts the mobilized shear strength of the soil. Owing to the presence of the roots, energized driving forces like surcharge, seepage action, lateral movement due to the earthquake, and water effect are minimized on the soil slope. Furthermore, the shearing resistance is increased by the root reinforcement which inevitably increases the factor of safety:

$$F.S. = \frac{S_{soil} + S_{root}}{S_m} \quad \text{Equation (2-22)}$$

The same overall global factor of safety divides the reinforcement that lead to the rise of the soil strength and shear resistance. It shows evidence that the rate of development and mobilization of soil reinforcement and shear resistances are the same. Slope/W utilizes an assumption made for this approach. It may likely but not entirely be a correct assumption. This research uses Slope/W to analyze the rooted soil slope, where vegetation roots are taken as reinforcements following the rule formulated in Equation (2-22).

CHAPTER 3

FIELD AND LABORATORY ANALYSIS OF MARSH VEGETATED SOIL

3.1 Introduction

It is presumed that, due to poor strength properties of fine-grained sediments in the beaches, marshes, and other wetlands, there are high rates of erosion in coastal Louisiana. It is also assumed that the increase of shear strength of the soil, as well as the reduction of erosion, can be done effectively by vegetation roots. Determining the changes in soil shear strength, owing to the existence of plant root systems, is the objective of this study. How root-enhanced shear strength behaves at different depths of a soil profile is an issue of study as well. Using field and laboratory experiments as well as theoretical models, the root reinforcement effect of *Spartina alterniflora* was examined to evaluate the potential of plant species growing in Louisiana coastal marshes. For the evaluation of the *Spartina alterniflora* roots contribution in strength enhancement of marsh soil direct shear tests of plain soil and various rooted soil, a layer sample was carried out in the laboratory. By using the simple perpendicular model of Wu *et al.* (1979) and inclined model of Gray *et al.* (1982), the root contribution was evaluated independently. Since information found on *Spartina alterniflora* plant root characteristics is not ample, there was a need to study the root distribution intensively, and root tensile strength tests were to be conducted in the laboratory. Root diameter to tensile strength relation was studied as well.

In this chapter, a new equation has been proposed for the increase in soil shear strength (C_r) due to the presence of plant roots in dredge sediment, using the total mobilized tensile strength of root fibers per unit area of soil (t_R) and based on direct shear tests.

3.2 Field Study

A field investigation was conducted on several locations of Cycle-1 in order to study the marsh contribution in enhancing soil strength. Cone penetration test through digital penetrometer as shown in **Figure 3-1** was done on the vegetated marsh of Cycle-1.

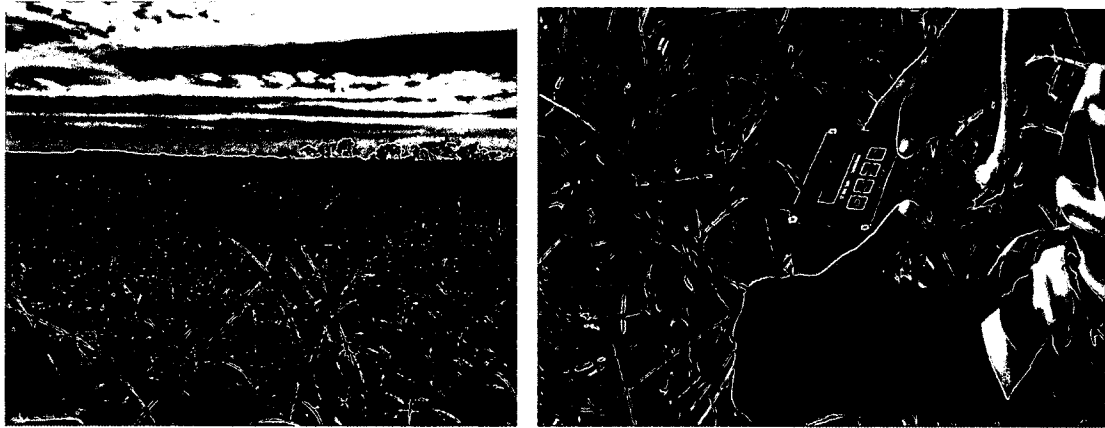


Figure 3-1: Vegetated Marsh (left) Penetration test (right).

The cone penetration tests provided a soil resistance distribution of vegetated soils through a depth of the top 800 mm. Significant enhancement noticed by roots of *Spartina alterniflora* for the top depth of 300 mm as shown in **Figure 3-2**. It turns out that the rooted soils behave like lightly consolidated weak clay. However, soil resistance dramatically increased beyond the depth of 800 mm, which might be the result of long-term self-consolidation of the original soils.

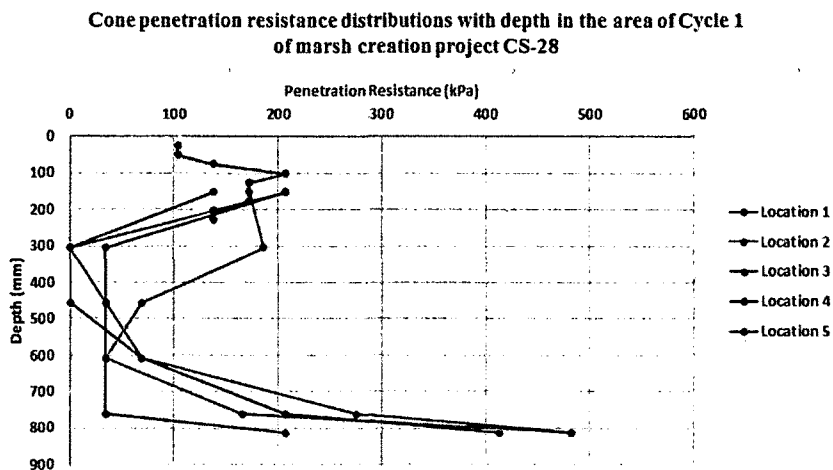


Figure 3-2: Cone penetration resistance distribution with depth in the area of Cycle-1.

3.3 Laboratory Study

To study the marsh soil and *Spartina* plant, 0.023 m³ of rooted soil sample were collected from a created marsh in Sabine National Wildlife Refuge, West of LA Highway 27 north and northwest of Brown's Lake in Cameron Parish, Louisiana as shown in **Figure 3-3**. The exact location of the site is near North Stark Canal, Louisiana with a Latitude of 29.959580 degrees and Longitude of -93.414259 degree.

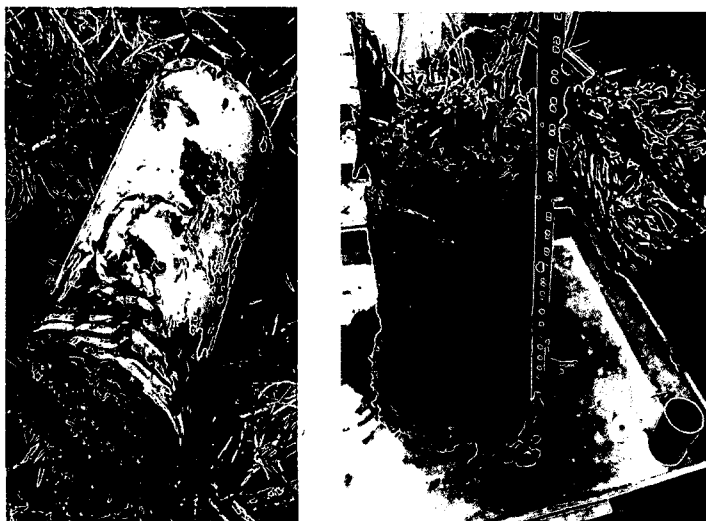


Figure 3-3: Collected marsh soil with vegetation from Cycle-1.

Moisture content, liquid limit, and plastic limit obtained from laboratory tests were 65%, 56% and 28%, respectively. The bulk density of the soil was 11 kN/m³.

3.3.1 Direct Shear Test

Consolidated drained direct shear test was performed on rooted and non-rooted soil samples. The strength parameters of soil, i.e., cohesion and friction angle, was obtained to study the effect of roots on the shear strength and the enhancement of slope stability. In order to perform a thorough direct shear evaluation, a minimum of three tests must be carried out (Bhudu, 2007). ASTM standard D3080 was consulted, where the inclusion of root matter in the test specimens deviated from the procedure. A total of three vertical loadings were selected based on the increase in effective stress due to the addition of fill media. The tests were run at vertical loadings of 0.7, 2.3, 3.2 and 5.47 kPa.

3.3.1.1 Direct shear test on rooted soil

Collected rooted soil core was divided into five different layers each with a depth of 3 inches. Top three layers were studied to evaluate the roots contribution at a different depth. Four different samples from each layer were tested to measure the soil strength parameters such as cohesion and friction angle. A cutter was used to get the sample directly from the layer and put into the shear box as shown in **Figure 3-4**.

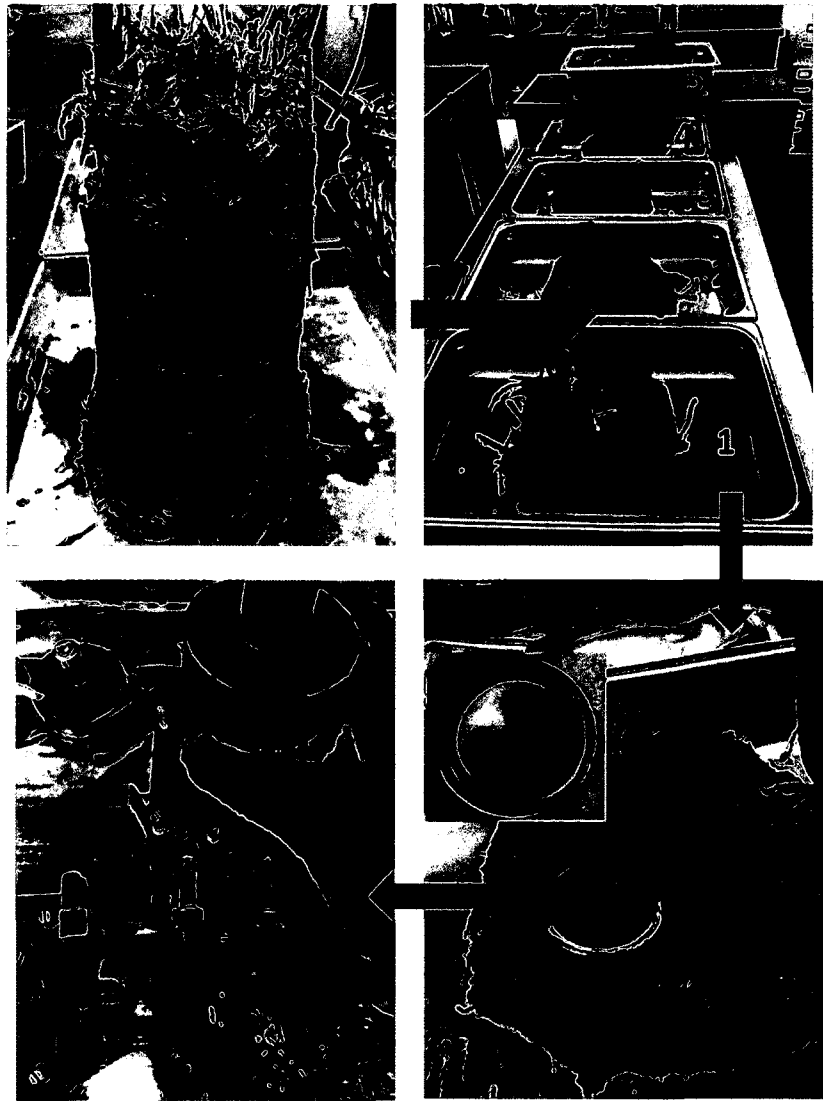


Figure 3-4: Sample preparation for the direct shear test.

3.3.1.2 Direct shear test on plain soil

Four different plain soil samples were prepared and tested to measure the soil strength parameters. Same normal stresses of 4.5, 15, 22 and 37 kPa that were used during the rooted soil analysis were assigned through lever arm loading.

3.3.2 Root Distribution Analysis

Root distribution was done by carefully washing the soil from the root zones as shown in **Figure 3-5(a)**. The combined and single plant was studied carefully to generate a more realistic root distribution model of the plant. During the washing process, it was

discovered that *Spartina* creates a strong root network with neighbor plants and it can be assumed that the combined root network system is the primary source of overall strength enhancement. Here, **Figure 3-5(b)** shows the root system of two plants where **Figure 3-5(c)** is for an individual plant. After carefully separating all the soil from the root system, **Figure 3-5(d)** shows the near surface roots distribution.

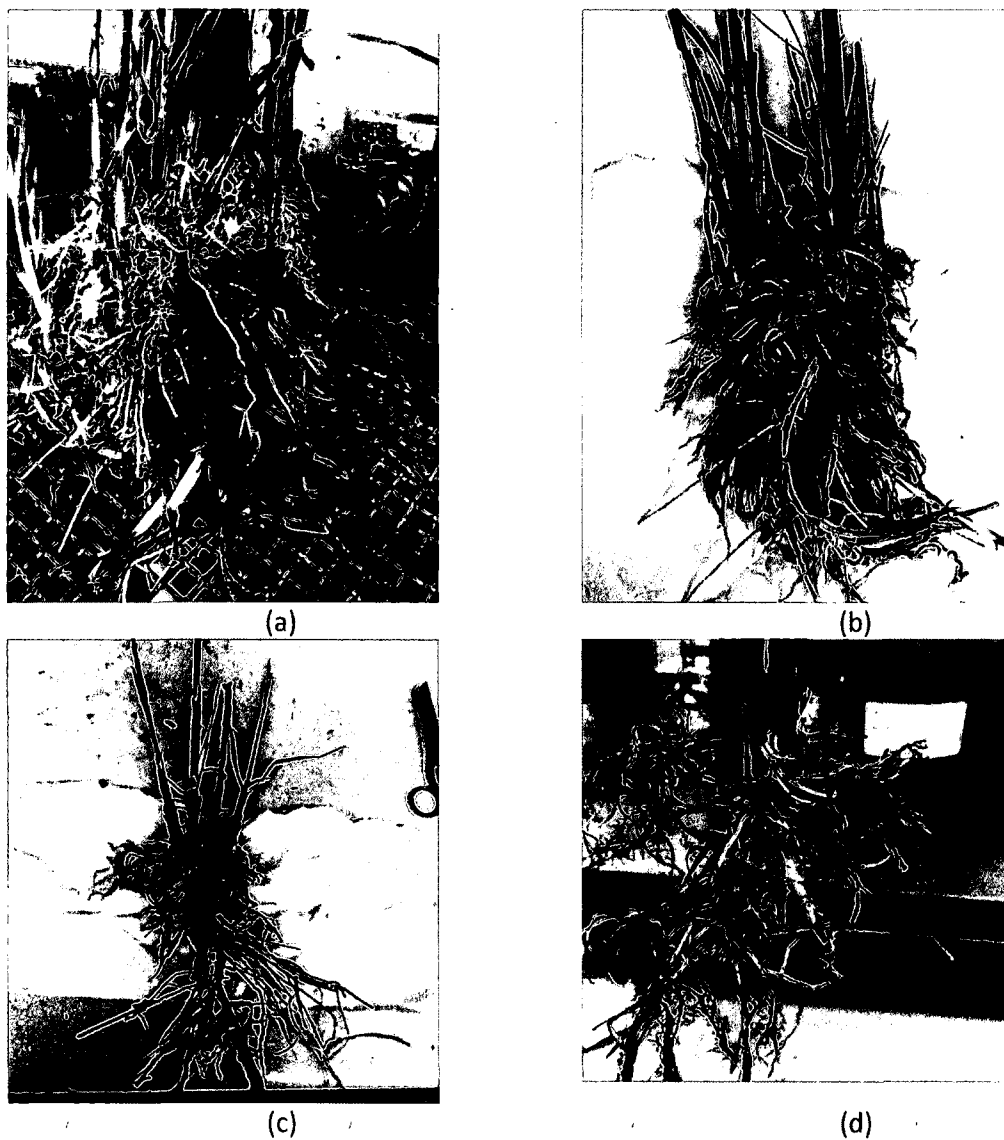


Figure 3-5: (a) Roots during the washing stage (b) Roots distribution of two plants (c) Root distribution of one single plant (d) Near surface root distribution.

Later by visible inspection the roots were divided into three parts named R1, R2 and R3 as shown in **Figure 3-6**. Where R1 and R2 can be considered as the source of strength and R3 serves as the nutrient collection pipe also provide some reinforcement to the soil. Physical parameters of the roots were provided in **Table 3-1**. The only visible characteristics that separate R1 from R2 are some finer roots growing from R1.

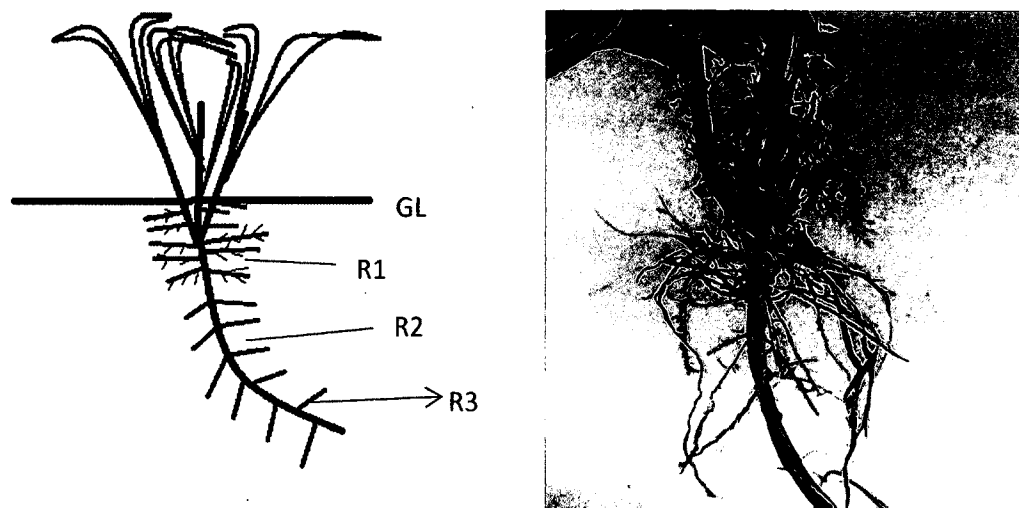


Figure 3-6: Root distribution of *Spartina alterniflora*.

Table 3-1 gives an estimate of the length and diameter of different kinds of roots.

Table 3-1: Root Physical Properties.

Root Type	Length (cm)	Diameter (cm)
R1	3.810-8.900	0.140
R2	11.430-16.500	0.114
R3	15.240-30.480	0.610

3.3.3 Tensile Strength Test on Roots

Three roots of the individual class were tested separately in a Universal Tensile Strength Test machine as shown in **Figure 3-7** equipped with a very low capacity load cell (667 N) and pneumatic controlled grips to ensure no slippage during the test. The grips

were holding onto the specimens at 25 mm apart and the tensile tests were performed using a universal tensile testing machine as shown in **Figure 3-7** at a rate of 0.50 mm/min.



Figure 3-7: (a) Types of Roots. (b) Tensile Test on Root.

Tensile strength at the rupture was calculated by dividing the maximum force required to rip each primary root over the cross-sectional area. In the tests, it was difficult from time to time to visualize the breakage with the naked eye due to the presence of fiber in the roots, and therefore, the tensile test was stopped at 10% drop from the peak load. Variations in tensile strength were observed in the roots (R1, R2, and R3) collected from different plants. In this research, three samples from each class were tested to study the tensile strength of respective kind.

3.3.4 Root Area Ratio Calculations

RAR is defined as the fraction of the soil cross-sectional area occupied by roots per unit area (Gray *et al.* 1982). A 2-inch diameter core was used to determine the RAR as shown in **Figure 3-8**. Core breakup method was utilized to measure the number of roots in a specific area. Three samples were collected from each layer and left to dry. The later dry soil core was broken into two different pieces and the roots were counted for both sides.

An average number of roots and diameter were used to determine the RAR for that specific layer.



Figure 3-8: Sample for RAR calculation.

3.4 Results

3.4.1 Tensile Strength of Roots

The peak tensile strength of the roots was considered as the strength at the rupture point. It was found in the tests that finer roots for each individual root type resisted higher tensile stress than the thicker roots as tensile stress was observed to increase as the root diameter tends to decrease as shown in **Figure 3-9**.

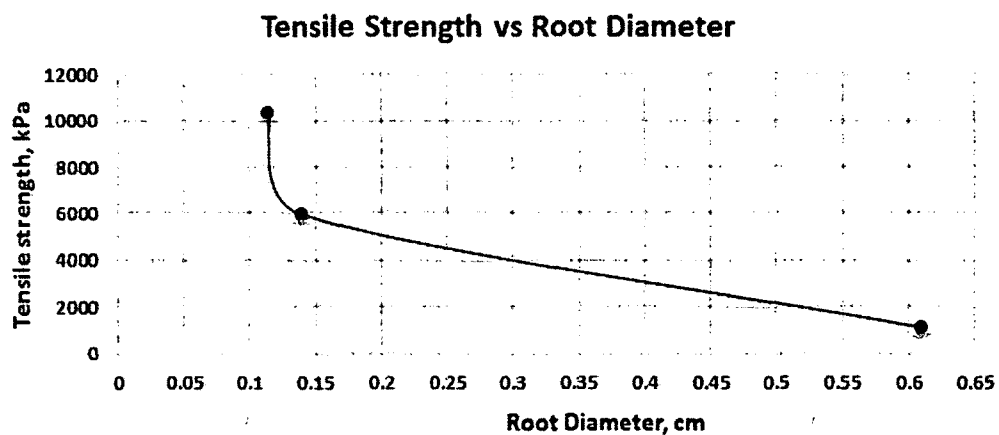


Figure 3-9: Tensile stress vs. root diameter comparison.

As presented in **Table 3-1**, three samples were taken and tested for each root class. Tensile strength versus root diameter was plotted as follows. It was also observed that the

maximum tensile strength of the roots was found for root type R2. In **Table 3-2**, detail physical properties and results of the tensile strength test of each root class has been presented.

Table 3-2: Physical properties of roots and resulted strength for each root.

Root Type	Length (cm)	Diameter (cm)	Sample #	Load (lb)	Tensile Strength (kPa)	Average Tensile Strength (psi)
R1	3.81-8.90	0.140	1	1.85	6074.28	5953.00
			2	1.96	6756.86	
			3	2.04	5026.28	
R2	11.43-16.50	0.114	1	1.97	10445.56	10347.00
			2	2.38	10941.98	
			3	2.80	9652.66	
R3	15.24-30.48	0.610	1	5.01	861.84	1096.00
			2	6.55	1185.89	
			3	8.12	1241.05	

3.4.2 Shear Strength of Plain and Rooted Soil

The corresponding stress-strain curves for plain and rooted soil are shown in **Figure 3-10** to **Figure 3-13**. The normal stresses were selected to cover the actual overburden earth pressure at the roots' depth.

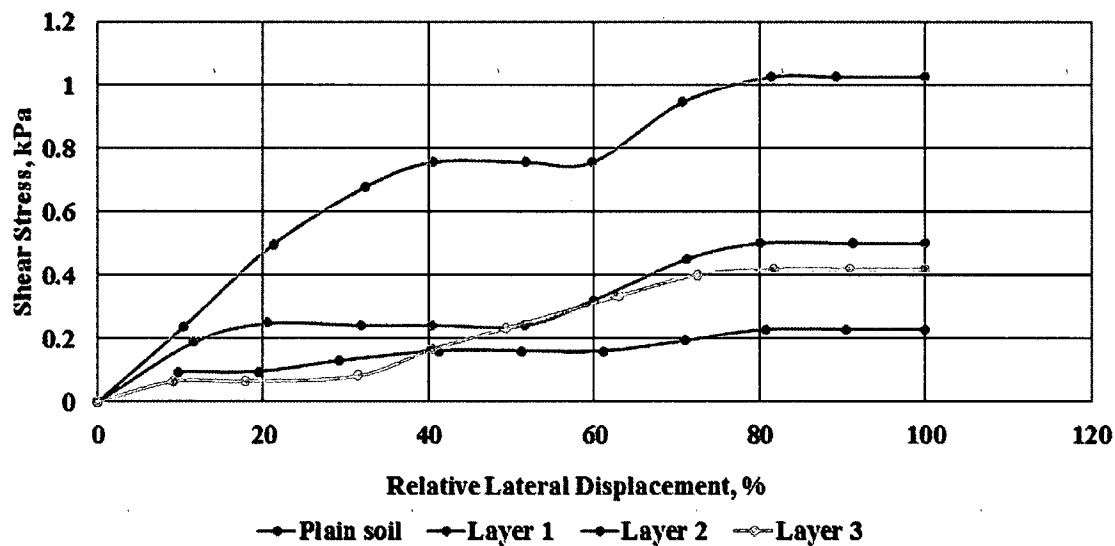


Figure 3-10: Stress-strain curve for plain and rooted soil for normal stress of 0.7 kPa.

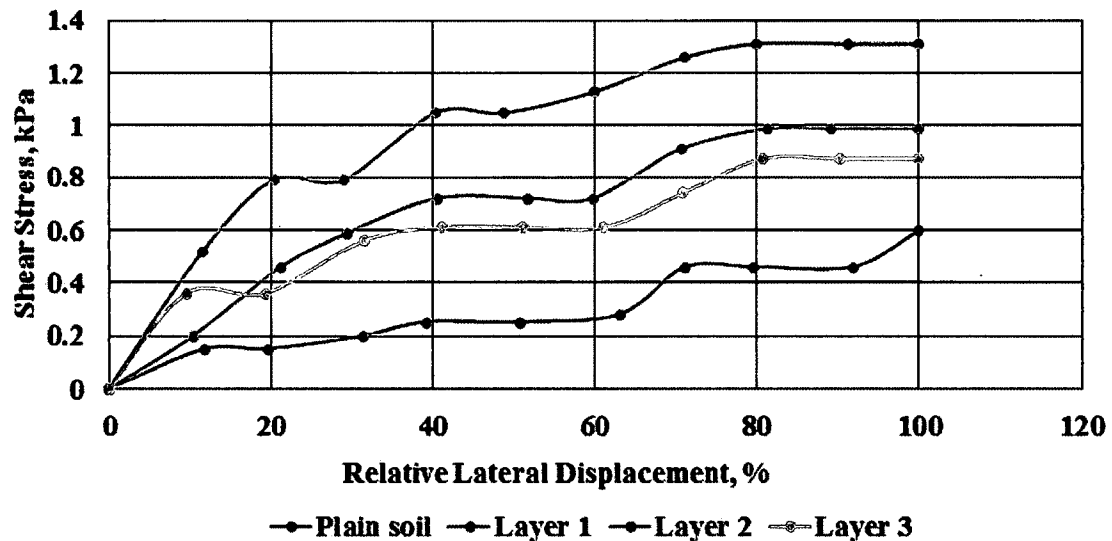


Figure 3-11: Stress-strain curve for plain and rooted soil for normal stress of 2.3 kPa.

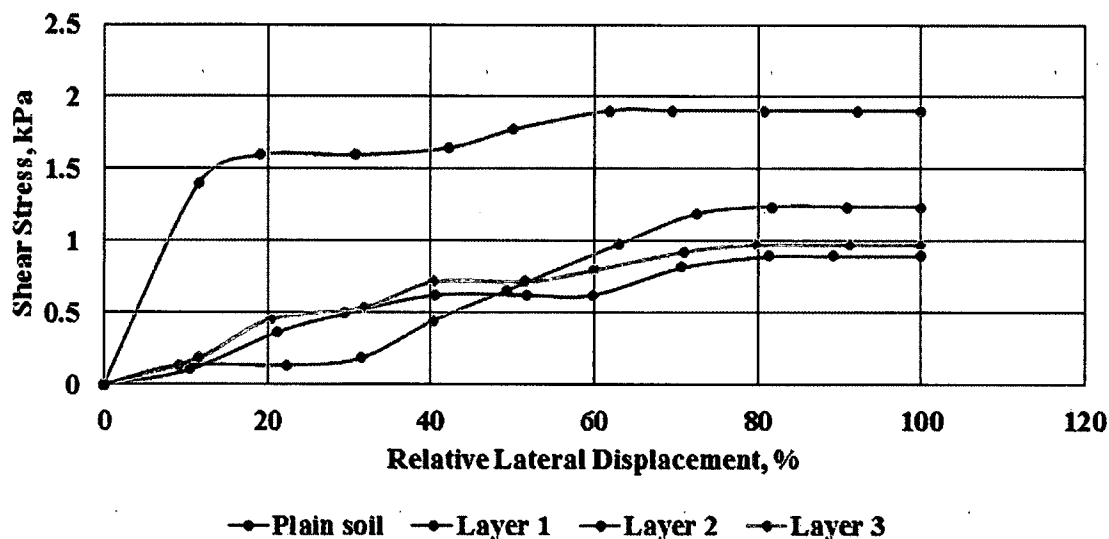


Figure 3-12: Stress-strain curve for plain and rooted soil for normal stress of 3.2 kPa.

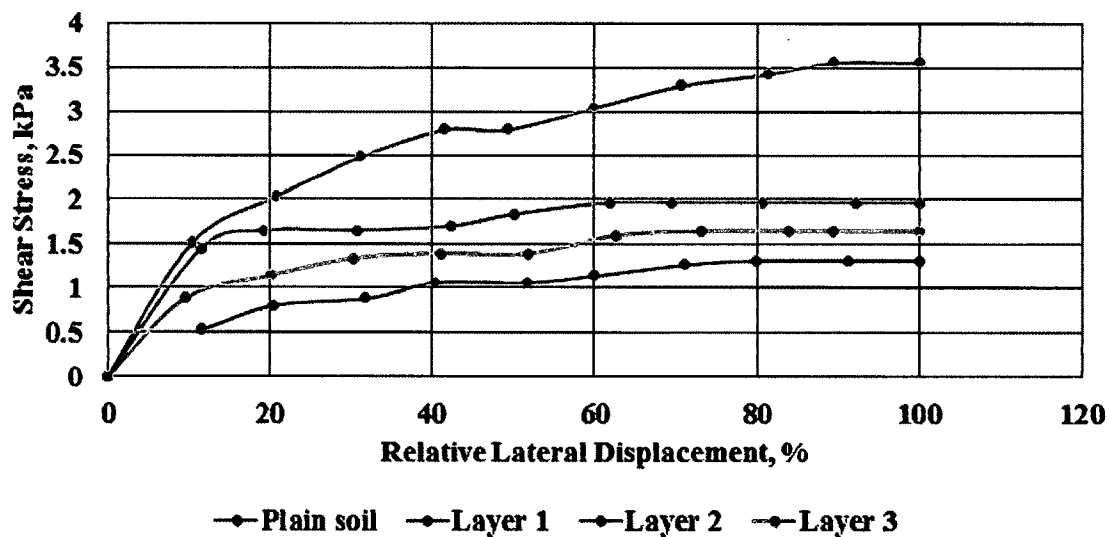


Figure 3-13: Stress-strain curve for plain and rooted soil for normal stress of 5.47 kPa.

The peak strengths and normal stresses corresponding to the different stress-strain curves were picked up and plotted in Figure 3-14, in which cohesions and friction angles were achieved for the plain and rooted soil layers, respectively. In general, the peak shear strengths were increased in the rooted samples. With the limited number of tested samples, it was found that the root reinforcement increased the cohesion of the soil by roughly 285% for layer 1, 217% for layer 2, and 168% for layer 3. The friction angle increased by 115%

for layer 1, 31% for layer 2, and 8% for layer 3. The reinforcing effect of the roots is more significant on cohesion than on the friction angle.

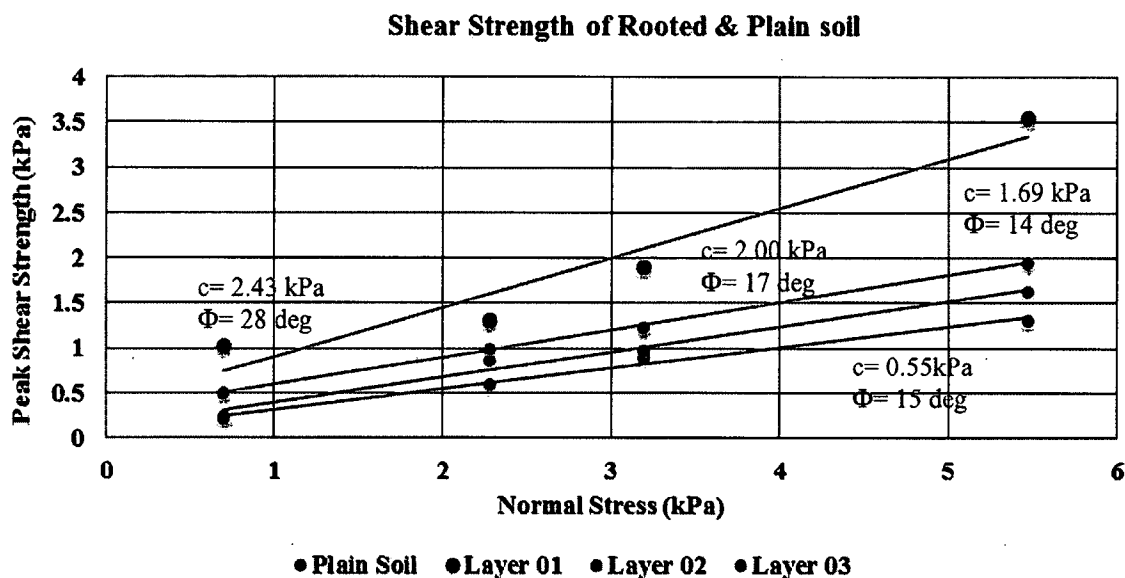


Figure 3-14: Stress-strain curve for plain and rooted soil.

Enhancement in the top layer was found to be significant compared to the bottom two layers. The top layer also produced friction angle enhancement where friction angle in the other two layers is insignificant as shown in Table 3-3.

Table 3-3: Soil strength parameter comparison.

Plain Soil Strength Parameters		Enhancement in strength parameter in Rooted Soil layers					
		Layer 1		Layer 2		Layer 3	
C (kPa)	Phi (degree)	C	phi	C	phi	C	phi
0.63	13	285%	115%	217%	31%	168%	8%

3.4.3 Root-Induced Cohesion in Soils

The perpendicular model by Wu *et al.* (1979) and the inclined model by Gray *et al.* (1982) discussed in Chapter Two were used to calculate root cohesion. Resulted root cohesion from both methods is presented in Table 3-4.

Table 3-4: Root cohesion for both models.

Layer #	Soil Area (As) (cm ²)	Average Number of Roots (#)	Average Root Diameter (cm)	Average Root Area (cm ²)	RAR	Average Root Tensile Strength (psi)	Tensile Stress (t_R) (kpa)	Root Cohesion (kPa)			
								Perpendicular Model	Inclined Model		
									15 deg	30 deg	45 deg
1	20.2	10	0.112	0.009	0.0048	8600	41.61	49.94	42.45	40.37	35.79
2	20.2	8	0.137	0.015	0.0059	6200	36.74	44.08	37.47	35.63	31.59
3	20.2	4	0.124	0.012	0.0023	6900	16.35	19.62	16.68	15.86	14.06

It was found that the analytical model overestimates the root-induced cohesion of dredge sediment by a big margin. In this research, direct relation between root tensile strength and cohesion was introduced by factorizing the direct shear test results. Correlation between root cohesion and root tensile strength found to be different in three layers due to variability in the cohesion production. Multiplication factor to be used with root tensile strength for layer 1, layer 2 and layer 3 are 0.043, 0.028 and 0.08, respectively. Based on the findings, a new estimation of root cohesion from tensile strength of the roots is provided as:

$$\Delta C \approx 0.05 t_R.$$

Equation (3-1)

CHAPTER 4

DELFT3D HYDRODYNAMIC MODEL CALIBRATION AND VALIDATION

4.1 Introduction

A hydrodynamic and wave model was initiated to support the study of vegetation contribution in reducing marsh erosion for the Lake Calcasieu estuarine system. To recognize the zones which are more inclined to erosion and to study the input of marsh vegetation in reinforcing the zones of interest are the principal objective for this combined hydrodynamic and wave modeling effort.

A two/three-dimensional modeling package integrating the influence of temporally varying wind fields, coupled with the range of conditions typical of the system, was required for the appropriate hydrodynamic analysis of Lake Calcasieu. Furthermore, available information including water elevation measurements and current measurements at key locations within the system was supplemented if there were a field data collection endeavor. The dataset, which was developed, formed the foundation for model boundary conditions as well as calibration and validation data. A wave model was incorporated into the two/three-dimensional circulation model after tracking the development of the calibrated/validated hydrodynamic model.

Sediment is transported by flowing water in river estuarine, and coastal environments. In spite of much of the sediment being transported close to the bed, a significant quantity may be transported higher in the flow. Additionally, the flow exerted

on the bed stresses the magnitude and direction of the shear, which is vital for determining the magnitude and direction of the sediment transport, signifying erosion/sedimentation location. This research focuses the main attention on the study of the bed shear stress on vegetated and non-vegetated marsh bed owing to Hurricane Ike and later used in the erosion study.

The Delft3D morphological modeling package (Deltares, 2011) was the primary modeling tool used in this study. Topographic and bathymetric surface changes based on the effects of waves, water levels, winds, and currents are determined by this package which consists of two models combined in one. Using the Simulating Waves Nearshore Model, wave propagation from the offshore to the nearshore area was estimated. The output waves of Delft3D Wave, as well as the varying water levels from offshore and the bathymetry, were utilized in the Delft3D-FLOW to determine the resulting currents, water levels, sediment transport, erosion, and deposition. The Delft3DFLOW model calculated the subsequent elevations of the topographic and bathymetric surface based on the estimated erosion and deposition at each time step and sends the updated bathymetry back to the Delft3D Wave model.

Depth-averaged flow velocity (2D approach) does not always give away the estimation of the erosion/sedimentation since noteworthy three-dimensional effects may occur. For instance, the spiral flow pattern commonly found in river bends, and the ‘undertow’ which is especially strong in breaking waves are some effects. As a result, for more accuracy, it has been considered during the hydrodynamic/Delft3D flow study even though the 3D approach requires more simulation time.

4.2 Chapter Structure

This chapter is structured as follows: Section 4.2 gives an overview of the collected data to assist with model calibration. Section 4.3 describes the set-up, calibration, and validation of the numerical models. Section 4.4 presents the results of the modeling study.

4.3 Gathered Data

4.3.1 Bathymetry

Bathymetry data has been acquired from various sources. Three sources were used for the Gulf of Mexico: NOAA's bathymetric sounding database, the Digital Nautical Chart database and the 5-minute gridded elevations/bathymetry for the world (ETOPO5) database. The Atlas and the Mississippi Coastal Analysis Lidar Projects were used for the floodplain topography. A height of 0.80 m was applied for marshland and -0.40 m for water at times when no data were available in the wetlands, conform the Louisiana Gap Analysis Project (LA-GAP). Data collected down the Mississippi and Louisiana coastline were by and large dated preceding Hurricane Katrina in August 2005. The bathymetry which was used for this research is depicted in Figure 4-1.

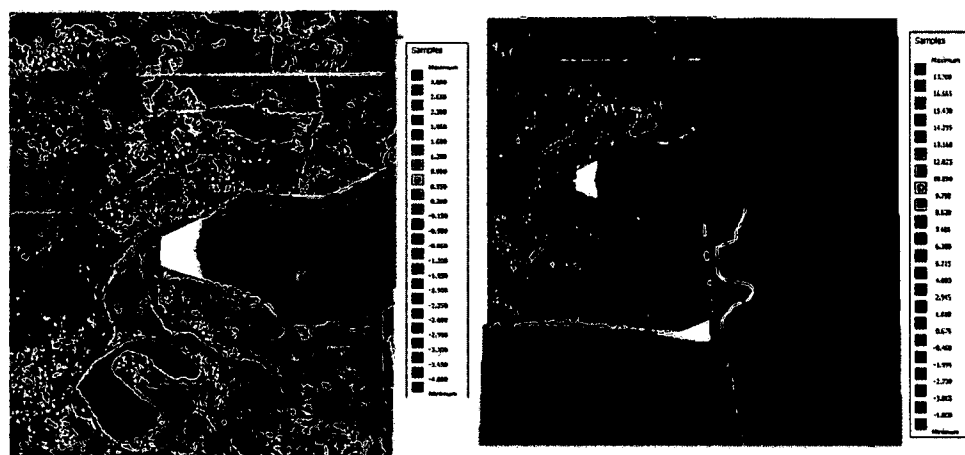


Figure 4-1: Sample data for floodplain (left) and overall model domain(right) bathymetry.

4.3.2 Reference Level

Along the Louisiana coastline, depth can be expressed in comparison to several reference levels. Of all other, NAVD88 and the tidal datums (e.g. MSL, MLLW) were the most important reference level for the data collected for this research. NAVD88 is an abbreviation for the North American Vertical Datum of 1988. The National Geodetic Vertical Datum of 1929 (NGVD29) also known as the Sea Level Datum of 1929 was substituted for it since that system was obsolete. Father Point/Rimouski, Quebec, and Canada are the primary tidal benchmark location of NAVD88. The new datum, exempting areas with known crustal motion, was published in 1990. Due to crustal motion, the Lower Mississippi Valley in Louisiana undergoes subsidence. The benchmark elevations published in 1992 are obsolete. Errors equal to 6 cm can occur (USACE FAQs, 2010). The program VDatum (VDatum, 2010) was used for the conversion between vertical data. NOAA initiated this program. GEOID transformation grids are required to convert NAVD88 to the tidal datum. Furthermore, the most recent version is the GEOID09 (NOAA GEOID, 2010). The benchmarks in Louisiana were updated for subsidence for each update of the hybrid geoid. The disparity between Local Mean Sea Level (LMSL) and NAVD88 is 0.27 meter. This signifies that when bathymetry is proportionate to NAVD88, the water level has to be increased by 0.27 meter in order to use Mean Sea Level (MSL) as a reference level. NAVD88 is used as reference datum throughout this research.

4.3.3 Water Level Data

Daily water level measurements for several locations in the Gulf of Mexico and nearby are being performed by the National Oceanic and Atmospheric Administration (NOAA). Several other institutes like US Geological Survey (USGS) and the U.S. Army

Corps of Engineers (Rivergages.com, 2010) have also taken on the endeavor of measuring water levels in the project area with the study area being mostly covered with marsh areas, very few data collection stations were available there. Calcasieu Pass (station# 8768094), which is the main station, is the source of tide collected at the entrance of Calcasieu Lake from the Gulf of Mexico as shown in **Figure 4-2**.

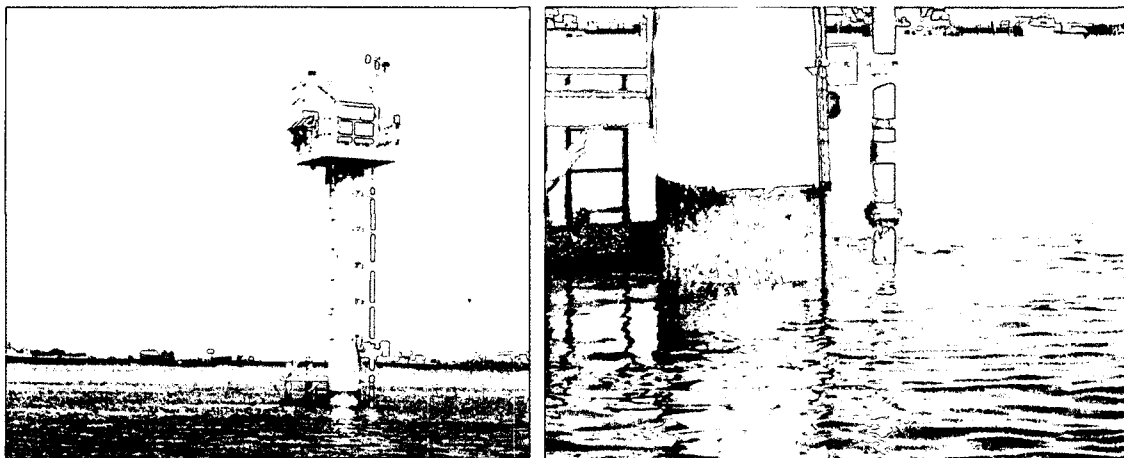


Figure 4-2: Photographs of Station 8768094 Calcasieu Pass, LA.

Tidal datum of the Calcasieu Pass station for different datum conditions is shown in **Figure 4-3**.

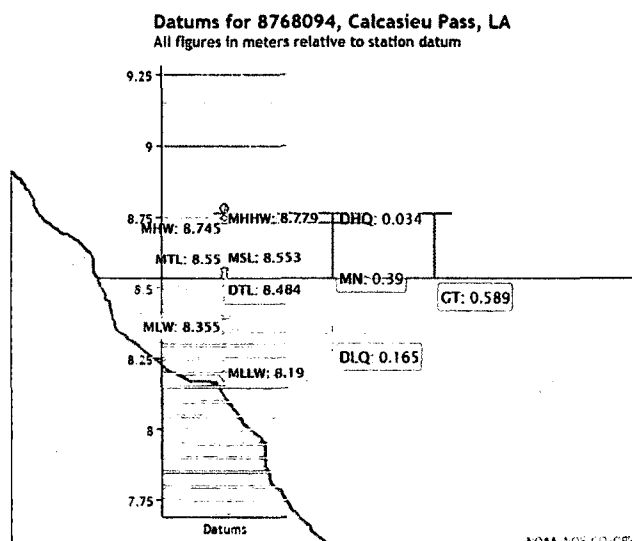


Figure 4-3: Tidal datum explanation for Calcasieu Pass station.

Along with the NOAA station the other seven stations of Office of Coastal Protection & Restoration (OCPR) are used to collect tide/water level data for calibration and validation purpose. Locations and source of data for all the stations were presented in Table 4-1.

Table 4-1: Summary of boundary and observation stations.

Station ID	Station Name	Station Type	Data Source	Latitude	Longitude	Data Type
WB	CRMS0641-H01	Boundary	OCPR	29.8963051	- 93.510596	Water Level/ Tide
EB	CRMS1738-H01	Boundary	OCPR	29.8538957	- 93.229349	Water Level/ Tide
SB	8768094 Calcasieu Pass, LA	Boundary	NOAA	29.760723	- 93.342941	Water Level/ Tide
OS1	CRMS0639-W01	Observation	OCPR	29.8897467	- 93.479397	Water Level/ Tide
OS2	CS20-15R	Observation	OCPR	29.8640416	-93.45145	Water Level/ Tide
OS3	CS20-14R	Observation	OCPR	29.8069199	- 93.396555	Water Level/ Tide
OS4	CRMS0655-H01	Observation	OCPR	29.799196	- 93.415882	Water Level/ Tide
OS5	CRMS1743-H01	Observation	OCPR	29.8905251	- 93.230987	Water Level/ Tide

The stations that were used to collect data for calibration and validation were termed observation station (OS). Three stations at three sides (East, West & South) of the study area were used to collect the model forcing/ boundary condition data. Observation and boundary stations are shown in **Figure 4-4**.

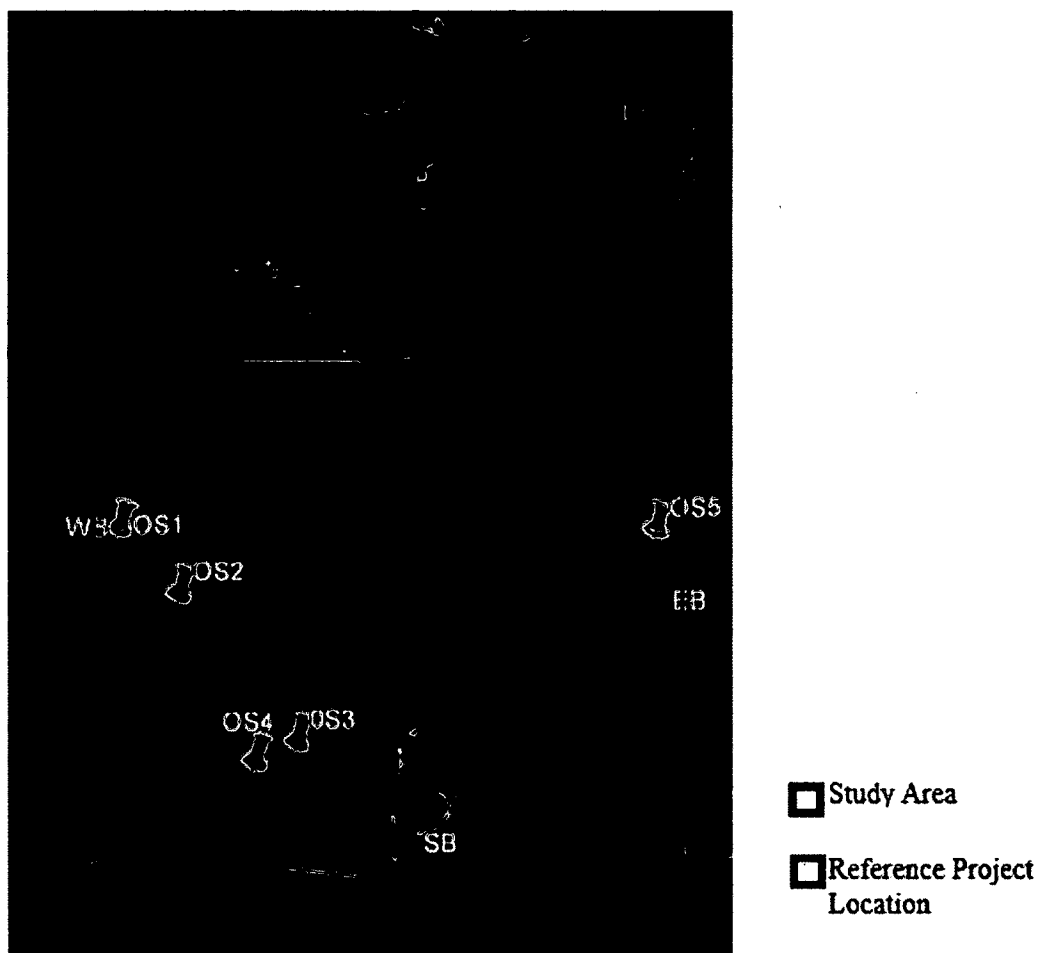


Figure 4-4: Boundary and observation stations.

4.3.4 Wind and Precipitation Data

Wind plays a major role in storm surge modeling. It is essential to consider winds while modeling shallow water zone as wind-generated wave produce significant stress. Delft3D can run with constant winds as well as spatially variable winds. Time-dependent wind data was obtained from Calcasieu Pass station for this research.

4.4 Model Setup

Model setup was done by using Delft3D preprocessing tools. RFGRID used for grid generation, QUICKIN used for assigning depth. Graphical User Interface (GUI) was used to assign boundaries and other forcing conditions.

4.4.1 Model Grid

Assembly of all grids are in spherical coordination. Mesh was generated in RFGRID which is Deltares's grid generation tool. As established before, the structured orthogonal curvilinear grid system was applied by Delft3D. In some required areas, such as connecting passes, the mesh was refined to be able to cover such locations. In this research, the structured grid was used effectively. **Figure 4-5** shows the computational grid for Delft3D flow.

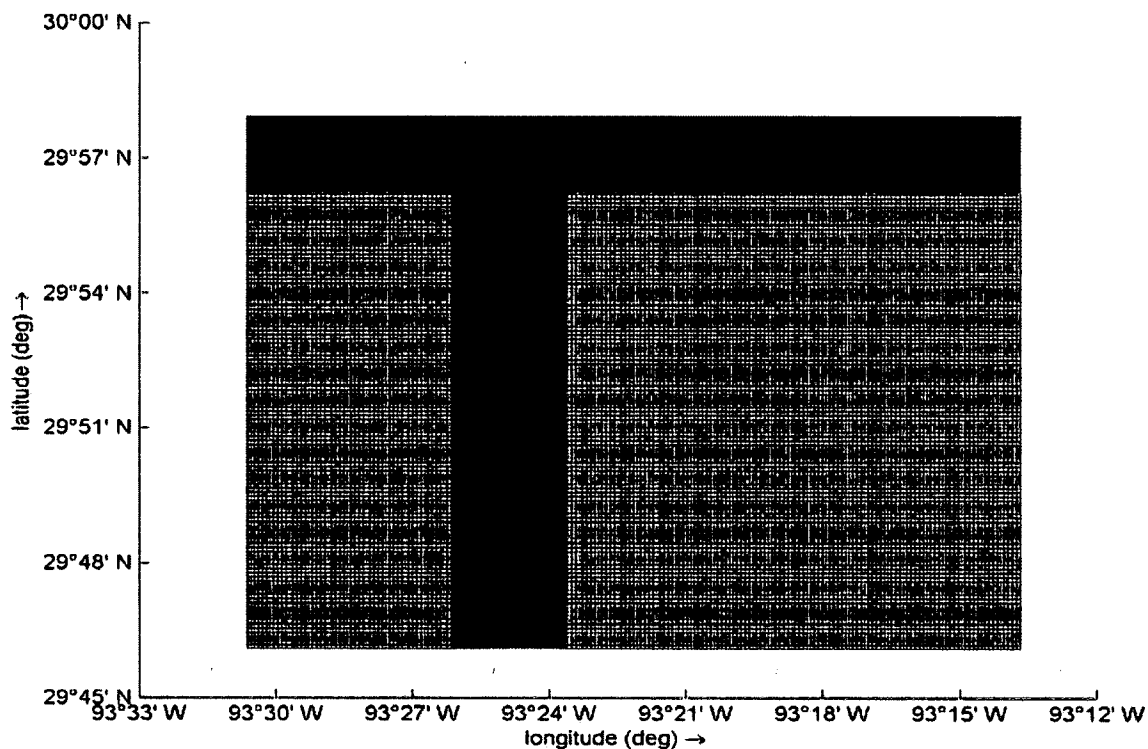


Figure 4-5: Delft3D FLOW grid.

An unstructured grid is far more expedient than a structured grid system for capture complex geometries. Additionally, if local refinements are done by any one of the grid in a specific location, unwanted areas will be extended by these refinements. The culmination of this will produce a waste of computation time. However, the structural grid is granted to be the most suitable option since dense data were accessible for the marsh areas and detail profile was an obligatory requirement for this kind of research.

Nine vertical sigma layers (10 sigma levels) were used for the hydrodynamic grid. Since the model had the wind module on, the layers distributed double parabolically with high resolution given to the surface and the bottom. **Figure 4-6** shows the percentage share of each layer deep inside the water column.

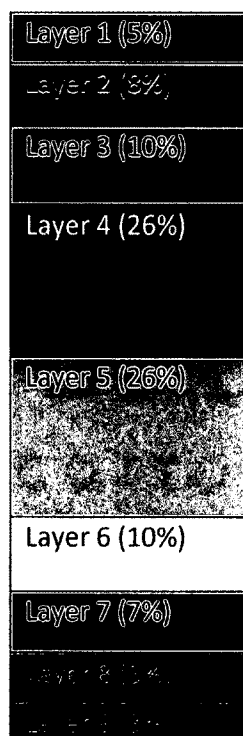


Figure 4-6: Layer distribution for Flow grid.

Delft3D wave grid was also generated through RGFRID. Wave grid is shown in **Figure 4-7**.

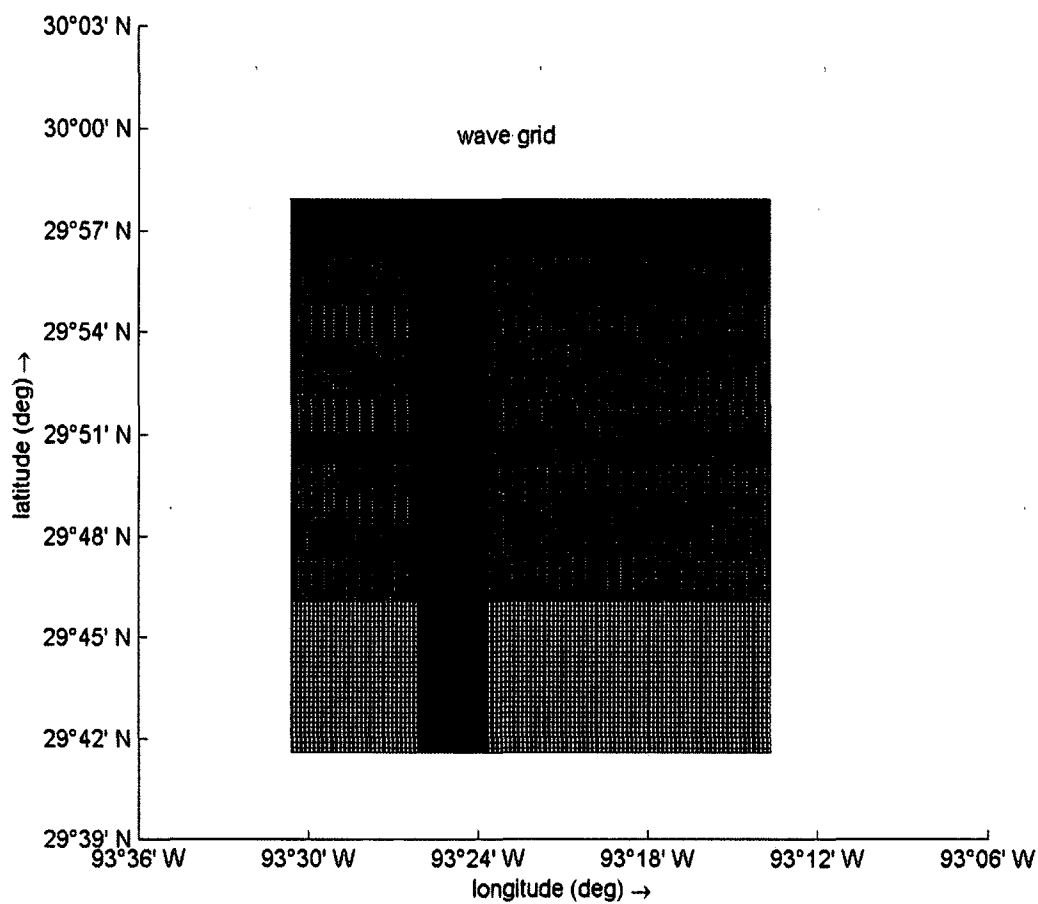


Figure 4-7: Delft3D WAVE grid.

Grid characteristics are summarized in Table 4-2. The model's developers (Deltares) have established guidelines for grid cell smoothing and orthogonality that were used.

Table 4-2: Grid characteristics.

Grid Properties	Flow Grid	Wave Grid
Number of Long-shore Cells	596	596
Number of Cross-shore Cells	306	336
Long-shore Spacing (m) -Min	3	3
Long-shore Spacing (m) - Max	50	50
Cross-shore Spacing (m) - Min	6	6
Cross-shore Spacing (m) - Max	60	250

Change in cell size between two rows of grid cells was represented through Smoothing. The cell size between two rows of grid cells increased by 10% is suggested by a smoothing value of 1.1. The maximum smoothing value is 1.2, which is recommended by Deltares. The angle between the long-shore and cross-shore grid lines was equal to the Orthogonality. At least 87.7-degree angles were supposed to be obtained between the long-shore and cross-shore grid lines within the area of interest and maintained for both grids properly.

The Calcasieu Lake and the floodplain were essentially covered by Delft3D flow grid where in spite of the wave grid being with the same dimension along long-shore, yet extended 8000 m more (highlighted with red) along cross-shore to cover the part of the Gulf of Mexico was included in the simulation. A combined flow wave grid is shown in **Figure 4-8**.

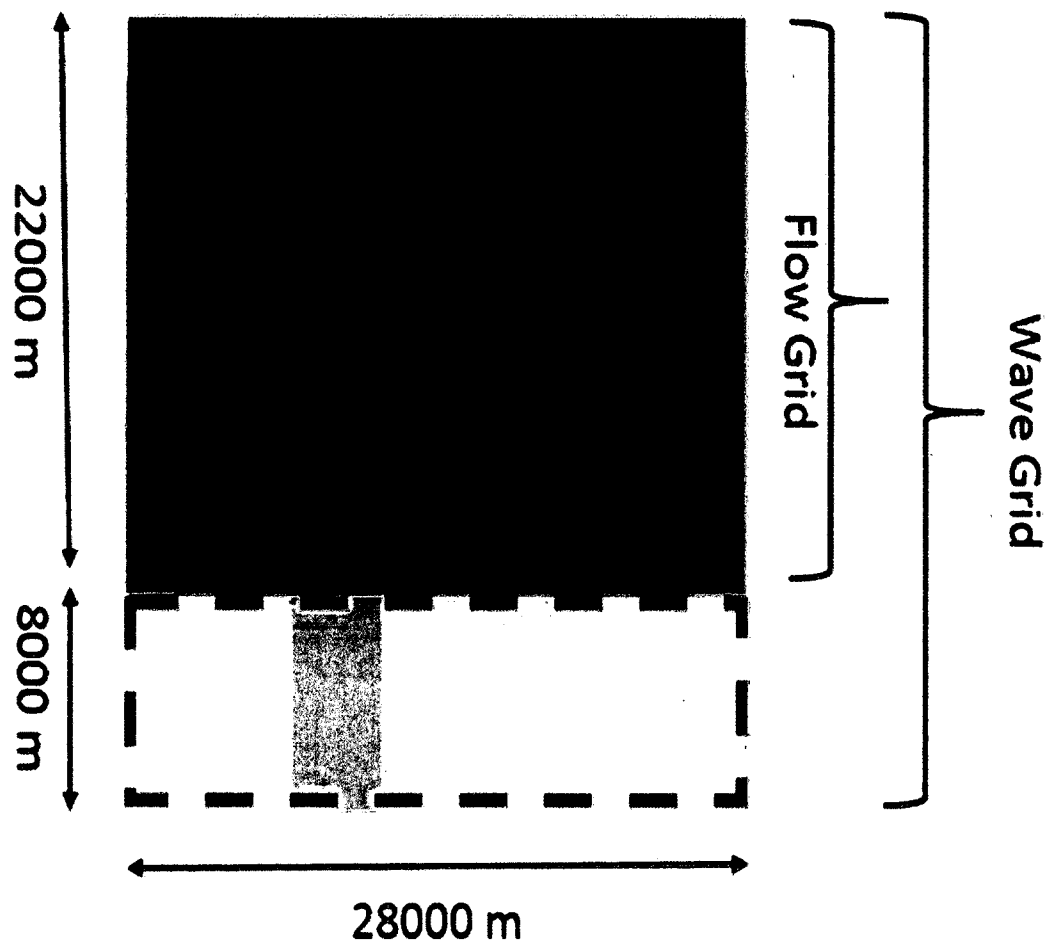


Figure 4-8: Delft 3D model grid.

4.4.2 Model Bathymetry

Delft3D Quickin assigned bathymetry to the respective grids. Five different methods are presented by this pre-processing tool of Delft3D for bathymetry interpolation including Average Value of Near Points, Value of Closest Point, Maximum Value of Near Points, Minimum Value of Near Points and Shepard. The Shepard method is a slanted average method. Both Flow and Wave model bathymetry are shown in **Figure 4-9** and **Figure 4-10** respectively. The depth is particularly mentioned at the grid cell's corner.

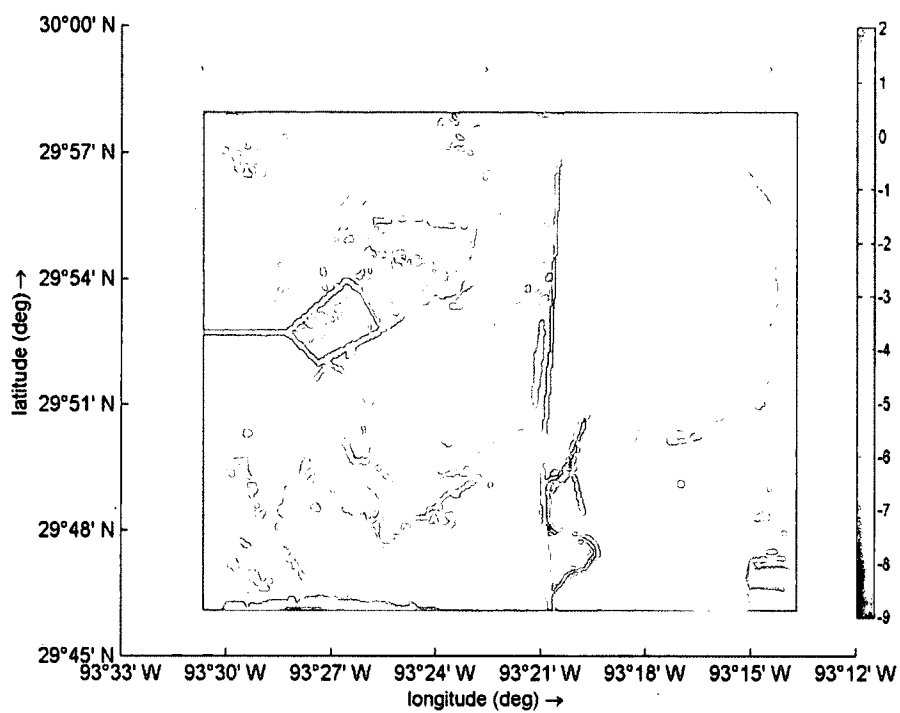


Figure 4-9: Flow model bathymetry.

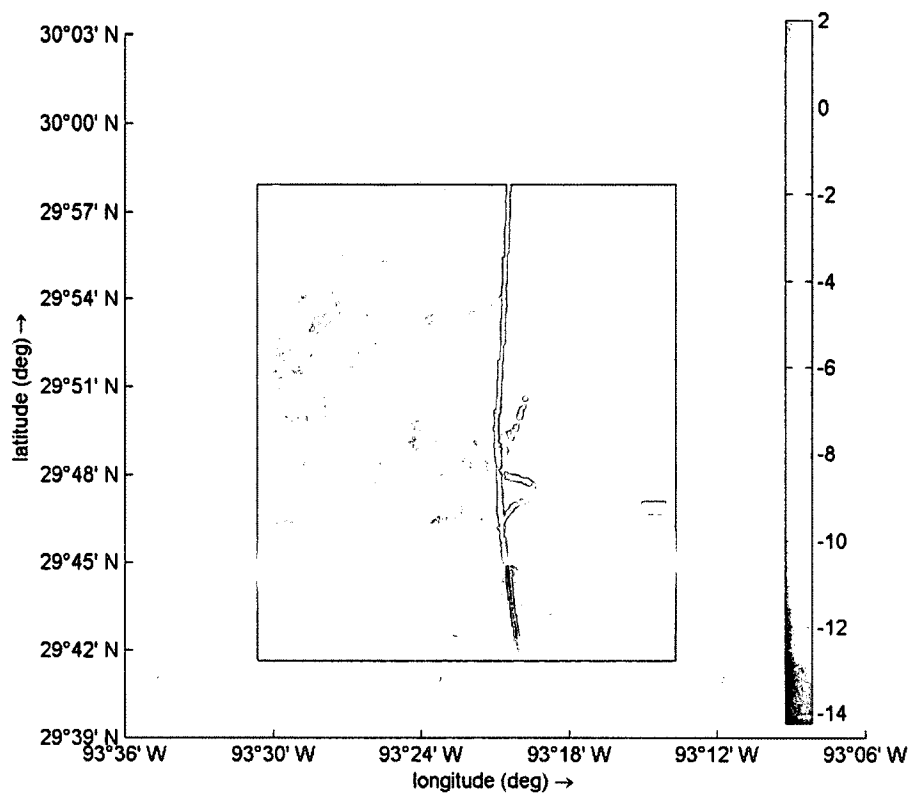


Figure 4-10: Wave model bathymetry.

4.4.3 Model Initial Condition

Propagation simulations have to be run in order to get the proper water level in the model to start appropriately. Both uniform and spatially varied initial conditions can be used by Delft3D. Preparing an initial conditions file is one of many other ways to define the initial condition. One can identify the initial conditions file easily because it is a typical ASCII file with an “ini” extension containing the required information in a gridded format. Also by using hot start, the initial condition can be defined. In contrast with the initial conditions file, the restart/hotstart file is a binary file which is an output of a previous run. Notably, in a coupled model wave the initial condition need not be specified since it will automatically be generated by using information of the flow run.

In this research, the water was circulated well enough to save a hot start after running the fully defined coupled model (i.e. including boundary and other forcing condition) a few days with the initial water level of 0.5 m in the whole domain. Then for the calibration process, the hot start was used for a major run in. **Figure 4-11** shows the water level in a hot start that was used as an initial condition.

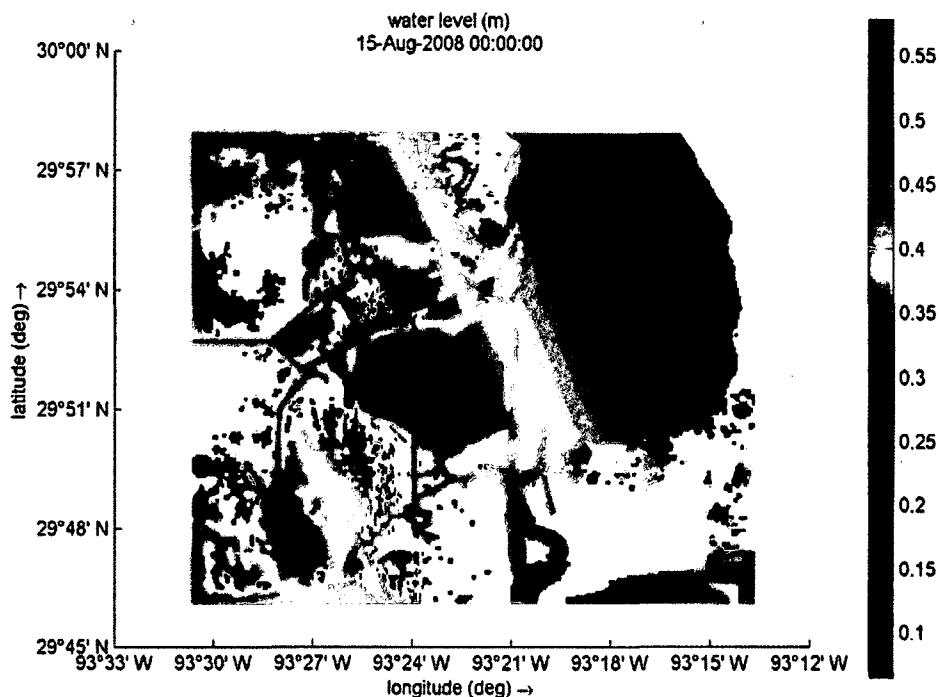


Figure 4-11: Initial condition of the Hydrodynamic model (water level).

4.4.4 Flow Model Forcing Conditions

4.4.4.1 Boundary

During this research, only water level was used as a main forcing condition in the hydrodynamic model. All the boundary stations and validation station are presented in **Figure 4-12**. Neumann boundary or zero cross-boundary water-level gradient condition was applied at the north end during simulation.

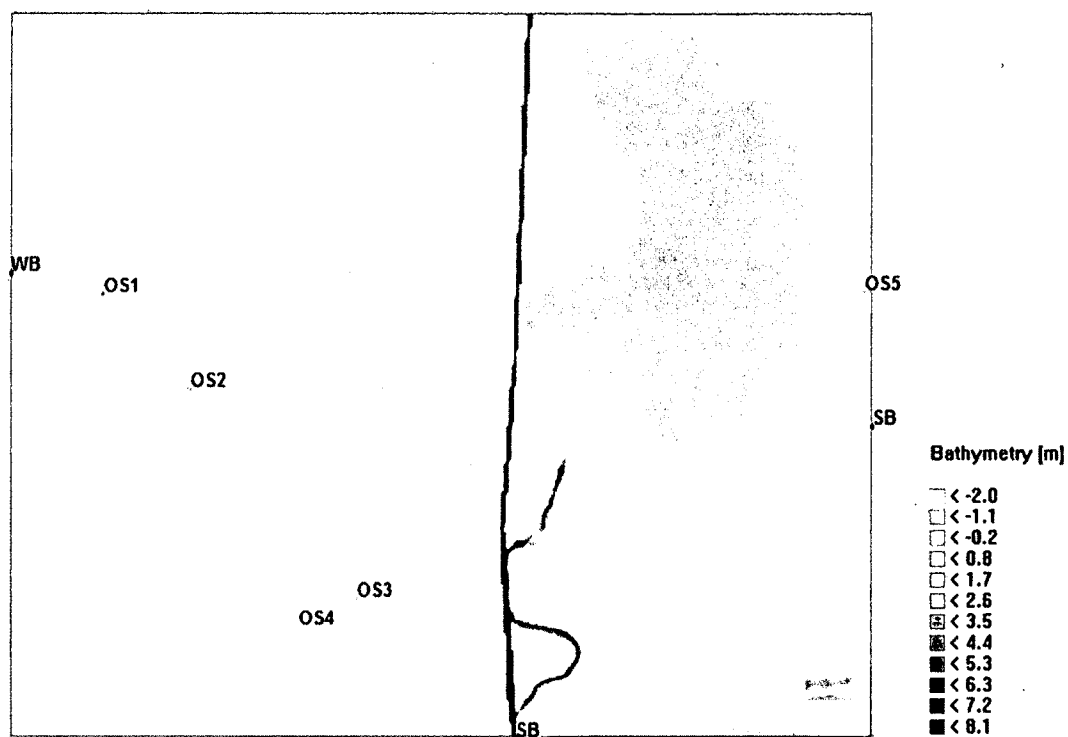


Figure 4-12: Model bathymetry and station locations.

Time series of the water level used as boundary forcing at West, East and South are presented in Figure 4-13, Figure 4-14 and Figure 4-15 respectively.

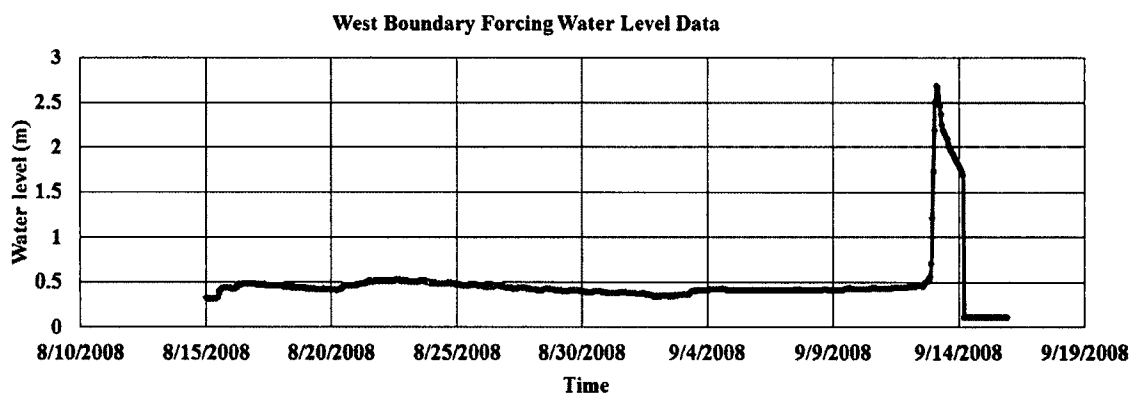


Figure 4-13: West boundary condition of the model.

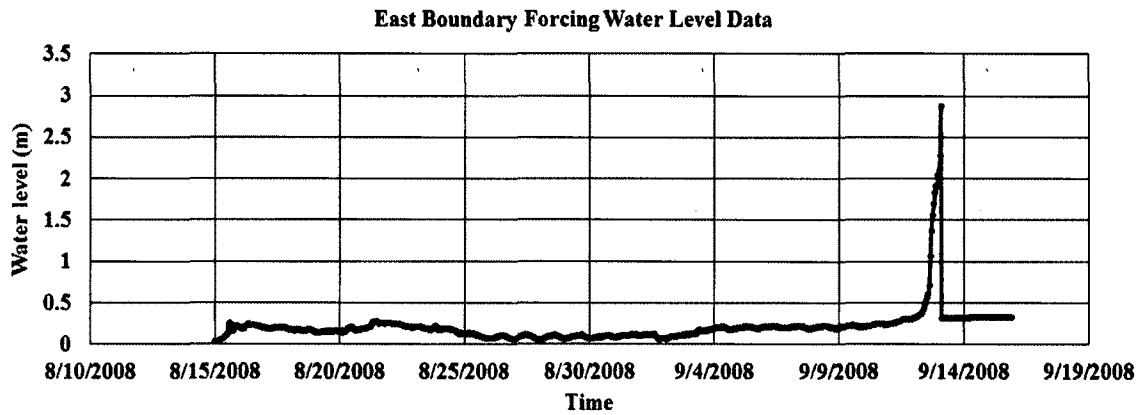


Figure 4-14: East boundary condition of the model.

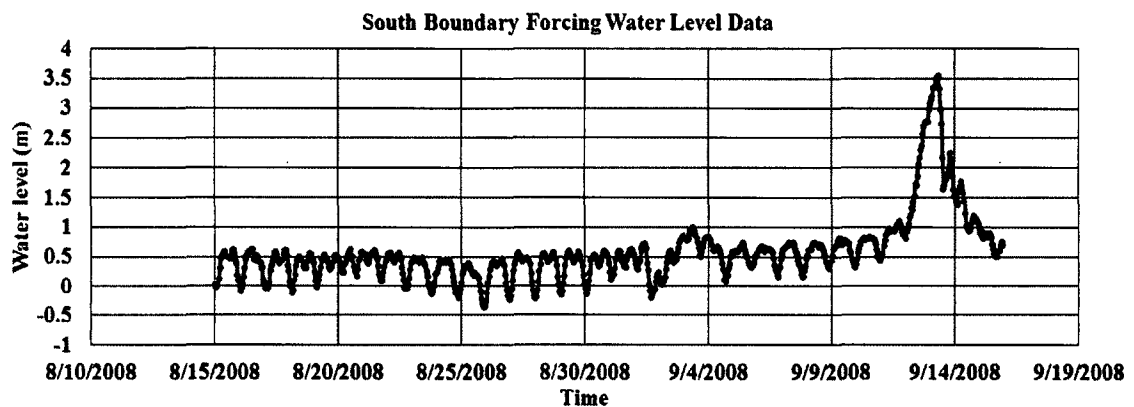


Figure 4-15: South boundary condition of the model.

4.4.4.2 Wind and precipitation forcing in the hydrodynamic model

As previously discussed, the wind has a significant effect in near shore areas it was included in the study. Based on the limitations of wind data collection station, wind data from the Calcasieu Pass station was used for wind forcing in the entire flow domain. **Figure 4-16** shows the wind speeds and wind directions applied on the model for the simulation period.

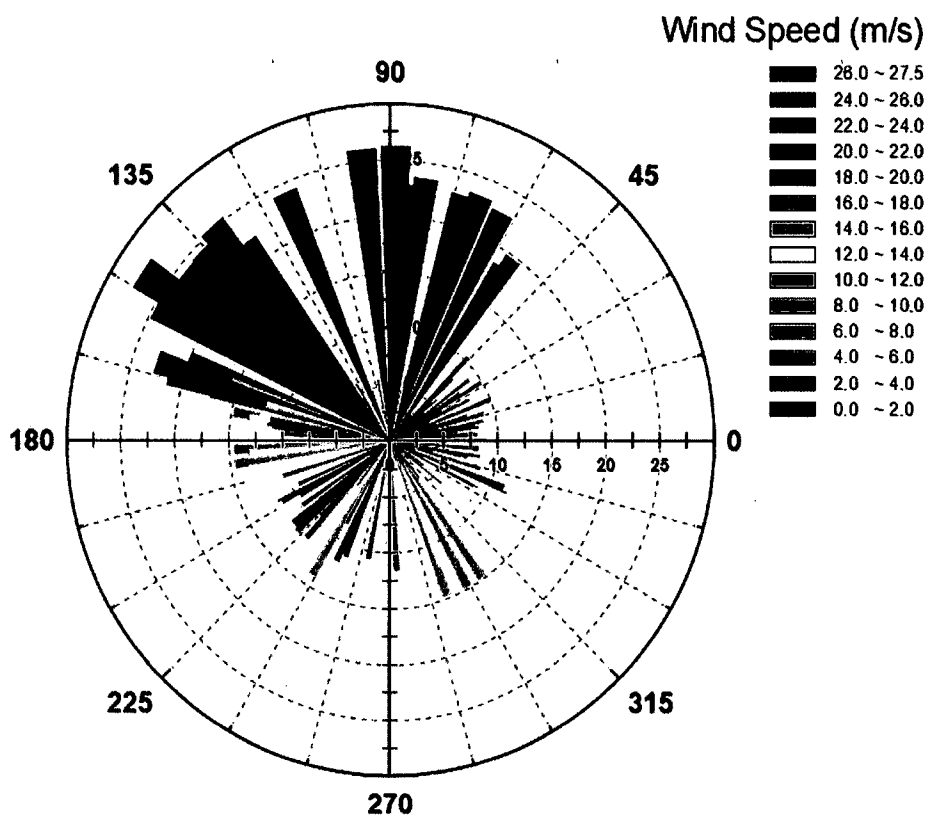


Figure 4-16: Wind rose (speed and direction) at Calcasieu Pass for the period of 15 August, 2008 to 15 September, 2008 used in Hydrodynamics model.

The simulation period involved two major hurricanes associated with high rainfall which can affect the water level during the simulation. During this study, precipitation data set was prepared by averaging precipitation data from nearby locations such as Lake Charles, LA and Port Arthur, TX shown in **Figure 4-17**.



Figure 4-17: Location of precipitation data collection stations.

Precipitation data forcing in the hydrodynamic model is presented in Figure 4-18.

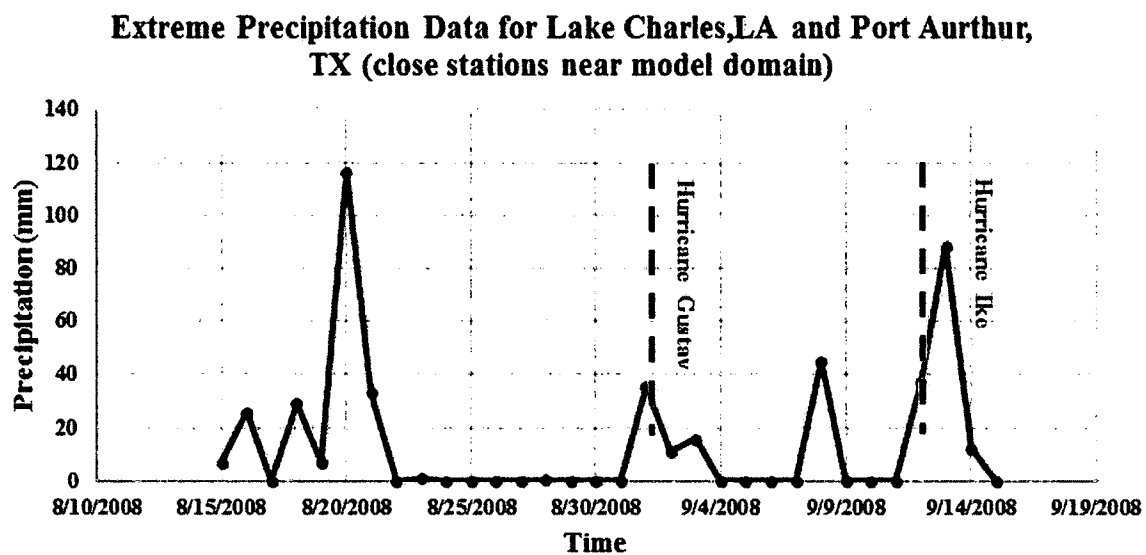


Figure 4-18: Extreme precipitation data used in Hydrodynamics model.

4.4.5 Additional Parameters for Flow Model

Additional important model parameters specified for the FLOW model are indicated in Table 4-3.

Table 4-3: Parameters used in Flow model.

Parameter	Value
Threshold Depth	0.1 m
Smoothing Time	60 min
Advection scheme for momentum	Flood
Horizontal Eddy Viscosity	1 m ² /s
Wall roughness slip condition	Free
Time Zone	GMT

4.4.6 Wave Model

During the calibration and validation, a calm sea was considered with the average wave height information near the Calcasieu Pass location obtained from NOAA website. Significant wave height normally varies from 0.3 m to 1 m with a peak period from 4 s to 8 s. Standard normal wave forcing was applied from offshore to onshore direction. **Table 4-4** shows the wave parameters used for boundary forcing in the wave model for calibration and validation. The wind was not included in the wave model input during the calibration phase.

Table 4-4: Wave parameters used for boundary conditions.

Parameter	Value
Significant Wave Height	0.5 m
Peak Period	8s
Direction	170 degree (SE)
Directional Spreading	4

To justify the assumption of general wave height near Calcasieu Pass, a most recent image of the graphical forecast is shown in **Figure 4-19**.

NDFD Graphical Forecast

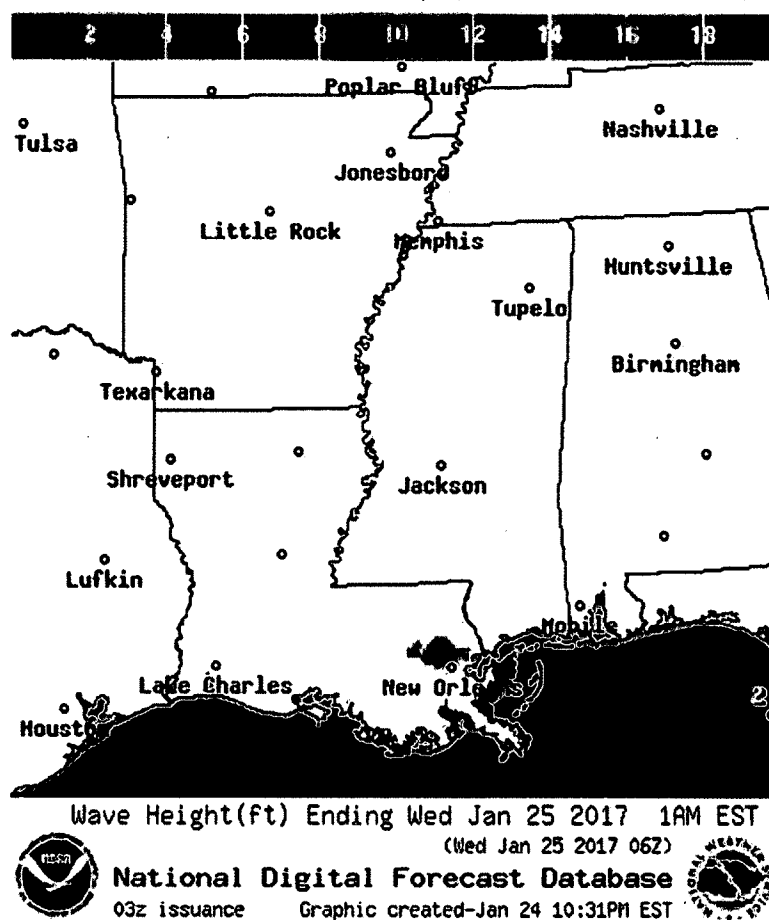


Figure 4-19: Regular/normal wave height data near study area.

4.4.7 Model Calibration

The realistic representation of the water level at various observation station location in the flow domain is the focal point in the flow-wave coupled model calibration. From August 15, 2008, to August 20, 2008, the coupled model was tested for calibration purpose. Several tests included a variation of bed roughness for co-efficiency and manually altering the depth at a different location to make sure the model works right. In **Figure 4-20** to **Figure 4-24** evaluation between observed and model value for different stations after calibration is presented.

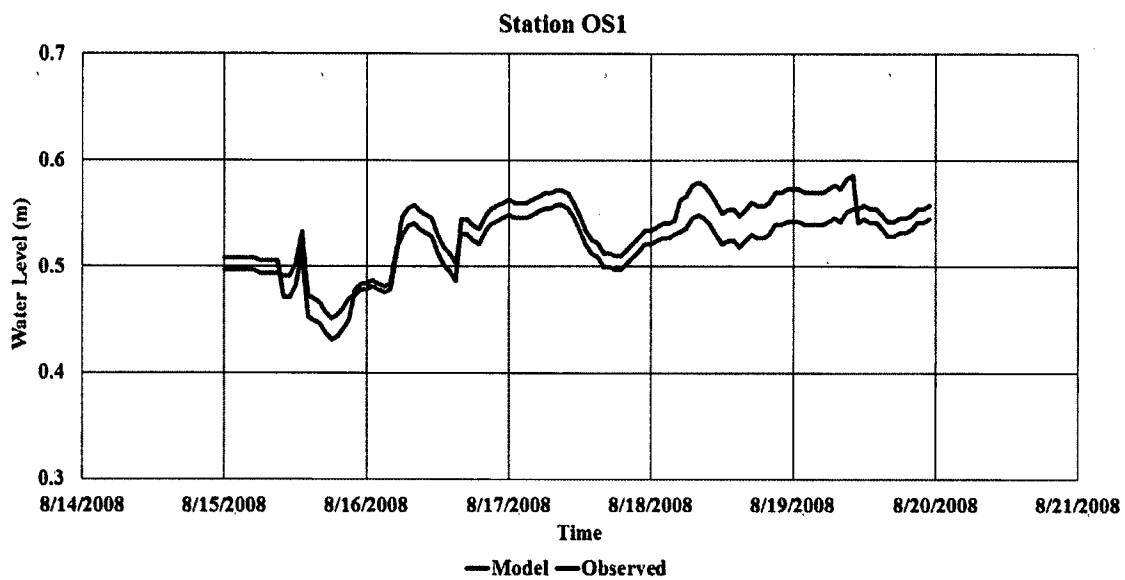


Figure 4-20: Model calibration for OS1.

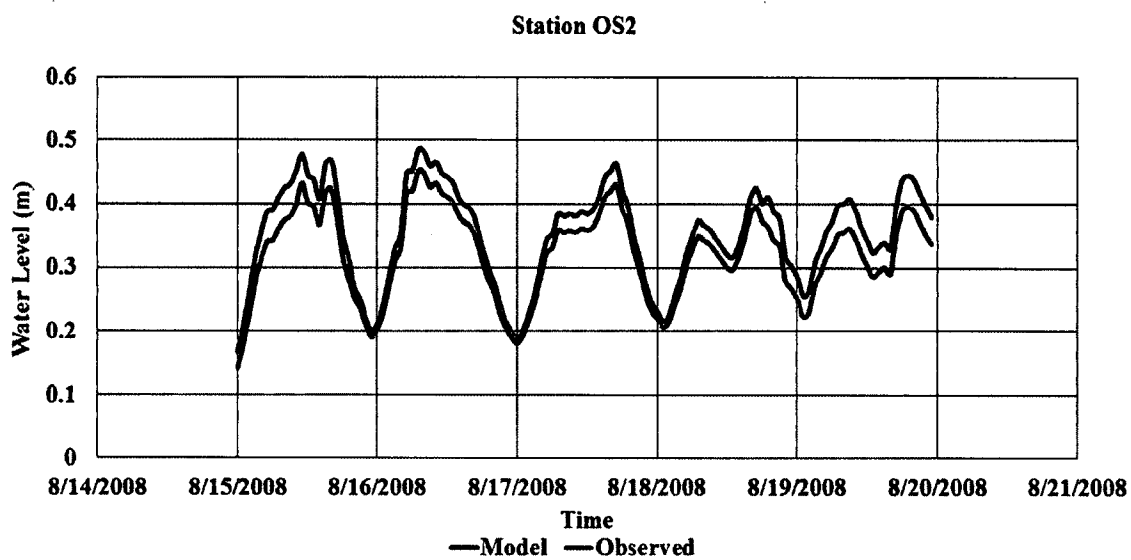


Figure 4-21: Model calibration for OS2.

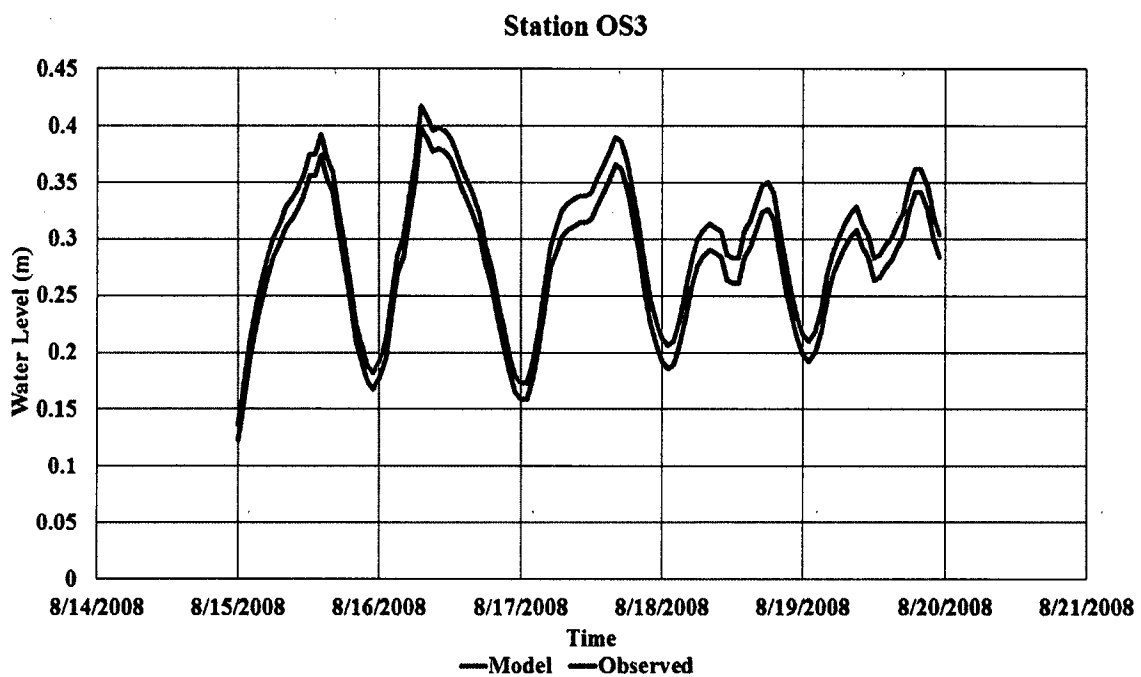


Figure 4-22: Model calibration for OS3.

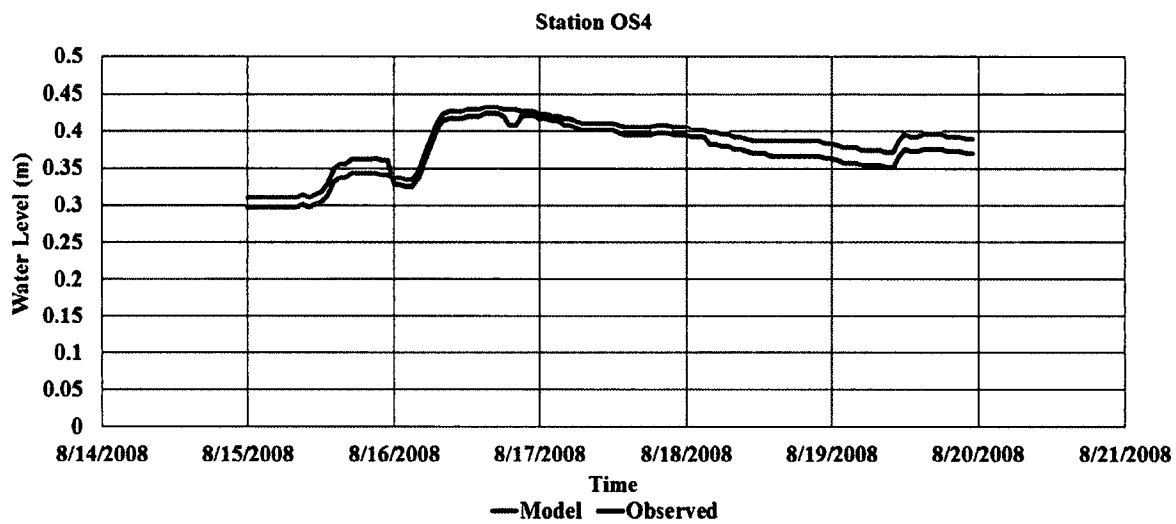


Figure 4-23: Model calibration for OS4.

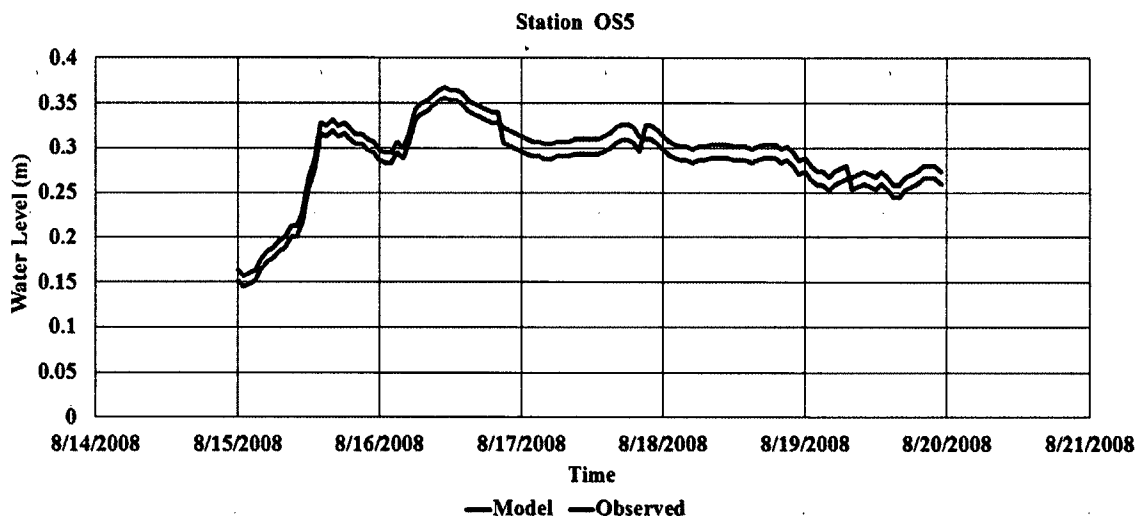


Figure 4-24: Model calibration for OS5.

The model shows good approximations of the observed water levels. To ensure that the model captures the essentials of the underlying waves and currents, the hydrodynamic model skill was evaluated using the ‘index of agreement’ or skill as proposed by Willmott (1981). Along with skill MAE (Mean Absolute Error) was also calculated to check calibration success. Skill varied between 0 (complete disagreement) and 1 (perfect agreement) where the MAE value of 0 suggested perfect agreement. Skill is dimensionless so comparison can be made over multiple parameters. Calculated MAE and skill are presented in **Table 4-5**.

Table 4-5: Comparison of RMAE and skill for calibration study.

Station	MAE	Skill
OS1	0.001	0.923
OS2	0.008	0.995
OS3	0.004	0.999
OS4	0.002	0.998
OS5	0.002	0.999

A conclusion of this calibration study can be made that, based on a calibration of the bed roughness in combination with default settings, the flow model yielded a good

agreement in surface elevation, flow from the Gulf through the estuary. The agreement between observed and modeled results makes this application a robust tool to investigate hydrodynamics and wave in future applications.

4.4.8 Model Validation

The model verification was performed for an approximate fifteen-day period, beginning 00 hours August 20, 2008, and ending 00 hours September 05, 2008. The modeled water surface elevations at the observation stations were selected and compared with measured ones for validation.

Model validations at different observation points are shown from **Figure 4-25** to **Figure 4-29**.

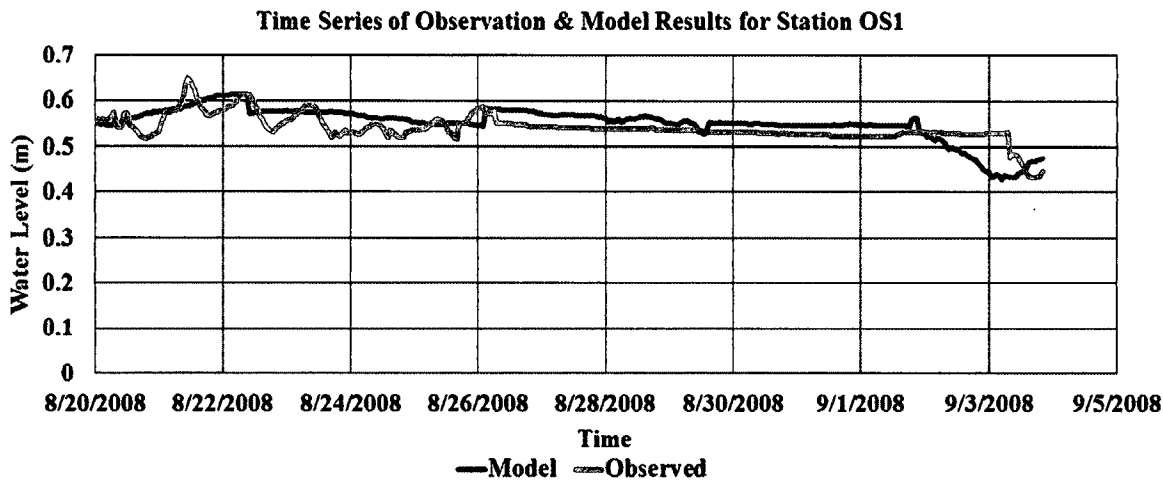


Figure 4-25: Model validation for OS1.

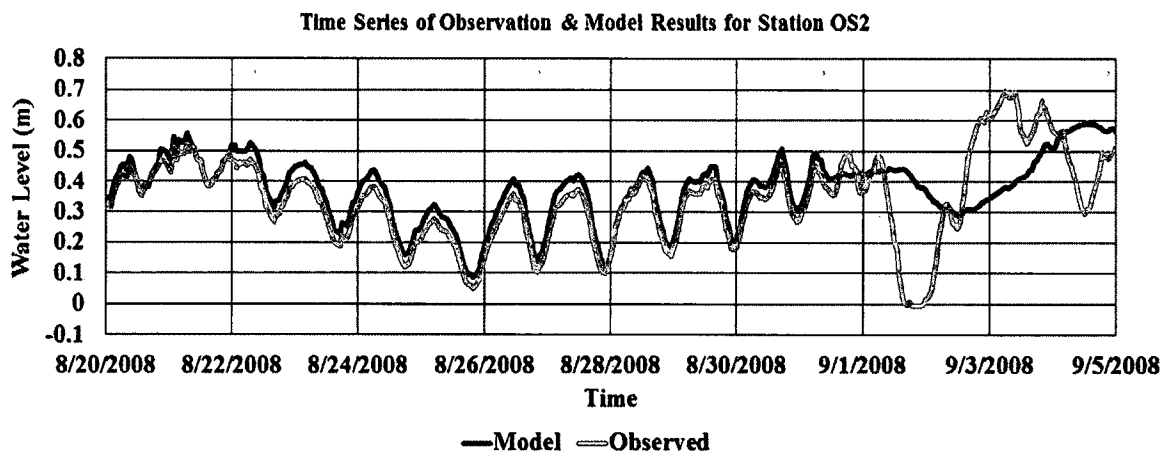


Figure 4-26: Model validation for OS2.

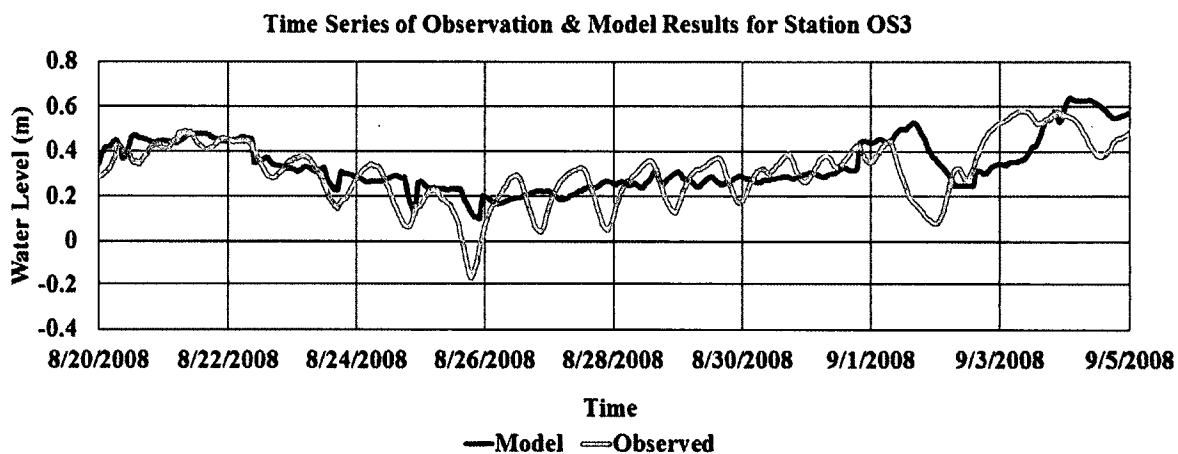


Figure 4-27: Model validation for OS3.

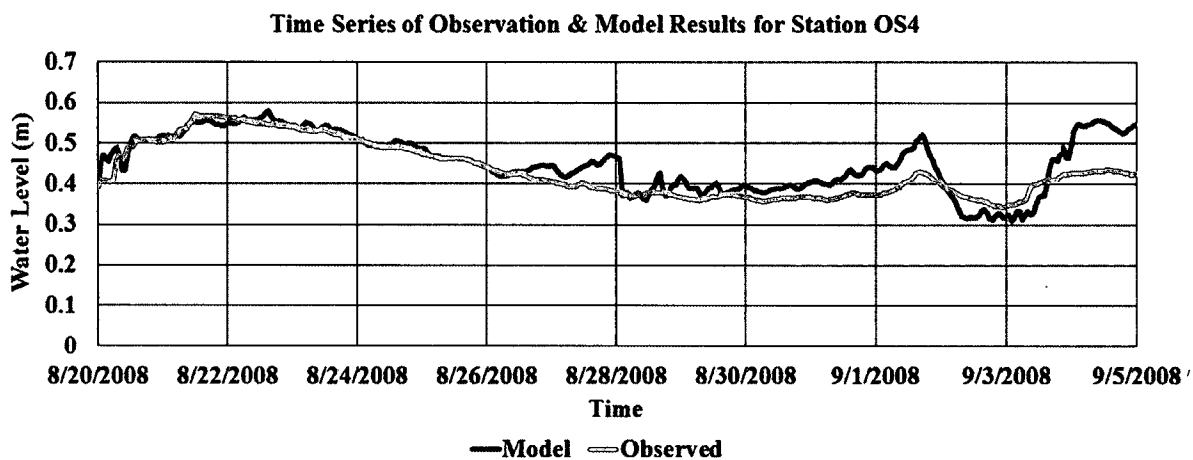


Figure 4-28: Model validation for OS4.

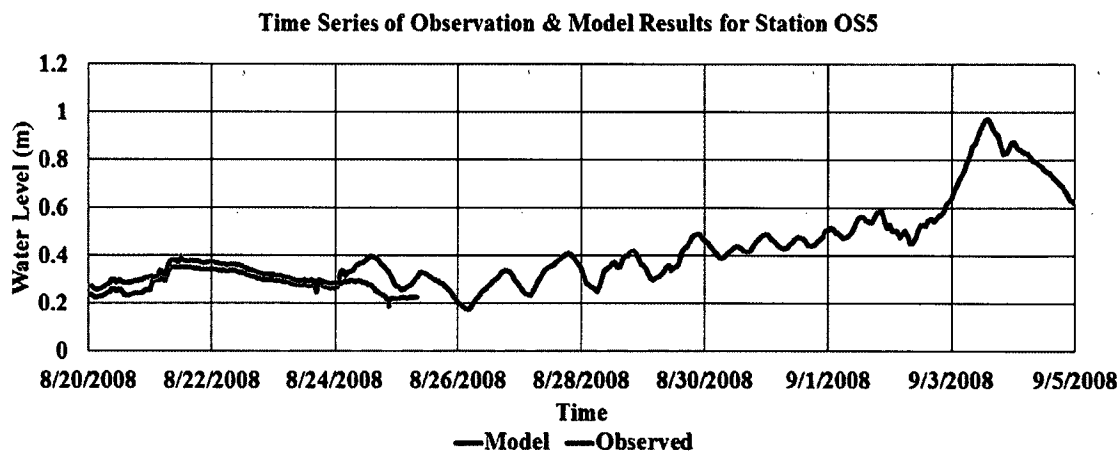


Figure 4-29: Model validation for OS5.

To ensure that the model captures the essentials of the underlying waves and currents, the hydrodynamic model skill and RMSE (Root Mean Square Error) were calculated and presented in **Table 4-6**.

Table 4-6: RSME and Skill comparisons for observation points.

Observation Points	RMSE	Skill
OS1	0.030	0.810
OS2	0.110	0.700
OS3	0.114	0.718
OS4	0.051	0.753
OS5	0.049	0.740

Skill value suggest a fair to good agreement for all the observation points.

4.4.9 Model Circulation Characteristics

For investigating the circulation characteristics of the Lake Calcasieu system, the final calibrated and validated model served as a useful tool. Current velocities and flow rates can be determined at any point in the model domain using model inputs of bathymetry and tide data. Hydrodynamic model possesses a very useful feature where a limited amount

of collected data can be continued to conclude the physical attributes of the system in areas where no physical data record exists.

Ebb dominance was found in the overall system after examining the flows in and out of the main channel. This is anticipated because of the micro tidal forcing within the Gulf of Mexico with the fresh water incessantly flowing inward, the system required less water to enter from the Gulf of Mexico on a flood cycle, in comparison to flow required to exit on an ebb cycle. Flow velocities are the strongest along the main channel of the Calcasieu. Depth-averaged velocities in the inlet generally peaked around 0.6-1.2 m/s for ebbing tides, and 0.4-0.8 m/s for flooding tides.

A close-up of the model output has been analyzed through extracting results at three different sections as shown in **Figure 4-30**.

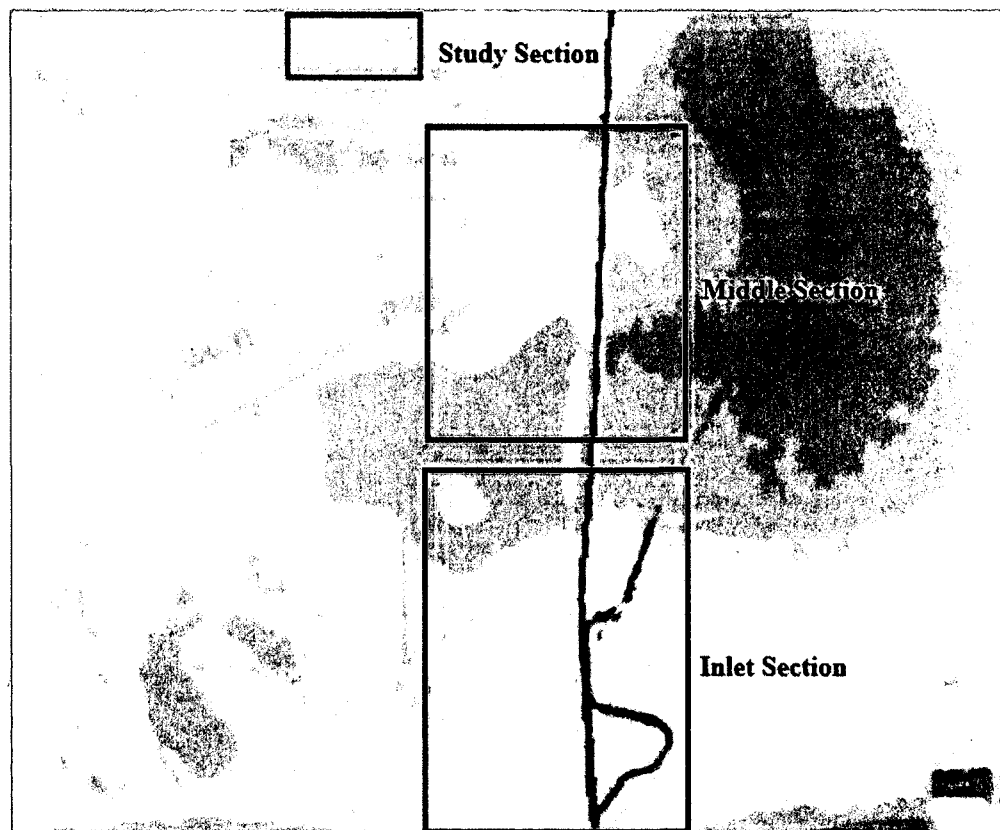


Figure 4-30: Sections of the model area to extract flow velocity results.

Ebb velocity and flood velocity contours for all these sections were presented in **Figure 4-31** to **Figure 4-36**. One tide cycle starting with ebb tide was analyzed for the model area. Maximum velocities found during the ebb tide for the inlet and middle sections where velocity fluctuated insignificantly at the study section during a normal tidal cycle.

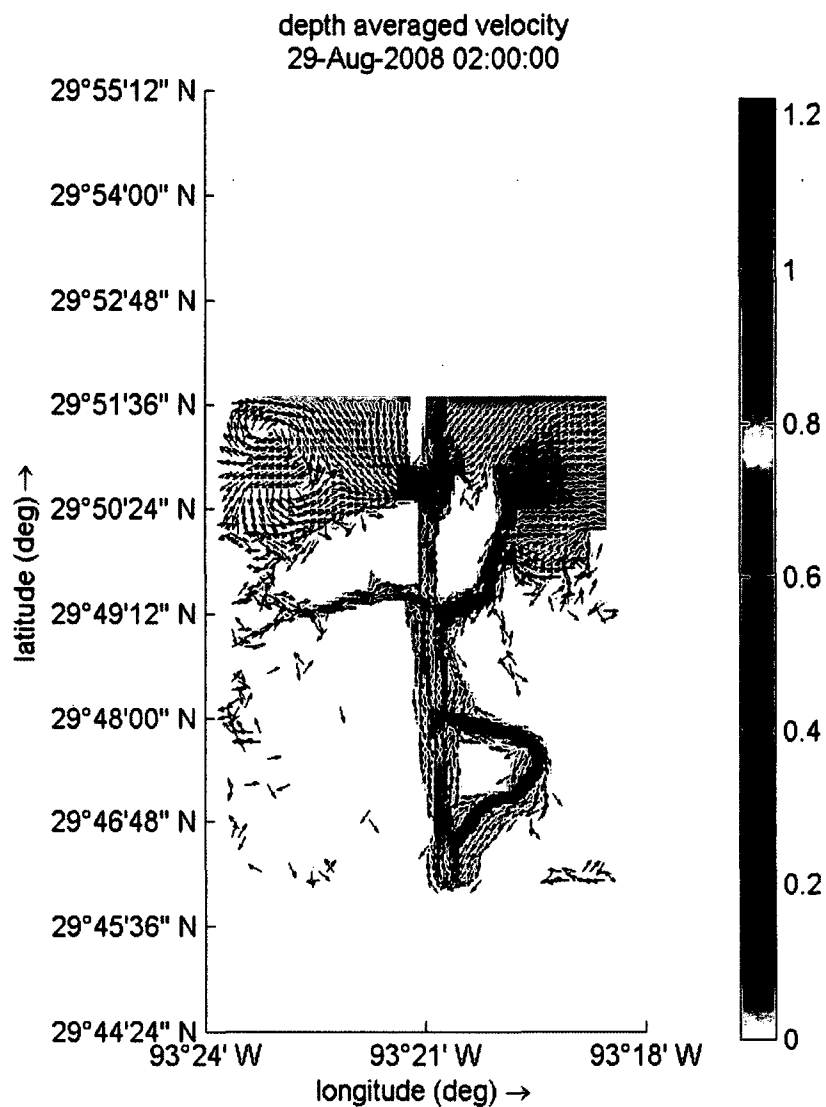


Figure 4-31: Flow velocity at the inlet section where maximum ebb velocities occur.

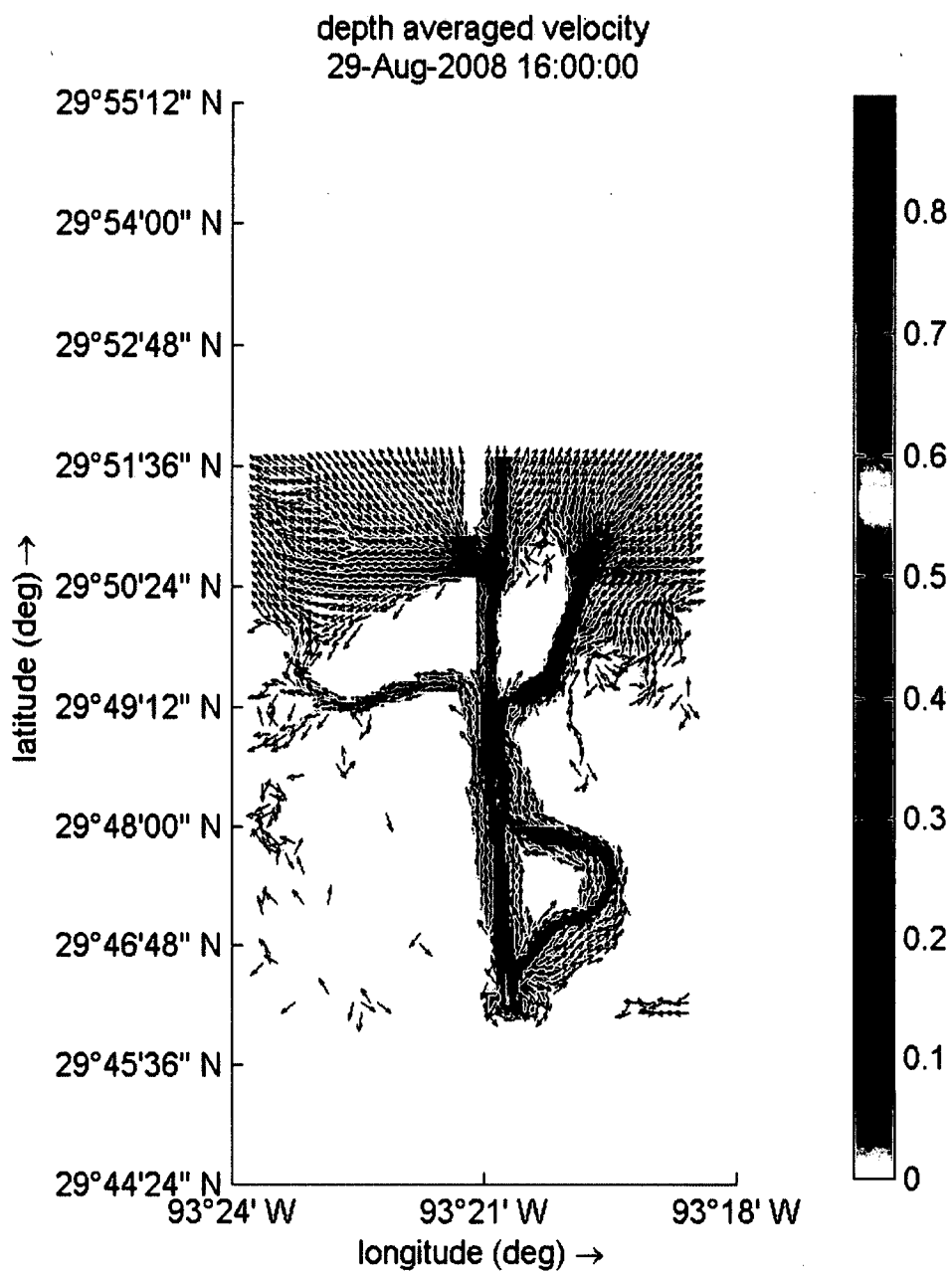


Figure 4-32: Flow velocity at the inlet section where maximum flood velocities occur.

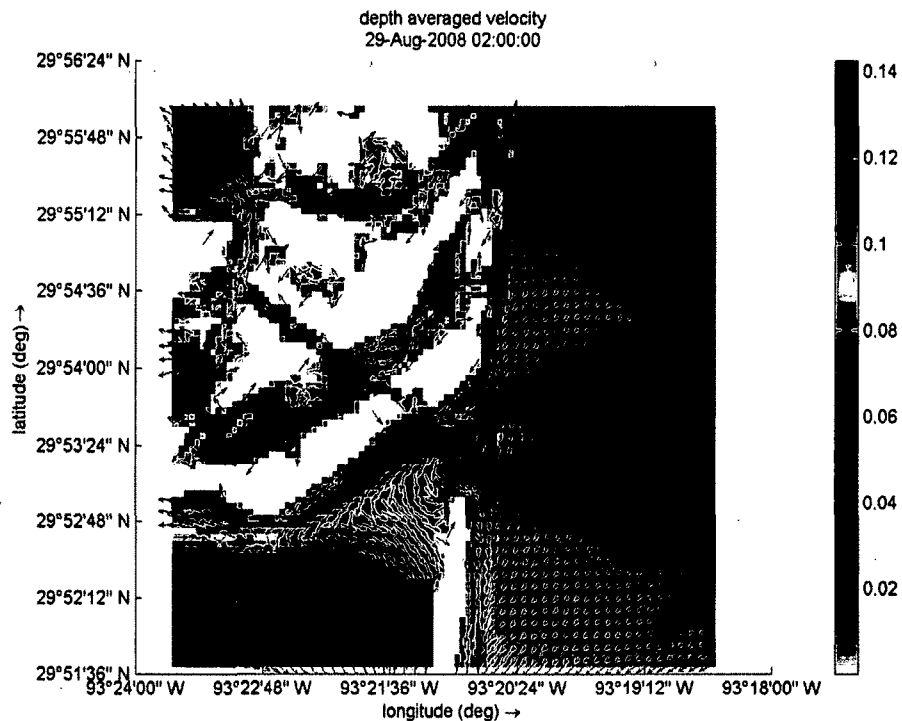


Figure 4-33: Flow velocity at the middle section where maximum flood velocities occur.

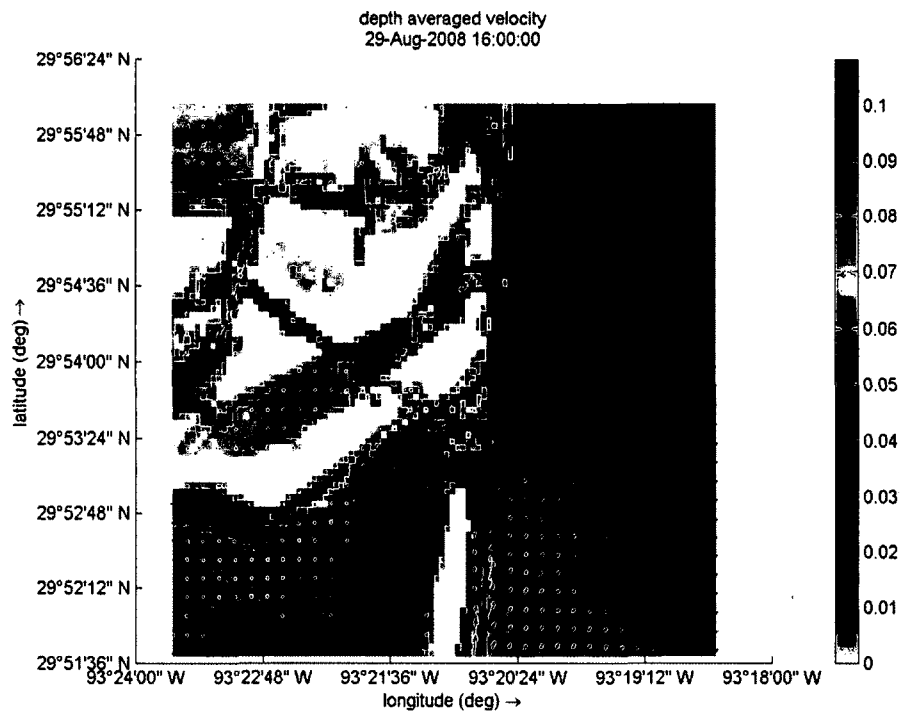


Figure 4-34: Flow velocity at the middle section where maximum flood velocities occur.

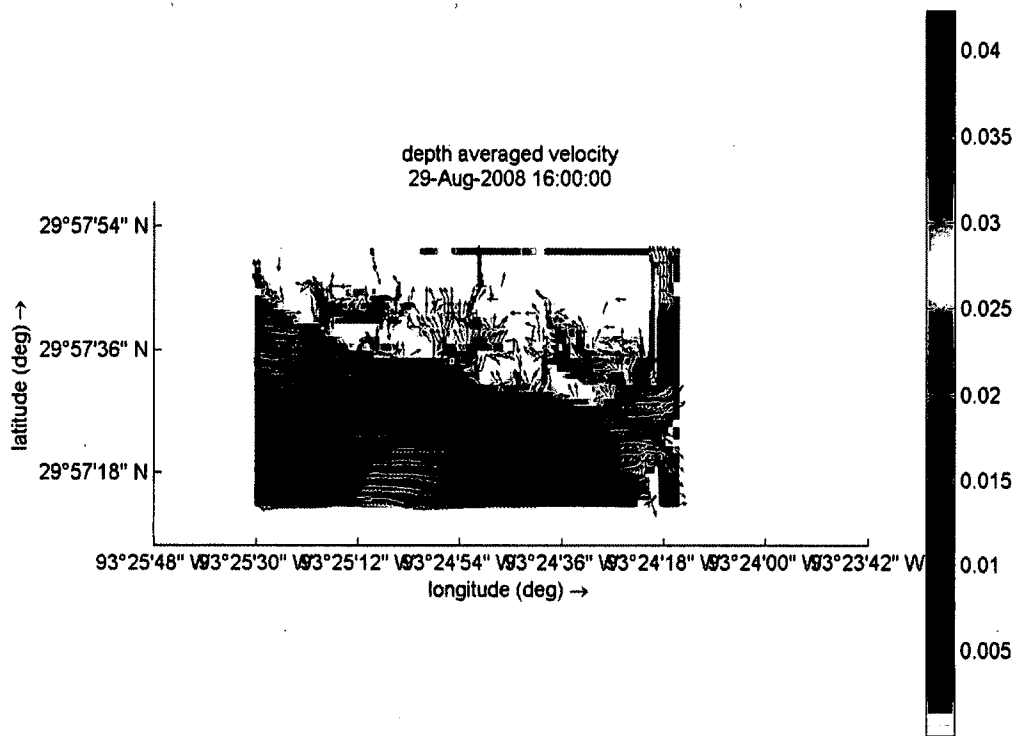


Figure 4-35: Flow velocity at the study section where maximum ebb velocities occur.

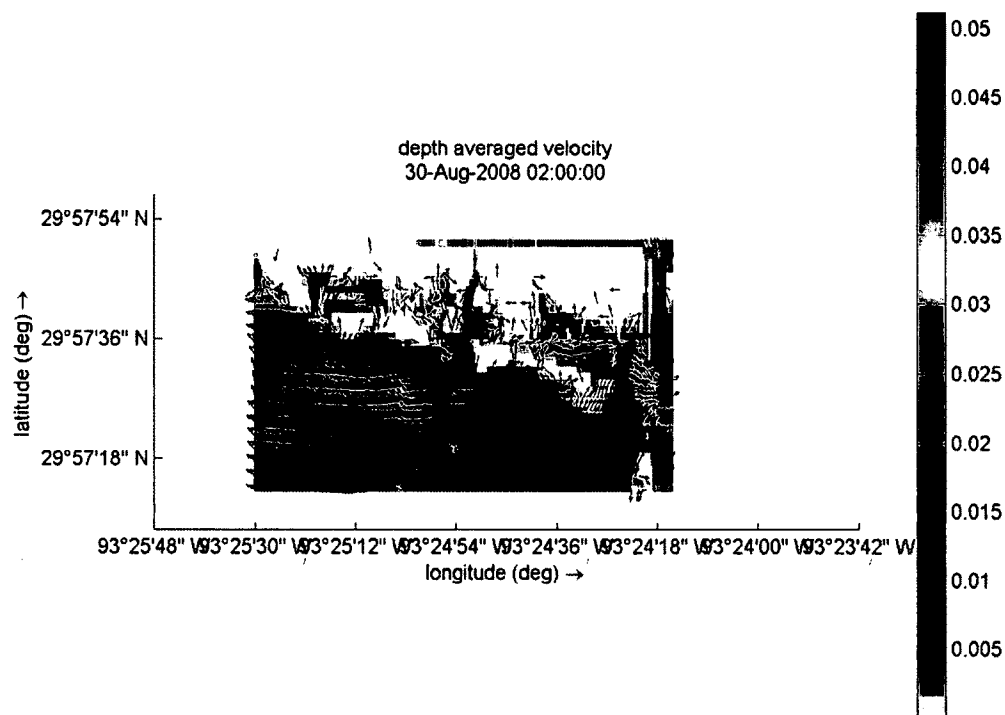


Figure 4-36: Flow velocity at the study section where maximum flood velocities occur.

CHAPTER 5

STUDY ON THE IMPACT OF HURRICANE IKE OVER *SPARTINA ALTERNIFLORA* MARSH SYSTEM

5.1 Introduction

The Louisiana and Texas (LATEX) Gulf Coast is located in a high tropical storm activity area. The Gulf Coast is typically approached by hurricanes through the northwestern Caribbean Sea. Most likely some of the intense hurricanes which started off thousands of miles away in the tropical Atlantic strike the Gulf Coast and other storms that hit the Gulf States develop in the Gulf of Mexico. Louisiana has a feature that is flat, a marshy coastline which intensifies hurricane danger. Approaching hurricane wave can reach from 10 to 20 feet high and spread as far as 25 miles inland. Coastal marsh damage during a hurricane period is not still well understood. According to CWPPRA (2012) project evaluation report, Cycle-1 of CS-28 project went through significant damages during Hurricane Rita where damage during hurricane Ike was moderate in terms of mass erosion incidence. It was noticed prior to this study that the model domain experienced two consecutive severe hurricanes, Hurricane Ike and Hurricane Gustav, with extreme precipitations during a very short period of time. However, this is not a common case, and moreover, the heavy precipitation during Hurricane Gustav flooded the study area before Hurricane Ike made its landfall. All these effects were included in this study to investigate the extreme conditions.

The principal objective of this chapter is to explore Hurricane Ike impact on the marsh mudflat of the study area. The calibrated and validated model from Chapter Four was used during this study through introducing hurricane information in the wave model. Shear stress generated on mud flat is the dominant contributor for marsh erosion. Different modeling scenarios were investigated during this study to understand the situation that creates maximum shear stress on the marsh bed and the study is included in this chapter. The hurricane effect on vegetated marsh bed was also studied through the vegetation model. Resulted stress from this chapter will be used in the next chapter to analyze the erosion of marsh flat under a hurricane. Contribution of vegetation (*Spartina alterniflora*) shoot system in terms of reducing hurricane impact is also studied in this chapter.

5.2 Chapter Structure

This chapter is structured as follows: Section 5.3 gives an overview of Hurricane Ike characteristics for the study area. Section 5.4 describes the set-up, boundary forcing and validation of the wave model. Section 5.5 presents different model scenarios to generate extreme hurricane conditions, and Section 5.6 presents the results of the modeling study.

5.3 Hurricane Ike

After entering the Gulf on September 9, 2008 at UTC 2030, Ike moved northwest and its wind field was expanded and strengthened until it reached a continuous 10 min wind speed of 37 m/s. When the center of the storm was approximately 300 km south of Isles Dernieres, LA, with tropical storm force winds extending 400 km from storm's center, the radius of maximum winds was 148 km at 0000 UTC on 12 September 2008 (31 h before landfall) (Berg 2009).

South of Isles Dernieres, LA (**Figure 5-1, Table 5-1**) tropical storm force winds broadened 400 km from the storm's center. At this point, significant wave heights were measured at over 8 m, 6 m, and 4 m in the mid-Gulf, to the south of Grand Isle, LA, and Galveston Island, respectively. Ike began to alter and track north-northwestward roughly around 13 h before landfall, then making landfall at Galveston Island, TX with a maximum wind speed of 41 m/s.

Table 5-1: Summary of Significant Times and Characteristics of Hurricane Ike.

Date-Time	Latitude	Longitude	Max Wind Velocity (m/s)	Category	Notes
Sep 01-0600 HR	17.2	37	13	Trop. Dep.	Trop.
Sep 04-0600 HR	22.4	55	54	4	Maximum Intensity
Sep 05-0430 HR	23.6	60.4	50	4	Enters SL18pTX33 Domain
Sep 05-1200 HR	23.4	62	46	3	OWI winds start
Sep 07-1300 HR	21	73.2	49	3	Landfall on Great Inagua
Sep 08-2100 HR	21.1	75.7	50	4	Landfall in Holguin Cuba
Sep 09-1400 HR	22.6	82.9	30	1	Landfall in Pinar del Rio Cuba
Sep 09-2300 HR	-	-	-	2	Enters Gulf of Mexico
Sep 12-0000 HR	26.1	90	37	2	
Sep 12-1200 HR	26.9	92.2	39	2	Peak in South Plaquemines
Sep 12-1800 HR	27.4	93	39	2	Shift in track WSE peak in NOLA
Sep 13-0000 HR	28.3	94.1	41	2	WSE peak in Lake Ponchartrain
Sep 13-0700 HR	29.3	94.7	41	2	Landfall at Galveston, TX
Sep 13-1200HR	30.3	95.2	37	1	
Sep 13-1800 HR	31.7	95.3	22	Trop. Storm	
Sep 14-0600 HR	35.5	93.7	15	Trop. Dep.	OWI winds end.
Sep 15-1200 HR		-			END

On 12 September 2008, Ike arrived at its max wind speed of 41 m/s in the Gulf of Mexico at 0430 UTC. After the strength weakened slightly, later on 12 September 2008, Ike reached a peak wind speed of 41 m/s before and at landfall at Galveston, TX, at 0700 UTC 13 September 2008. In Chambers County, TX, located to the northeast of Galveston Island, Ike formed the highest measured surge at landfall of 5.3 m **Figure 5-1** (FEMA 2008).

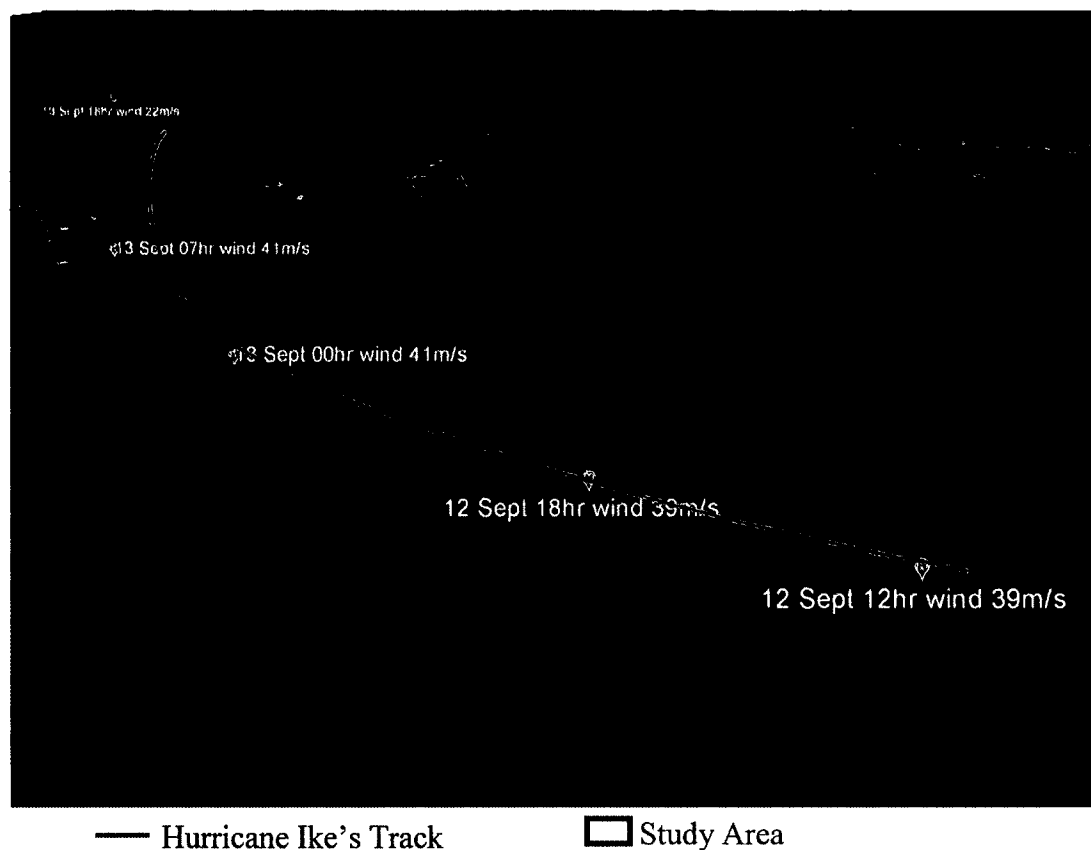


Figure 5-1: Hurricane Ike tracking with corresponding wind speed data.

From the study of the hurricane's path and time of landfall adjoining to our study area, as shown in **Table 5-1** and **Figure 5-1**, the simulation time for coupled model with Hurricane Ike force was selected for the period of 00 hours, 12 September, 2008, to 00 hours, 14 September, 2008.

5.4 Model Setup

5.4.1 Model Grid and Bathymetry

The same grid and bathymetry profile assigned to the flow and wave model in Chapter Four was used in this study to investigate hurricane impact and vegetation contribution. Model grids for flow and wave model are shown in **Figure 5-2** and **Figure 5-3**, respectively.

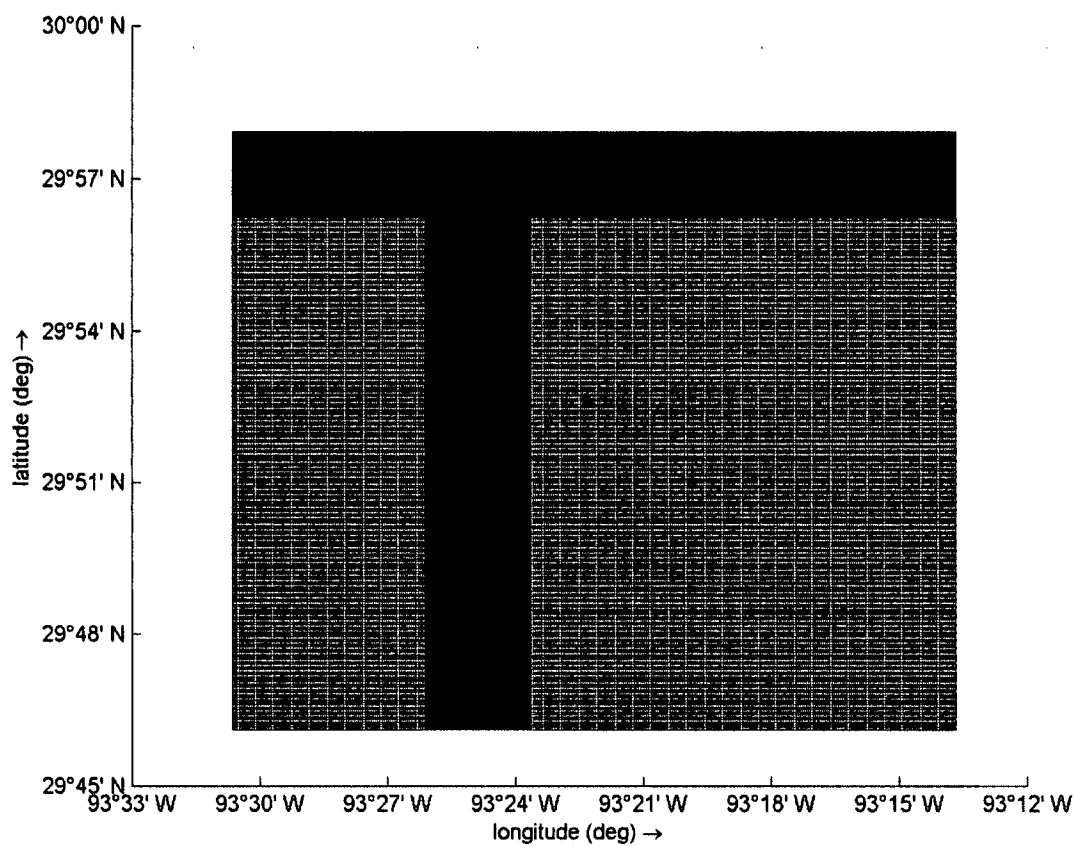


Figure 5-2: Model flow grid.

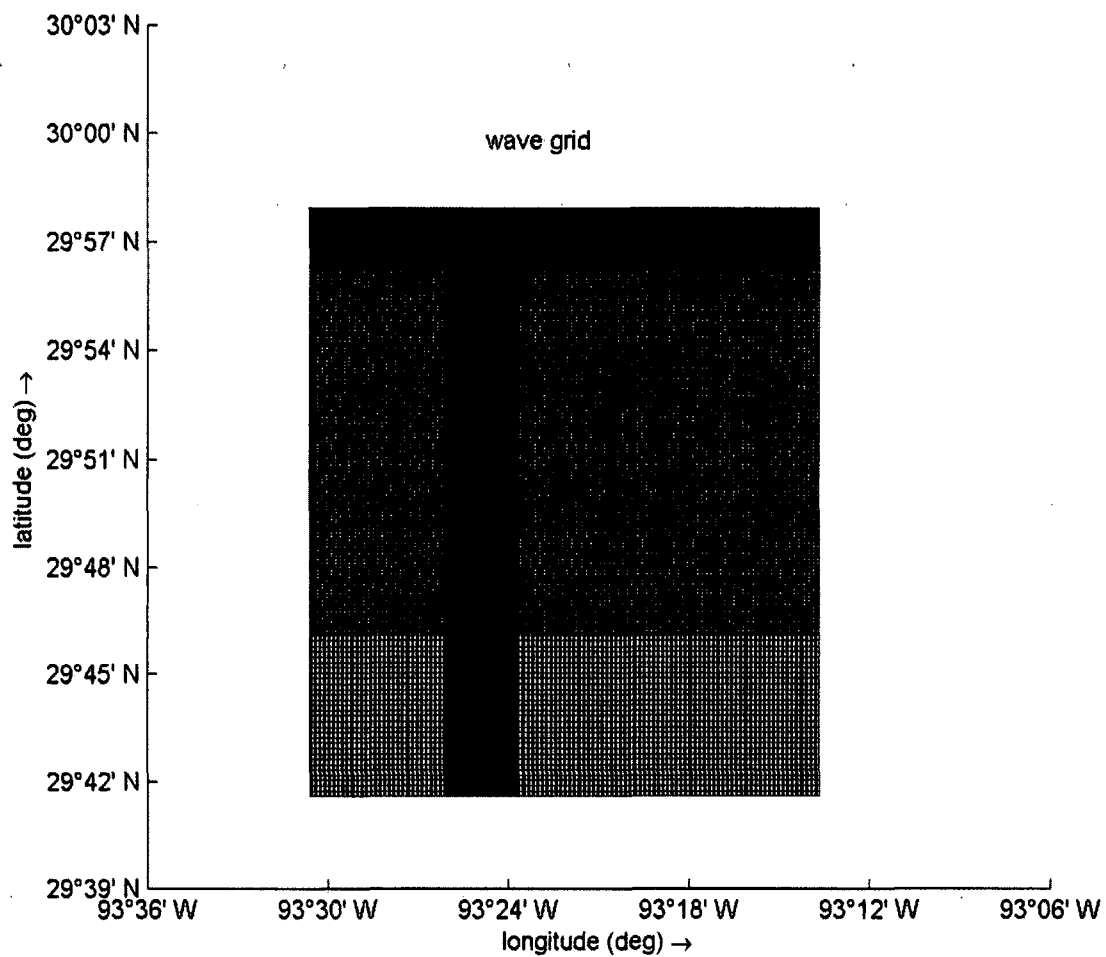


Figure 5-3: Model wave grid.

Flow and Wave model bathymetry are obtained from Chapter Four and are presented in **Figure 5-4** and **Figure 5-5**, respectively. The depth is particularly mentioned at the grid cell corner.

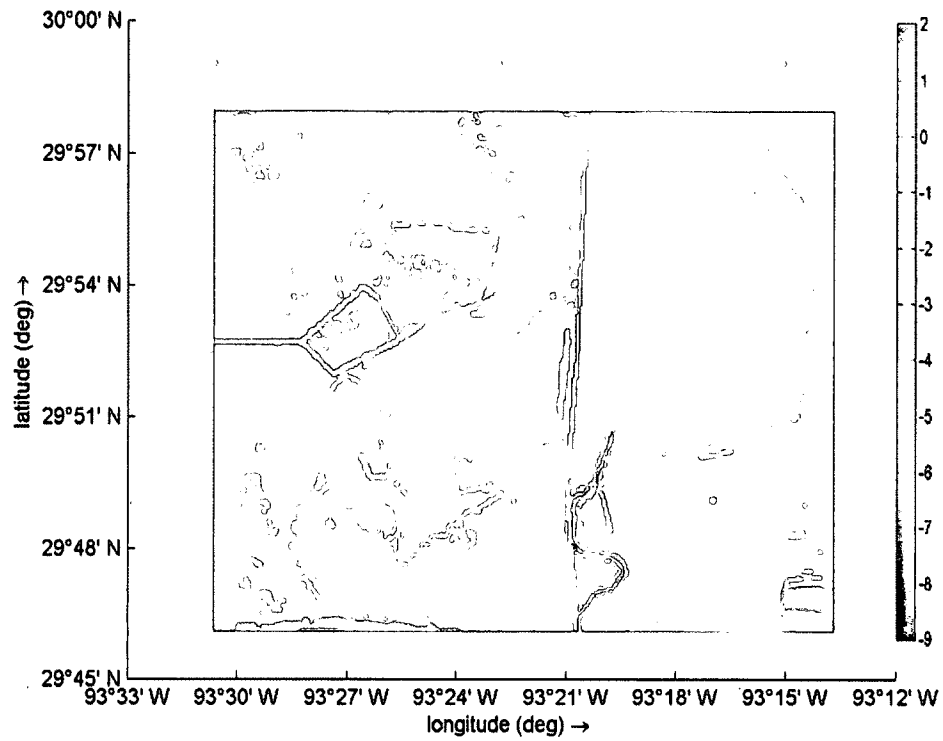


Figure 5-4: Flow bathymetry

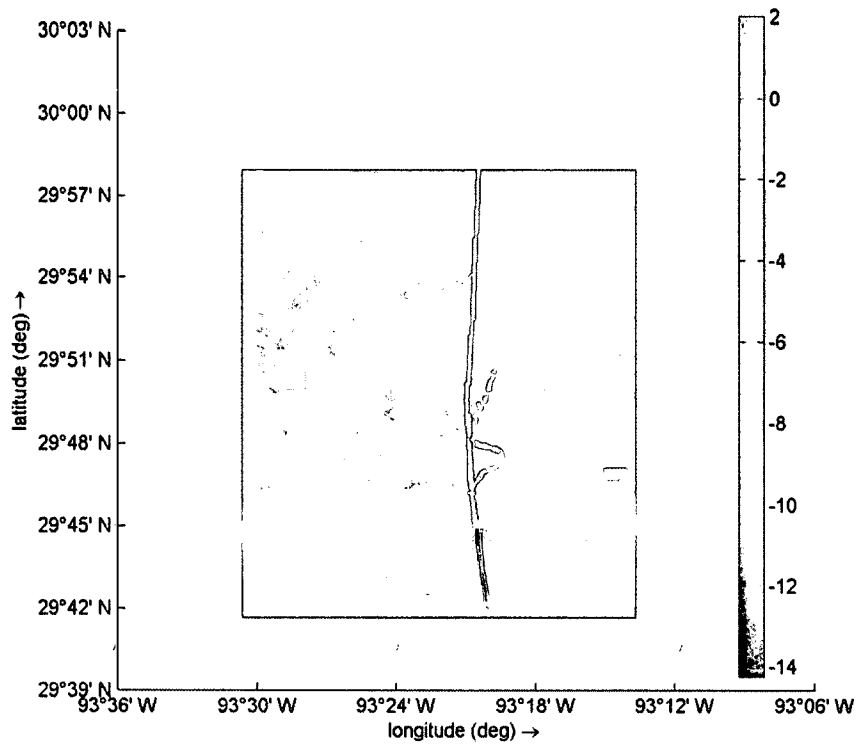


Figure 5-5: Wave bathymetry

5.4.2 Initial Condition

As discussed earlier, the coupled model initial condition mainly depends on the flow module so only the flow initial condition is discussed here. Both uniform and spatially varied initial conditions can be used by Delft3D. Preparing an initial conditions file is one of many other ways to define the initial condition. One can identify the initial conditions file easily because it is a typical ASCII file with an “ini” extension containing the required information in a gridded format. Also, by using hotstart file, initial condition can be defined. In contrast with the initial conditions file, the restart/hotstart file is a binary file which is an output of a previous run. Restart file saved during validation study for 12 September, 00 hours was used as the initial condition of the hydrodynamic model. The initial condition of the flow model which is termed “Submerged” condition is presented in **Figure 5-6**.

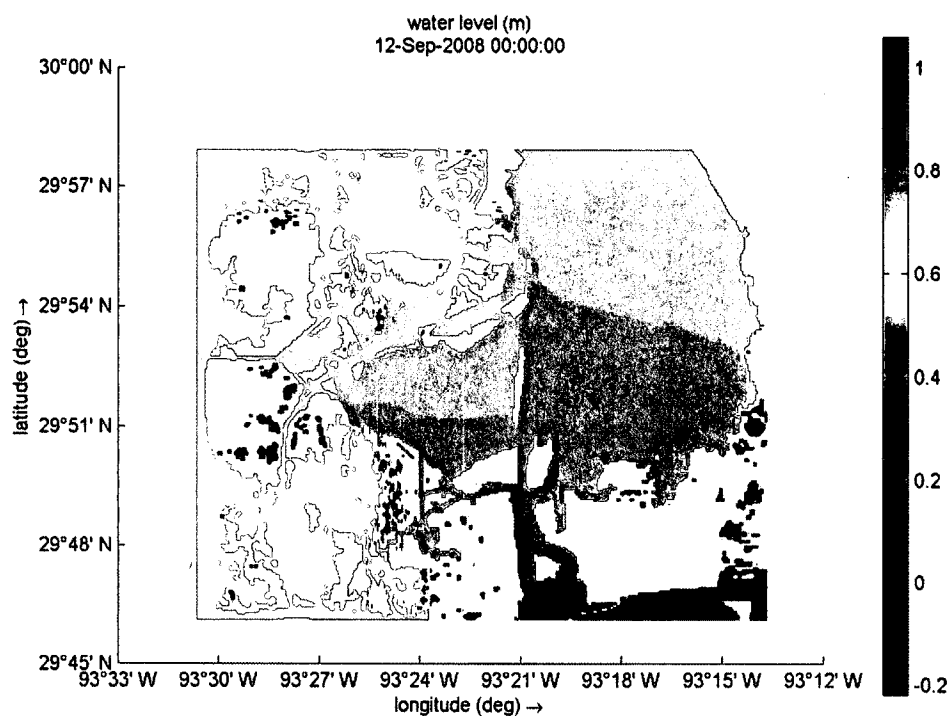


Figure 5-6: Submerged initial condition.

Along with the submerged initial condition, another initial condition termed “Dry” condition was selected and used in this research to understand the effect of drought condition in the model domain prior to a hurricane. This concept emerges from the CWPPRA project evaluation report that states that the effect of Hurricane Rita (single hurricane over a short period) was severe compared to Hurricane Ike (came along with Hurricane Gustave during a short period). In order to conduct an in-depth study of the marsh bed behavior under a hurricane-induced wave and current actions, the regular water level in the model domain was also considered as an initial condition. In this dissertation, the original initial condition that was extracted from a previous simulation run for 00 hours September 12 is termed submerged initial condition and the special one which is the regular water level condition (selected restart file: 00 hours August 15), prior to Hurricane Gustav effect will be termed as dry initial condition. **Figure 5-7** represents the dry initial condition that was used in this study.

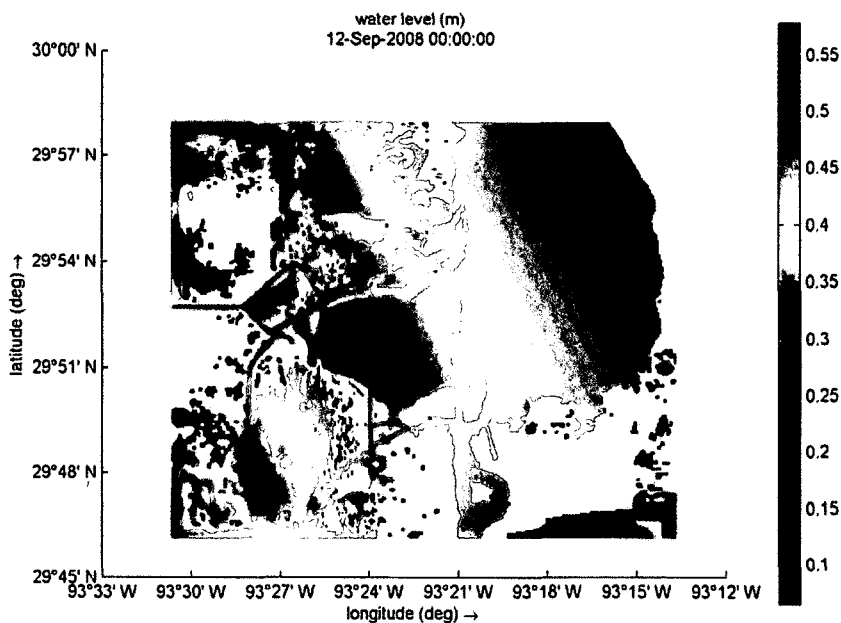


Figure 5-7: Dry initial condition.

5.4.3 Boundary Condition

It should be noted that the wave flow coupled model with inclusion of Hurricane Ike discussed in this chapter is just a part of the overall model that was validated in Chapter Four. The overall model discussed in Chapter Four was for the period of 30 days, from 15 August 2008 to 15 September 2008. On the other hand, the hurricane forced coupled model discussed in this chapter was for the period of 48 hours starting from the beginning of 12 September 2008 and ending at the end of 14 September 2008. All the boundary conditions for the Flow model were the same as discussed earlier but only for this short simulation period. To make it simple for the readers, the boundary forcing graph for the flow model during this period is also included in this chapter.

5.4.3.1 Flow

Flow boundary condition was applied from three sides of the domain in the form of the water level. Neumann boundary or zero cross-boundary water-level gradient condition was applied throughout the north side during simulation. Boundary condition data were used in the model are presented in **Figure 5-8**, **Figure 5-9** and **Figure 5-10**.

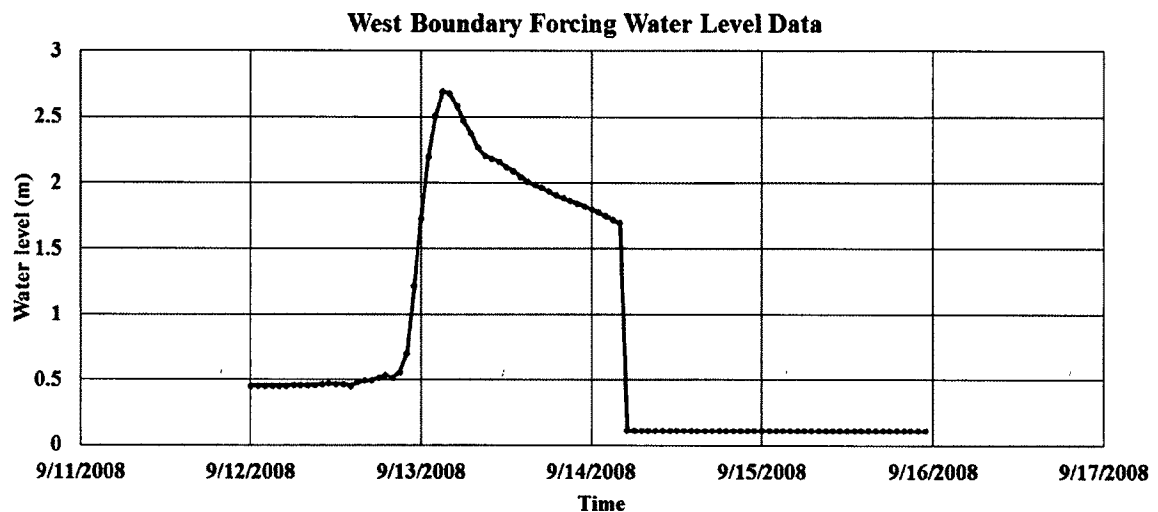


Figure 5-8: West boundary condition of the model.

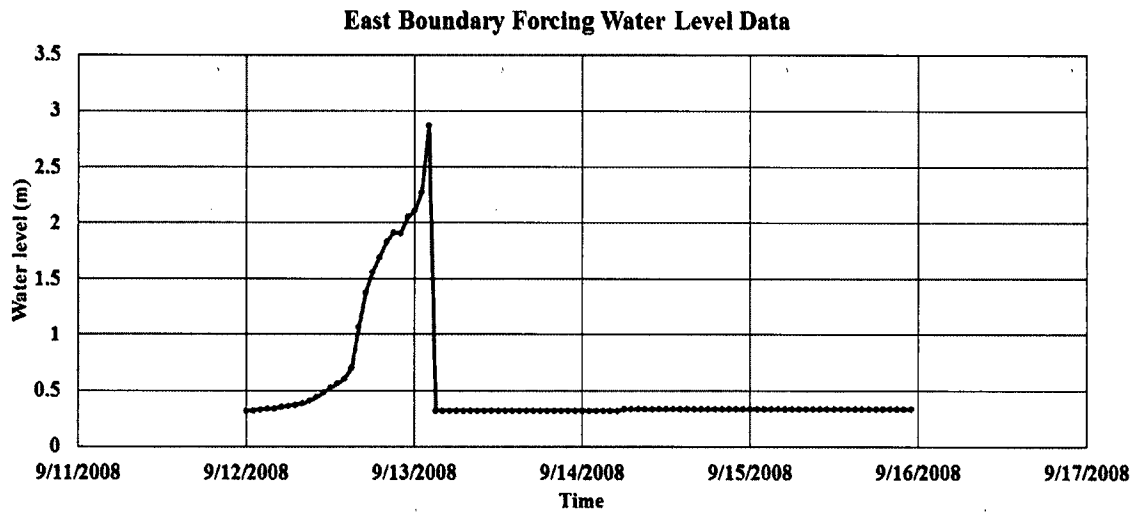


Figure 5-9: East boundary condition of the model.

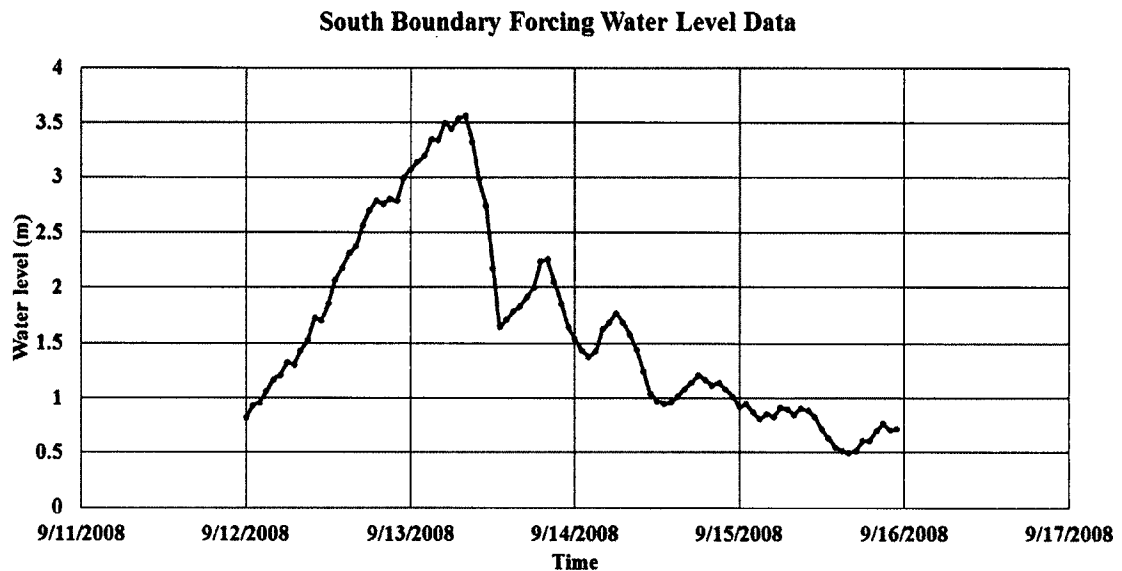


Figure 5-10: South boundary condition of the model.

5.4.3.1.1 Wind forcing

Based on the limitation of wind data collection station, wind data collected from the Calcasieu Pass station was used for wind forcing in the entire flow domain. **Figure 5-11** shows the wind speed and wind directions applied on the model for the simulation period.

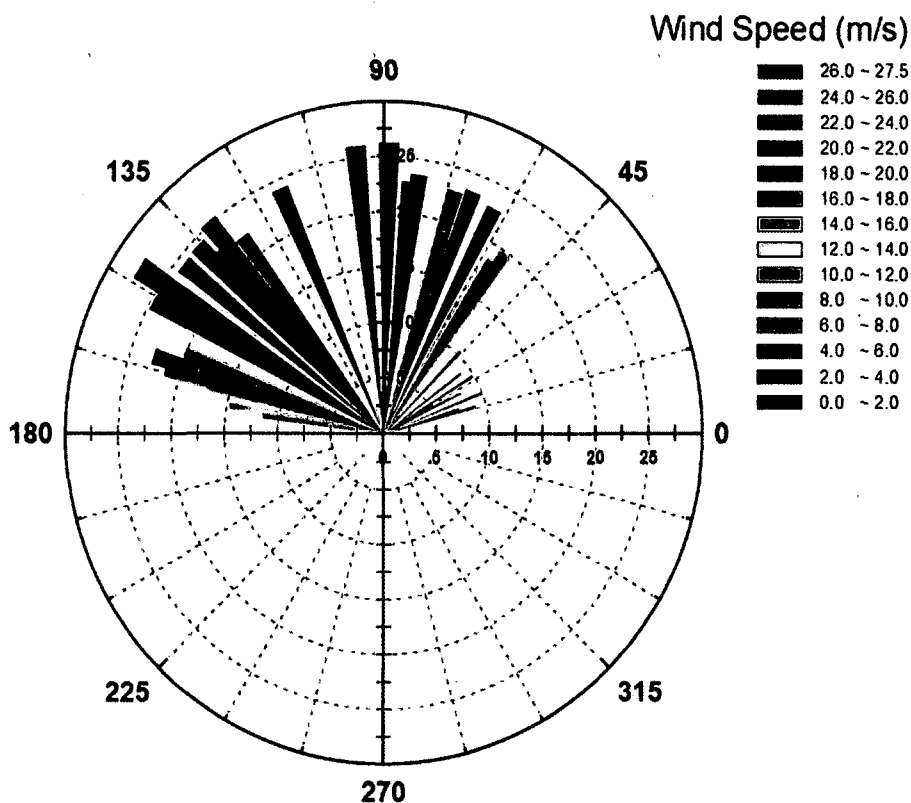


Figure 5-11: Wind rose (speed and direction) at Calcasieu Pass for the period of 12 September, 2008 to 15 September, 2008 used in the Hydrodynamics model.

5.4.3.2 Wave Model

Wave model boundary forcing data was collected for the simulation period from Hurricane Ike study by East *et al.* (2008). Key wave forcing parameter such as significant wave height, mean period, wind velocity and directions were provided by including a self-written WAVECON file in the model directory. Details of WAVECON file is presented in **Figure C-1** in the **APPENDIX-C**. Significant wave height and mean period data obtained for Station NDBC 42305 are presented in **Figure 5-12** and **Figure 5-13**, respectively.

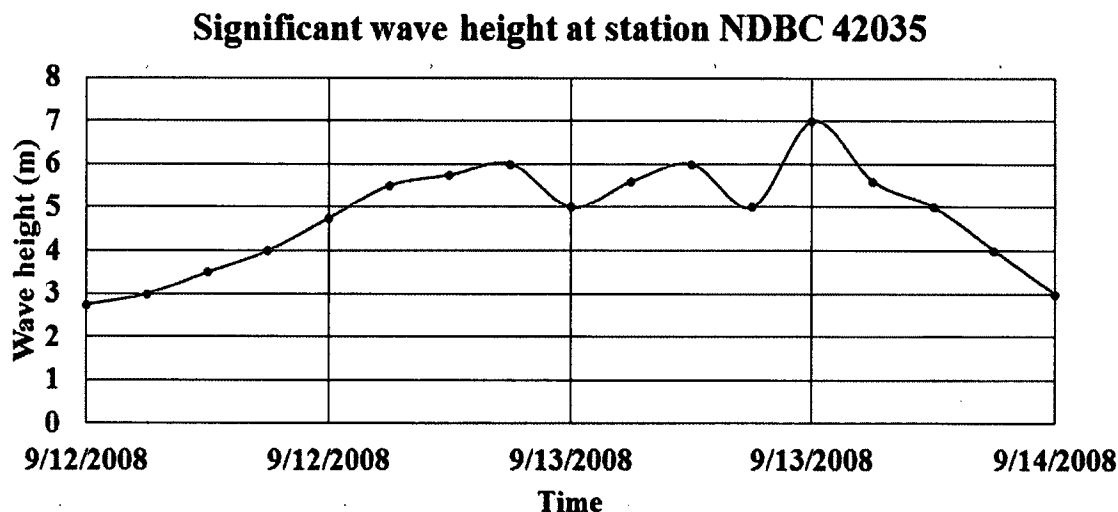


Figure 5-12: Significant wave height boundary data for the simulation period.

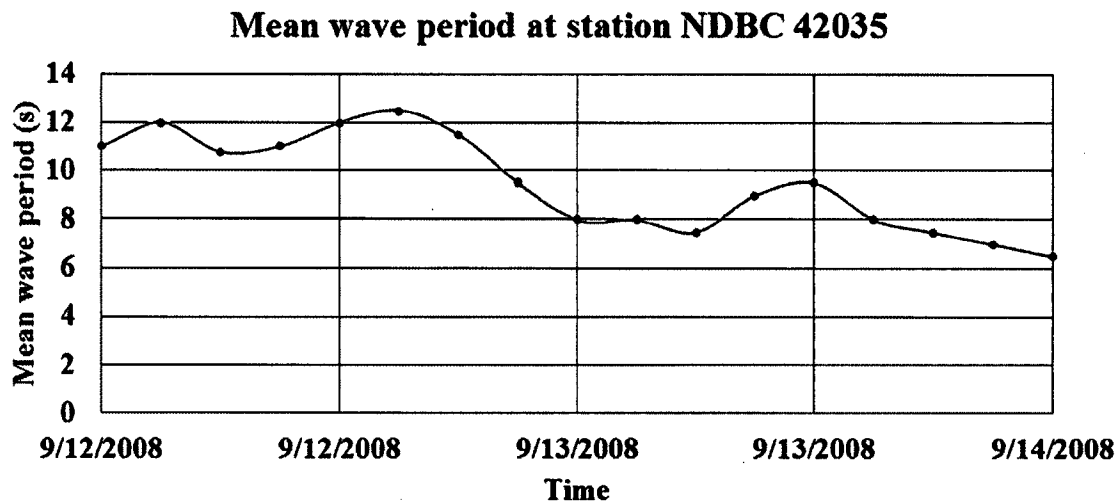


Figure 5-13: Significant wave height boundary data for the simulation period.

Wave direction during a hurricane is mainly controlled by the direction of the wind. Wind direction presented in **Figure 5-11** was used as wave direction during the simulation period.

5.4.4 Model Coupling

Finally, the flow model was set to run with a time step of 3.6 s. The time step is largely related with the size of the grid cell. The time step was checked by calculating the

Courant number. Time step of 3.6 s generates a Courant number below 10, which is acceptable for this kind of simulation (Delft 2007). The flow and wave modules of Delft3D communicate via the ‘online’ coupling method, in which the flow and wave modules communicate with each other at each time step, establishing a two-way wave current interaction. Wave condition was updated each (hydrodynamic) hour. Details of wave flow model input files are attached in **APPENDIX-A**.

5.4.5 Model Validation

Observed data for wave validation was provided by East *et al.* (2008). Only two stations positioned in the model domain of all 59 sensors served during this validation study as the remainders were located outside of the model domain. Wave heights in the observation stations were referenced to NAVD88. Locations of the two stations used for wave validation are presented in **Table 5-2**.

Table 5-2: Location of observation station.

Station Name	Latitude	Longitude
Calcasieu Pass	29.959716796875	-93.4212684631348
USGS LA-CAM-003	29.798883689880	-93.3296662597656

Figure 5-14 and **Figure 5-15** show the wave height comparison for the observation stations. Results show a satisfactory wave prediction in the coupled model.

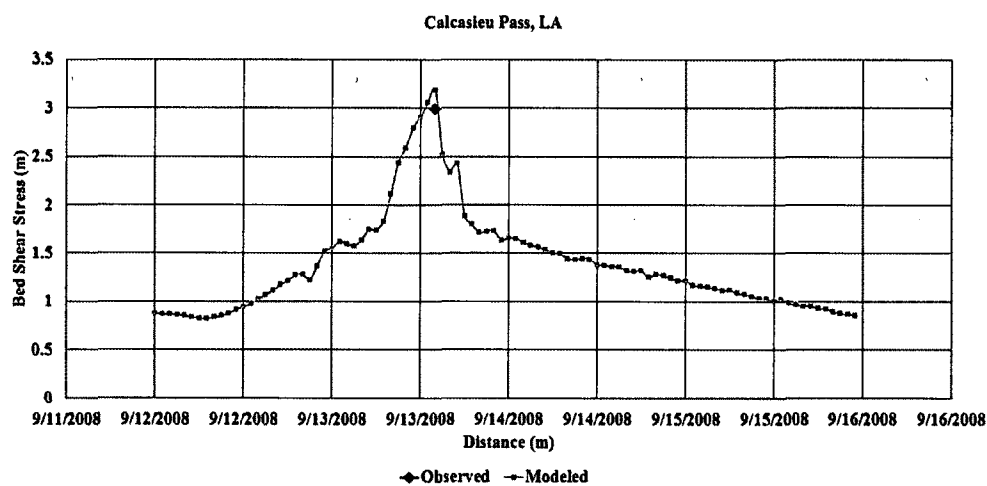


Figure 5-14: Validation time-series plot for Calcasieu Pass station.

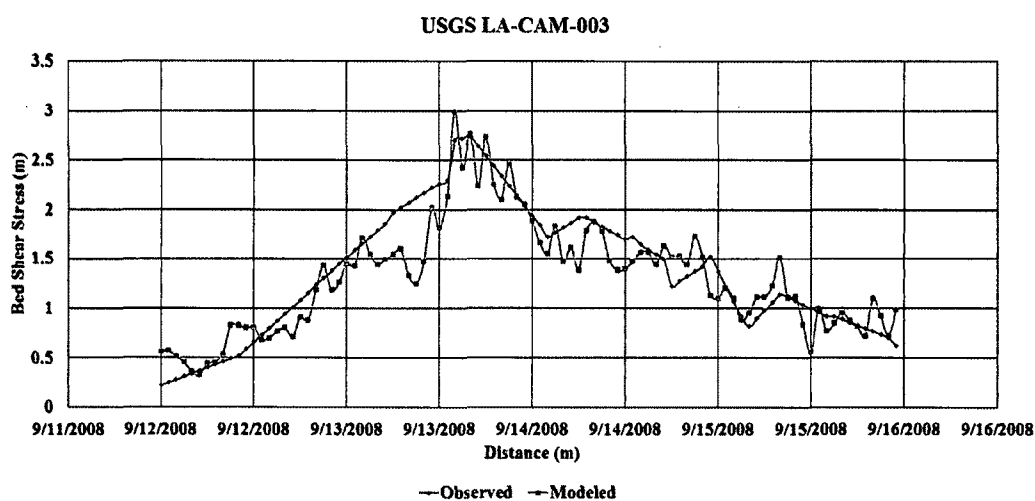


Figure 5-15: Validation time-series plot for USGS LA-CAM-003.

5.4.6 Vegetation Model

After the coupled model was successfully run and satisfactory wave results were obtained, the model was then modified by including vegetation on the mud flat. This study aimed to give an insight on the marsh contribution in reducing the impact of hurricane-induced wave and current. Vegetation cover was introduced to the model by including polygon map of the cover. **Figure 5-16** shows the polygon covering for Cycle-1, which was used to indicate the marsh field in the vegetation model study.

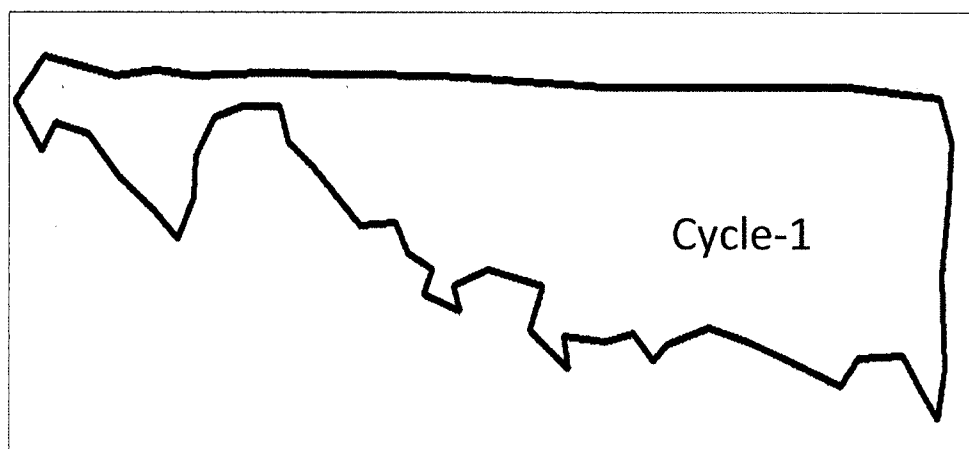


Figure 5-16: Polygon for Cycle-1 vegetation map input in the model.

Vegetation data were obtained from Station CRMS 6301 for *Spartina alterniflora Loisel* as presented in Chapter Two. They were used to define vegetation shoot system in the Delft3D coupled model. **Table 5-3** shows the key input parameters in Delft3D vegetation model. Vegetation model input files for Delft3D model is presented in **APPENDIX- B**.

Table 5-3: Vegetation input parameters.

Parameter	Value
Vegetation Type	Reed
Height	107 cm
Stem Diameter	0.6 cm
Plant Density	100/m ²

5.5 Model Scenarios

The validated wave flow coupled model with hurricane forcing was tested with a total of four scenarios to investigate the extreme condition for mass erosion. The scenarios tested in this study is explained in **Figure 5-17**.

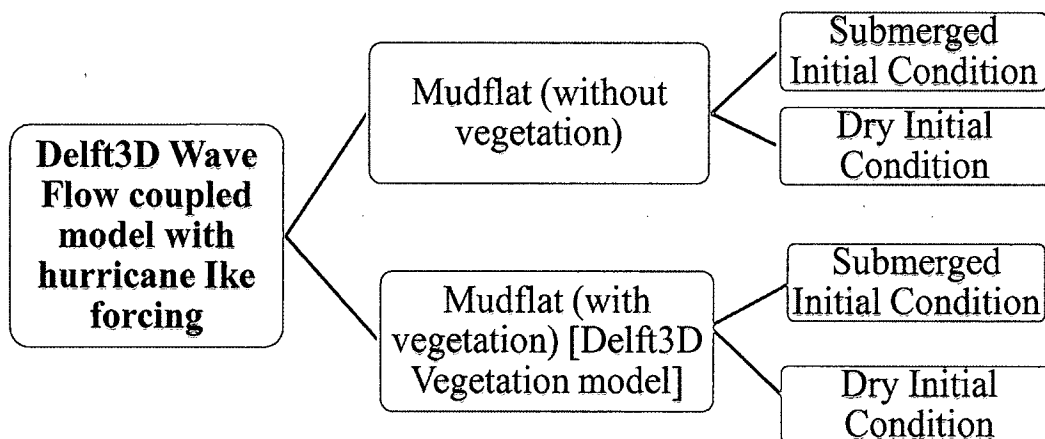


Figure 5-17: Modeling scenarios for Delft3D wave flow coupling with Hurricane Ike forcing.

5.6 Results

Result analysis was done by comparing all the results for the following two extreme periods during Hurricane Ike as mentioned in **Table 5-4**.

Table 5-4: Result observation condition.

Condition Name	Time
Land Fall	12 September at 18:00 hours
Peak Surge	13 September at 02:00 hours

All results for the study area extracted and viewed through using the segment presented in **Figure 5-18** of the model domain.

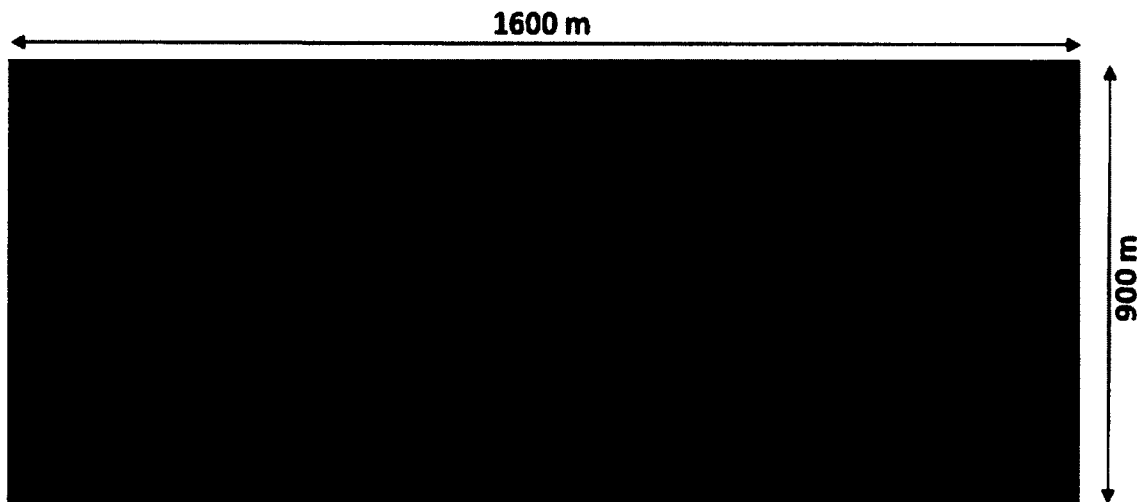


Figure 5-18: Segment of the overall domain to extract results for Cycle-1 mudflat.

5.6.1 Result Analysis for Mudflat (Without Vegetation)

Wave and current induced bed shear stress on mudflat due to two different initial conditions revealed that the mudflat experienced higher bed shear stress while dry at the beginning of a hurricane generation. The bed shear stress contour for submerged and dry initial conditions during hurricane landfall and hurricane peak are presented in **Figure 5-19** and **Figure 5-20** respectively. Wave and current induced shear stress on mudflat during Hurricane Ike found to be maximum while considering the dry initial condition approach. During hurricane landfall, the maximum shear stress increased to 29.04 N/m^2 from 5.77 N/m^2 while considering dry condition analysis. Similarly, maximum shear stress during hurricane peak for submerged condition was found to be 4.72 N/m^2 where it increased to 46.39 N/m^2 for dry condition analysis.

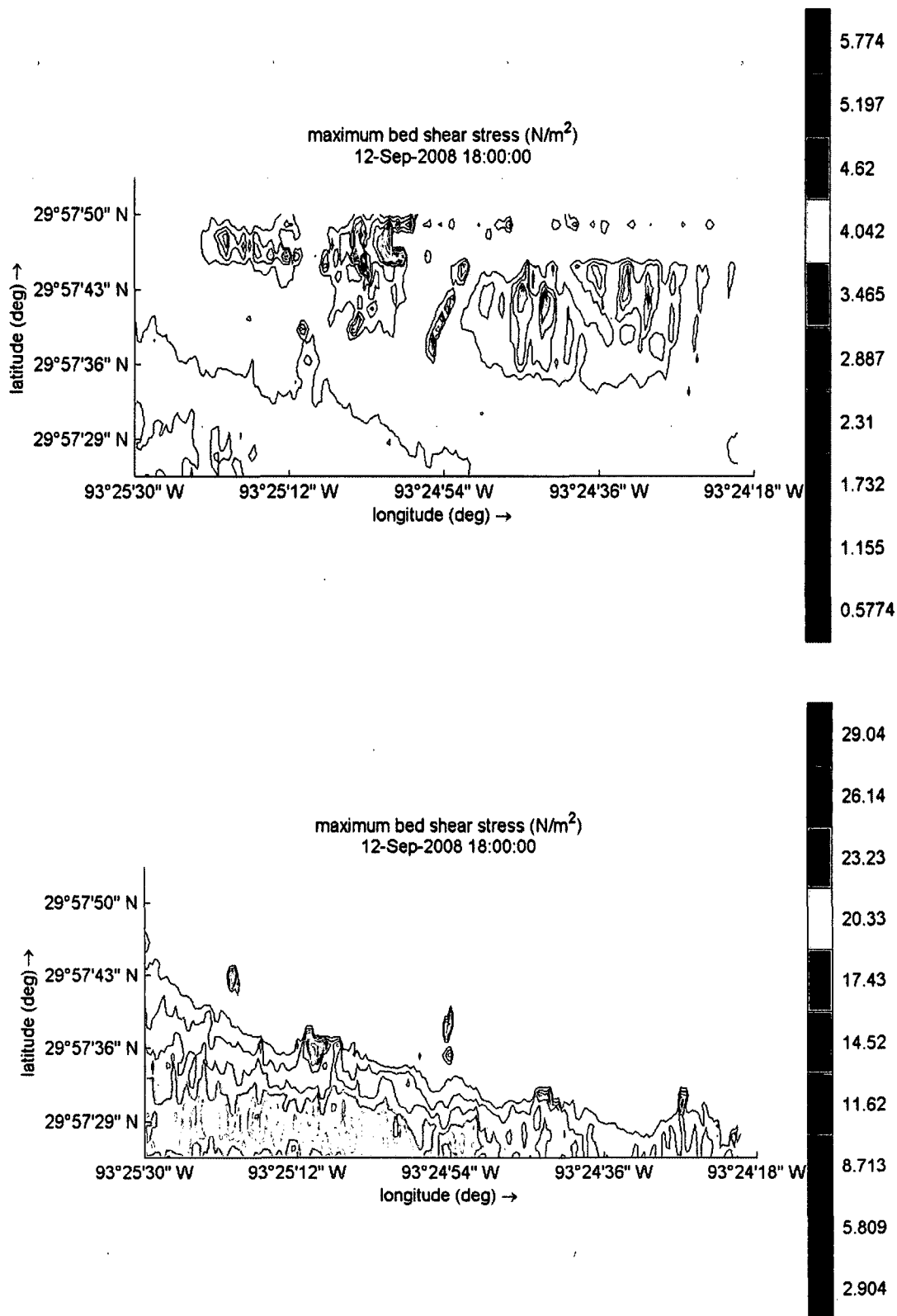


Figure 5-19: Wave and current induced bed shear stress on mudflat for submerged (top) and dry (right) initial condition during hurricane landfall.

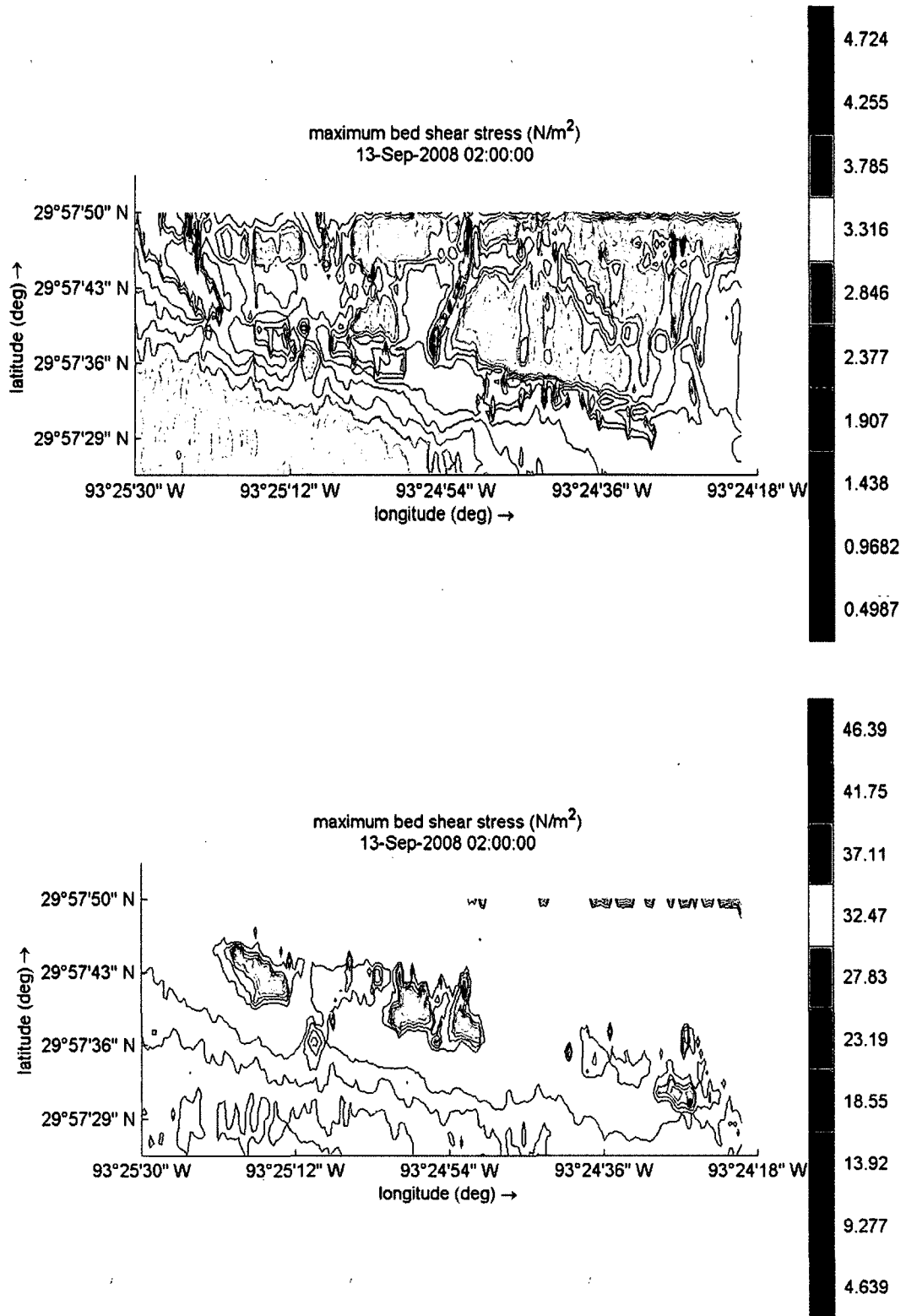


Figure 5-20: Wave and current induced bed shear stress on mudflat for submerged (top) and dry (right) initial condition during hurricane peak.

Figure 5-21 and Figure 5-22 show the water depth contours over the mudflat (Cycle-1) during the landfall and peak time of the hurricane, generated from two different initial conditions. Water depth during hurricane landfall on mudflat found to be close to zero where the area found to be flooded with around 0.8 m depth of water with submerged analysis. During hurricane peak, both condition created inundation over the area with slightly lower water depth value for dry condition analysis.

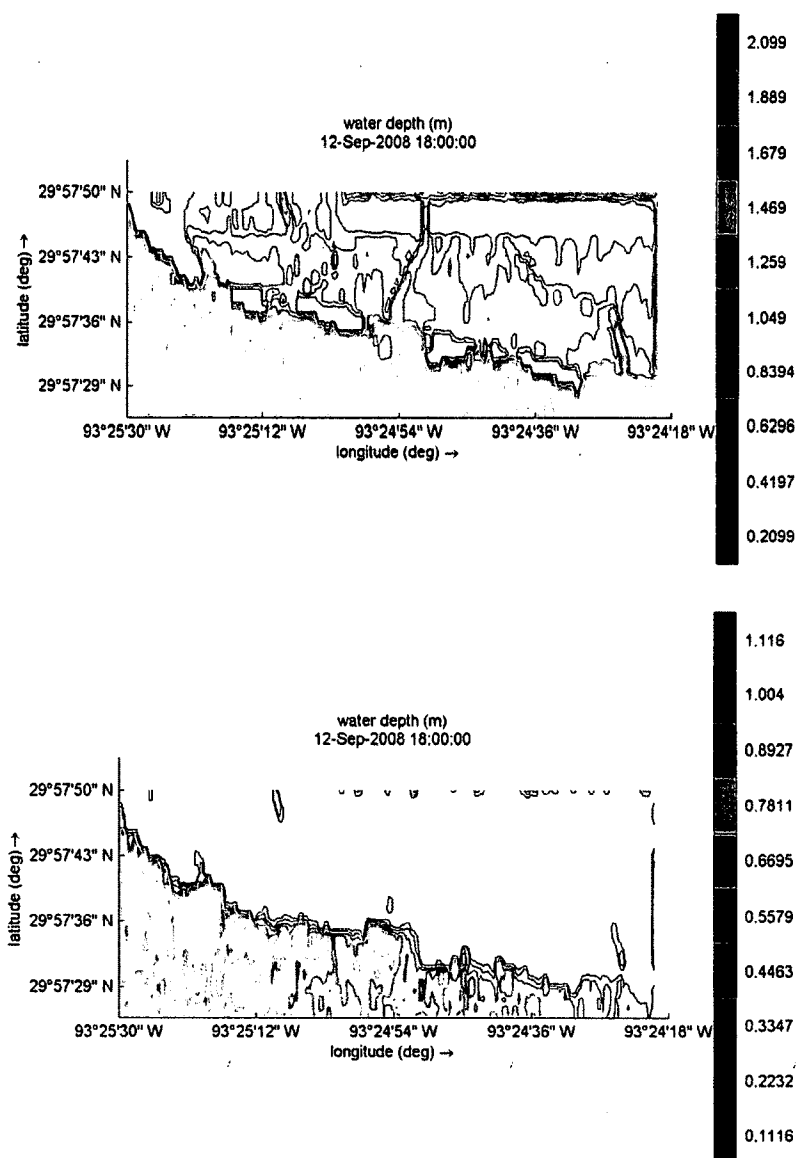


Figure 5-21: Water depth on mudflat for submerged (top) and dry (right) initial condition during hurricane landfall.

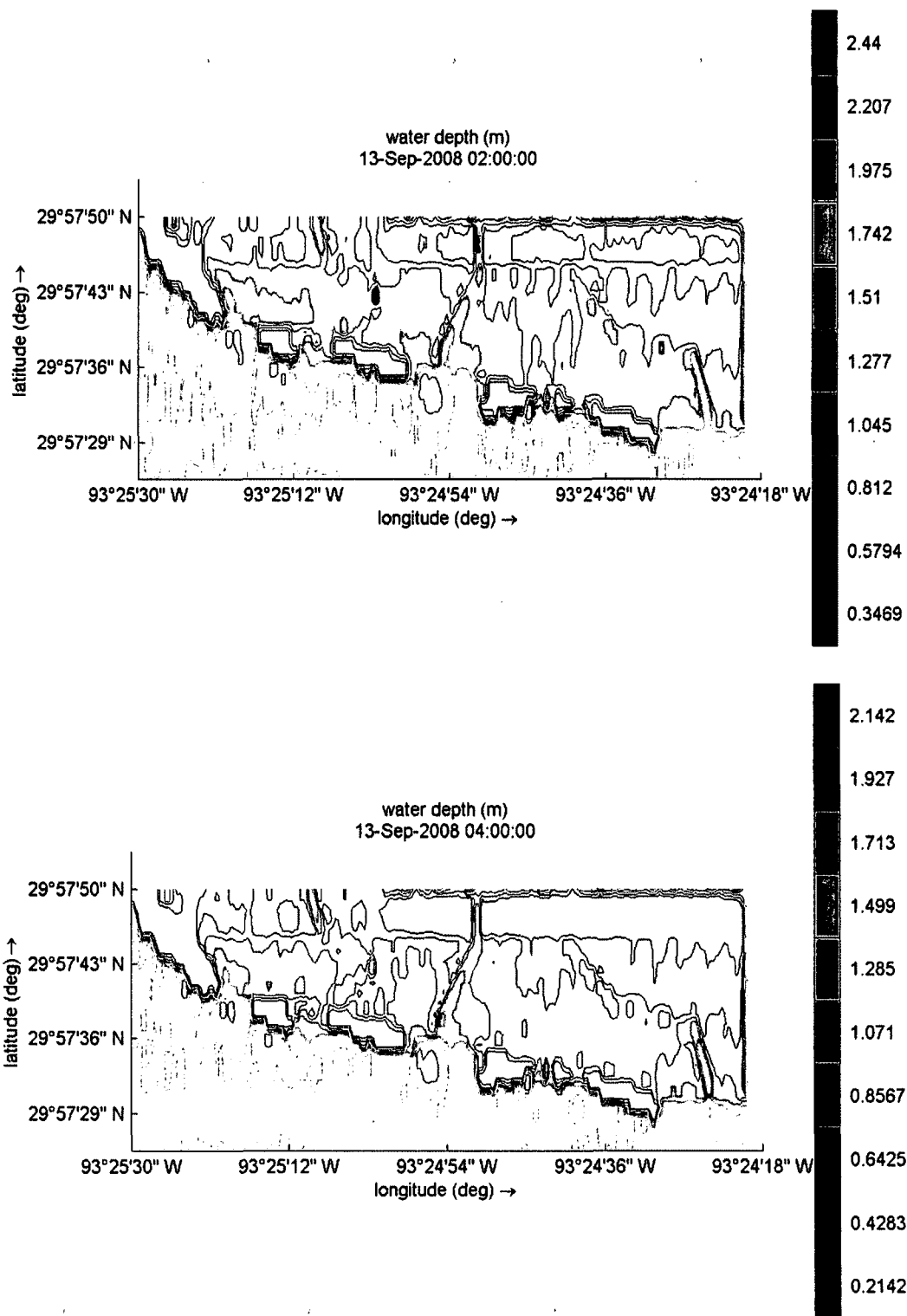


Figure 5-22: Water depth on mudflat for submerged (top) and dry (right) initial condition during hurricane peak.

5.6.1.1 Maximum bed shear stress and corresponding water depth

To extract the results on marsh the bed, three longshore sections (LS) and three cross-shore sections (CS) were taken to illustrate the shear stress distributions. **Table 5-5** presents the length of the sections that were used for result analysis. Locations of both types of the sections are presented in **Figure 5-23**. The selection of sections, locations and dimensions were controlled through results observations of maximum stress contour. LS1 and LS3 were considered as 1000 m long where LS2 was 1200 m as noticeable stress was observed in the contour plot at the middle right part of the mudflat as shown in **Figure 5-18** (top) and **Figure 5-19** (top). Similarly, to cover the critical spots, the length of CS2 was kept at 300 m longer than CS1 and CS2.

Table 5-5: Description of result extraction section.

Result Extraction Section	Length (m)
Longshore Section 1 (LS1)	1000
Long Section 2 (LS2)	1000
Long Section 3 (LS3)	1200
Cross-shore Section 1 (CS1)	500
Cross-shore Section 2 (CS2)	800
Cross-shore Section 3 C(S3)	500

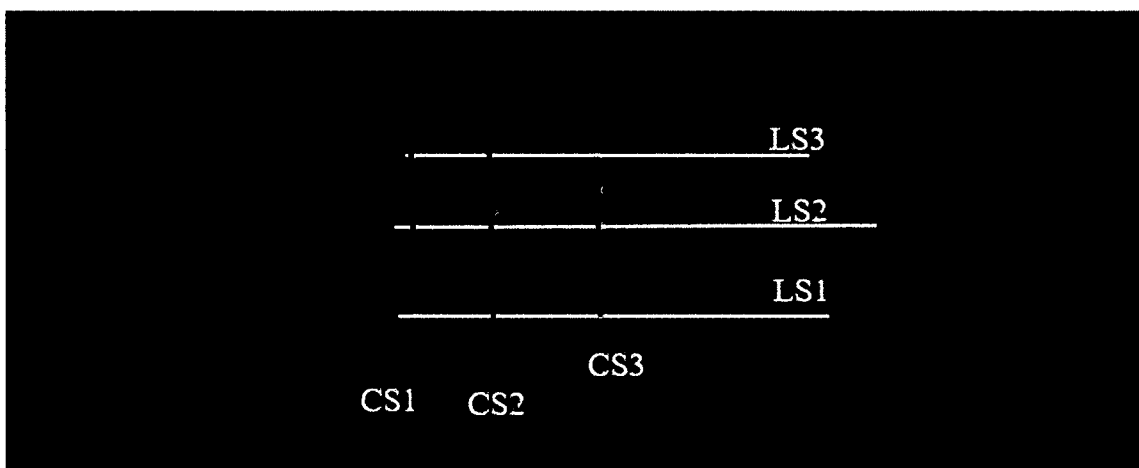


Figure 5-23: Sections for result extraction.

Bed shear stresses along all the sections were found in a range from as low as 0.001 N/m² to as high as 46 N/m². The results revealed that the LS1 which is closest to the shore provides maximum stress during landfall and significantly higher stress also observed during peak for this section as shown in **Figure 5-24**. Water depth results for this section exposed that the water depth was very low while maximum stress generated on this location during landfall with dry condition analysis are shown in **Figure 5-25**.

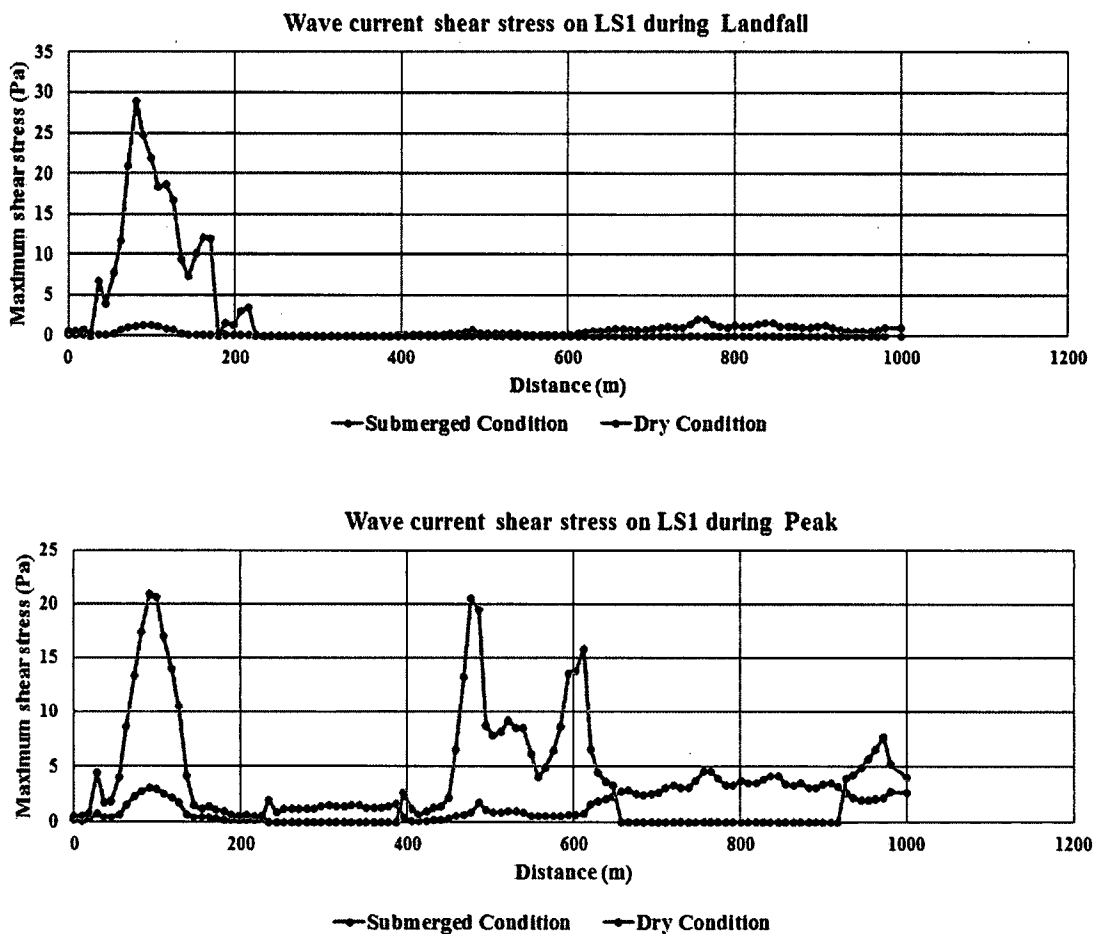


Figure 5-24: Wave current shear stress on LS1.

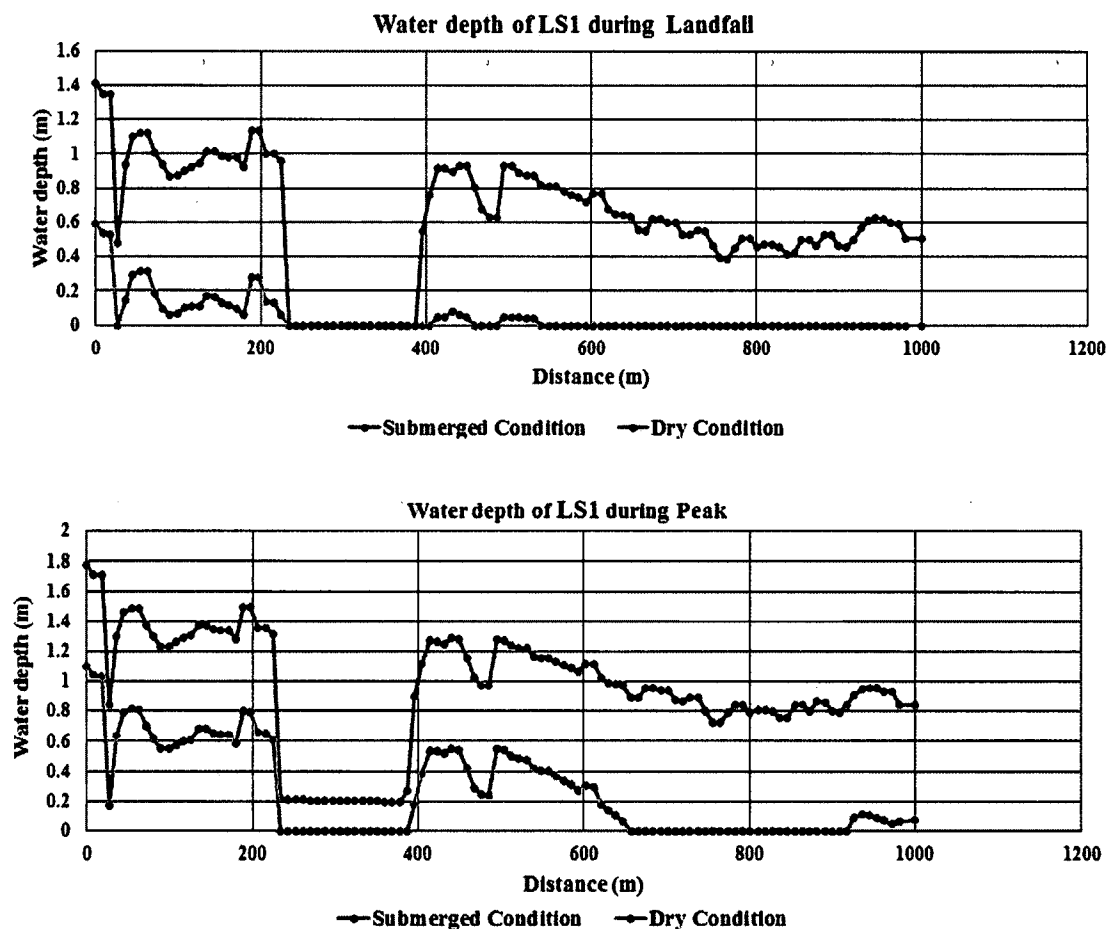


Figure 5-25: Water depth on LS1.

In the intermediate section LS2, mostly no stress generated during landfall as no wave reached the section. Maximum stress observed in this section during peak for dry condition where the stress generated from submerged condition analysis remain insignificant as shown in Figure 5-26. Water depth on this section location was found significantly lower with dry condition analysis compared to submerged condition analysis as shown in Figure 5-27.

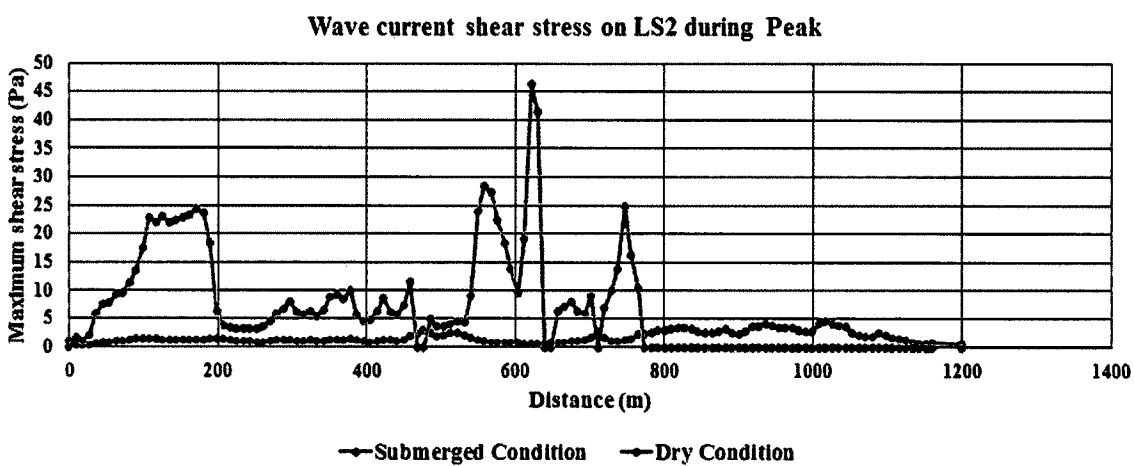
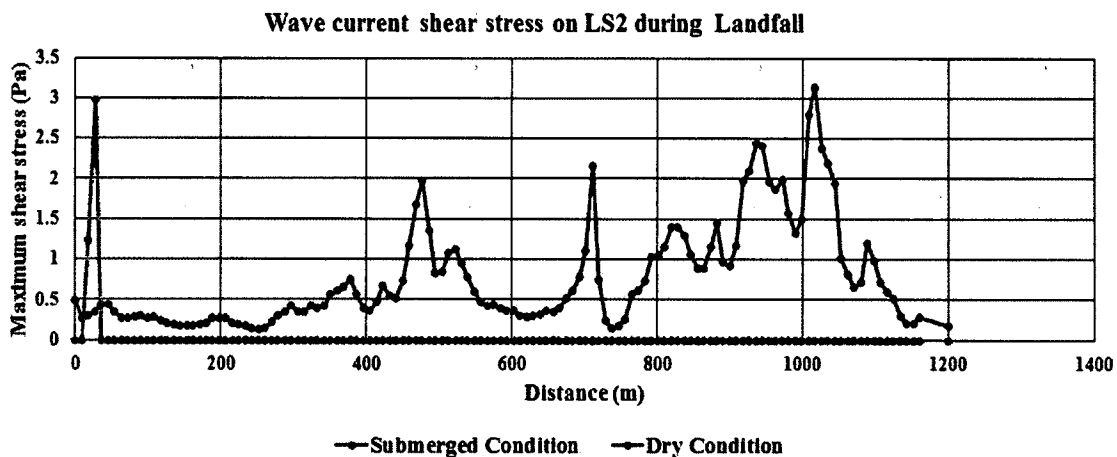


Figure 5-26: Wave current shear stress on LS2.

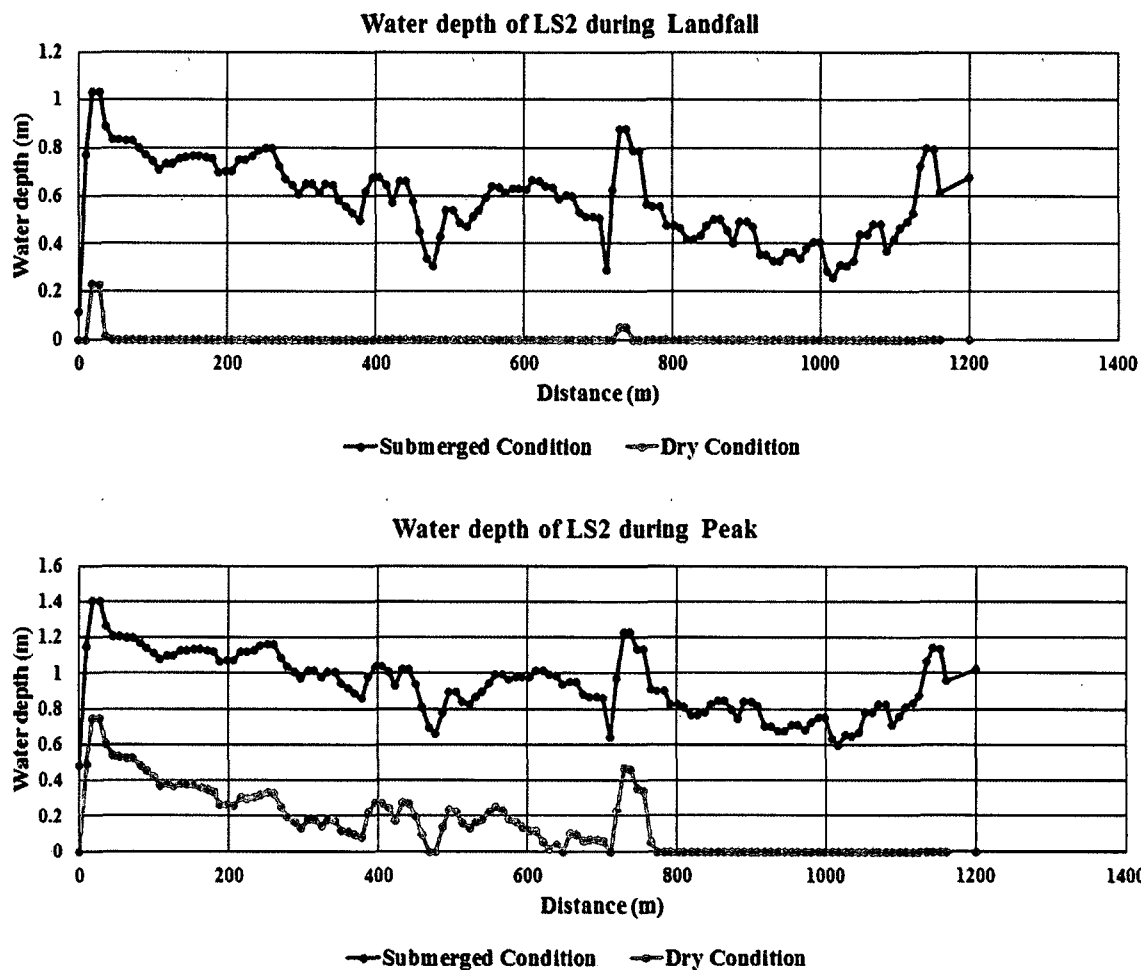


Figure 5-27: Water depth on LS2.

In the furthest section from the marsh edge, LS3 generated stresses during the hurricane period for two different conditions were almost similar as shown in **Figure 5-28**. The water depth on this section during hurricane simulation with dry condition remained very low compared to submerged condition analysis as shown in **Figure 5-29**.

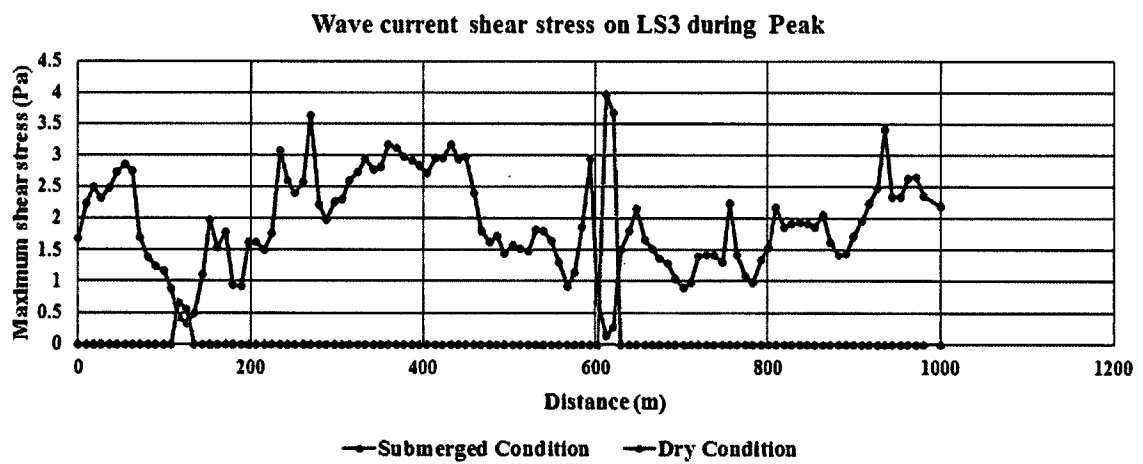
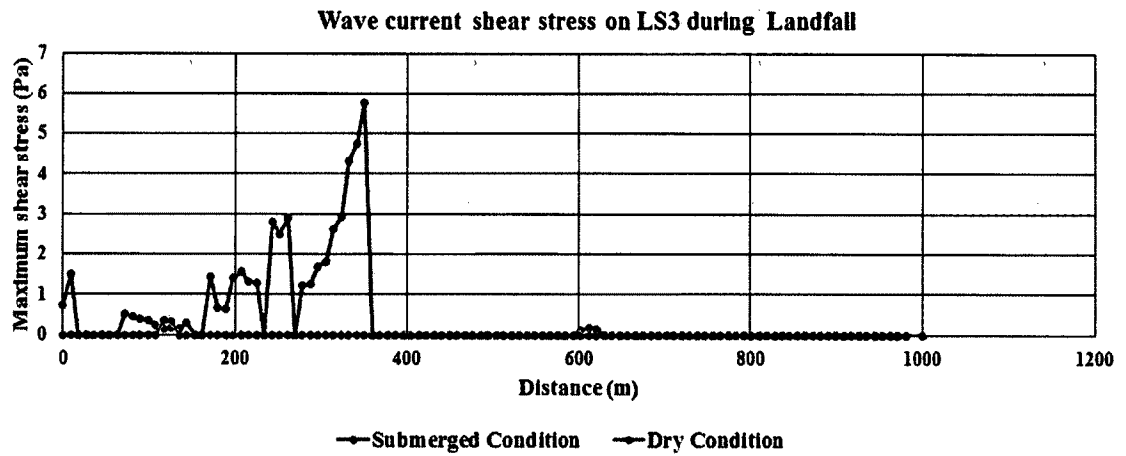


Figure 5-28: Wave current shear stress on LS3.

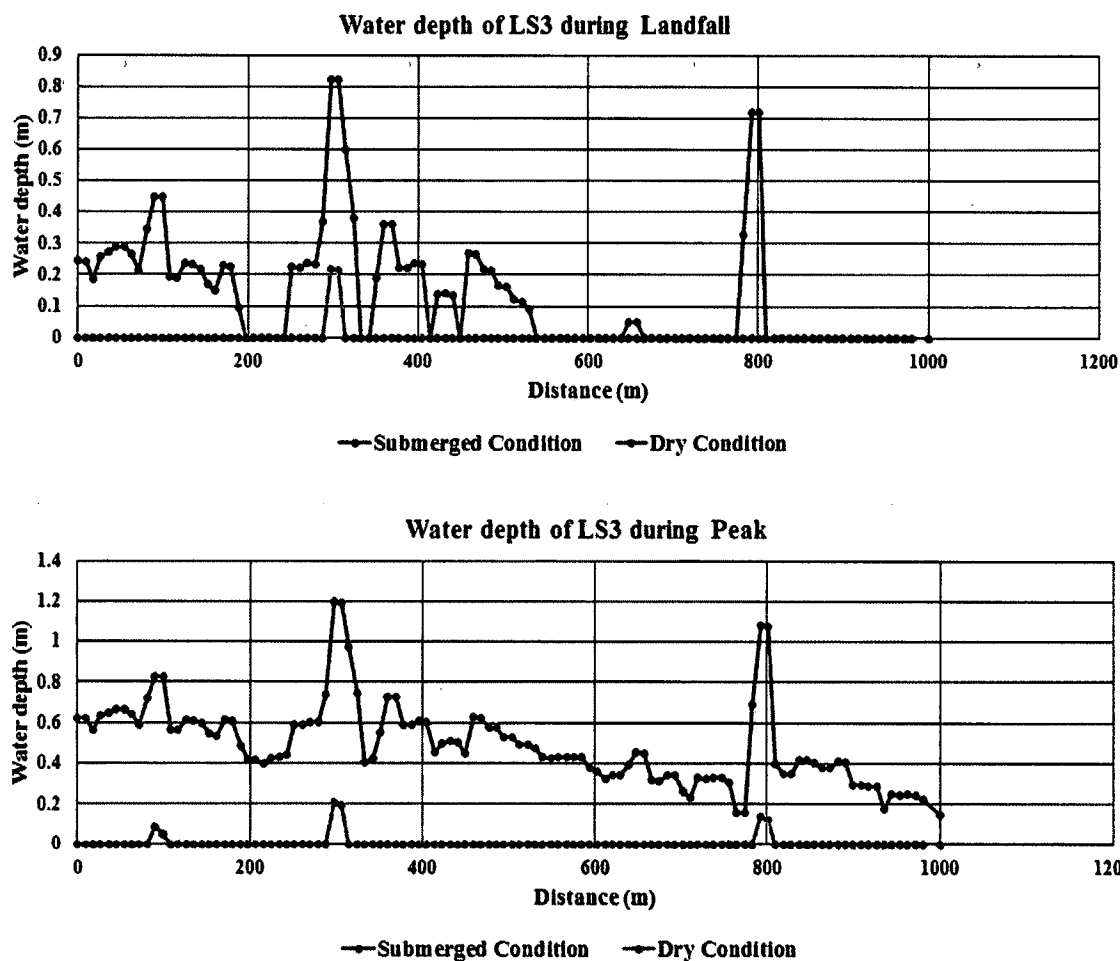
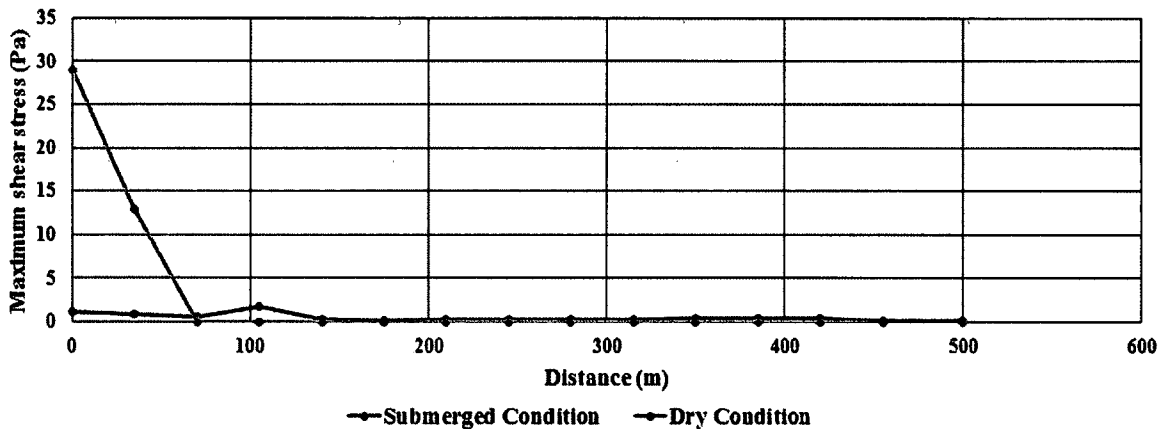


Figure 5-29: Water depth on LS3.

The maximum shear stress and water depth over cross-shore sections CS1, CS2 and CS3 are presented in Figure 5-30 to Figure 5-35. Shear stress output over these sections revealed almost a similar type of conclusion that came from longshore analysis. Locations close to the mud edge produced higher stress while remaining in shallow water during the wave landfall and maximum stress situation occurred on mud flat during the peak time of the hurricane and for the dry condition analysis.

Wave current shear stress on CS1 during Landfall



Wave current shear stress on CS1 during Peak

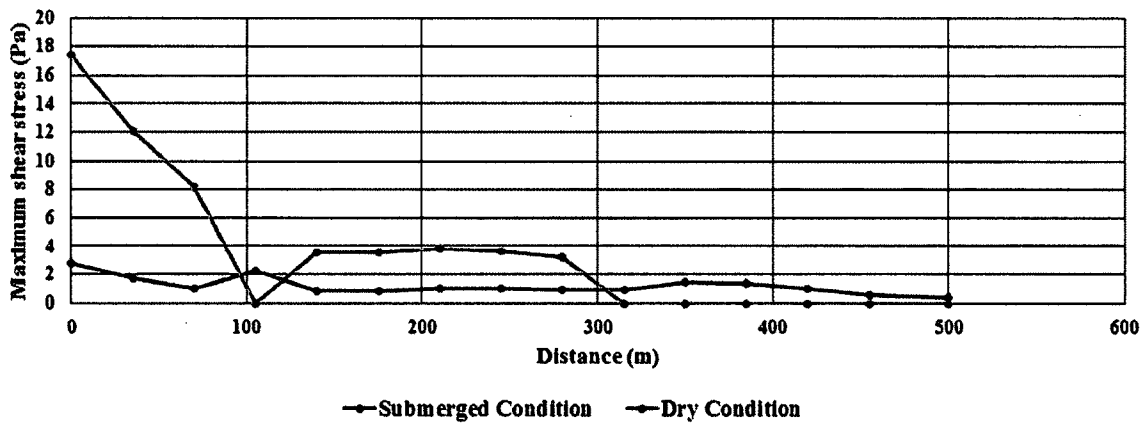


Figure 5-30: Wave current shear stress on CS1.

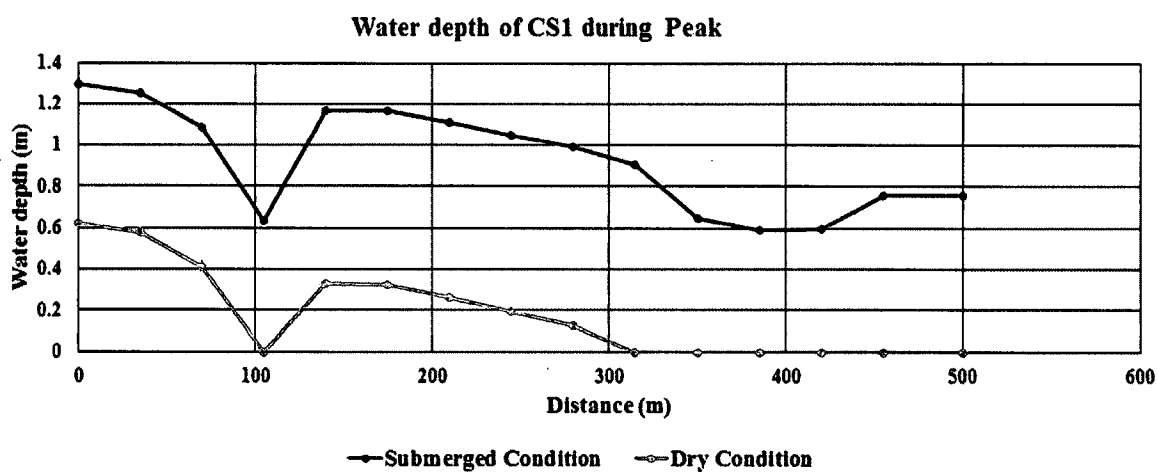
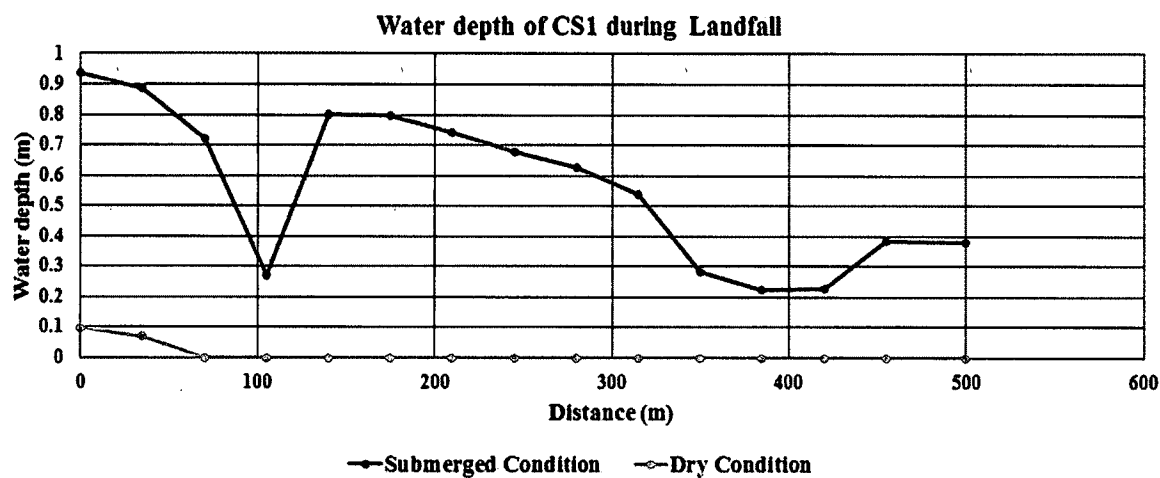


Figure 5-31: Water depth on CS1.

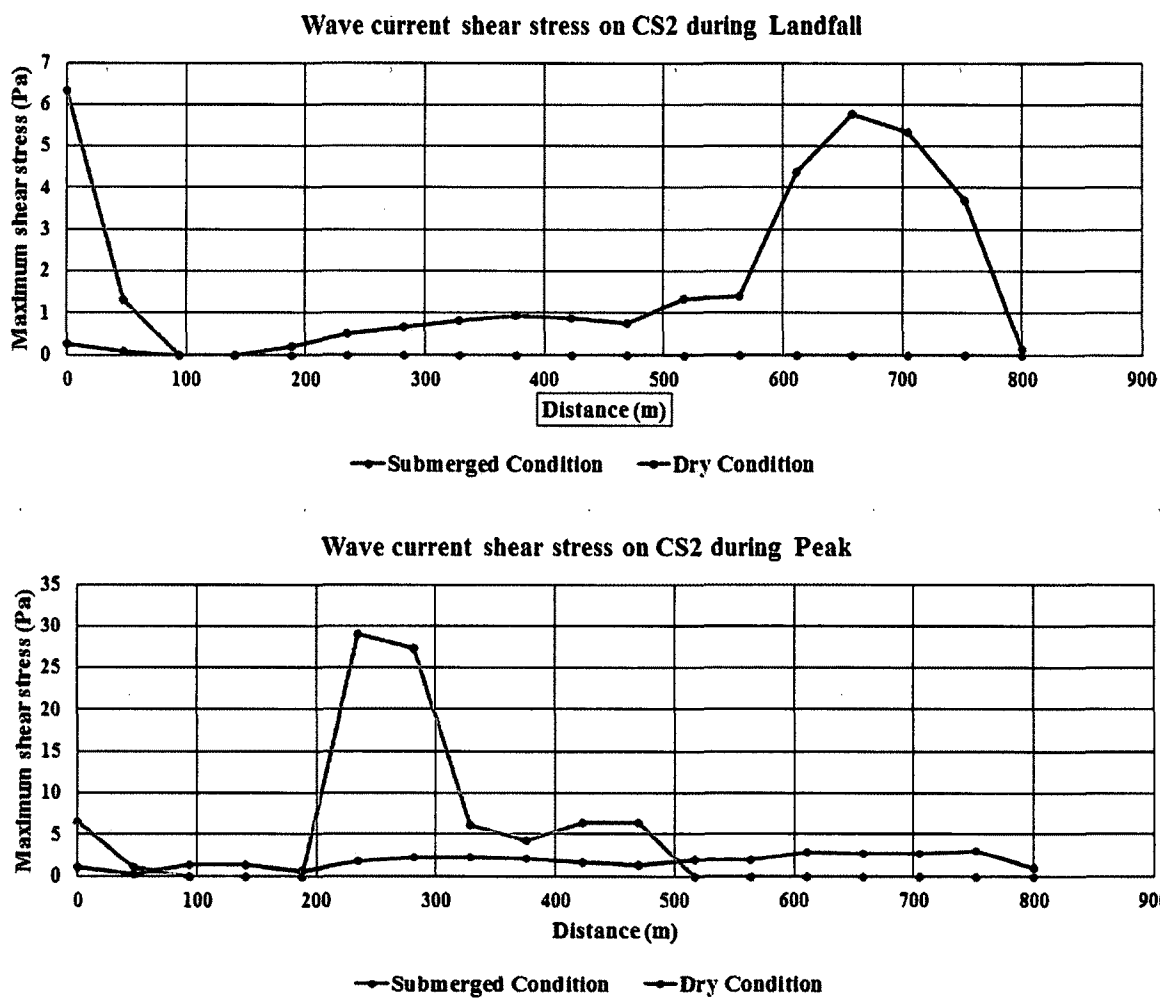


Figure 5-32: Wave current shear stress on CS2.

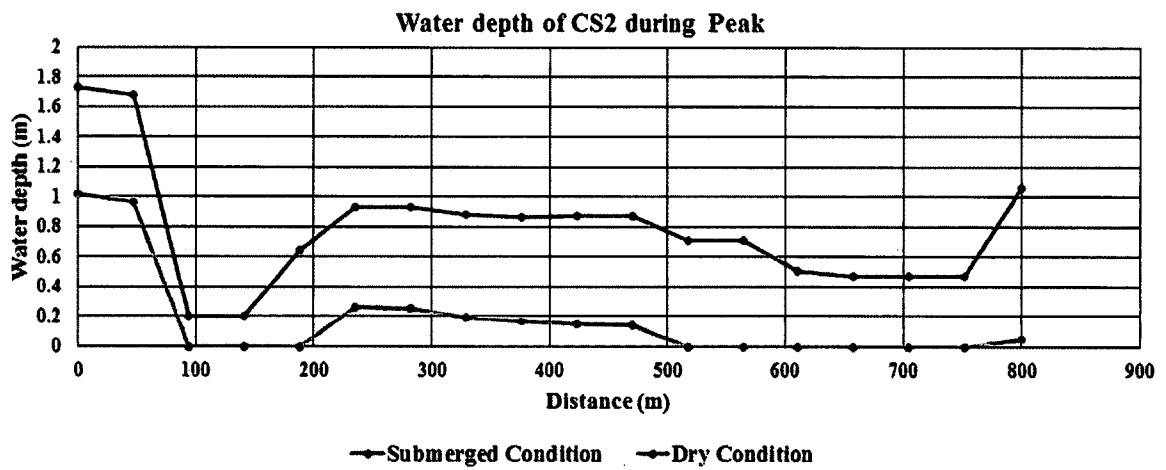
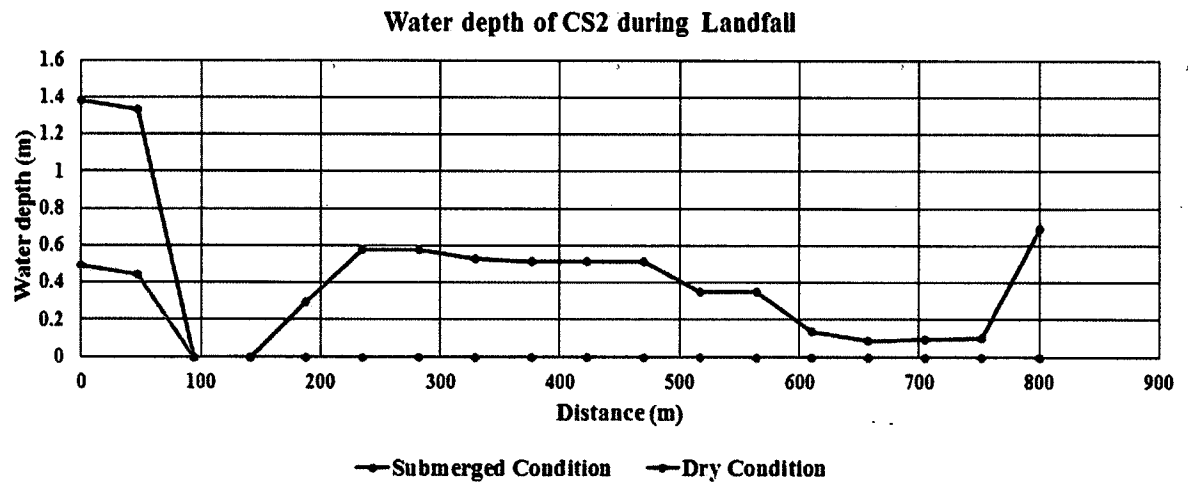


Figure 5-33: Water depth on CS2.

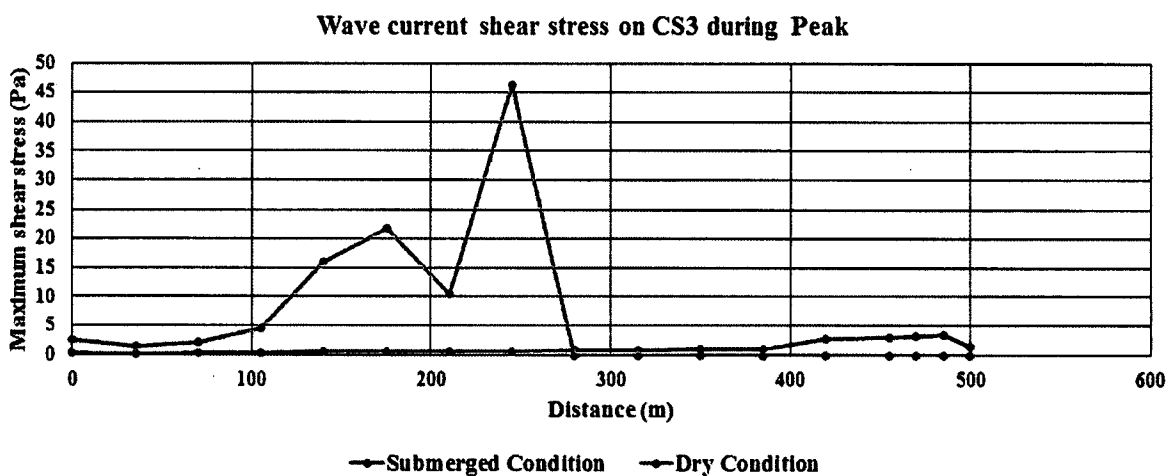
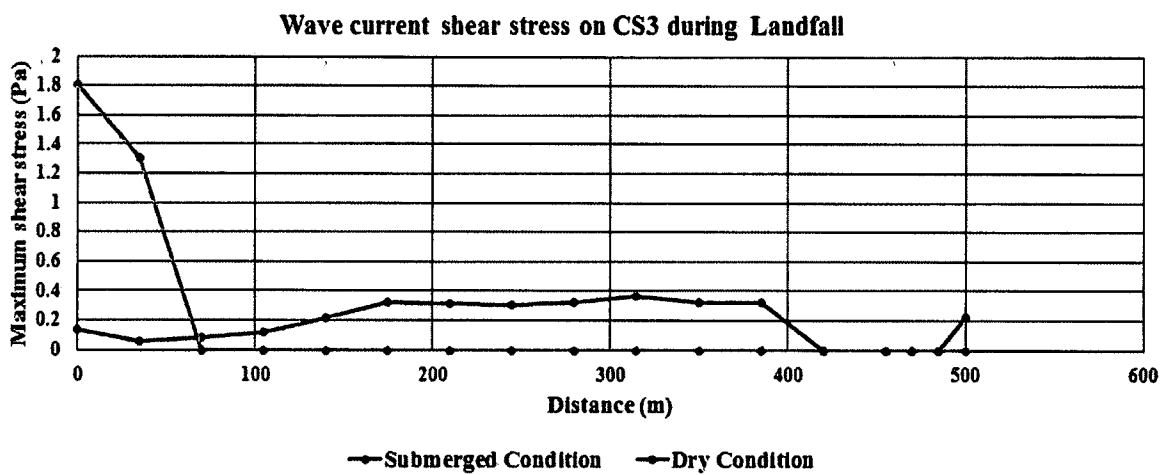


Figure 5-34: Wave current shear stress on CS3.

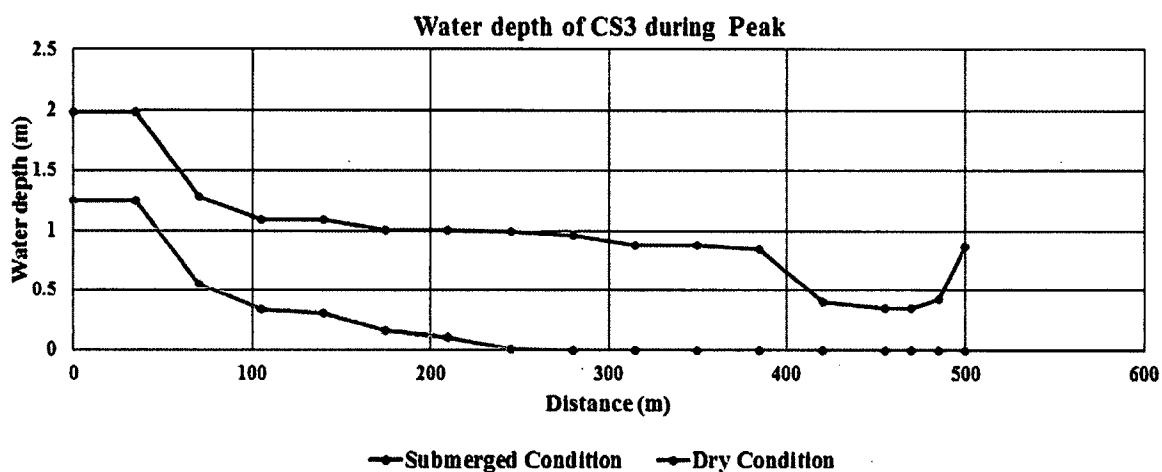
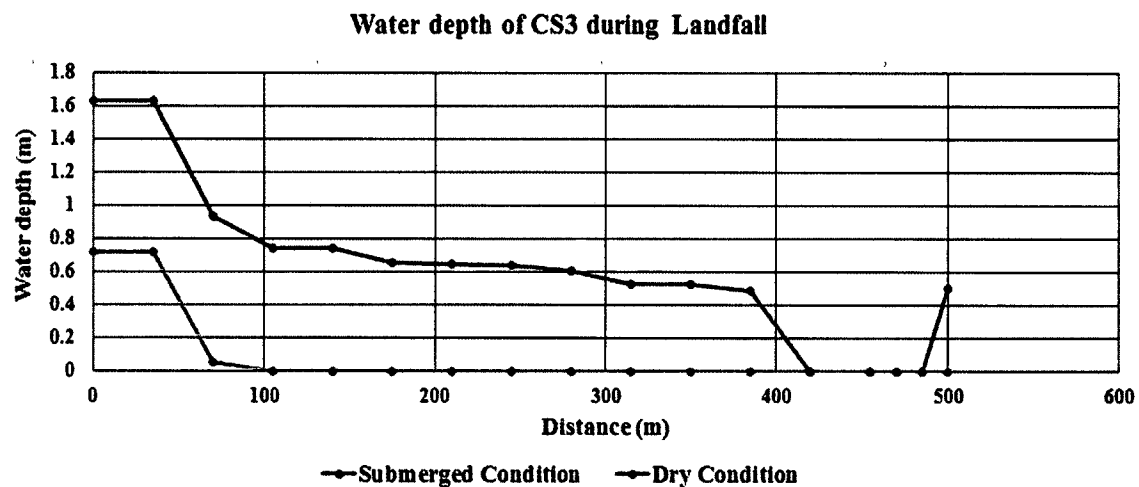


Figure 5-35: Water depth on CS3.

5.6.1.2 Locations of critical zones

After analyzing the maximum bed shear stress distributions over longshore and cross-shore sections, three most vulnerable locations, point A, B and C, are shown in

Figure 5-36.

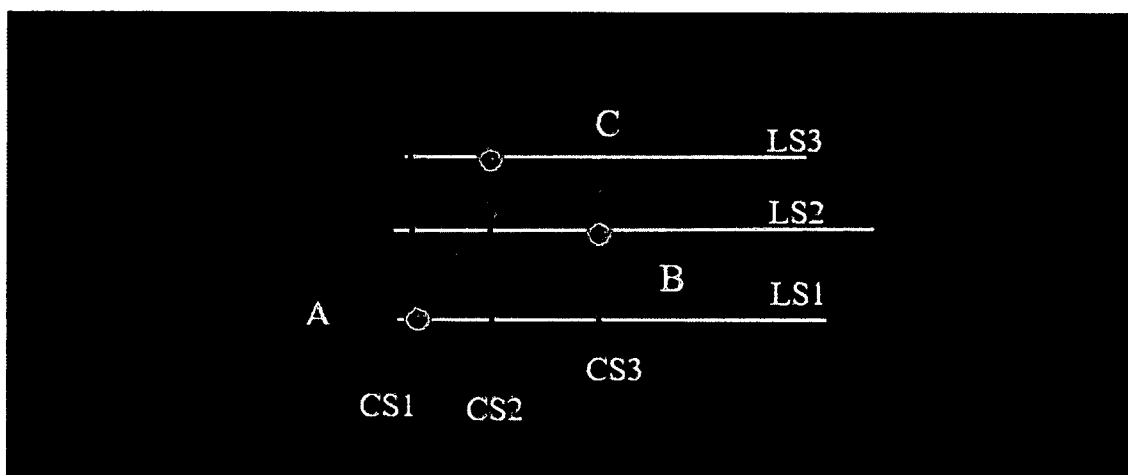


Figure 5-36: Sections for result extraction.

The latitude and longitude of the extraction points are listed in **Table 5-6**. Location A is most vulnerable during hurricane landfall as this location fell on the marsh edge. Location B is vulnerable during hurricane peak condition and most stress developed while the hurricane impact developed during a drought condition. Location C experienced some stresses during the hurricane period, which is insignificant compared to stress generated on location A and location B.

Table 5-6: Extraction point location.

Extraction Point ID	Latitude	Longitude
A	29°57'36.36"N	93°25'8.50"W
B	29°57'42.04"N	93°24'54.40"W
C	29°57'45.87"N	93°25'1.32"W

5.6.2 Result Analysis for Marsh Mudflat (With Vegetation)

Wave and current induced bed shear stress on vegetated mudflat due to two different initial condition revealed that the mudflat experienced higher bed shear stress while dry at the beginning of a hurricane generation. The bed shear stress contour for

submerged and dry initial conditions during hurricane landfall and hurricane peak are presented in **Figure 5-37** and **Figure 5-38**, respectively.

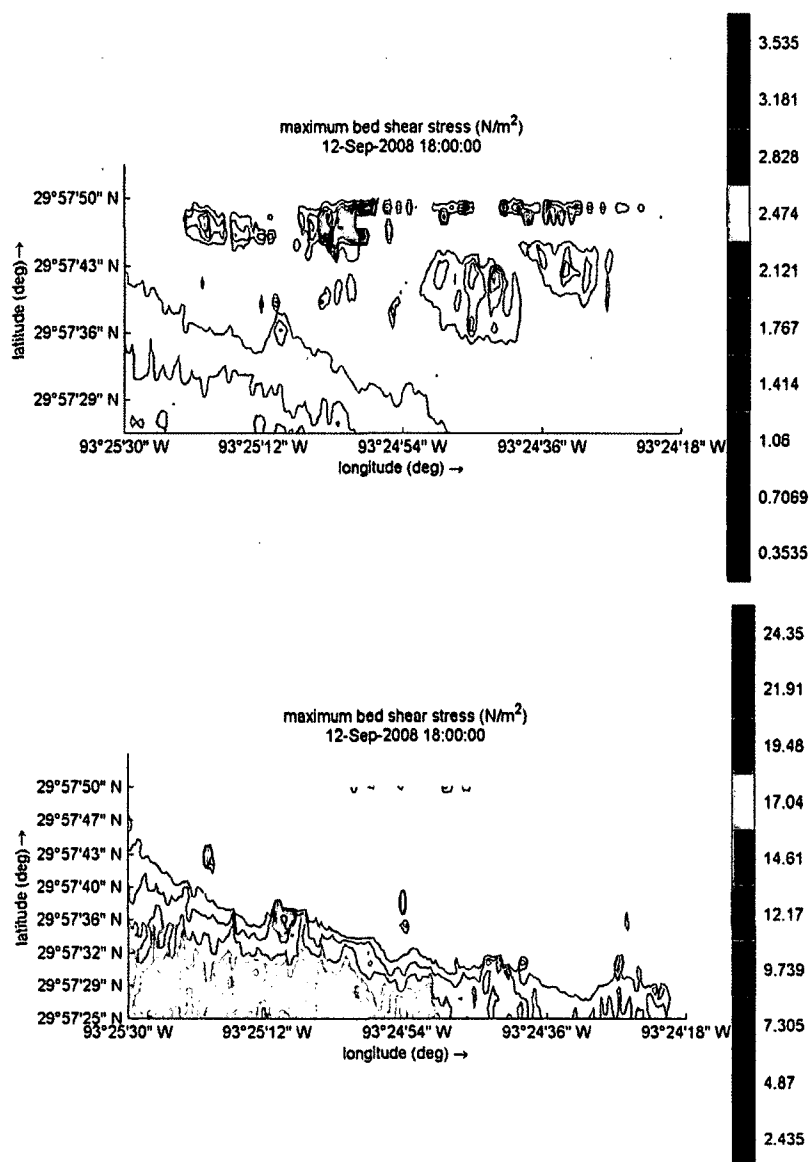


Figure 5-37: Wave and current induced bed shear stress on vegetated mudflat for submerged (top) and dry (right) initial condition during hurricane landfall.

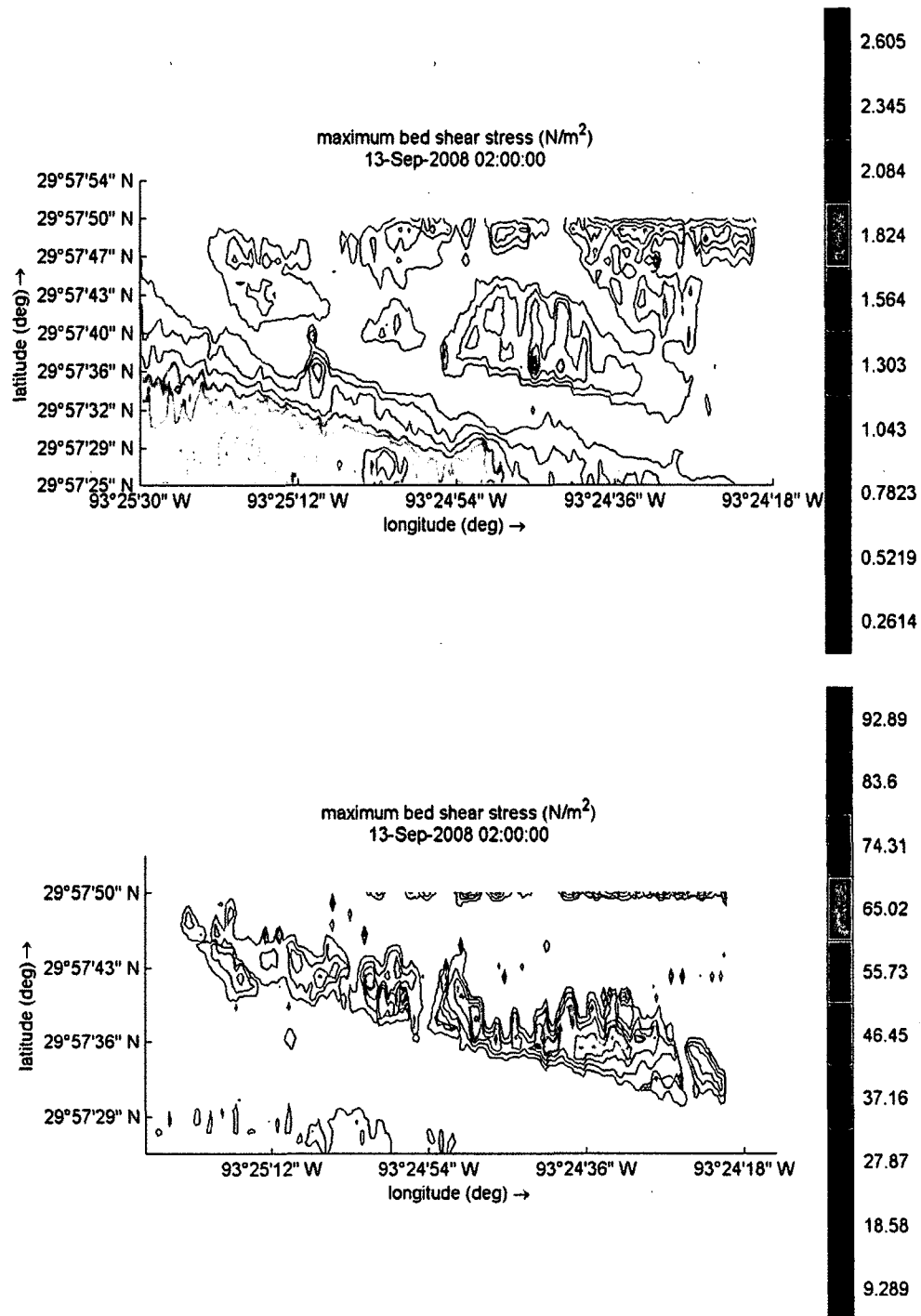


Figure 5-38: Wave and current induced bed shear stress on vegetated mudflat for submerged (top) and dry (right) initial condition during hurricane peak.

It was also noticed that the vulnerable location remained the same while including vegetation into the study. The generated stress found to be lower during hurricane landfall

with both dry and submerged condition with vegetation present. During hurricane peak, vegetation reduced maximum stress on mudflat for submerged condition compared to non-vegetated mudflat, but increased the maximum stress for dry condition analysis. A detailed result analysis was conducted to explain the hurricane impact on vegetated and non-vegetated marsh and is presented in the following section.

5.6.3 Result Comparison for Vegetated and Non-Vegetated Mudflat

To analyze the wave and current induced bed shear stress distributions for vegetated and non-vegetated marsh bed, time dependent analysis was conducted in the next section for the vulnerable location of point A and B. Location C produced insignificant results in terms of mass erosion phenomena and deducted from future analysis as this research mainly focused on the mass erosion of marsh mudflat. Results of location A revealed the hurricane impact near the marsh edge where results of location B provided insight of the hurricane impact on marsh interior flat surface.

Maximum shear stress generated at location A reduced in the presence of vegetation for both types of condition analysis as shown in **Figure 5-39**. No significant influence of vegetation on water depth was observed during the hurricane period as shown in **Figure 5-40**.

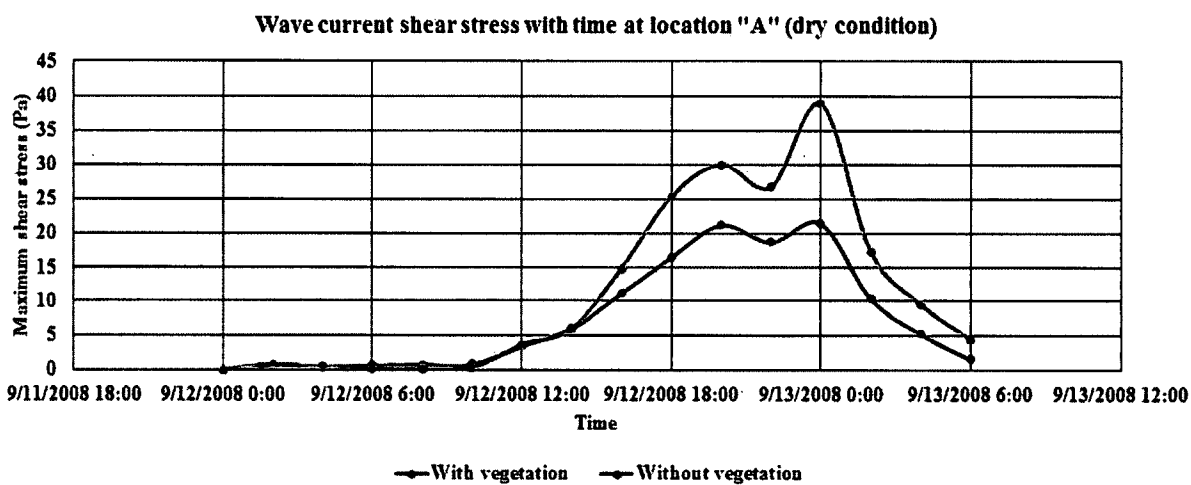
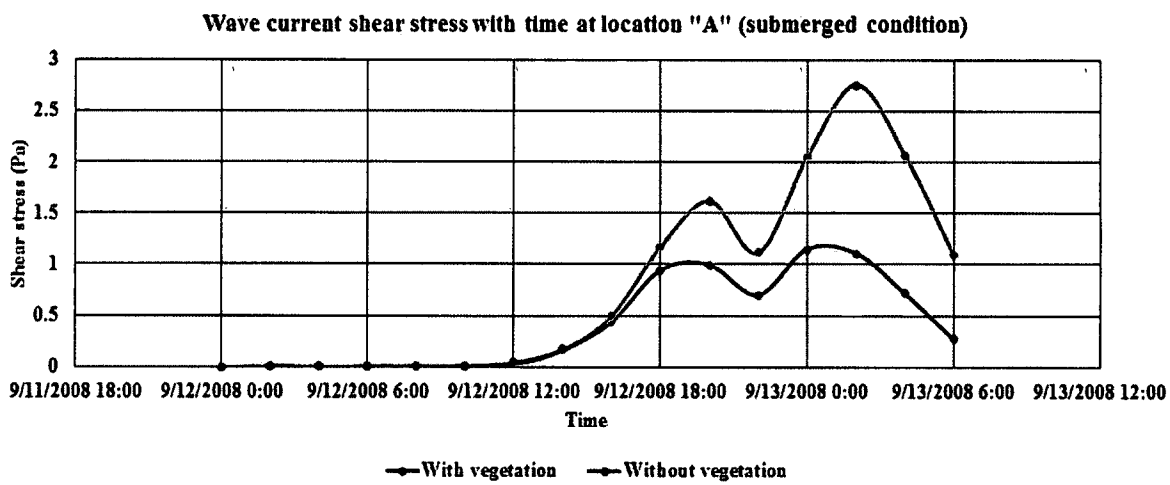


Figure 5-39: Wave and current induced bed shear stress with time at location "A" from submerged (top) and dry (bottom) condition analysis for vegetated and non-vegetated mudflat.

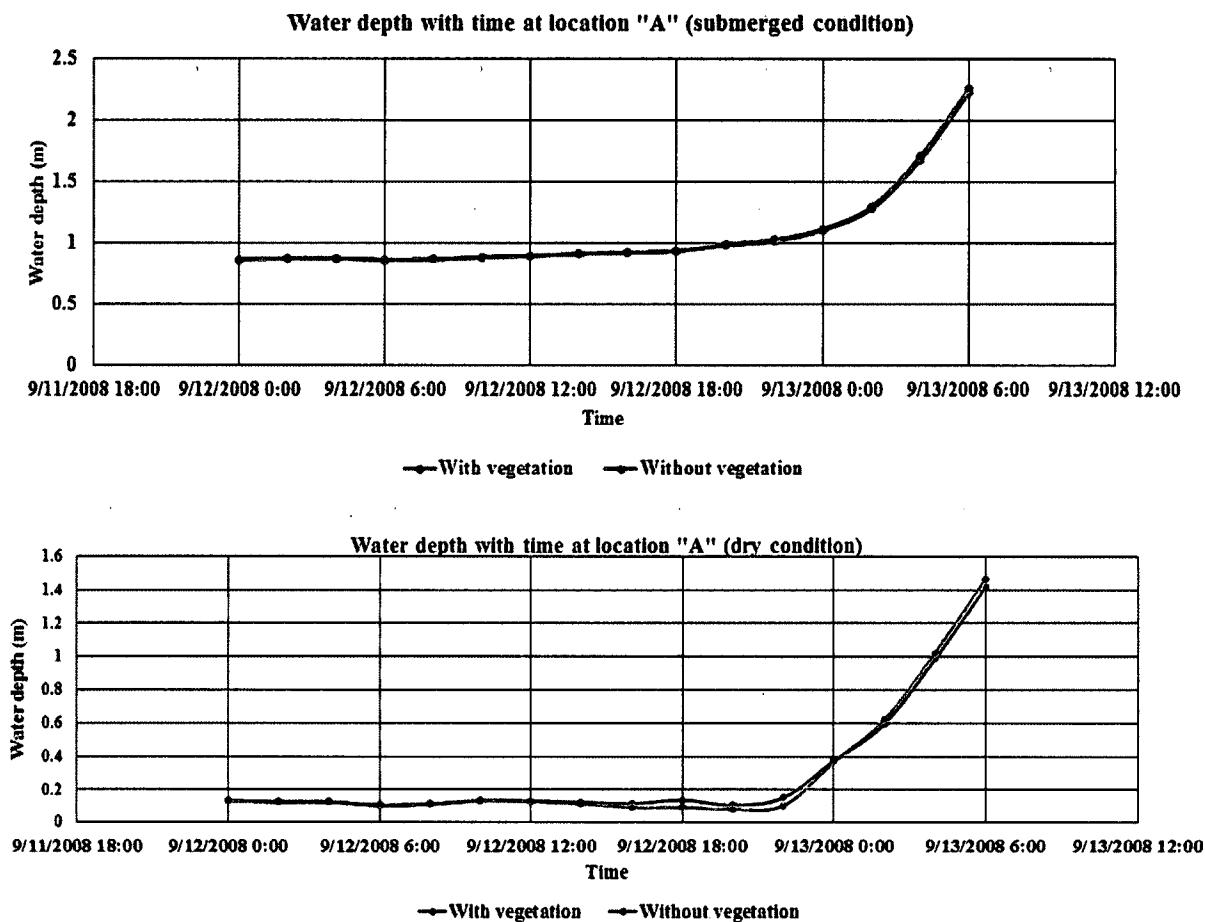


Figure 5-40: Water depth with time at location "A" from submerged (top) and dry (bottom) condition analysis for vegetated and non-vegetated mudflat.

Result analysis at location B indicated that the maximum stress reduced in the presence of vegetation for submerged condition but increased significantly for dry condition analysis is shown in **Figure 5-41**. No significant fluctuation in water depth during peak for dry condition analysis observed while analyzing vegetated and non-vegetated marsh bed is shown in **Figure 5-42**. However, it was noticed that only during dry condition and peak time of a hurricane wave made direct contact with the marsh bed with maximum impact and produced significant stresses on mudflat for both vegetated and non-vegetated conditions. It can be summarized that the additional resistance from vegetation friction producing the higher stress on vegetated bed compared to non-vegetated

bed. Although vegetation found to be very effective during a low energy wave impact, they can be self-destructing during a high-energy wave setting like hurricane wave and with the condition where they are completely exposed to the wave. Vegetated marsh still can survive the hurricane impact while they stayed inundated/submerged.

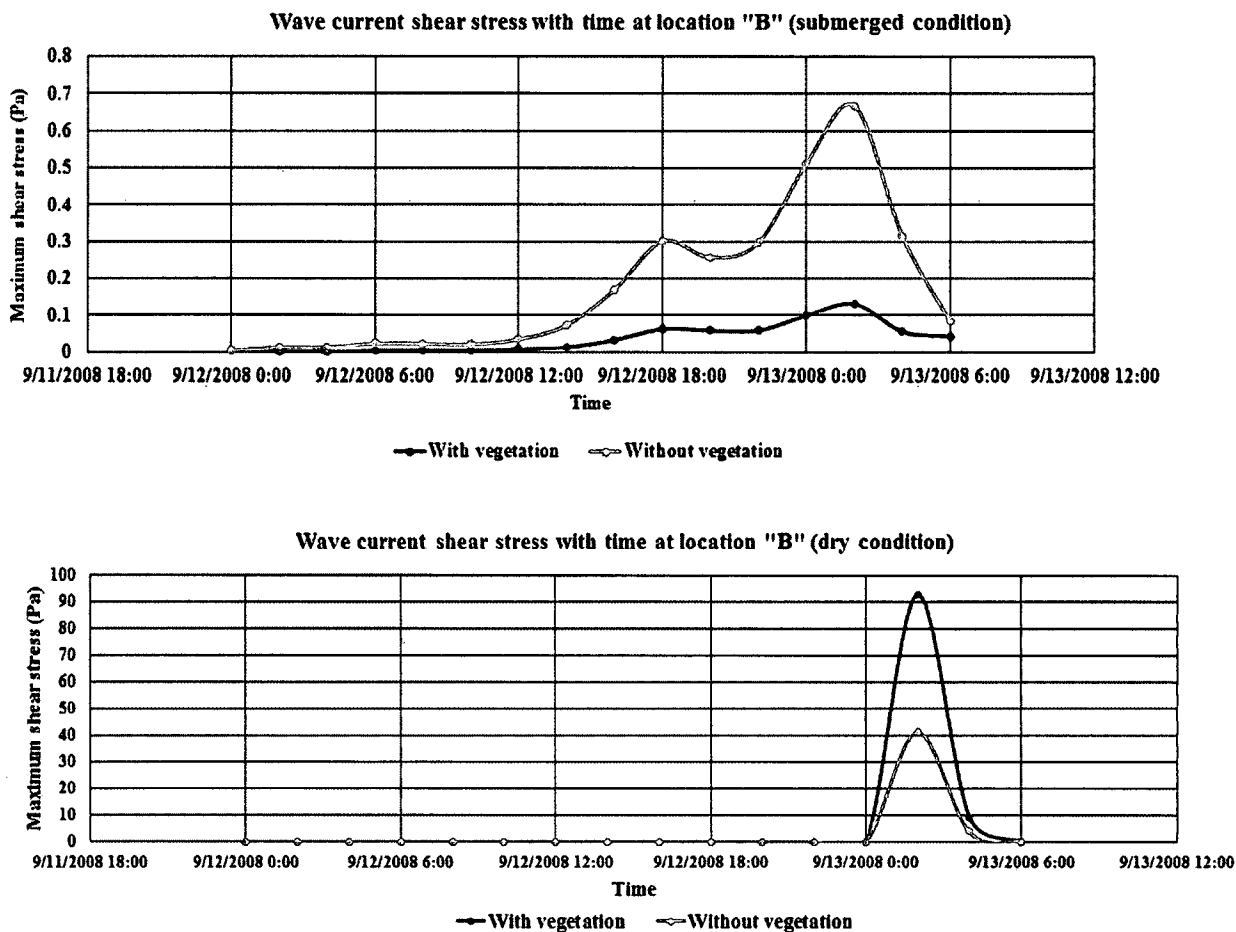


Figure 5-41: Wave and current induced bed shear stress with time at location "A" from submerged (top) and dry (bottom) condition analysis for vegetated and non-vegetated mudflat.

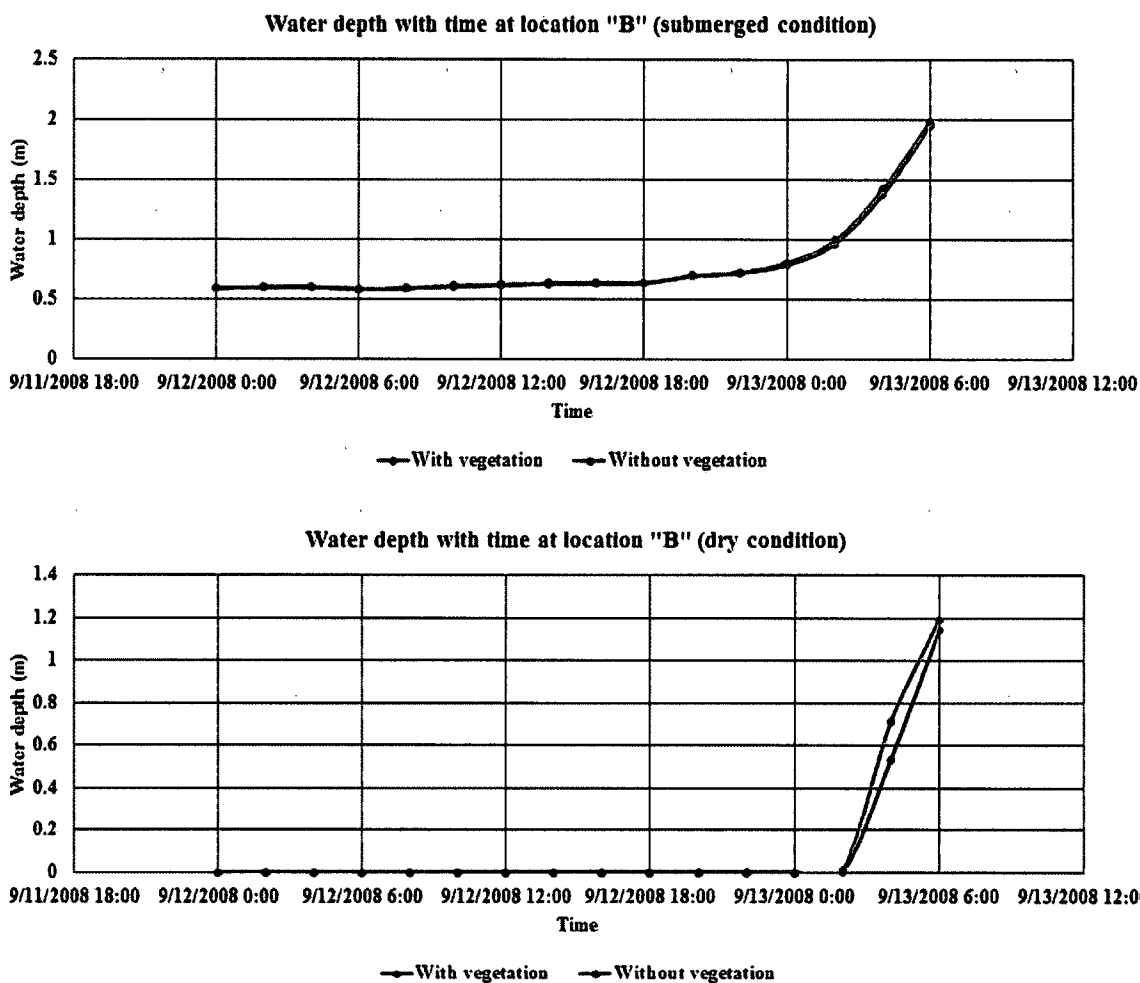


Figure 5-42: Water depth with time at location "A" from submerged (top) and dry (bottom) condition analysis for vegetated and non-vegetated mudflat.

Velocity profile through canopy/marsh during different hurricane impact scenarios revealed that vegetation shoot structure reduced the velocity for all types of scenarios as shown in **Figure 5-43** to **Figure 5-46**.

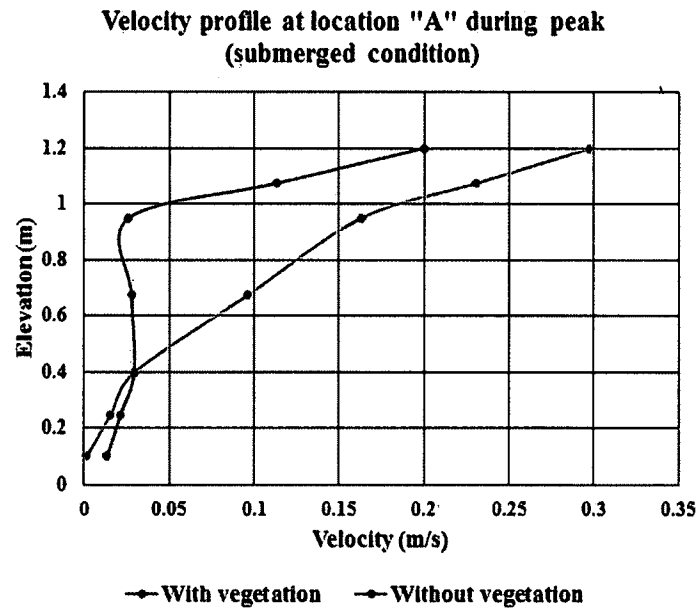


Figure 5-43: Velocity profile at location A during peak (submerged condition).

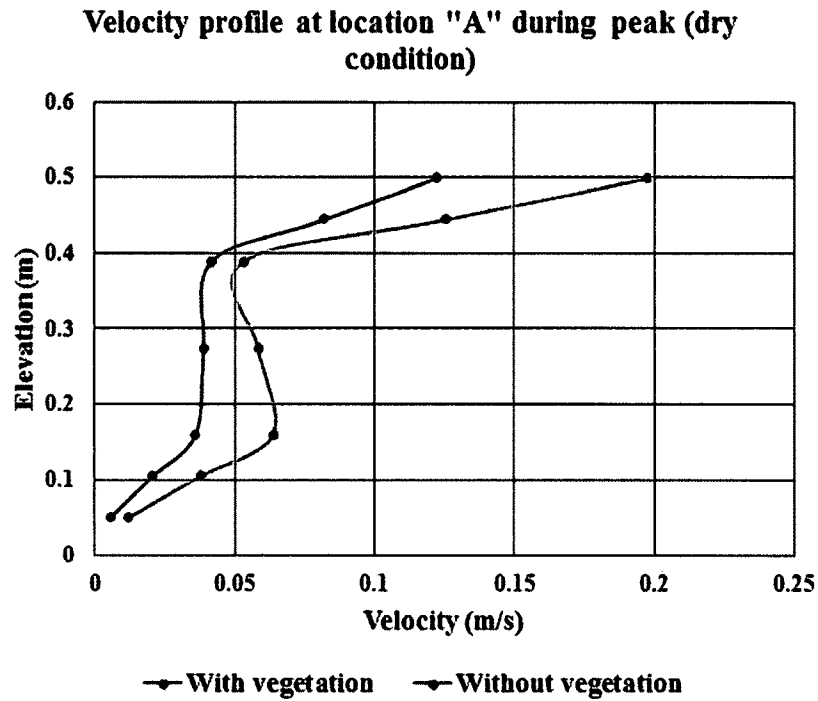


Figure 5-44: Velocity profile at location A during peak (dry condition).

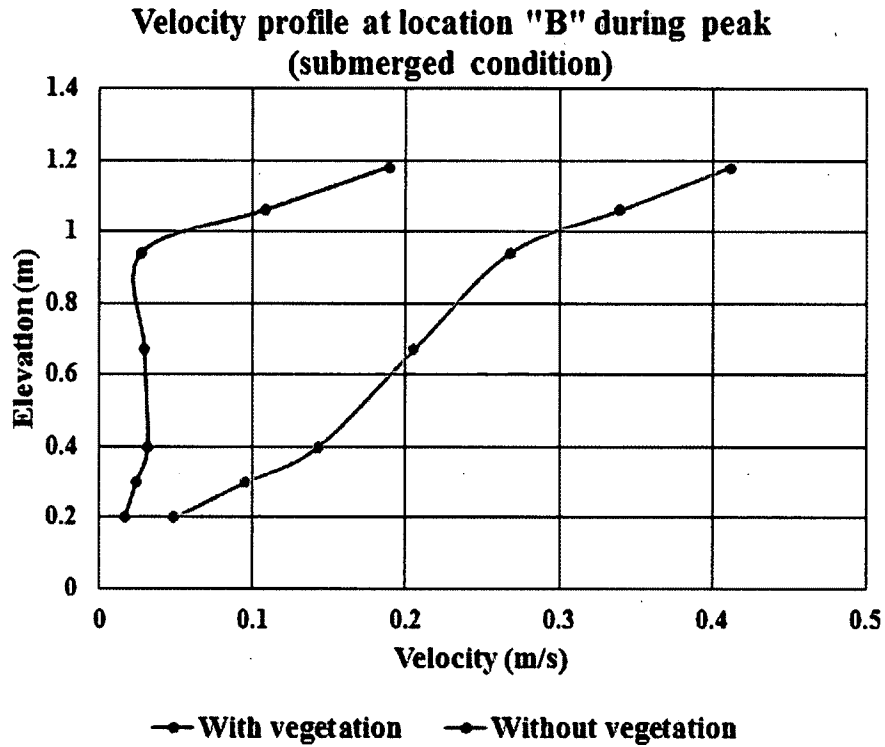


Figure 5-45: Velocity profile at location B during peak (submerged condition).

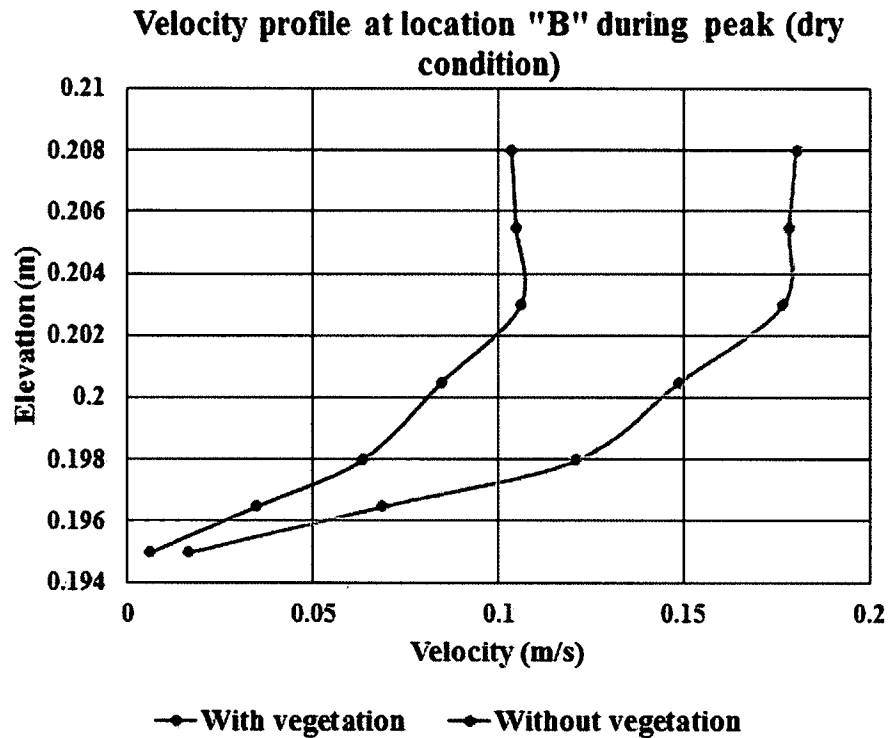


Figure 5-46: Velocity profile at location B during peak (dry condition).

5.6.4 Summary

It has been found that the presence of shoot system around the weak spot reduces bed shear stress significantly, especially while the marsh bed is submerged or under a low wave energy field. However, completely exposed vegetation during the peak of a hurricane found to be most vulnerable and supposed to experience severe mass erosion/marsh shears. The vegetation model was not intended to lead to a conclusion that the vegetation shoot system is enough to reduce the wave and current action while submerged as there might be no/less shoots available around the critical zones. However, effective use of the shoot system in absorbing wave energy can largely help to protect the critical zones of the coastal marsh area.

CHAPTER 6

EROSION PREDICTION STUDY OF *SPARTINA ALTERNIFLORA* MARSH SYSTEM UNDER HURRICANE IKE

6.1 Introduction

Root reinforcement incorporates the utilization of vegetation and engineering structures for slope stability enhancement and soil scouring reduction. In this study, we treated the major types of surface erosion as a special slope stability problem on the shallow surfaces. The study presented in this chapter is based on the research methods developed by Shahriar *et al* (2016) in which a study was conducted to quantify the root effect of the Johnson grass roots on shallow slope stability along the potential slip surfaces parallel to soil slopes in an effort to evaluate soil-binding or anti-erosion ability of the roots. It was assumed that factors of safety against these shallow slip surfaces are a direct measure of resistance to the surface erosion and not a direct measure of the overall slope stability.

The role of root reinforcement against soil erosion was evaluated by calculating factors of safety of the shallow slip surfaces. The roots were modeled using the Smeared Method (SM) by raising the overall rooted soil strength or using the Anchor Reinforcement Method (ARM), in which the roots were modeled as independent reinforcing anchors. Configurations of the root bundles, locations and distributions of individual roots were effectively taken into account in the ARM method.

During this study, only the SM method was used as the vegetation root effects were investigated in terms of contribution at different soil layer through overall enhancement in soil shear strength in the presence of roots.

Again, the surface erosion analysis in the study of Shahriar *et al* (2015) was conducted for Johnson grass on a steeper slope. The soil strength was also much higher compared to dredged sediment and to study the root contribution, very shallow slip surfaces were used during that analysis. The study presented in this dissertation includes nearly flat surface or surface with very little slope angle. It should be noted that a flat slope with no load on it is fairly stable, and instability might only occur under different loading condition on the slope surface. As a result, no specified slip surface was required for this study, and the global factors of safety was used as a measure of erosion of the mudflat surface.

This chapter summarizes the special erosion analysis of marsh bed by using Delft3D model results for the hurricane-induced tides and current waves at Calcasieu-Sabine Basin marsh area described in Chapter 4. The slope stability analyses were performed by utilizing commercial software program Slope/W to evaluate the grass soil-binding capability following the Smeared Method (SM). It should be also noted that the slope stability analysis is a static analysis but the impact of the hurricane is a dynamic process. Therefore, hurricane impact was studied for two critical periods of Hurricane Ike, namely hurricane landfall and hurricane peak as discussed in Chapter Five.

6.2 Erosion Prediction Model

6.2.1 Model Setup

Two different sections from the area of interest have been considered for erosion analysis. One section is the mudflat with a flat slope as shown in **Figure 6-1**.

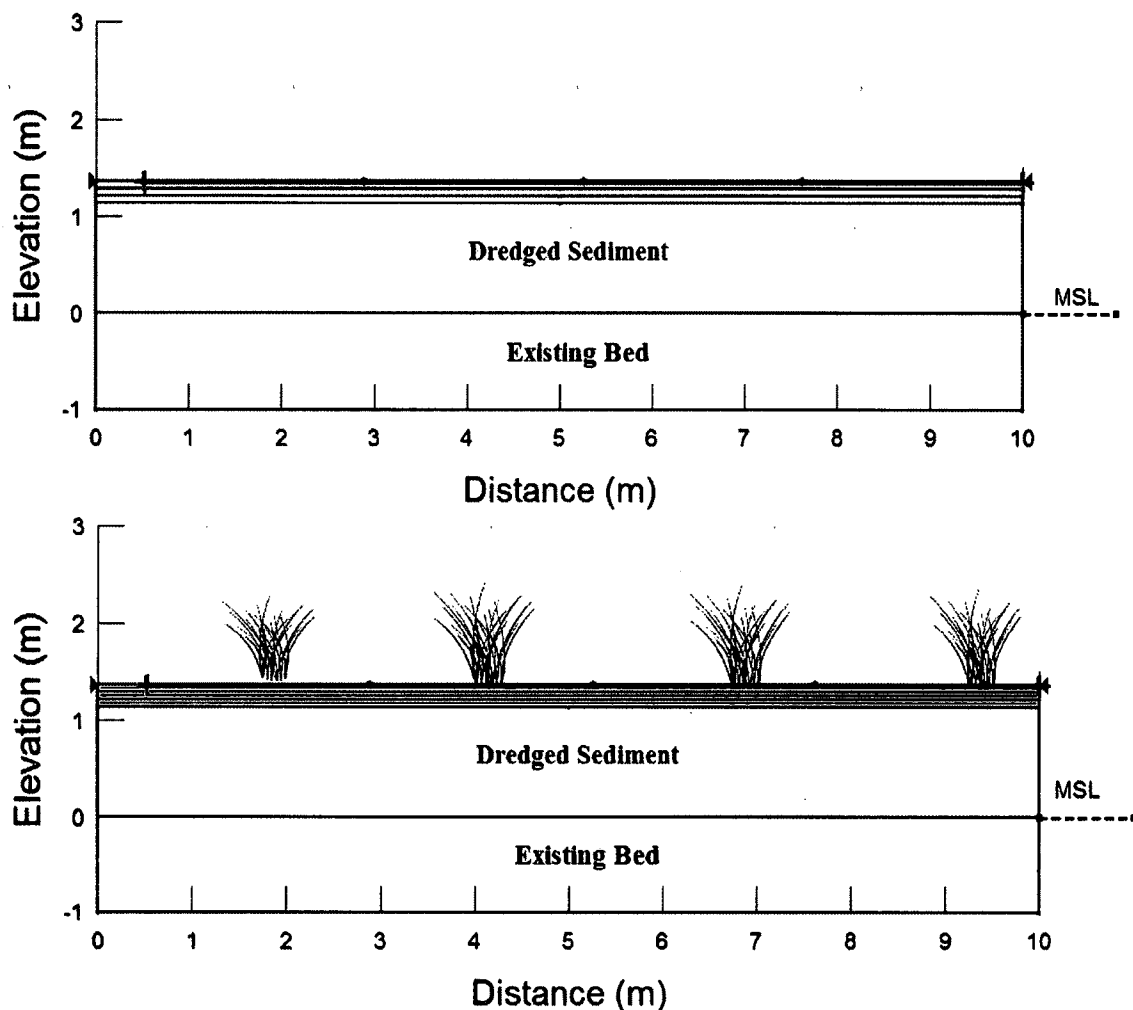


Figure 6-1: Mudflat section for plain soil (top) and rooted soil (bottom).

Another one is the marsh edge section as shown in **Figure 6-2**. During the marsh creation, dredged sediments was placed over the existing bed up to an elevation of 1.37 m (CPRA project monitoring report) and the dredged sediment layer in this study was considered with the same thickness. Section lengths were selected based on the study of the Delft3D output. Considering the maximum stress generation point at the middle, the results were observed for stress variation over the length and section length with no significant change in stress they were considered for both types of sections. Slope length of 10 m selected for the marsh flat model study and for marsh edge section, slope was considered over 5 m horizontal surface with 1V:30H slope as obtained from Delft3D dry

bed level elevation study for the specified length. In the case of the marsh edge section, only the slope of the marsh edge was considered during load application.

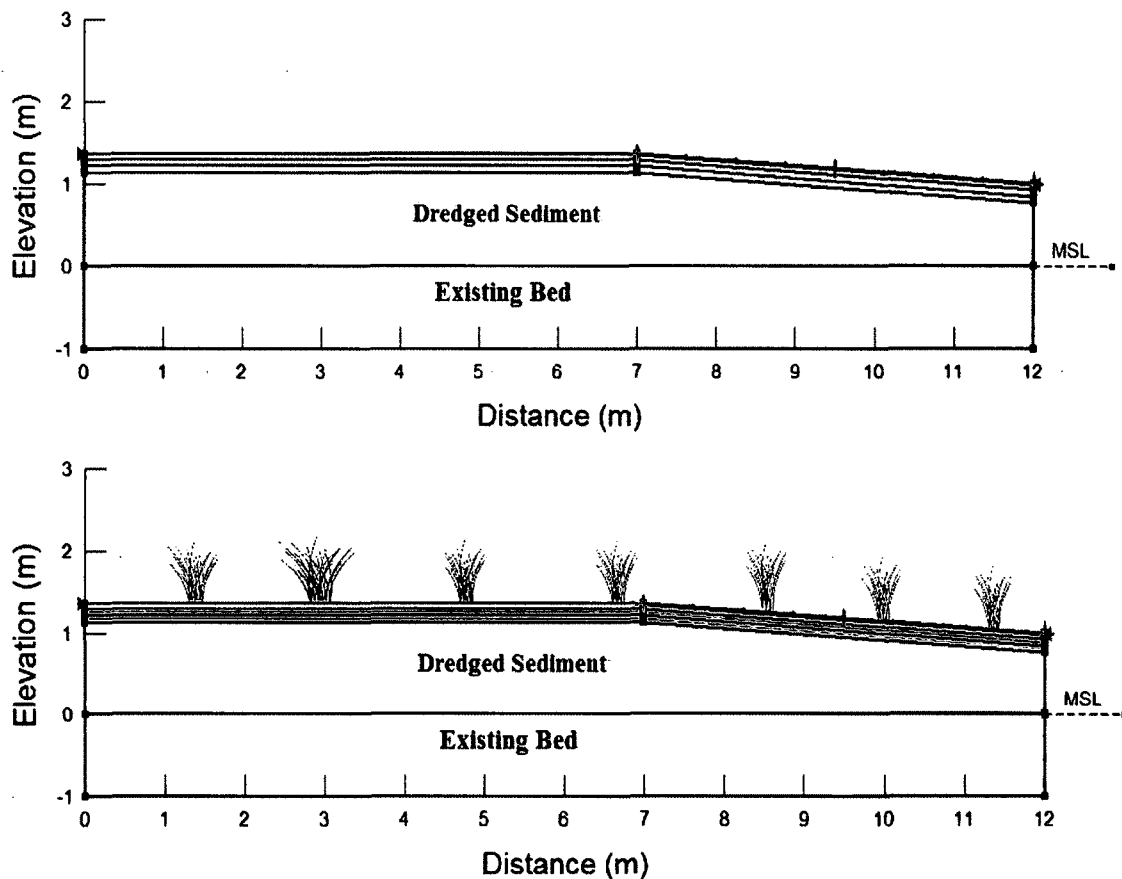
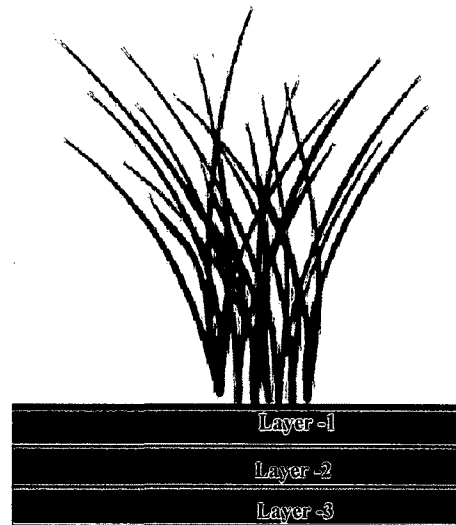


Figure 6-2: Marsh edge section for plain soil (top) and rooted soil (bottom).

6.2.2 Material Properties

Material properties used in the erosion analysis were obtained from the lab experiment results for rooted and non-rooted soil documented in Chapter 3. The soil profile is divided into three layers at the top for vegetated model input as shown in **Figure 6-3**, and thickness of each layer were selected based on the layer distribution method adopted in Chapter 3. Summary of the soil strength properties for the different layers is presented in **Table 6-1**.



Dredged sediment/ plain soil

Figure 6-3: Layer distribution of marsh soil.

Table 6-1: Material properties used in erosion model.

Soil profile	Layer characteristics	Layer thickness (m)	Soil strength parameters	
			C (kPa)	Phi (degree)
Layer 1	Rooted soil	.076	2.43	28
Layer 2	Rooted soil	076	2	17
Layer 3	Rooted soil	076	1.69	14
Dredged sediment	Plain soil	1.37*	0.63	13

*Thickness is total sediment layer thickness and in presence rooted layer at top it decreases accordingly.

6.2.3 Model Scenarios

In order to study all the effects during a hurricane over coastal marsh, a total of 16 scenarios were studied. A list of all scenarios are presented in **Table 6-2**. Hurricane landfall, time and peak time were determined as September 12, 18:00 hours and September 13, 02:00 hours, respectively. To make it easily understandable, all the scenarios are highlighted with different colors in four segments, where each segment presents the same

study location and hurricane time. In this chapter, model inputs and outputs are discussed mainly based on two different times of the hurricane.

Table 6-2: Model scenarios for erosion analysis.

Scenario #	Time during hurricane	Location	Inundation condition	Vegetation presence
1	Landfall	Marsh edge	Submerged	No
2	Landfall	Marsh edge	Submerged	Yes
3	Landfall	Marsh edge	Dry	No
4	Landfall	Marsh edge	Dry	Yes
5	Landfall	Marsh flat	Submerged	No
6	Landfall	Marsh flat	Submerged	Yes
7	Landfall	Marsh flat	Dry	No
8	Landfall	Marsh flat	Dry	Yes
9	Peak	Marsh edge	Submerged	No
10	Peak	Marsh edge	Submerged	Yes
11	Peak	Marsh edge	Dry	No
12	Peak	Marsh edge	Dry	Yes
13	Peak	Marsh flat	Submerged	No
14	Peak	Marsh flat	Submerged	Yes
15	Peak	Marsh flat	Dry	No
16	Peak	Marsh flat	Dry	Yes

6.2.4 Model Loading Condition

Hurricane generated stress and water depth for each scenario were obtained from Delft3D and applied accordingly into the model. To study the extreme effects during a hurricane, results were obtained at location A used for marsh edge analysis and results were obtained from location B used for marsh flat analysis as these points were physically located on marsh edge and marsh flat surface respectively. The shear stress acts tangential to the surface of the marsh and is multiplied by the area over which it acts to calculate total wave force. The stress was assumed constant over the surface and force calculation was conducted by taking the unit's width of the surface. The calculated force was then

distributed at each unit interval over the surface. The key input parameters, i.e., shear stress and water depth for all the scenarios (SC) are presented in **Table 6-3**.

Table 6-3: Model input conditions.

SC #	Time during hurricane	Location	Inundation condition	Vegetation presence	Max shear stress (Pa)	Water depth (m)
1	Landfall	Marsh edge	Submerged	No	1.180	0.937
2	Landfall	Marsh edge	Submerged	Yes	0.940	0.940
3	Landfall	Marsh edge	Dry	No	29.04	0.098
4	Landfall	Marsh edge	Dry	Yes	16.58	0.14
5	Landfall	Marsh flat	Submerged	No	0.302	0.640
6	Landfall	Marsh flat	Submerged	Yes	0.063	0.640
7	Landfall	Marsh flat	Dry	No	0	0
8	Landfall	Marsh flat	Dry	Yes	0	0
9	Peak	Marsh edge	Submerged	No	2.760	1.300
10	Peak	Marsh edge	Submerged	Yes	1.710	1.280
11	Peak	Marsh edge	Dry	No	17.380	0.620
12	Peak	Marsh edge	Dry	Yes	10.410	0.600
13	Peak	Marsh flat	Submerged	No	0.670	0.990
14	Peak	Marsh flat	Submerged	Yes	0.130	0.970
15	Peak	Marsh flat	Dry	No	46.390	0.012
16	Peak	Marsh flat	Dry	Yes	9.890	0.006

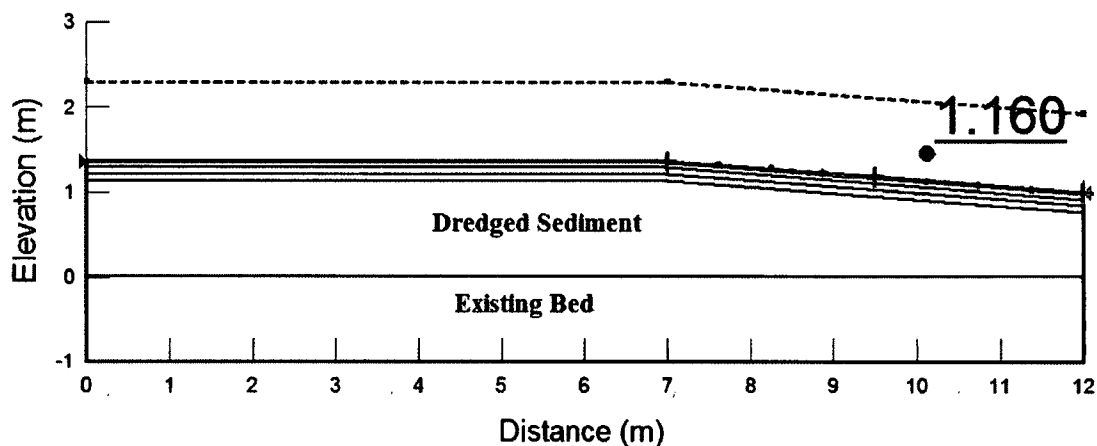
6.2.5 Results

Results for all scenarios are presented in **Table 6-4**. Erosion study results revealed that the erosion occurred for scenarios 3, 4, 9, 11, 15 and 16. It is difficult to understand the erosion significance of erosion just by analyzing the factors of safety value as it is just proving the weakest slip surface and might be located at very shallow depth without damaging the marsh root structure. As this study mainly focused on the mass erosion event or uprooting of vegetation roots under a hurricane impact, a detail analysis was conducted to understand the failure path during different scenarios. As there was no hurricane force for scenarios 7 and 8, both of the scenarios were excluded during the erosion model study.

Table 6-4: Erosion prediction model results

SC #	Time during hurricane	Location	Inundation condition	Vegetation presence	FOS	Prediction
1	Landfall	Marsh edge	Submerged	No	1.16	No erosion
2	Landfall	Marsh edge	Submerged	Yes	2.71	No erosion
3	Landfall	Marsh edge	Dry	No	0.22	Erosion
4	Landfall	Marsh edge	Dry	Yes	0.84	Erosion
5	Landfall	Marsh flat	Submerged	No	13.76	No erosion
6	Landfall	Marsh flat	Submerged	Yes	33.62	No erosion
7	Landfall	Marsh flat	Dry	No	-	-
8	Landfall	Marsh flat	Dry	Yes	-	-
9	Peak	Marsh edge	Submerged	No	0.58	Erosion
10	Peak	Marsh edge	Submerged	Yes	1.66	No erosion
11	Peak	Marsh edge	Dry	No	0.29	Erosion
12	Peak	Marsh edge	Dry	Yes	1.13	No erosion
13	Peak	Marsh flat	Submerged	No	5.98	No erosion
14	Peak	Marsh flat	Submerged	Yes	14.62	No erosion
15	Peak	Marsh flat	Dry	No	0.34	Erosion
16	Peak	Marsh flat	Dry	Yes	0.57	Erosion

Results of all scenarios were investigated to understand the failure of the surface during the hurricane's impact. All resulted scenarios are presented from **Figure 6-4** to **Figure 6-17**.

**Figure 6-4: Factors of safety for scenario 1.**

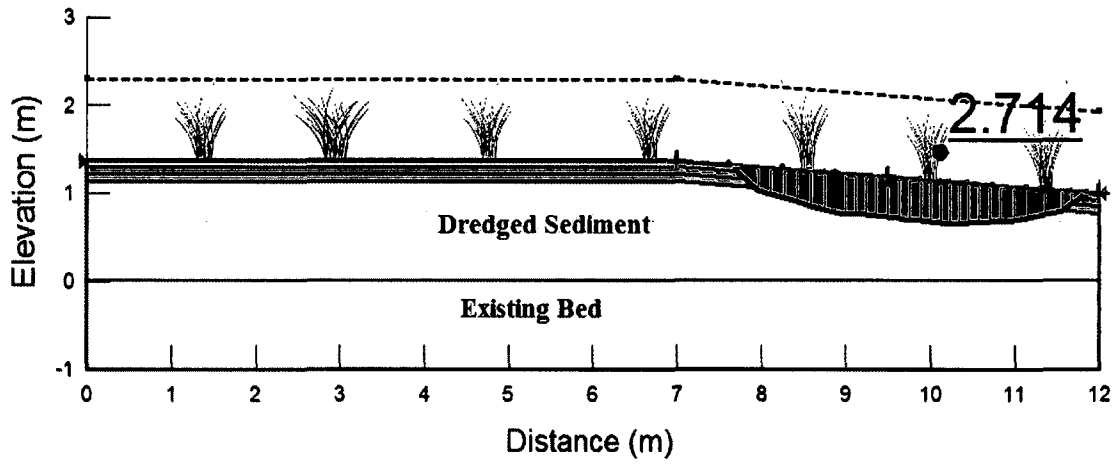


Figure 6-5: Factors of safety for scenario 2.

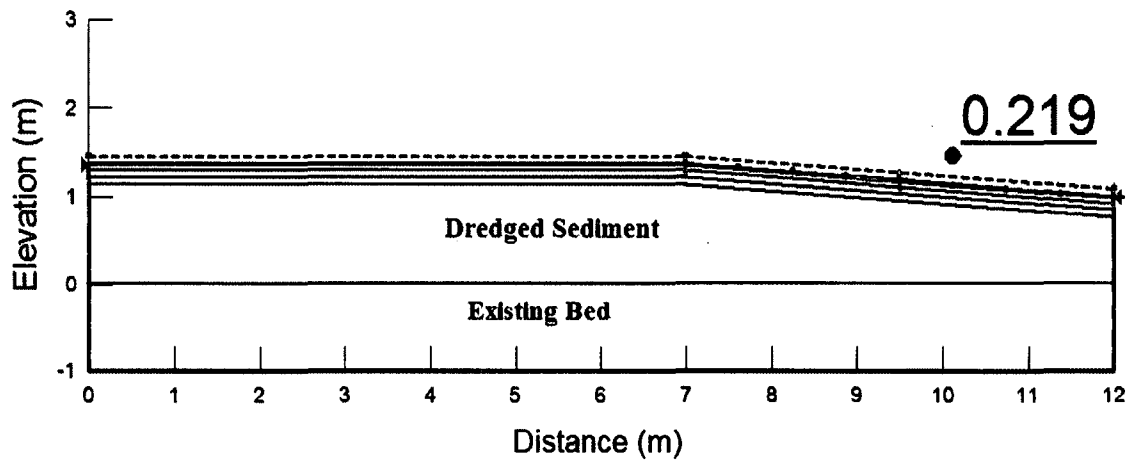


Figure 6-6: Factors of safety for scenario 3.

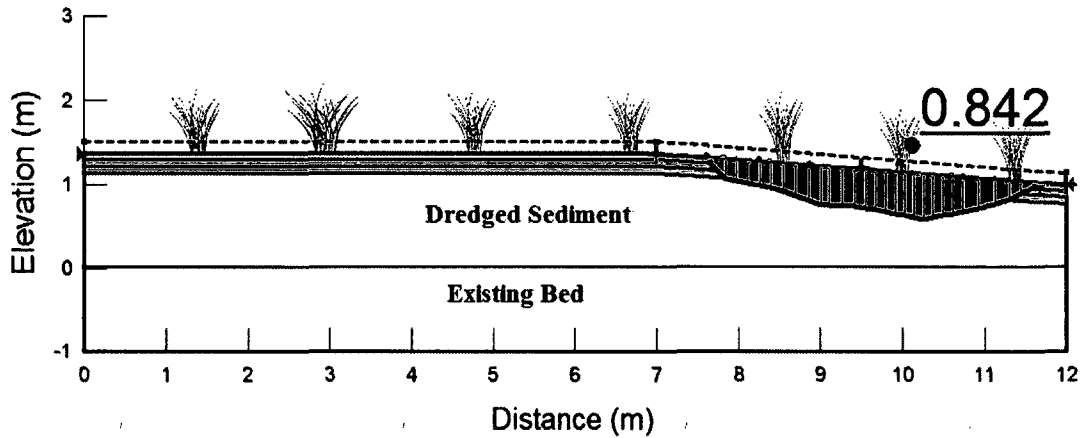


Figure 6-7: Factors of safety for scenario 4.

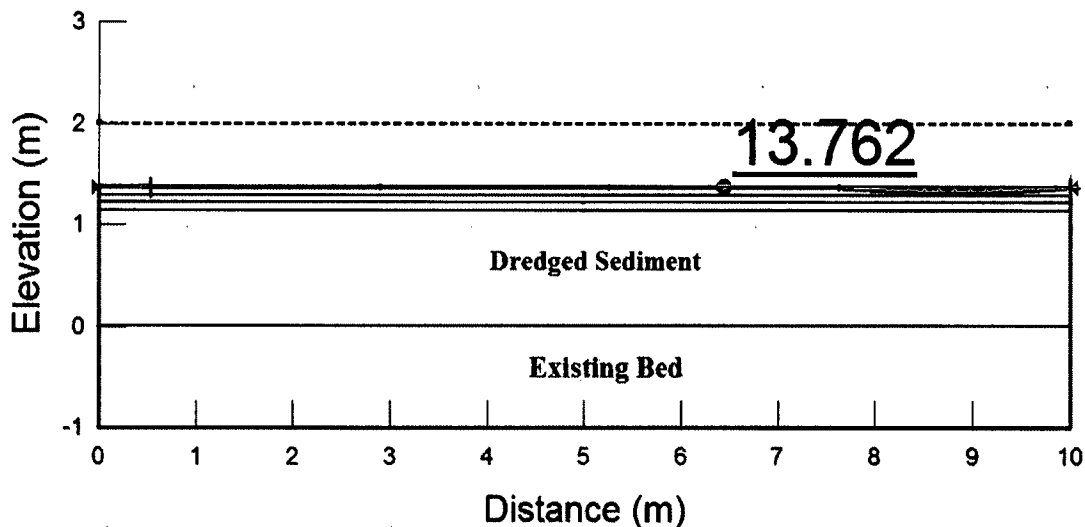


Figure 6-8: Factors of safety for scenario 5.

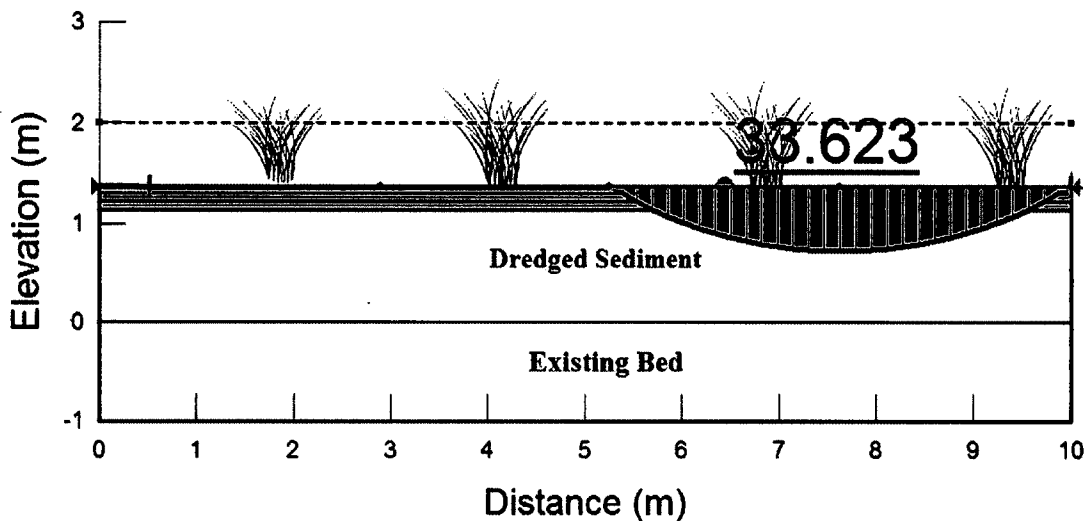


Figure 6-9: Factors of safety for scenario 6.

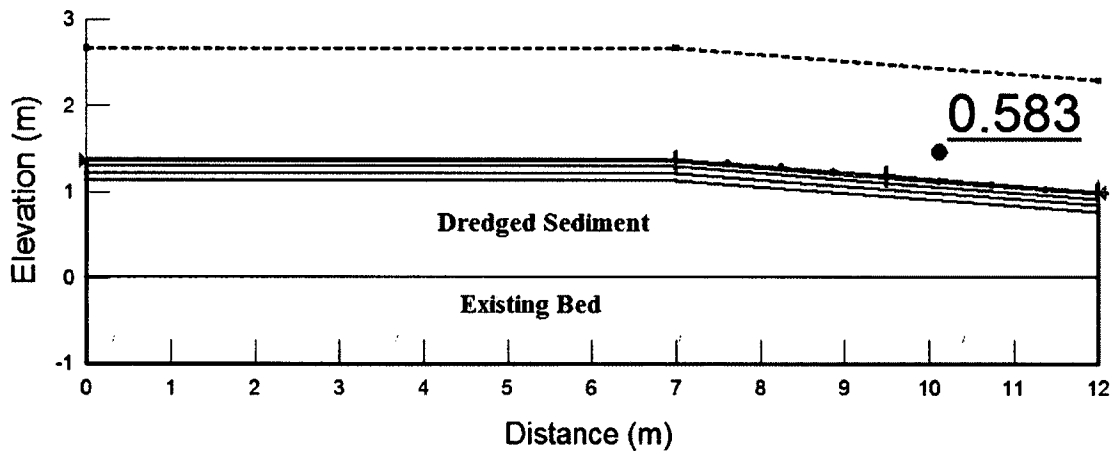


Figure 6-10: Factors of safety for scenario 9.

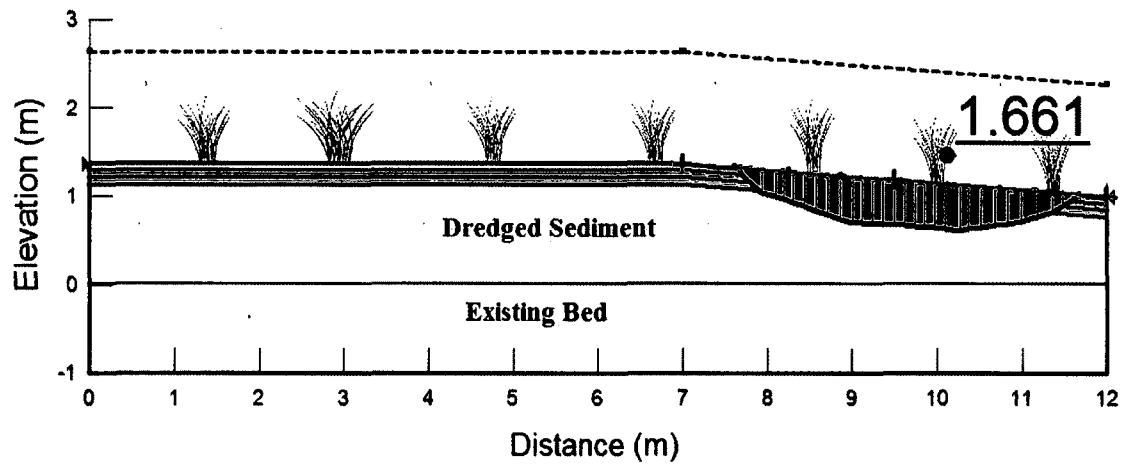


Figure 6-11: Factors of safety for scenario 10.

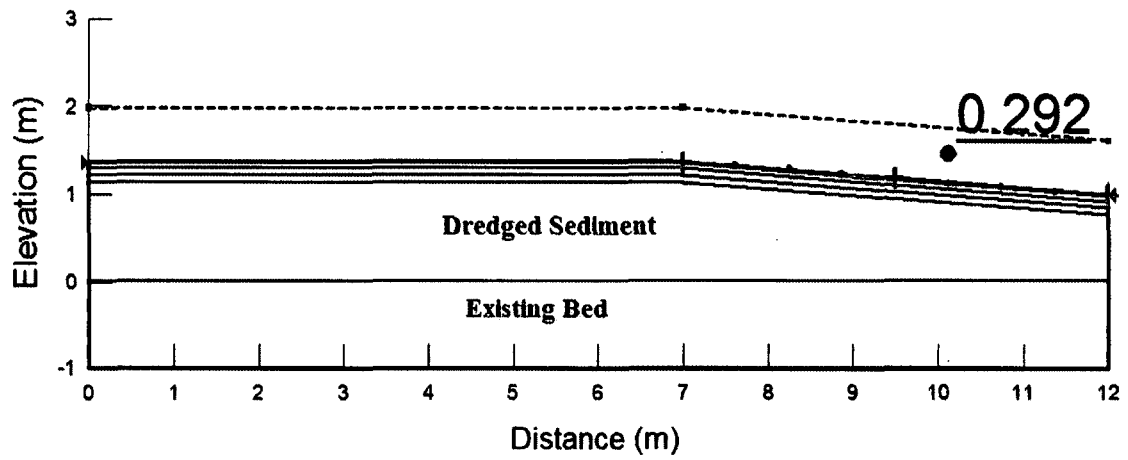


Figure 6-12: Factors of safety for scenario 11.

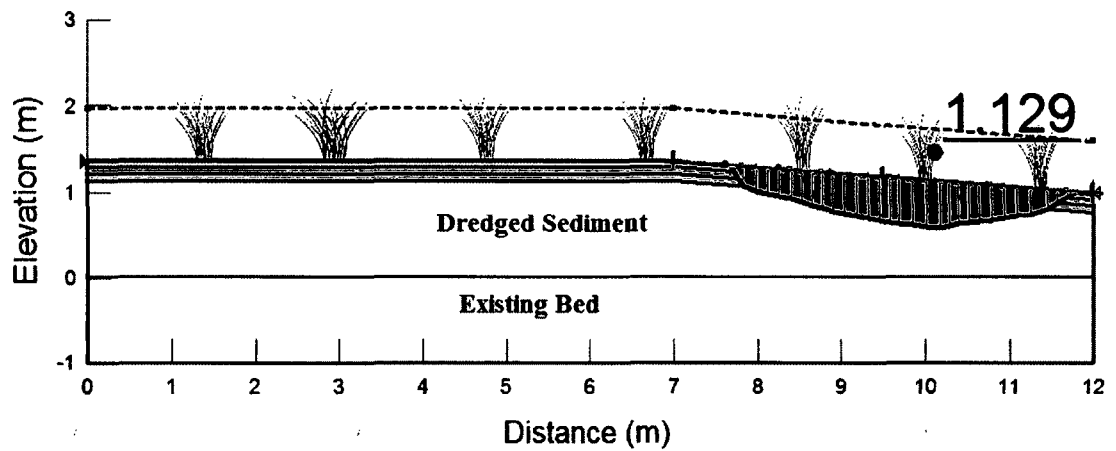


Figure 6-13: Factors of safety for scenario 12.

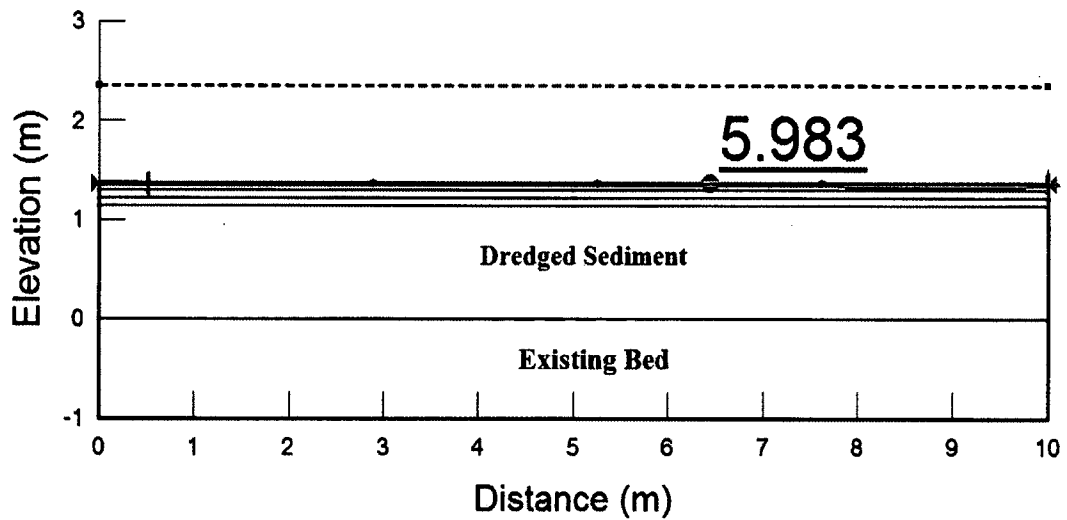


Figure 6-14: Factors of safety for scenario 13.

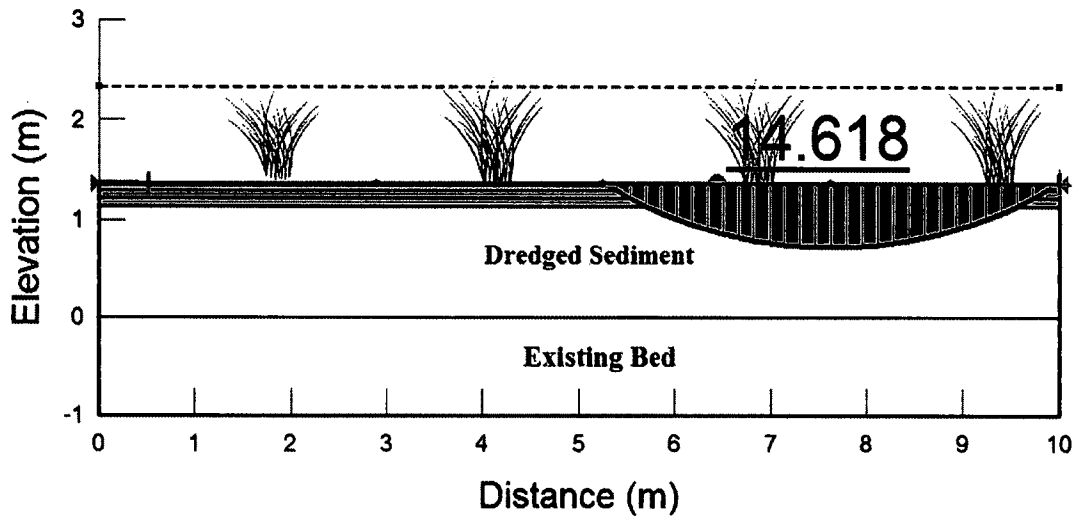


Figure 6-15: Factors of safety for scenario 14.

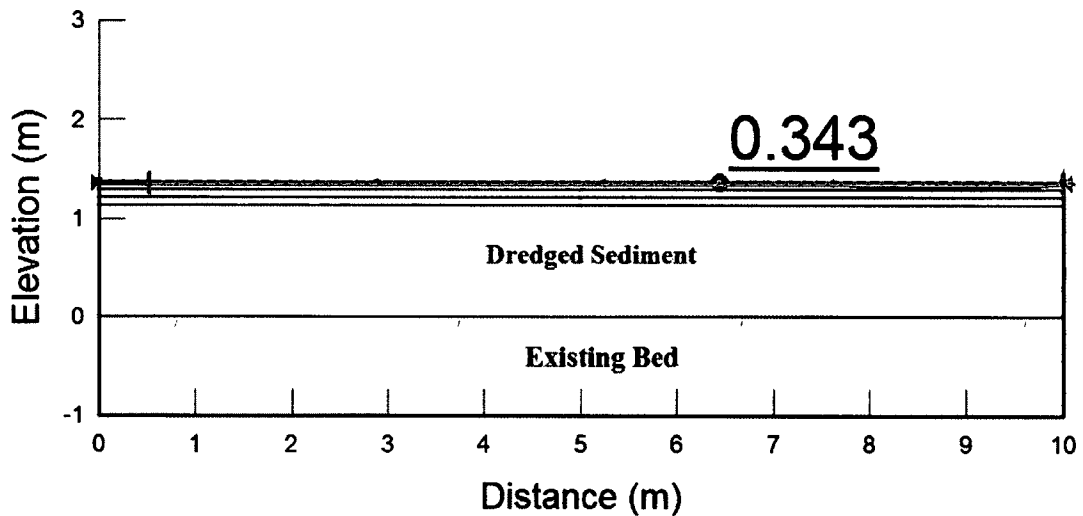


Figure 6-16: Factors of safety for scenario 15.

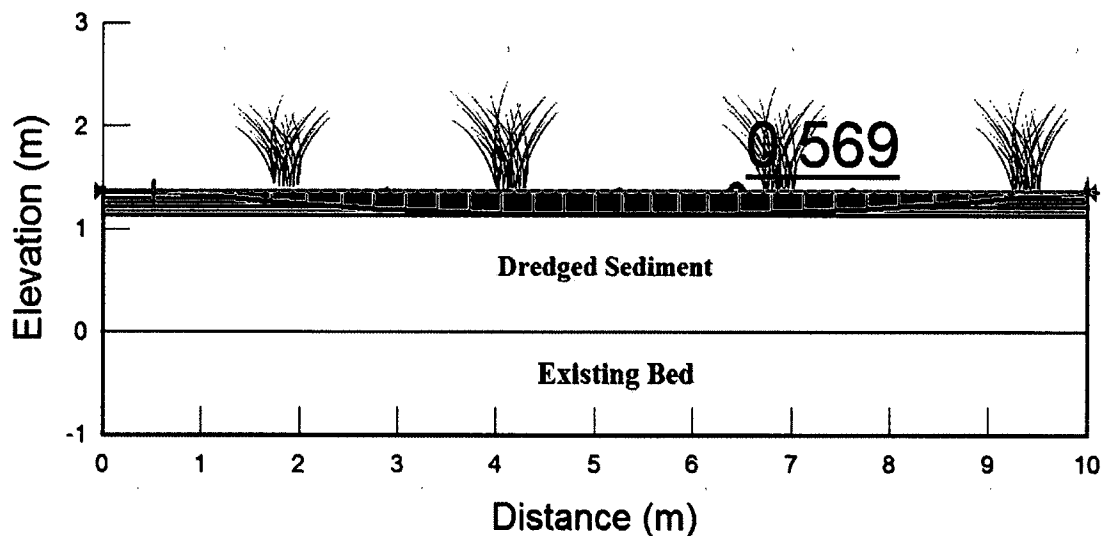


Figure 6-17: Factors of safety for scenario 16.

6.2.6 Summary

It was found that the marsh mudflat is prone to experience significant erosion while in drought condition during the hurricane's impact. It was observed that the vegetation is very capable of reducing wave current induced shear stress under low wave energy setting, but behave differently when high wave directly impact hit the marsh surface.

Erosion study outputs are summarized in **Table 6-5**. It was observed that the erosion was predicted for a number of cases but uprooting or mass erosion only occurred during two scenarios. Near the marsh edge, mass erosion occurred during the hurricane's landfall with the condition that the marsh edge was above water prior to hurricane's impact. On marsh flat, mass erosion occurred during the peak of the hurricane when analyzed with drought condition prior to the hurricane.

Table 6-5: Model results.

Scenario #	Time during hurricane	Location	Inundation condition	Vegetation presence	FOS	Prediction
1	Landfall	Marsh edge	Submerged	No	1.16	No erosion
2	Landfall	Marsh edge	Submerged	Yes	2.71	No erosion
3	Landfall	Marsh edge	Dry	No	0.22	Erosion
4	Landfall	Marsh edge	Dry	Yes	0.84	Uprooting
5	Landfall	Marsh flat	Submerged	No	13.76	No erosion
6	Landfall	Marsh flat	Submerged	Yes	33.62	No erosion
7	Landfall	Marsh flat	Dry	No	-	-
8	Landfall	Marsh flat	Dry	Yes	-	-
9	Peak	Marsh edge	Submerged	No	0.58	Erosion
10	Peak	Marsh edge	Submerged	Yes	1.66	No erosion
11	Peak	Marsh edge	Dry	No	0.29	Erosion
12	Peak	Marsh edge	Dry	Yes	1.13	No erosion
13	Peak	Marsh flat	Submerged	No	5.98	No erosion
14	Peak	Marsh flat	Submerged	Yes	14.62	No erosion
15	Peak	Marsh flat	Dry	No	0.34	Erosion
16	Peak	Marsh flat	Dry	Yes	0.57	Uprooting

CHAPTER 7

SUMMARY, CONCLUSIONS AND RECOMMENDATIONS

7.1 Summary

This research includes extensive *in-situ* and laboratory testing of shear strength of vegetated and non-vegetated marsh soil in coastal Louisiana. A marsh creation project site was selected for the study. Additionally, shear strength enhancement of soil in the presence of *Spartina alterniflora* roots was summarized in an equation based on additional cohesion.

To study the hydrodynamic and wave impact on coastal marsh, as a wave flow coupled model covering the study area was developed, calibrated and validated against field data. Delft3D was found to be very capable in producing proper current circulation throughout the domain. Hydrodynamic and wave coupled model was later used to study the impact of a major hurricane (Ike) on coastal marshes. The model was tested with different scenarios to investigate the extreme conditions. Major scenarios involved the inclusion of vegetation and generating hurricane impact over a drought marsh. The hurricane model results indicated that the presence of vegetation shoots had dominant effect on reducing bed shear stresses for most cases while less effective during high wave impact and expedite loss if completely exposed to hurricane waves during the peak hour.

Finally, results of lab experiments and hurricane model were used simultaneously to predict erosion during different periods of the hurricane. A total of 16 scenarios were

studied for the hurricane impact on marsh edge and marsh flat surface. Results revealed that the hurricane's impact was severe near edges during landfall and most devastating on marsh flat while marsh bed was fully exposed during the peak. Slope/W was found to be a very productive tool in predicting marsh erosion, especially in predicting extreme erosion/uprooting of marsh during the extreme event.

7.2 Conclusions

In this dissertation, research achievements are presented on the significance of coastal marsh under severe hurricane condition. From the results obtained, the following conclusions can be made.

The *Spartina alterniflora* root system effectively increased the soil shear strength up to a shallow depth. The lab study was conducted for three layers from the top surface. The vegetation root enhanced the shear strength by roughly 285%, and for the bottom two layers, strength enhancements were roughly 217% and 186%, respectively. The reinforcing effect of roots is more significant on cohesion than on the friction angle. In this research, a direct relation between root tensile strength and cohesion was introduced by factorizing the direct shear test results. It was concluded that the root enhances the cohesion of dredged sediment by 5% of its tensile strength.

The tide and wave of the Calcasieu estuary has been successfully modeled. The model was calibrated and validated for the periods of August 15, 2008 to September 15, 2008, which included Hurricane Gustav and Hurricane Ike. The model effectively responded to the flooding and drying condition during the hurricane period which indicates high capability of Delft3D in generating hydrodynamic and wave condition in a coastal marsh environment.

It was found that the edge and flat soil mass react differently under hurricane-induced waves and current actions, especially when time dependent analysis was considered. At the beginning of a hurricane generation, mudflat showed higher stability where the marsh edge was found to be vulnerable. Significant reduction in stability was discovered in mudflat during the peak period of the storm and that can result in a higher erosion rate than the edge erosion. It was also observed that the presence of a shoot system around the weak spot reduced bed shear stress significantly, especially while the marsh bed was submerged or under a low wave energy field. Yet, the completely exposed vegetation during the peak of a hurricane was found to be most vulnerable and supposed to experience severe mass erosion/marsh shears. The vegetation model did not intend to lead to a conclusion that the vegetation shoot system was enough to reduce the wave and current action while submerged as there might be no/less shoots available around the critical zones. However, effective use of the shoot system in absorbing wave energy can largely help to protect the critical zones of the coastal marsh area.

It was observed that significant damage might have occurred in the study area if there were no Hurricane Gustav before Hurricane Ike. The extreme precipitation and indirect flooding during Hurricane Gustav reduced the damaging effect of Hurricane Ike which came later. The results also explained the severe erosion in the study area during Hurricane Rita; 95% of the marsh in Cycle-1 was eroded during Hurricane Rita, where the same location experienced minor/no erosion during Hurricane Ike. It can be concluded that the drought condition over the vegetated marsh field during Hurricane Rita impact led to severe erosion/uprooting of marsh in the area of interest.

The Slope/W-based analyses indicated that the commercial software can be used as a robust tool to predict erosion on the marsh surface under extreme hurricane conditions.

It was found that the marsh mudflat is prone to experience significant erosion while in drought condition during the hurricane's impact. It was observed that the vegetation is very capable of reducing wave current induced shear stress under low wave energy setting, but behave differently when high waves directly hit the marsh surface.

From the outcomes of the erosion prediction analyses, it was observed that the uprooting or mass erosion only occurred during two scenarios among sixteen scenarios. Near the marsh edge, mass erosion occurred during the hurricane's landfall with the condition that the marsh edge was above water prior to the hurricane's impact. On marsh flat, mass erosion occurred during the peak times of the hurricanes while analyzed with drought condition prior to the hurricanes.

7.3 Recommendations

Based on the findings of this research, the following recommendations can be made:

- 1) The low elevated marsh land that stayed submerged prior to a hurricane's impact tends to experience less damage during the hurricane. Further study to determine the elevation of the marsh bed should be conducted.
- 2) The vegetated marsh experienced higher hurricane stress while completely exposed during the hurricane's peak time. This most probably occurred due to the direct stress resulting from wave breaking over the vegetated marsh. Wave-generated shear stress depends on the wave friction factor f_w . Delft3D has the ability to generate a wave friction factor and frictional resistance for vegetation

based on the model inputs such as vegetation height, stem diameter and plant distributions. However, a further study is recommended for proper assessment of the *Spartina alterniflora* friction resistance with variable vegetation height, stem diameter and plant distribution.

- 3) It should also be noted that lower marsh/submerged marsh will allow more wave induced current to the city/commercially important location resulting in significant economic loss. On the other hand, exposed marsh was not found to be sufficient in resisting higher energy wave, which also led to replanting in major locations of the marsh creation projects. Based on the findings, it is highly recommended to study the combined approach (soft and hard engineering techniques) while considering projects for reducing marsh erosion. Different marsh creation projects considering two to three segments of marsh land from offshore to inshore can be studied for further improvement in the marsh creation projects.
- 4) Hurricane energy-absorption capacity of marshes should be carried out for different vegetation communities which will provide a valuable opportunity for further improvements. Sensitivity studies of bed shear stress to minor variations in stem characteristics are also recommended.
- 5) Before taking up an investment project, it is recommended that the whole area be divided into smaller areas/segments and local model with closure grid spacing be developed for each area/segment in order to study the feasibility of the project based on this master model developed during this research.

APPENDIX A
DELFT3D MODEL INPUTS

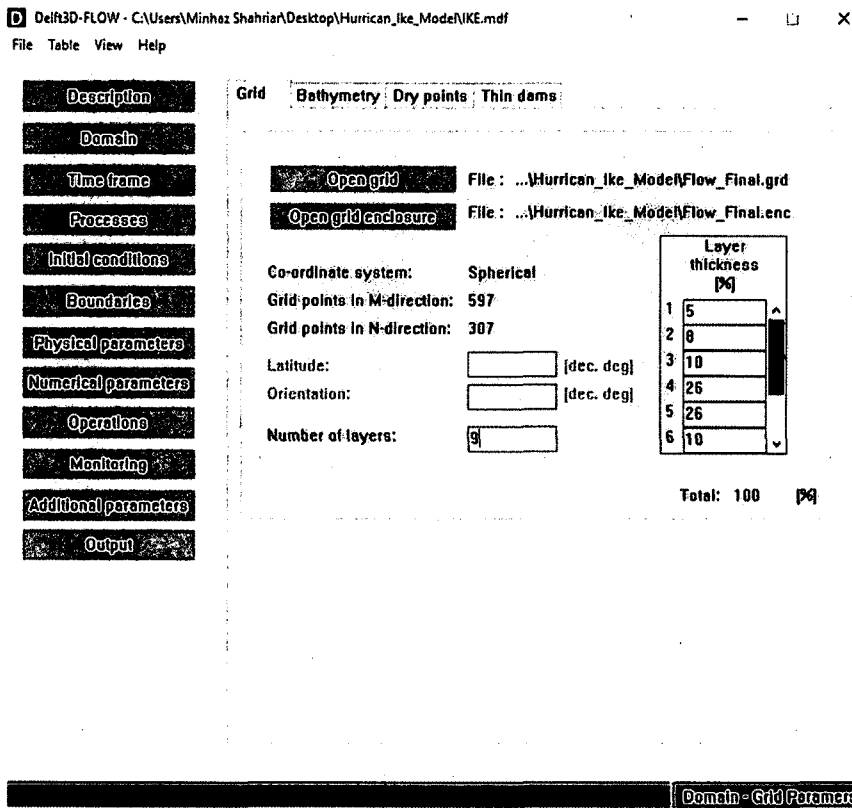


Figure A-1: Delft3D Flow grid input through GUI.

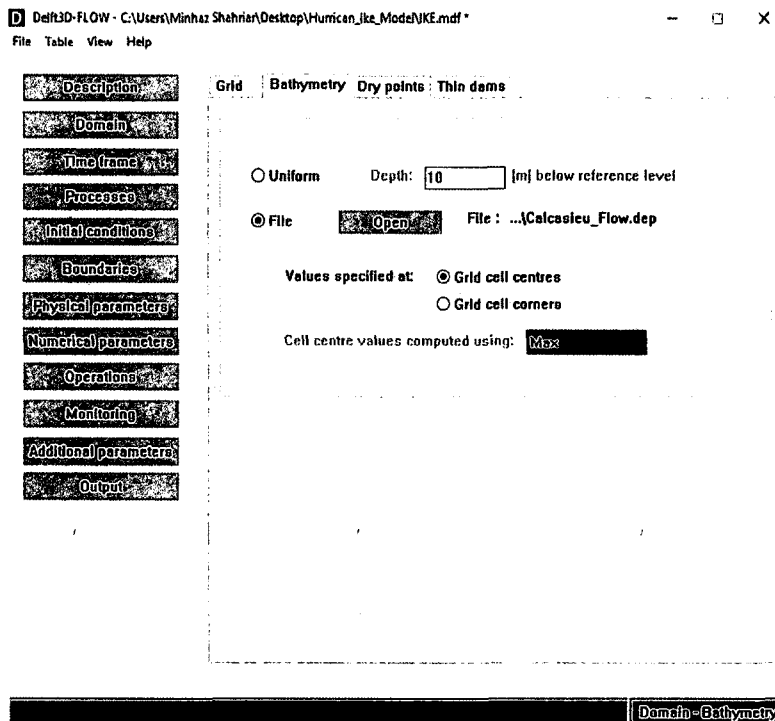


Figure A-2: Delft3D Flow depth input through GUI.

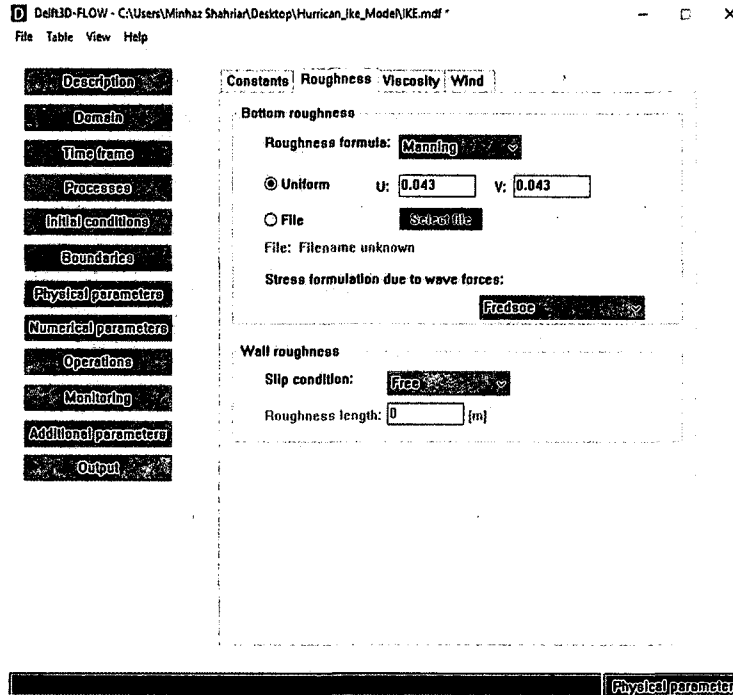


Figure A-3: Delft3D Flow roughness input through GUI.

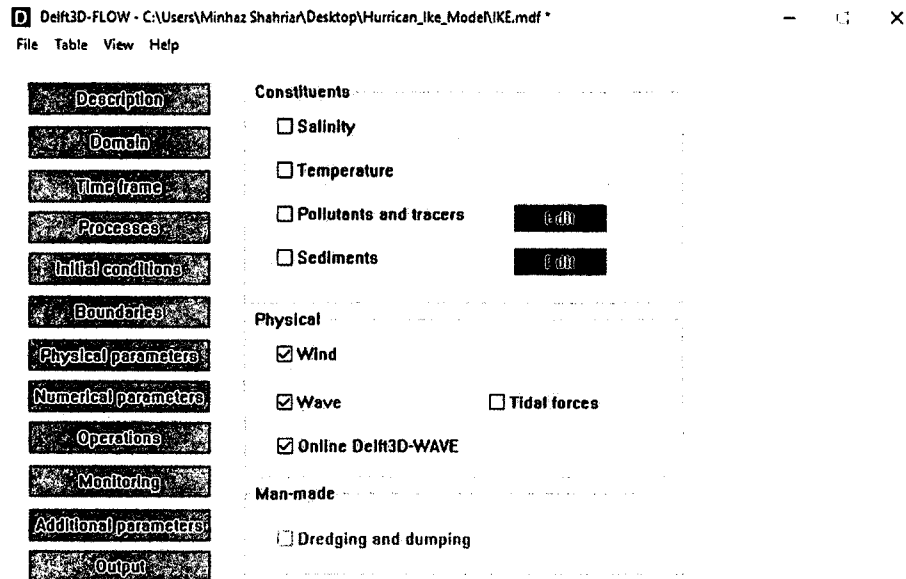


Figure A-4: Delft3D Flow process input through GUI.

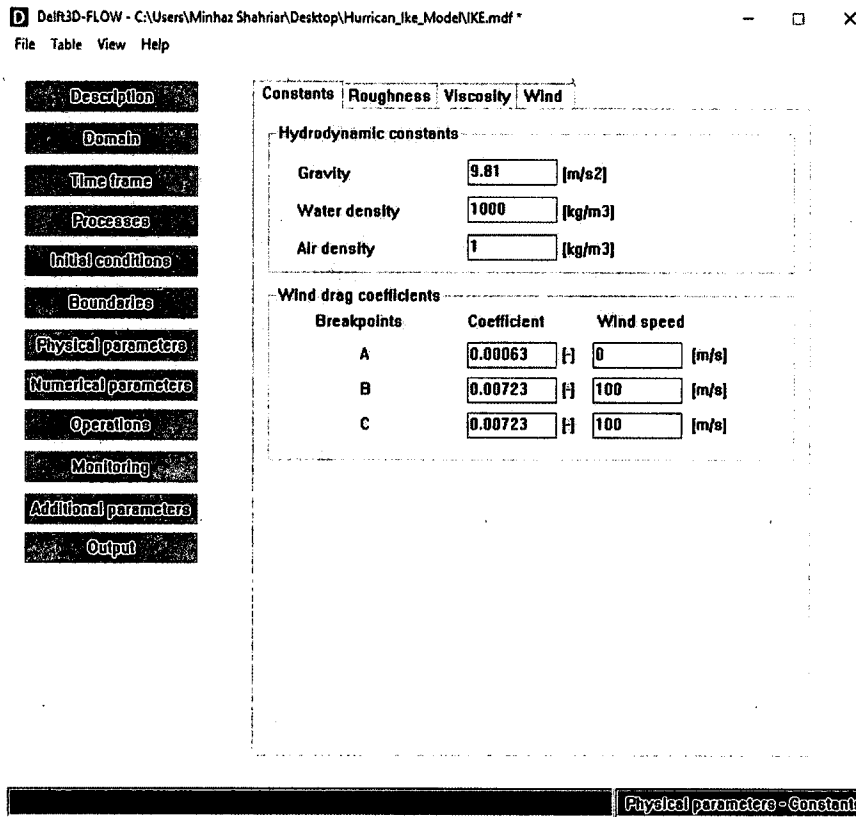


Figure A-5: Delft3D Flow constant input through GUI.

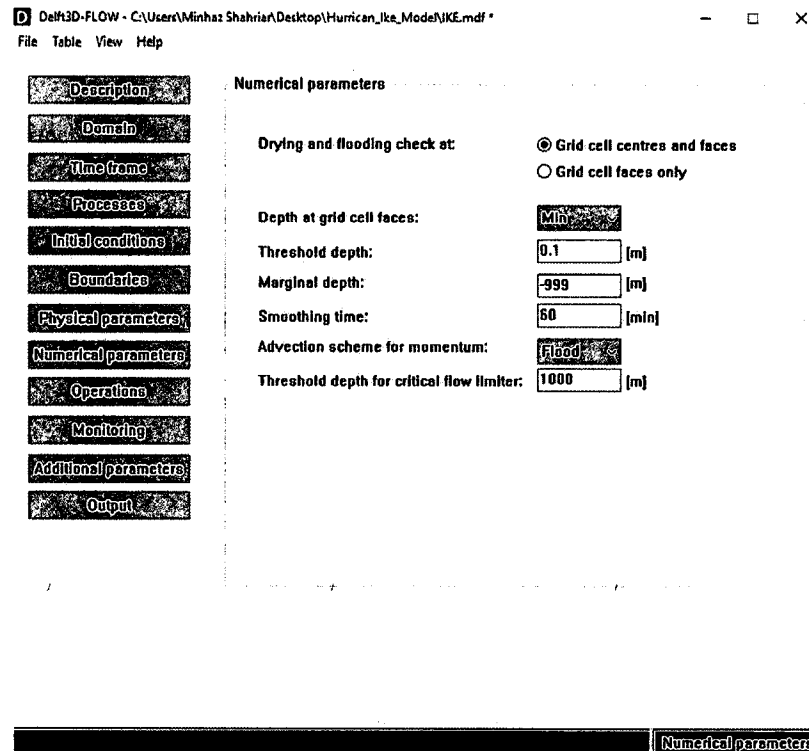


Figure A-6: Delft3D Flow numerical parameters input through GUI.

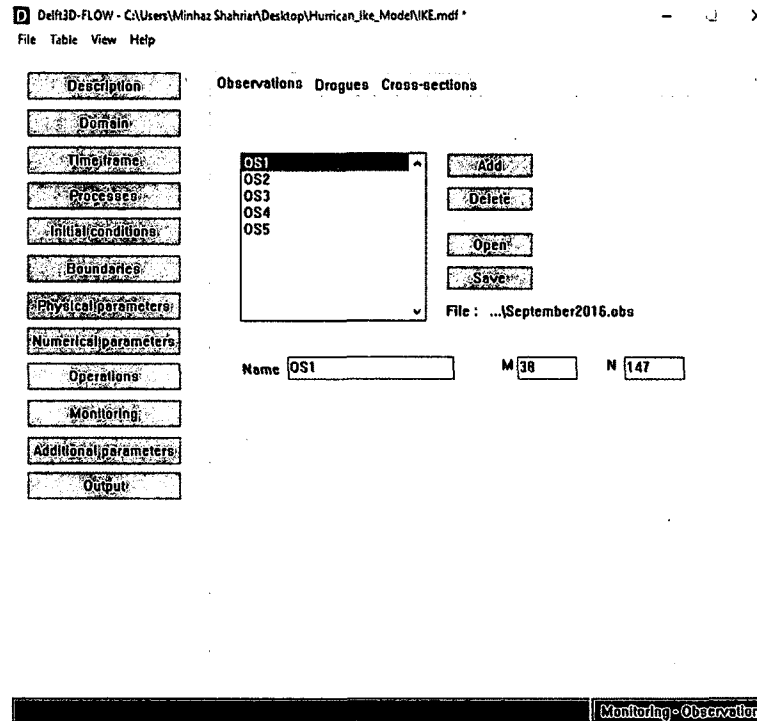


Figure A-7: Delft3D Flow observation points input through GUI.

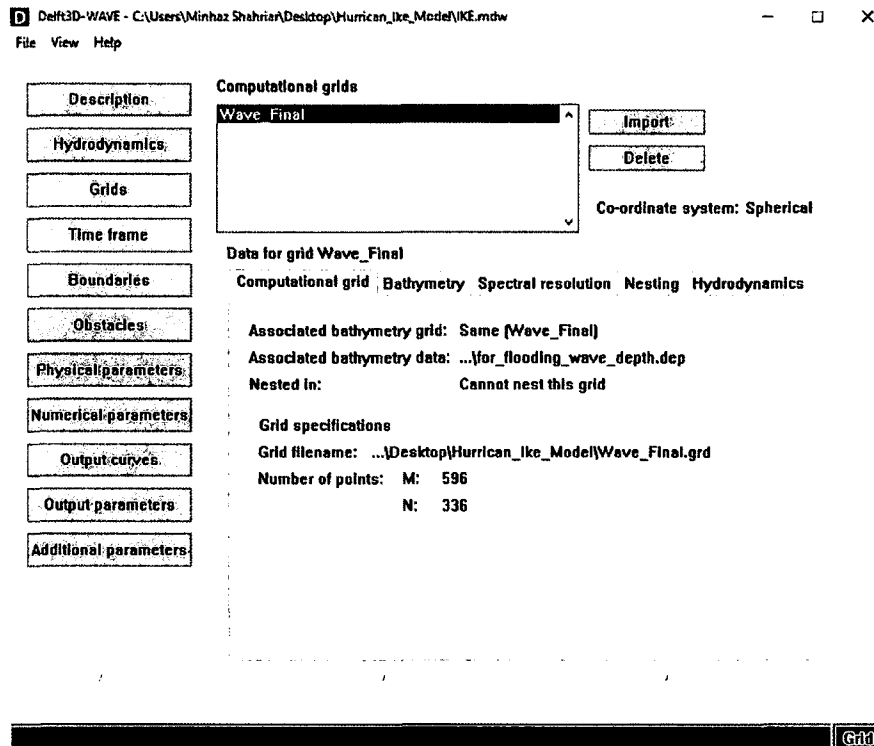


Figure A-8: Delft3D Wave grid input through GUI.

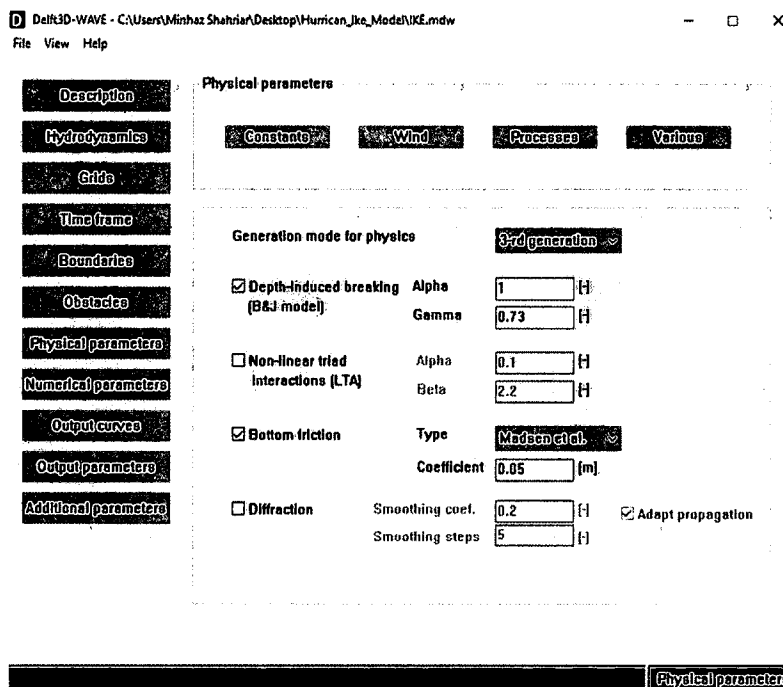


Figure A-9: Delft3D Wave physical parameters input through GUI.

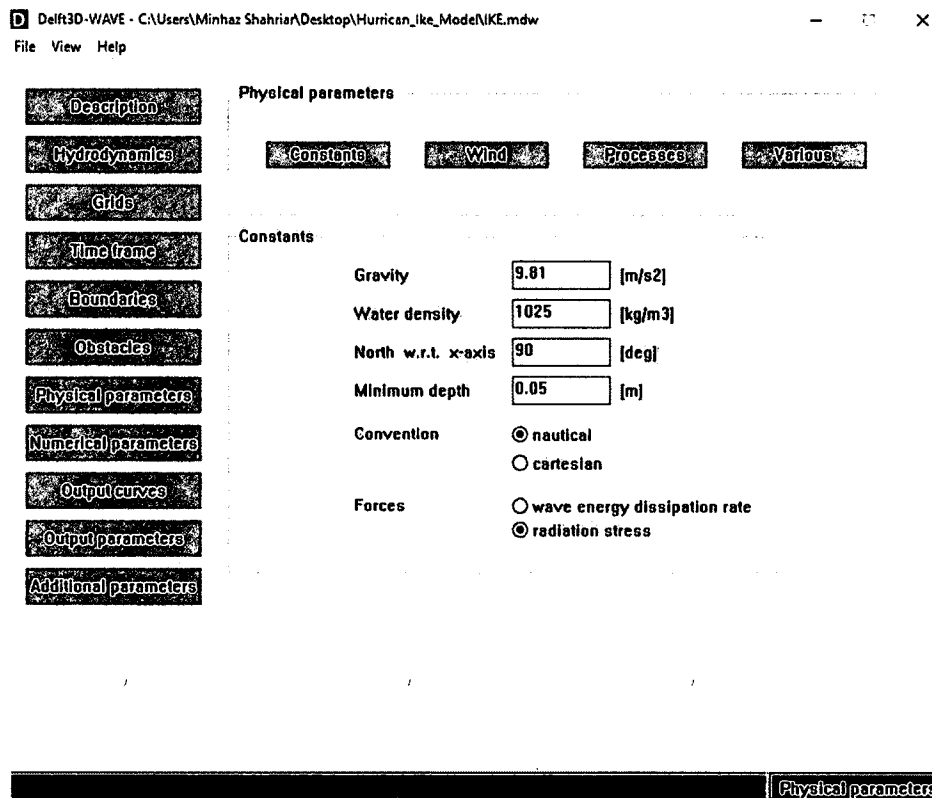


Figure A-10: Delft3D Wave physical parameters input through GUI.

Delft3D-WAVE - C:\Users\Minhas\Shahria\Desktop\Hurricane_ike_Model\IKE.mdw
File View Help

Description

Hydrodynamics

Grids

Time frame

Boundaries

Obstacles

Physical parameters

Numerical parameters

Output curves

Output parameters

Additional parameters

Geographical space

First-order (SWAN 40.01) / Second-order (SWAN 40.11)

Third-order (not yet operational)

Spectral space

Directional space (CDD): [H] (0.0-1.0)

Frequency space (CSS): [H] (0.0-1.0)

CDD and CSS determine the numerical scheme: 0 = central, 1 = upwind

Accuracy criteria (to terminate the iterative computations)

Relative change	Percentage of wet grid points
Hs-Tm01: <input type="text" value="0.02"/> [H]	<input type="text" value="98"/> [%]
Relative change w.r.t. mean value	Maximum number of iterations
Hs: <input type="text" value="0.02"/> [H]	<input type="text" value="15"/>
Tm01: <input type="text" value="0.02"/> [H]	

Numerical parameters

Figure A-11: Delft3D Wave numerical parameters input through GUI.

APPENDIX B

DELFT3D VEGETATION INPUT FILES

```

*
* Directional Point Model of Vegetation input file
*
[VegetationFileInformation]
  FileCreatedBy   = Minhaz Shahriar
  FileCreationDate = 04-12-2014
  FileVersion     = 01.00
[General]
  PolygonFile     = cycle1.pol
  ClPlant = 0.80   [ - ] Turbulence length scale coefficient between stems
  ItPlant = 50     [ - ] Number of time steps between updates of plant arrays

[Vegetation]
  Type = reed
  *
  * height [m]      stem diameter [m]      nr of stems [-]      cd coefficient [-]
  *
  Vps = 0.0         0.006                   1                    2.0
  Vps = 0.90        0.006                   1                    2.0
  Vps = 0.91        0.006                   1                    2.0
[Area]
  VegetationType = #reed#           [ - ] must match a vegetation group in this file
  Polygon        = #reed#           [ - ] must match a polygon in the PolygonFile
  NPlants        = 100              [ /m2 ]

```

Figure B-1: Delft3D vegetation input file script.

B.1 Delft3D Vegetation Map File for *Spartina alterniflora*

File Name: Spartina (Cycle-1).pol
Spartina alterniflora Polygon map
reed

52	2
-9.3428096E+01	2.9960800E+01
-9.3428780E+01	2.9961391E+01
-9.3429873E+01	2.9962160E+01
-9.3430761E+01	2.9963047E+01
-9.3431717E+01	2.9963284E+01
-9.3432127E+01	2.9962692E+01
-9.3432947E+01	2.9963757E+01
-9.3432059E+01	2.9964704E+01
-9.3429942E+01	2.9964290E+01
-9.3428712E+01	2.9964409E+01
-9.3427619E+01	2.9964291E+01
-9.3425502E+01	2.9964351E+01
-9.3420311E+01	2.9964292E+01
-9.3415393E+01	2.9964057E+01
-9.3408221E+01	2.9964057E+01
-9.3405489E+01	2.9963821E+01
-9.3405147E+01	2.9962874E+01
-9.3405216E+01	2.9961631E+01
-9.3405420E+01	2.9960034E+01
-9.3405352E+01	2.9958022E+01
-9.3405557E+01	2.9956957E+01
-9.3406035E+01	2.9957548E+01
-9.3406581E+01	2.9958318E+01
-9.3407879E+01	2.9958258E+01
-9.3408425E+01	2.9957667E+01
-9.3409928E+01	2.9958199E+01
-9.3411157E+01	2.9958613E+01
-9.3412319E+01	2.9958909E+01
-9.3413548E+01	2.9958554E+01
-9.3413958E+01	2.9958199E+01
-9.3414572E+01	2.9958790E+01
-9.3415392E+01	2.9958613E+01
-9.3416621E+01	2.9958731E+01
-9.3416485E+01	2.9958021E+01
-9.3417646E+01	2.9958849E+01
-9.3417236E+01	2.9959796E+01
-9.3418876E+01	2.9960150E+01
-9.3419900E+01	2.9959795E+01
-9.3419695E+01	2.9959263E+01
-9.3420788E+01	2.9959618E+01
-9.3420515E+01	2.9960150E+01
-9.3421266E+01	2.9960505E+01

-9.3421608E+01 2.9961156E+01
-9.3422701E+01 2.9961097E+01
-9.3424067E+01 2.9962339E+01
-9.3424819E+01 2.9962871E+01
-9.3425092E+01 2.9963641E+01
-9.3426185E+01 2.9963640E+01
-9.3427004E+01 2.9963403E+01
-9.3427551E+01 2.9962575E+01
-9.3427619E+01 2.9961687E+01
-9.3428096E+01 2.9960800E+01

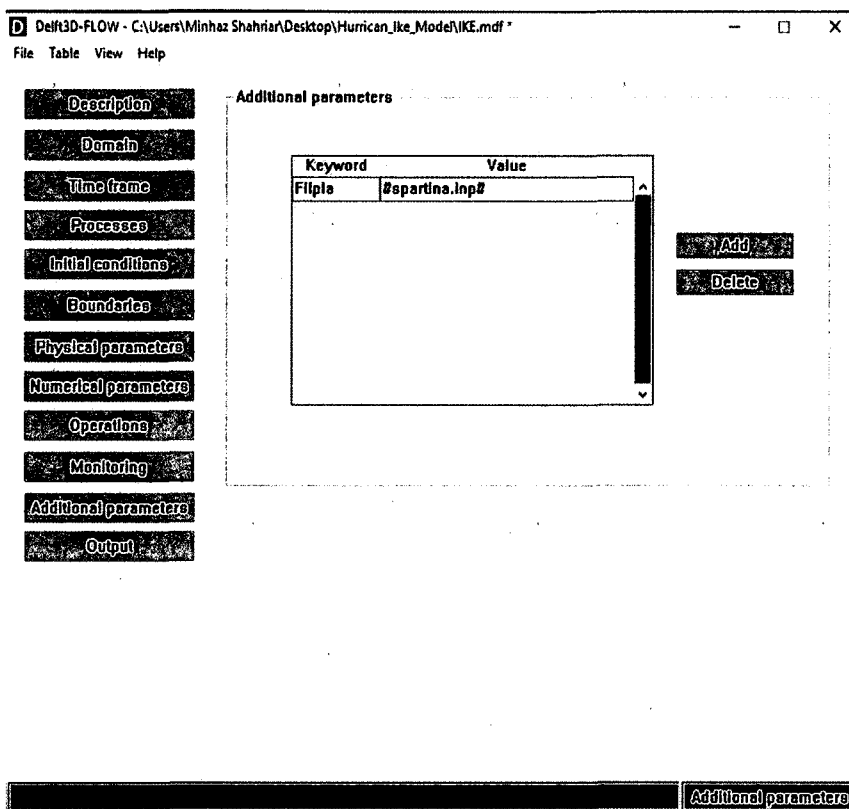


Figure B- 2: Keyword input to initiate vegetation model.

APPENDIX C
DELFT3D MODEL FILES

C.1 Delft3D Wave Boundary File

```
## File Name: wavecon.Hurricane_Ike.mdw
## Hurricane Ike Wave Input File
## Created by: Minhaz Shahriar
## mms040@latech.edu
```

```
* Idate Hs Tp Dir(°) ms wl windspeed wind dir.(°)
```

```
BL01
```

```
17 8 * number of rows number of columns
```

0	2.75	11	30.00	4	0	5.20	30.00
180	3	12	18.00	4	0	5.80	18.00
360	3.5	10.75	16.00	4	0	9.00	16.00
540	4	11	27.00	4	0	8.20	27.00
720	4.75	12	46.00	4	0	10.40	46.00
900	5.5	12.5	63.00	4	0	13.80	63.00
1080	5.75	11.5	73.00	4	0	19.20	73.00
1260	6	9.5	57.00	4	0	18.60	57.00
1440	5	8	82.00	4	0	23.60	82.00
1620	5.6	8	96.00	4	0	26.10	96.00
1800	6	7.5	133.00	4	0	22.70	133.00
1980	5	9	131.00	4	0	25.30	131.00
2160	7	9.5	162.00	4	0	22.80	162.00
2340	5.6	8	164.00	4	0	18.30	164.00
2520	5	7.5	165.00	4	0	17.20	165.00
2700	4	7	171.00	4	0	13.30	171.00
2880	3	6.5	169.00	4	0	12.30	169.00

C.2 Wave Flow Coupled Run Script

```

& echo off
rem
rem This script is an example for running Delft3D-FLOW 6.00 online with Delft3D-WAVE (Windows)
rem Adapt and use it for your own purpose
rem
rem mas040@latech.edu
rem 10 April 2014
rem
rem
rem This script starts a single-domain Delft3D-FLOW computation online with Delft3D-WAVE on Windows

rem Set the config file and ndw file
rem
set argfile=config_d_hydro.xml
set ndwfile=Hurricane_IKE.ndw

rem
rem Set the directories containing the executables
rem
set ARCH=win64
set D3D_HOME=...\bin
rem set D3D_HOME=c:\Program Files (x86)\Deltares\Delft3D 4.01.00
set flowexedir=%D3D_HOME%\%ARCH%\flow2d2d\bin
set wavexedir=%D3D_HOME%\%ARCH%\wave\bin
set swanexedir=%D3D_HOME%\%ARCH%\swan\bin
set swanbatdir=%D3D_HOME%\%ARCH%\swan\scripts

rem
rem No adaptations needed below
rem

rem Start FLOW
set PATH=%flowexedir%;%PATH%
start "Hydrodynamic simulation" "%flowexedir%\d_hydro.exe" %argfile%

rem Start WAVE
title Wave simulation
set PATH=%wavexedir%;%swanbatdir%;%swanexedir%;%PATH%
"%swanexedir%\wave.exe" %ndwfile% 1
title %CD%

rem To prevent the DOS box from disappearing immediately: remove the rem on the following line
rem pause

```

C.3 Wave Run Script

```

@echo off

set swanexe=1322_HOCHT\ARCH3\swan\bin\swan_4072ABCDE_del_w64_illomp.exe

rem
rem swan40.72AB and newer runs parallel, using the total number of cores on the machine
rem to force the number of parallel processes, remove the "rem" in front of the following line and adjust the number
rem set OMP_NUM_THREADS=1

@echo SWAN batchfile executed for Delft3D
@echo Using swan.bat in directory %~dp3
@echo Using %swanexe%
@echo Performing wave computation for: %1.swn

if exist PRINT del PRINT
if exist INPUT del INPUT
if exist swaninit del swaninit
if exist Errfile del Errfile
if exist errpts del errpts
if exist %1.erf del %1.erf
if exist %1.erp del %1.erp
if not exist %1.swn goto error1
if not exist "%swanexe%" goto error2
copy %1.swn INPUT

mod.exe -l "26" "INTEGRID _" INPUT
mod.exe -l "27" "FRICTION CURV 0. 0. 326 328" INPUT
mod.exe -l "28" "READING FRICTION 1.0 'cyclic.mod' 4 0 FREE" INPUT
mod.exe -a "FRIC JON      0.0670" "FRICTION MADSEN km=0.05" INPUT

"%swanexe%"

copy PRINT %1.pst
if exist errfile copy errfile %1.erf
if exist errpts copy errpts %1.erp
if exist swaninit del swaninit
goto finish
:error1
@echo
@echo .....
@echo          SWAN input file %1.swn does not exist
@echo .....
pause
goto finish
:error2
@echo
@echo .....
@echo          SWAN executable does not exist
@echo          (%swanexe%)
@echo .....
pause
goto finish
:finish
@echo on
rem exit

```

REFERENCES

Abernethy B, Rutherford ID. 2001. The distribution and strength of riparian tree roots in relation to riverbank reinforcement. *Hydrological Processes* 15, pp. 63–79.

Automated Tropical Cyclone Forecast Archive, available online at <ftp://ftp.nhc.noaa.gov/atcf/>

Barras, J.A., P.E. Bourgeois, and L.R. Handley. 1994. Land loss in coastal Louisiana 1956-90. National Biological Survey, National Wetlands Research Center Open File Report 94-01. 4, pp. 10 color plates.

Barras, J.A. 2003. Changes to Cote Blanche Hydrologic Restoration (TV-04) Area after Hurricane Lili: U.S. Geological Survey, National Wetlands Research Center, map-id USGS-NWRC 2003-11-112. poster.

Barras, J.A. 2006. Land area change in coastal Louisiana after the 2005 hurricanes—a series of three maps: U.S. Geological Survey Open-File Report 2006-1274, available online at <http://pubs.usgs.gov/of/2006/1274/>

Barras, J.A. 2007a. Land area changes in coastal Louisiana after Hurricanes Katrina and Rita, in Farris, G.S., Smith, G.J., Crane, M.P., Demas, C.R., Robbins, L.L., and Lavoie, D.L., eds., *Science and the storms—the USGS response to the hurricanes of 2005*: U.S. Geological Survey Circular 1306, pp. 98-113, available online at <http://pubs.usgs.gov/circ/1306/>

Barras, J.A. 2007b. Satellite images and aerial photographs of the effects of Hurricanes Katrina and Rita on coastal Louisiana: U.S. Geological Survey Data Series 281, available online at <http://pubs.usgs.gov/ds/2007/281/>

Barras, J.A., Bernier, J.C., and Morton, R.A. 2008. Land area change in coastal Louisiana—A multidecadal perspective (from 1956 to 2006): U.S. Geological Survey Scientific Investigations Map 3019, scale 1:250,000, 14 p. pamphlet, available online at <http://pubs.usgs.gov/sim/3019/>

Barras, J.A. 2009. Land area change and overview of major hurricane impacts in coastal Louisiana, 2004-08: U.S. Geological Survey Scientific Investigations Map 3080.

Benoit, W. L., & Nill, D. M. 1998. Oliver Stone's defense of JFK. *Communication Quarterly*, 42, 127-143. doi: 10.1080/01463379809370091
1:250,000, 6 p. pamphlet.

- Bernier, N. B., K. R. Thompson. 2007. Tide-surge interaction off the east coast of Canada and northeastern United States, *J. Geophys. Res.*, 112, C06008, doi:10.1029/2006JC003793
- Berg, R. 2009. Tropical Cyclone Report, Hurricane Ike, 1–14 Sep, p. 55, NOAA/National Hurricane Cent., Miami, Fla.
- Booij, N., R. C. Ris, and L. H. Holthuijsen. 1990. A third-generation wave model for coastal regions, 1, Model description and validation, *J. Geophys. Res.*, 104, C4.
- Budhu, M. 2007. *Soil Mechanics and Foundations*. 2nd ed., Wiley, Hoboken, NJ.
- Calcasieu pass station image, available online at <https://tidesandcurrents.noaa.gov/stationhome.html?id=8768094/>
- Coastal Protection and Restoration Authority. 2011. Fiscal Year 2012 Annual Plan: Integrated Ecosystem Restoration and Hurricane Protection in Coastal Louisiana. Coastal Protection and Restoration Authority of Louisiana. Baton Rouge, LA, available online at http://www.lacpra.org/assets/docs/2012%20ANNUAL%20PLAN/CPRA_Annual_Plan_4-28-11_Web_Format.pdf/
- Deltares. 2011. User Manual Delft3D-FLOW. Simulation of Multi-Dimensional Hydrodynamic and Transportation Phenomena, Including Sediments. Deltares, Delft, The Netherlands.
- Dingemans, M. W. 1997. Water Wave Propagation Over Uneven Bottoms, part 1, Linear Wave Propagation, *Adv. Ser. Ocean Eng.*, 13, p. 471, World Sci., River Edge, N. J.
- East, J. W., M. J. Turco, and R. R. Mason Jr. 2008. Monitoring inland storm surge and flooding from Hurricane Ike in Texas and Louisiana, September 2008, U.S. Geol. Surv. Open File Rep, p. 1365.
- Endo, T., Tsuruta, T. 1969. Effects of tree's roots upon the shearing strengths of soils. In 18th Annual Report of the Hokkaido Branch, Government Forest Experimental Station, Tokyo, pp. 167–179.
- FEMA 2008. Texas Hurricane Ike rapid response coastal high water mark collection, FEMA-1791-DR-Texas, Washington, D. C.
- Fredsøe, J. 1984. Turbulent boundary layer in wave-current motion, *J. Hydraul. Eng.*, 110(8), pp. 1103–1120.
- Gray, D. H., A.T. Leiser. 1982. *Biotechnical slope protection and erosion control*. Van Nostrand Reinhold Company. New York.
- Gray, D. H., R. B. Sotir. 1996. *Biotechnical and soil bioengineering slope stabilization: A practical guide for erosion control*. John Wiley and Sons, New York.
- Greenway, D. R. 1987. Vegetation and slope stability. In *slope stability*, edited by M. F. Anderson and K. S. Richards. Wiley and Sons, New York.

Gosselin, M., M. Levasseur, P. A. Wheeler, R. A. Horner, and B. C. Booth .1998. New measurements of phytoplankton and ice algal production in the Arctic Ocean, *Deep Sea Res., Part II*, 44(8), pp. 1623–1644, doi:10.1016/ s0967-0645(97)00054-4.

Hayes, M.D. 1967. Hurricanes as geological agents. case studies of Hurricanes Carla, 1961, and Cindy, 1963. University of Texas at Austin, Bureau of Economic Geology, Report of Investigation 61, p. 54.

Hasselmann, K., *et al.*, 1973. Measurements of wind-wave growth and swell decay during the Joint North Sea Wave Project (JONSWAP, Dtsch. Hydrogr. Z. Suppl., 12A8, pp. 1–95.

Henkel, D.J. 1970. The role of waves is causing submarine landslides, *Geotechnique* 20(1), pp. 75-80.

Holthuijsen, Leo H. 2007. *Waves in oceanic and coastal waters*. Cambridge: Cambridge University Press.

Johnston, J.B., Watzin, M.C., Barras, J.A., and L.R. Handley.1995. Gulf of Mexico coastal wetlands: case studies of loss trends. In: LaRoe *et al.*, (eds.) *Our living resources: a report to the nation on the distribution, abundance, and health of U.S. plants, animals and ecosystems*. U.S. Department of the Interior, National Biological Service, Washington, D.C., pp. 269-272.

Louisiana Coastal Wetlands Conservation and Restoration Task Force. 2012. *The 2012 Evaluation Report to the U.S. Congress on the Effectiveness of Coastal Wetlands Planning, Protection and Restoration Act Projects*, available online at https://lacoast.gov/reports/rtc/RTC_2012_1-18-13.pdf/

Louisiana State University, cited. 2004: Louisiana Lidar, available online at <http://atlas.lsu.edu/lidar/>

Menashe, E. 2001. *Proceedings of the Conference: Native Plant Propagation and Restoration Strategies*. Haas, DI and R. Rose Editors. Nursery Technology Cooperative and Western Forestry and Conservation Association. Eugene OR, available online at <http://depts.washington.edu/uwbg/wordpress/wpcontent/uploads/BiostructuralErosionControlMenashe.pdf>

Mei, C. C. 1983. *The Applied Dynamics of Ocean Surface Waves*, John Wiley, New York.

Miller, K.G., and Snyder, S.W.1997. *Proceedings of the Ocean Drilling Program, Scientific Results, 150X: College Station, TX (Ocean Drilling Program)*, p. 388.

Morton, R. A., and Paine, J. G. 1985. Beach and vegetation-line changes at Galveston Island, Texas; Erosion, deposition, and recovery from Hurricane Alicia: The University of Texas at Austin, Bureau of Economic Geology Geological Circular 85(5), p. 39.

Morton, R.A.1988. Interactions of storms, seawalls and beaches of the Texas coast, in Kraus, N.C., and Pilkey, O.H., *Effects of seawalls on the beach: Journal of Coastal Research, Special Issue 4*, pp. 113-134.

Morton, R. A., and Miller, T. L. 2005. National Assessment of Shoreline Change: Part 2: Historical Shoreline Changes and Associated Coastal Land Loss along the U.S. Southeast Atlantic Coast: U.S. Geological Survey Open-file Report 2005-1401.

National Geophysical Data Center. 1988. Data announcement 88-MGG-02, digital relief of the surface of the Earth. National Oceanic and Atmospheric Administration, Boulder, CO, available online at <http://www.ngdc.noaa.gov/mgg/global/etopo5.html/>

National Digital Forecast Database, available online at <http://graphical.weather.gov/sectors/southmissvlyMarineWeek.php?zoom=OFF#tabs/>

NOAA's bathymetric sounding database, available online at <https://maps.ngdc.noaa.gov/viewers/bathymetry/>

Nummedal, D., R. Manty, and S. Penland. 1980. Bar morphology along the Mississippi Sound Margin: Gulf Coast Association of Geological Societies V.30, pp. 465-466.

O'Loughlin, C.L. 1974. The effect of timber removal on the stability of forest soils. *Journal of Hydrology* V.13, pp.121-134.

Paille, R.F., 1996, Lower Atchafalaya Basin reevaluation study—planning aid report on freshwater inflows to the Terrebonne Basin: Lafayette, La., U.S. Fish and Wildlife Service, Ecological Services, p. 28.

R.L. Soulsby, L. Hamm, G. Klopman, D. Myrhaug, R.R. Simons, G.P. Thomas. 1993. Wave-current interaction within and outside the bottom boundary layer *Coast. Eng.* p. 4169.

Robson B.J. 1999. Hydrodynamics of shallow mediterranean estuaries, and relevance to come biogeochemical processes affecting *Nodularia* blooms. New South Wales, Australia. University of New South Wales. PhD Thesis.

Sasser, C.E., Visser, J.M., Mouton, Edmond, Linscombe, Jeb, and Hartley, S.B. 2014. Vegetation types in coastal Louisiana in 2013: U.S. Geological Survey Scientific Investigations Map 3290, 1 sheet, scale 1: 550,000, available online at <https://dx.doi.org/10.3133/sim3290/>

Schmidt, K.M. Roering, J.J. Stock, J.D. Dietrich, W.E. Montgomery, D.R. Schaub, T. 2001. The variability of root cohesion as an influence on shallow landslide susceptibility in the Oregon Coast Range. *Canadian Geotechnical Journal* 38, pp. 995–1024.

Shahriar, M.M. Wang, J.X. Alam, S. and Patterson, W.B. 2016. Soil-binding ability of vegetation roots in enhancing erosion resistance of a shallow slope. *International Journal of Geotechnical Engineering*. doi:10.1080/19386362.2016.1168608

Treffers, R. 2009. Wave-Driven Longshore Currents in the Surfzone. Master of Science thesis, Delft University of Technology.

- U.S. Army Corps of Engineers. 2010. Waterborne Commerce of the United States, Calendar Year 2009. Alexandria, VA: Institute for Water Resources, U. S. Army Corps of Engineers, available online at <http://www.ndc.iwr.usace.army.mil/wcsc/statenm09.html/>
<http://www.ndc.iwr.usace.army.mil/wcsc/portton09.html/>
- Uittenbogaard, R.E. and Blumberg, A.F. 2000. 3D modelling of horizontal transport and vertical mixing in Lake Victoria. Hydroinformatics 2000, Cedar Rapids (IOWA).
- Van Ballegooyen, R. and Taljaard, S. 2001. Application of Delft3D – FLOW to stratified estuaries in South Africa.
- VDatum, 2010. Vertical Datum Transformation Software, available online at <https://vdatum.noaa.gov/welcome.html/>
- Walden, J. 1996. The New England gillnet effort survey. NOAA, NMF S, NEFSC, Woods Hole, Massachusetts. NEFSC [Northeast Fisheries Science Center] Ref. Doc. 99(10), p. 38.
- Waldron, L. J. 1977. The shear resistance of root-permeated homogeneous and stratified soil, Soil Science Society of America Proceedings 41, pp. 843-849.
- Waldron LJ, Dakessian S. 1982. Effect of grass, legume and tree roots on soil shearing resistance. Soil Science Society of America Journal 46, pp. 894–899.
- Walkup, C. J. 1991. *Spartina alterniflora*. In: Fire Effects Information System, [Online]. U.S. Department of Agriculture, Forest Service, Rocky Mountain Research Station, Fire Sciences Laboratory (Producer), available online at <http://www.fs.fed.us/database/feis/>
- Wiegel, Robert L. 1964. Oceanographic engineering, Prentice-Hall, Inc.
- Willmott, C. J. 1981. On the validation of models, Phys. Geogr. 2, pp. 184–194.
- Winterwerp, J. C. 1999. On the dynamics of high-concentrated mud suspensions. PhD thesis, Delft University of Technology, Delft, The Netherlands.
- Whitham G.B. 1974. N. Linear and Nonlinear Waves, John Wiley, New York, p. 55.
- Wu, T. H. McKinnel, W. P., and Swanston, D. N. 1979. Strength of tree roots, landslides on Prince of Wales Island, Alaska. Canadian Geotechnical Journal 16, pp. 19-33.
- Zeimer, R. R. and D. N. Swanston. 1977. Root strength changes after logging in southeast Alaska. U.S.D.A. Forest Service, PNW Research Station, Portland, Oregon.